INFORMATION TO USERS

This manuscript has been reproduced from the microfilm master. UMI films the text directly from the original or copy submitted. Thus, some thesis and dissertation copies are in typewriter face, while others may be from any type of computer printer.

The quality of this reproduction is dependent upon the quality of the copy submitted. Broken or indistinct print, colored or poor quality illustrations and photographs, print bleedthrough, substandard margins, and improper alignment can adversely affect reproduction.

In the unlikely event that the author did not send UMI a complete manuscript and there are missing pages, these will be noted. Also, if unauthorized copyright material had to be removed, a note will indicate the deletion.

Oversize materials (e.g., maps, drawings, charts) are reproduced by sectioning the original, beginning at the upper left-hand corner and continuing from left to right in equal sections with small overlaps. Each original is also photographed in one exposure and is included in reduced form at the back of the book.

Photographs included in the original manuscript have been reproduced xerographically in this copy. Higher quality 6" x 9" black and white photographic prints are available for any photographs or illustrations appearing in this copy for an additional charge. Contact UMI directly to order.

UMI®

Bell & Howell Information and Learning
300 North Zeeb Road, Ann Arbor, MI 48106-1346 USA
800-521-0600

Biophysical mechanisms underlying the recruitment process in walleye pollock (*Theragra chalcogramma*)

Sarah Hinckley

A dissertation submitted in partial fulfillment of the
requirements for the degree of

Doctor of Philosophy

University of Washington
1999

Program Authorized to Offer Degree: Fisheries

In presenting this thesis in partial fulfillment of the requirements for the Doctoral degree at the University of Washington, I agree that the Library shall make it's copies freely available for inspection. I further agree that extensive copying of the dissertation is allowable only for scholarly purposes, consistent with "fair use" as prescribed in the U.S. Copyright Law. Requests for copying or reproduction of this dissertation may be referred to University Microfilms, 1490 Eisenhower Place, P.O. Box 975, Ann Arbor, MI 48106, to whom the author has granted "the right to reproduce and sell (a) copies of the manuscript in microform and/or (b) printed copies of the manuscript made from microform."

Signature Sarah Hwidley

Date 5-18-99

University of Washington
Graduate School

This is to certify that I have examined this copy of a doctoral dissertation by

Sarah Hinckley

and found that it is complete and satisfactory in all respects,
and that any and all revisions required by the final
examining committee have been made.

Chair of Supervisory Committee:

Robert C. Francis

Reading Committee:

Robert C. Francis

Donald Gunderson

Bernard A. Megrey

Date: 5-18-99.

University of Washington

Abstract

Biophysical mechanisms underlying the recruitment process in walleye pollock (*Theragra chalcogramma*)

Sarah Hinckley

Chairperson of the Supervisory Committee:

Professor Robert C. Francis
Fisheries

Recruitment variability in marine fish species is not well understood, yet is very important as a component of fishery management. This dissertation describes a set of coupled biological and physical simulation models designed to examine mechanisms underlying the recruitment process for walleye pollock, *Theragra chalcogramma,* in the western Gulf of Alaska. These models consist of (1) a three-dimensional hydrodynamic model of the region driven by winds and fresh-water runoff, (2) an individual-based model of the early life stages (egg through 0-age juvenile) of pollock, which uses a Lagrangian float-tracking scheme to follow fish through space and which keeps track of many characteristics of individual fish, and (3) a three-dimensional nutrient-phytoplankton-zooplankton model which includes the dominant prey species of pollock larvae. Methods of coupling large simulations models are discussed. Six sets of model experiments and hindcasts are described. Important findings of the work include the following. An explanation for the consistency of the timing and location of spawning of pollock in Shelikof Strait is presented, as it relates to transport to the juvenile nursery area and spatial and temporal dynamics of the prey. Support is found for the hypothesis that eddies (specifically cyclonic eddies) are good feeding environments for larvae and aid in transporting them to the nursery areas. The depth of an individual is shown to be an important life history trait which makes a significant contribution to growth and survival. This modelling shows that

spatial variability in physical factors such as temperature and salinity at the scales resolved by these models, as well as the spatial and temporal dynamics of the prey resources, have important effects on individuals and significant consequences at the level of the population. The match-mismatch theory of recruitment success is supported. A possible mechanism for the effect of wind-induced turbulence on growth and survival is explored. It is hoped that what has been learned from this type of modelling can be integrated into our growing knowledge of the recruitment process for walleye pollock and other marine fish species.

TABLE OF CONTENTS

LIST OF FIGURES

LIST OF TABLES

Preface

The research described in this dissertation would not have been possible without the participation of Drs. A. Hermann and B. Megrey, researchers in the Fisheries Oceanography Coordinated Investigations Program, NOAA. Much of this work has been published under the coauthorship of myself, Hermann and Megrey, in Hinckley et al. 1996a and 1996b, Hermann et al. 1996, Hinckley et al. In Press, Hermann et al. In Press, and Megrey and Hinckley In Press.

Acknowledgements

I would like to express my appreciation for the support and encouragement I have had from my chair, Bob Francis, and from Bern Megrey, Al Hermann, Art Kendall and Gary Stauffer over a long period of time. All of the scientists in the Fisheries Oceanography Coordinated Investigations program at NOAA contributed greatly to this work by sharing their expertise and data. My committee members, Ken Rose, Don Gunderson and Barbara Hickey have all been very helpful along the way. I owe Judy Gray a big thank you for getting me going on this project and for the career change it represented. The Electric Power Research Institute funded some of the early work, my thanks to them. But I couldn't have done it without my friends. To Steve, Susi, Marianne, Whipple and Kris. To my family. To the people at CQS and QERM. And to the Allegro for coffee and table space.

Chapter 1. Introduction

1.1 Background

The question of what causes variability in year-class strength in marine fish populations has been the focus of research for many decades. In particular, the underlying causes of year-to-year changes in the number of young fish surviving to enter a fishery (recruitment) are not well understood (Wooster and Bailey 1989). It has been thought since the early 1900's that factors affecting the survival of early life stages of marine fish cause large fluctuations in the abundance of fish populations. Variability in recruitment is of central importance to fishery managers (Rothschild 1986, Sissenwine 1984, Kendall et al.1996). This is because management of a fish stock usually includes development of projections of future abundances based on different harvest and recruitment scenarios. Recruitment is usually the most poorly known of the variables used in stock projection models.

Many hypotheses have been developed to explain recruitment variability. Hjort's (1914, 1928) "critical period" hypothesis proposed that variation in food production for first-feeding larvae was important. However, little evidence of a clear link has been shown (Leggett and DeBlois 1994) and Legget and DeBlois conclude that the available evidence does not support the "critical period" hypothesis as a major contributor to recruitment variation. Cushing's (1972, 1974) "match-mismatch" hypothesis proposed that the timing of the spring bloom in relation to the timing of larval production was critical. This proposal implies that feeding conditions during the entire larval period have a major effect on recruitment. The available evidence supports this hypothesis, but recent studies suggest that other factors may dominate (Leggett and DeBlois 1994). The effect of conditions of stratification and turbulence on larval food and feeding success (Lasker 1975, Rothschild and Osborn 1988, MacKenzie et al. 1994, MacKenzie and Kiørboe 1995) has also been thought to be important to the feeding, growth and survival process.

The effect of predation on recruitment variability, reviewed by Bailey and Houde (1989), has not been extensively studied, so its effects have not been resolved. As stated by Leggett and DeBlois (1994) "food-mediated changes in larval growth, condition and performance are likely to alter both the frequency, and the intensity of predation on post-yolk-sac stages of most, if not all, marine fish larvae". Several recent hypotheses depend on the interaction between food and predation. The "bigger is better" hypothesis (Leggett and DeBlois 1994), holds that larger larvae have increased foraging capability and are less susceptible to predation (implying that larger initial size or faster growth are critical). The "stage duration" (Cushing 1975) states that larvae which experience better feeding conditions grow faster, and therefore experience a smaller cumulative (total) mortality due to shortened duration of earlier stages when mortalities are high than do larvae experiencing poorer feeding conditions. The present consensus about the "bigger is better" hypothesis (Cowan et al. 1997) seems to be that such a simple conceptual model as decreasing vulnerability with increased size, is not widely applicable because fish are exposed to a complex and changing mixture of predators that may vary in abundance, size and type, and that differ in their preferences and behavior. In some cases, larger larvae may be more vulnerable than smaller larvae. The relative importance of density-dependent versus density-independent factors is unclear. Density-dependent effects of adult population size on recruitment (spawner-recruit relationships) have been proposed and studied in depth, but relationships are usually weak, and traditional stock-recruitment models have performed poorly in helping to understand recruitment.

Studies of the recruitment process have often focused on population-level phenomena, such as correlations among environmental factors, stock factors and recruitment levels, or alternatively, on single processes occurring at the level of individual organisms or single life stages, for example, predation or starvation. However, the idea is becoming more generally accepted that mechanisms operating on different time, space, or organizational (individual, population, species) scales may all be important, and that overall recruitment levels are unlikely to be controlled by one factor or process at one life stage alone. A

complex set of factors are involved which may act sequentially or simultaneously through compounded interactions to affect year-class strength.

Numerical biophysical modeling can help us to explore mechanisms affecting recruitment and the interactions of these mechanisms. Due to the complexity of the involved processes , "progress in understanding how selective forces shape recruitment will depend increasingly on modeling, such as the individual-based approaches now being applied to examine how habitat, environment and predation affect recruitment variability" (Pope et al. 1994). In order to examine hypotheses about differential growth and mortality among individuals, we believe it is necessary to include individuals explicitly in this model. We also believe that an appropriate model to study recruitment processes of some marine fish species should also include spatial factors, such as ocean circulation patterns and the distributions of abiotic and biotic factors, as we believe that these factors may significantly affect recruitment.

At present, the majority of marine population and ecosystems models are formulated in terms of aggregate properties of each model component, for example, the mean biomass of fish per unit volume or area. In effect, such models follow the evolution of the "mean individual" of represented populations through time. Ecologists have increasingly used models which deal explicitly with individuals in order to generate system dynamics (DeAngelis and Gross 1992, Judson 1994). These models keep track of a number of distinct individuals within a population, each of which may interact with other individuals or with the physical environment based on its present state and possibly its past history. Such models are frequently stochastic in design.

This increase in models dealing with individuals has arisen for several reasons. Simple, aggregated models ignore two basic aspects of biology: that all individuals are different, and that interactions between individuals take place locally (Huston et al. 1988, DeAngelis and Gross 1992, Judson 1994). However, analytical approaches to the examination of such issues are often intractible. The rise of individual-based models (IBMs) has been

facilitated by increases in computer power over the past decade, which allows the simultaneous tracking of many individuals and their attributes. This was previously impossible.

Individual-based models are usually divided into two main types: "i-state distribution" models and "i-state configuration" models (Metz and Diekmann 1986, Caswell and John 1992). I-state distribution models aggregate individuals into age, size or stage groups, within which all individuals are assumed to be homogenous. I-state configuration models treat each individual as a unique entity. I-state distributions can be derived from i-state configuration models by reducing the configuration to a distribution function.

The advantages and disadvangtages of i-state configuration models have been described by DeAngelis and Rose (1992). They conclude that these models are useful in studying problems where the population size is small and there is high sensitivity to initial conditions, in large or small populations where there is stochasticity in growth and mortality and where fluctuations in i-state variables may be amplified in some individuals relative to other individuals, or where all individuals at the same point in state-space are not assumed to encounter the same environment due to incomplete population mixing. Under these circumstances, i-state configuration IBMs are able to capture dynamics that are lost when aggregated models are used. Such models enable exploration of processes at higher levels of complexity at different time and space scales, and the inclusion of many different i-state variables. Recent examples of the IBM approach include DeAngelis et al. (1991), Rice et al. (1993), Crowder et al. (1993), Rose and Cowan (1993), Werner et al. (1993, 1996).

There are certainly disadvantages and difficulties in the use of the i-state configuration models. The biological data needs increase greatly (although parameters are usually easier to understand), and it is often very difficult to obtain truly individual information. There are few measurements over time on the same individual. There are also practical limits to the attributes that can be measured for each fish (Van Winkle et al. 1993). Selection on, and heritability of traits is often not addressed (Chambers 1993). Often modelers are forced to use population-level estimates of parameters, such as means and variances of an attribute, or even simply the mean, due to the lack of truly individual information

(Pepin and Miller 1993). In the case of spatially explicit models, spatially varying estimates of parameters are difficult to obtain. Moreover, these models are less amenable to standard techniques of mathematical analysis than aggregated models. Results can be voluminous and difficult to interpret. The choice of output variables to examine is often not obvious, and interactions among variables can be confusing. The meaning of standard statistical methods used on model output is a largely undeveloped area. Finally, these models can require massive amounts of computing resources (CPU time, storage and memory).

There is debate about whether i-state configuration models are so specific to a particular system that they preclude generality (Smith 1974, Lomnicki 1992), or conversely, whether they can actually unify ecological theory (Huston et al. 1988). IBMs appear to offer one of the few options for addressing the ecological effects of individual variation (Chambers and Trippel 1997). In the end, however, the choice of whether to use i-state configuration, i-state distribution, or simple aggregated population models depends on the specific objectives of the study and the attributes of the system under examination.

The inclusion of spatial factors is crucial for understanding the growth and survival of many marine species. Different life stages may occupy substantially different physical environments. For example, eggs may be laid in a near-bottom, near-coastal environment, while larvae develop near the surface in shallow continental shelf waters, and juvenile and adult years are spent in the deeper ocean. Even for marine species with no appreciable horizontal transport, systematic vertical migration through light, temperature and prey concentration gradients may play a significant role in determining growth and survival. Movements of individuals may be due purely to physical forcing, for example in the passive early life stages, or to active responses to the biotic or abiotic environment, for example in later life stages which are capable of controlling their position.

Spatial variability in circulation and environmental conditions which causes differential gowth and mortality among individual young fish may be important to overall levels of recruitment. For many marine fish species with planktonic early life stages, mesoscale

and larger circulation features may influence the success of a year class (Incze et al. 1990, Kendall and Nakatani 1992, Schumacher et al. 1993, Bograd et al. 1994), especially in regions with strong and variable currents. Circulation factors may act directly, through transport of early life stages to appropriate nursery areas, or indirectly, by mediating encounters of young fish with prey and predators. In regions with complex horizontal current patterns, the trajectories of individual fish may differ widely, causing individual histories of exposure to environmental variables (such as temperature, salinity, predators and prey) also to differ. This may lead to variability in growth or the probability of survival among individuals.

Historically, ecological models intended to predict mean population properties which vary in space have done so through the use of a spatially fixed (Eulerian) numerical grid. While straightforward stochastic methods may allow for random influences of a fluctuating environment (Nisbet and Gurney 1982), they cannot easily deal with systematic changes in the environment which result from an individual's advection or migration into new habitats over the course of its lifetime. Models involving heterogeneous spatial effects are generally analytically intractable, and necessitate the use of numerical simulation (DeAngelis and Rose 1992). The inclusion of spatial variability in IBM's is relatively recent (Tyler and Rose 1994, Werner et al. 1993, 1996). Thus far, most individual-based models do not include spatial tracking, that is, they include no information about where the individuals exist in their environment as they grow and develop. Those that are spatially explicit have tended to have little biological detail (Neill 1979, Bartsch et al. 1989, Walters et al. 1992, Tyler and Rose 1994).

Spatially explicit biological models may be constructed using either Eulerian or Lagrangian frames of reference, a distinction drawn by other plankton modelers (e.g. Lande and Lewis, 1989). An Eulerian biophysical model is here defined as one which follows the evolution of some quantity at discrete, fixed physical locations. Typically these locations are the fixed grid points used by a numerical model, although analytical solutions throughout the domain are sometimes possible for simple Eulerian models. Changes

in any quantity are due not only to local biological processes, but also to advective and diffusive exchange with adjacent locations, e.g.:

$$\frac{d}{dt}B(\underline{x}, t) = -\underline{u}(\underline{x}, t) \bullet \nabla B(\underline{x}, t) + \nabla \bullet (\underline{k} \nabla B(\underline{x}, t)) + f_E(B, \underline{x}, t) \qquad \text{(EQ 1.1)}$$

Here, B represents the modeled quantity, $\underline{u} = (u,v,w)$ is the fluid velocity, ∇ is the gradient operator, $\underline{k}$ represents horizontal and vertical eddy diffusion coefficients, $\underline{x} = (x,y,z)$ is the spatial location, t is time, and f_E represents changes due to biological processes (birth, growth, death, etc.) at a fixed location. This can be expressed verbally as

Local rate of change = advective change + diffusive change + nonconservative biological change

Note that f_E is a function of space and time, and may be either deterministic or probabilistic. This Eulerian biological model, with f_E deterministic, is the form typically used by the oceanographic community for NPZ (nutrient, phytoplankton,zooplankton) dynamics (e.g. Jamart et al. 1977, Jamart et al. 1979, Frost 1987, 1993, Wroblewski 1977, Lewis et al. 1994, Moisan and Hofmann 1996a, Moisan et al. 1996, Frank and Walstad 1997).

In the hydrodynamic literature, a Lagrangian reference frame is one which moves with a discrete parcel of fluid. By extension, we may define a Lagrangian biological model as one which follows an individual organism or group of organisms moving through space as it is advected by the ambient currents. Mathematically, we represent changes following an individual (or group) i as:

$$\frac{dB_i}{dt} = f_L(B_i(t), \underline{x}_i(t), t) \qquad \text{(EQ 1.2)}$$

where,

$$\underline{x}_i(t) = \int_0^t \underline{u}_i(\underline{x}_i(t))dt \qquad \text{(EQ 1.3)}$$

Here, $B_i(t)$ represents some property of the individual (or group) at time t, $\underline{x}_i(t) = (x_i(t),y_i(t),z_i(t))$ represents the spatial path through time, and f_L represents any nonconservative changes due to biological processes. Such changes may include processes based on past history. The quantity $\underline{u}_i$ represents each component of the fluid velocity $\underline{u}$ plus any directed motions, such as vertical migration due to buoyancy or locomotion. Note the potentially "individual-based" nature of the Lagrangian model, though in fact such models need not be IBMs per se. Examples of Larangian models which are not individual-based include those of Flierl and Davis (1993), Botsford et al. (1994), and Moisan and Hofmann (1996b).

When a conservative (or linearly decaying) substance is being tracked ($f_E=f_L=0$), the density of "individuals" represents the concentration of the substance. In that case, the Lagrangian and the Eulerian approaches are mathematically equivalent. The Lagrangian approach is often found to yield better resolution of strong gradients (fronts and streaks) of concentration, due to spurious diffusion introduced by numerical techniques used to solve the Eulerian equations.

Conversely, the Eulerian approach is more useful when broad spatial coverage is required (i.e. relatively uniform concentration over a wide area). Some pollutant dispersal models use the Lagrangian approach in the initial stages of dispersion from a point source, then extrapolate particle densities onto an Eulerian grid to model the later stages of dispersion (Dimou and Adams, 1992).

A Lagrangian approach (e.g. an IBM which tracks positions) is especially preferable to the Eulerian approach when past history influences present response to the environment. This is the case when individual fish move around through the physical environment, and we need to keep track of how their history of movement and exposure to physical vari-

ables affects their present situation. However, as in pollutant dispersal models, Lagrangian IBMs may require huge numbers of individuals to ensure adequate spatial coverage of the modeled population in its domain. The problem is especially acute when mortality is high and dispersion is rapid. In these situations, some way must be found of reseeding the population to make up for lost individuals. Even with such reseeding, there may be a steady loss of fine-scale information about the concentration field of remaining individuals. Rose et al. (1993) and Scheffer et al.(1995) have explored ways of reseeding lost individuals in spatially aggregated, high-mortality situations through random sampling of the current surviving population.

There are practical and theoretical limits to both physical and biological simulations. First, we cannot resolve all scales of motion in the modelled fluid, no matter how fine the resolution of the numerical model. Second, we have limited access to physical or biological data for initialization of such a model, or for assimilation into the model as it runs. In general, the best we can presently achieve is a physical model which captures the broad features of the mean circulation, while yielding variability (e.g. meanders and eddies) which matches the character of the true field in some statistical sense. For example, we cannot hope to produce eddies at precisely the observed locations and times, but we can reasonably expect the model to produce approximately the same number of eddies as are observed per year, in the same general location as observed. In a similar fashion, we seek to model individuals whose statistics are representative of the true population, without necessarily replicating the precise life history of any single individual.

This biophysical modeling effort focuses on walleye pollock, *Theragra chalcogramma* in the western Gulf of Alaska. Walleye pollock forms the basis for one of the worlds largest single-species fisheries with catches in the Bering Sea and the Gulf of Alaska exceeding 1 million metric tons per year (Kinoshita et al. 1995). A large stock of pollock spawns in Shelikof Strait in the western Gulf of Alaska every year. This stock reached peak abundances in the mid- to late 1970's and the early 1980's. Since 1989, catches have been restricted due to reduced population size (Hollowed et al. 1993). There were few strong

year classes in mid and late 1980's but moderately good years in 1984, 1985 and 1988; and especially poor years in 1982, 1986, 1987 and 1989-91. A time series of recruitment since 1962 shows that year classes in the late 1970's were unusually strong (Megrey et al. 1995), and that variability in recruitment of this stock is large (Fig. 1.1). For this reason, and due to its commercial importance (as well as the relative tractability of field studies), this species was chosen for study in the Fisheries Oceanography Coordinated Investigations (FOCI) of the National Oceanic and Atmospheric Administration (NOAA), which began in 1984. The primary goal of this program has been to examine the abiotic and biotic factors that influence the recruitment of pollock. Biological processes such as starvation, predation, transport, feeding and growth, and the physical factors (such as climate, atmosphere and ocean circulation) that affect them have been studied (Kendall et al. 1996).

As described in Kendall et al. (1996), adult pollock spawn at depths of 150-250m in late March and early April at the western end of Shelikof Strait between Kodiak Island and mainland Alaska (Fig. 1.2). The spawning region and time, and the distribution of eggs varies little among years (Kendall and Picquelle 1990). A large patch of eggs is formed due to the aggregated nature and the short duration of spawning, as well as the lack of strong currents at the depths of spawning (Kendall et al. 1996). Larvae hatch at about 4.5 mm standard length (SL) (Bailey and Stehr 1986) after a period of about 2 weeks. These larvae quickly rise to the upper 50 m of the water column and drift in the prevailing currents, generally to the southwest, for the next several weeks (late April to mid-May). Larger larvae (greater than 6.0 mm SL) undergo diel migrations between 15 and 50 m, in which they are deepest during the day and shallowest at night (Kendall et al. 1994). Currents may carry the larvae south-westward along the Alaska Peninsula, or offshore along the shoreward edge of the Shelikof sea valley southwest of Shelikof Strait. Although the transport of early life stages is dominated by advection, there exists a high degree of horizontal and vertical variability of the currents in time and space, and the occurrence of mesoscale eddies, convergence zones, plumes and a deep counterflow are thought to affect the growth and survival of young pollock.

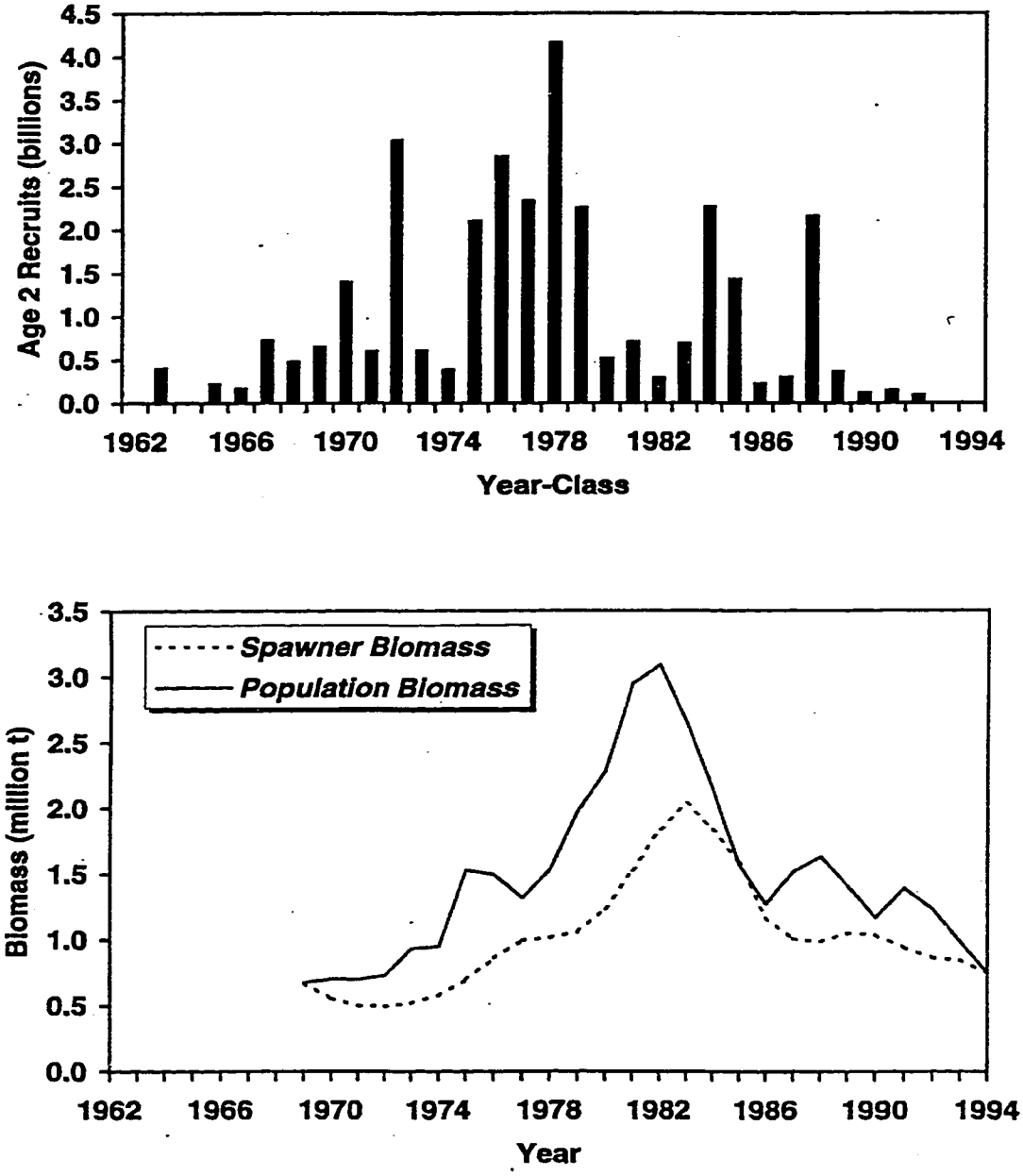

Figure 1.1. Time series of age-2 walleye pollock recruitment (top panel) and spawner and population biomass (bottom panel) derived from application of fisheries-dependent and fishing-independent data to a stock asssessment model. Figure from Megrey et al. (1996).

Considerable interannual variation exists in the distribution and abundance of larvae by late May (Incze et al. 1989, Kendall and Picquelle 1990, Hermann et al. 1996b). The main prey of larvae consists of the naupliar stages of copepods, the size range of which increases as larvae grow (Kendall et al. 1987). Variability in the timing and magnitude of prey production, and in the overlap of larvae and prey may affect the growth and survival of larvae (Incze et al. 1989, Incze and Ainaire 1994, Bailey et al. 1996a). The abundance of prey has been found to affect the nutritional condition of larvae (Theilacker et al. 1996). It appears that larvae may be vulnerable to starvation during the first two weeks after first feeding. Larvae become juveniles at about 25 mm SL, several months after hatch. By mid-summer, many of the surviving juveniles have been advected to nursery grounds near the Shumagin Islands, ~350 km to the south-west of the spawning site (Fig 1.3) (Hinckley et al. 1991, Wilson et al. 1996). Although juveniles are seen in some years in bays around Kodiak Island, the Shumagin Islands region most consistently contains large numbers of juveniles (Spring and Bailey 1991, Walters et al. 1985).

Year class strength in this species is thought to be set within the first few months of life (Bailey and Spring 1992), however the particular life stage at which recruitment appears to be determined varies among years. Although a large number of fish surviving the larval stage doesn't necessarily mean a good year class, ie. events occurring during the juvenile stage may significantly affect recruitment, a large number of larval survivors is necessary to produce a good year class (Bailey and Spring 1992).

The circulation in the western Gulf of Alaska is dominated by two current systems (Fig. 1.4). The Alaskan Stream follows the continental slope over deep water (Reed 1984, Musgrave et al. 1992). The Alaska Coastal Current (ACC) follows the Alaska coast and flows through Shelikof Strait (Royer 1981, Schumacher et al. 1989, Stabeno et al. 1995b). The ACC extends for 1500 km along the coast and is one of the strongest coastal currents in the world, with speeds between 25 and 100 cm s^{-1} (Stabeno et al. 1995b). The ACC is forced primarily by winds and fresh water runoff. Observed mean volume transport through Shelikof Strait is 0.85 x 10^6 m^3s^{-1}, with wind-forced pulses of greater than 3.0 x

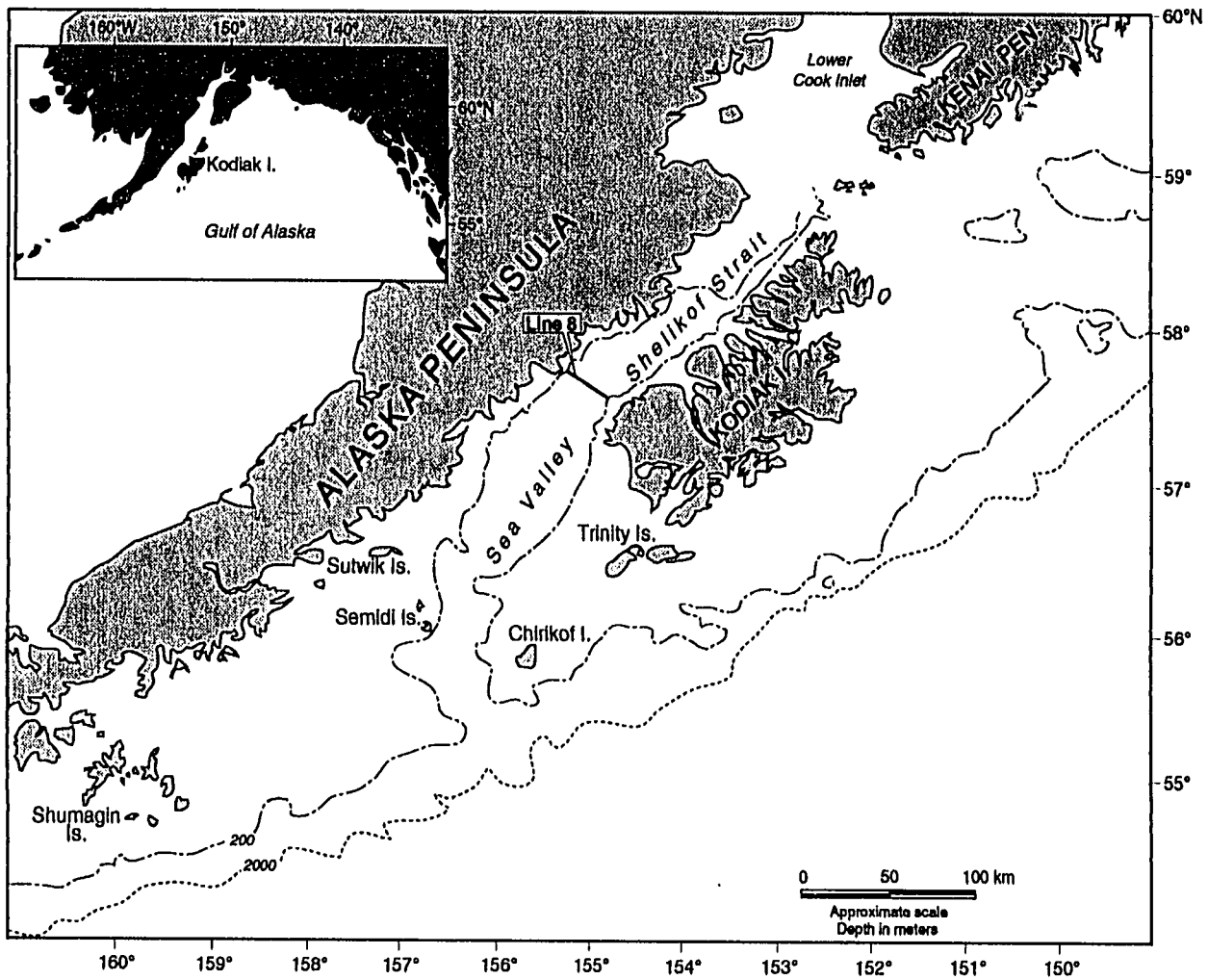

Figure 1.2. Location of the study area with place names and bathymetry (in fathoms); 1 fathom = 1.83 m). The insert indicates the typical upper-ocean circulation.

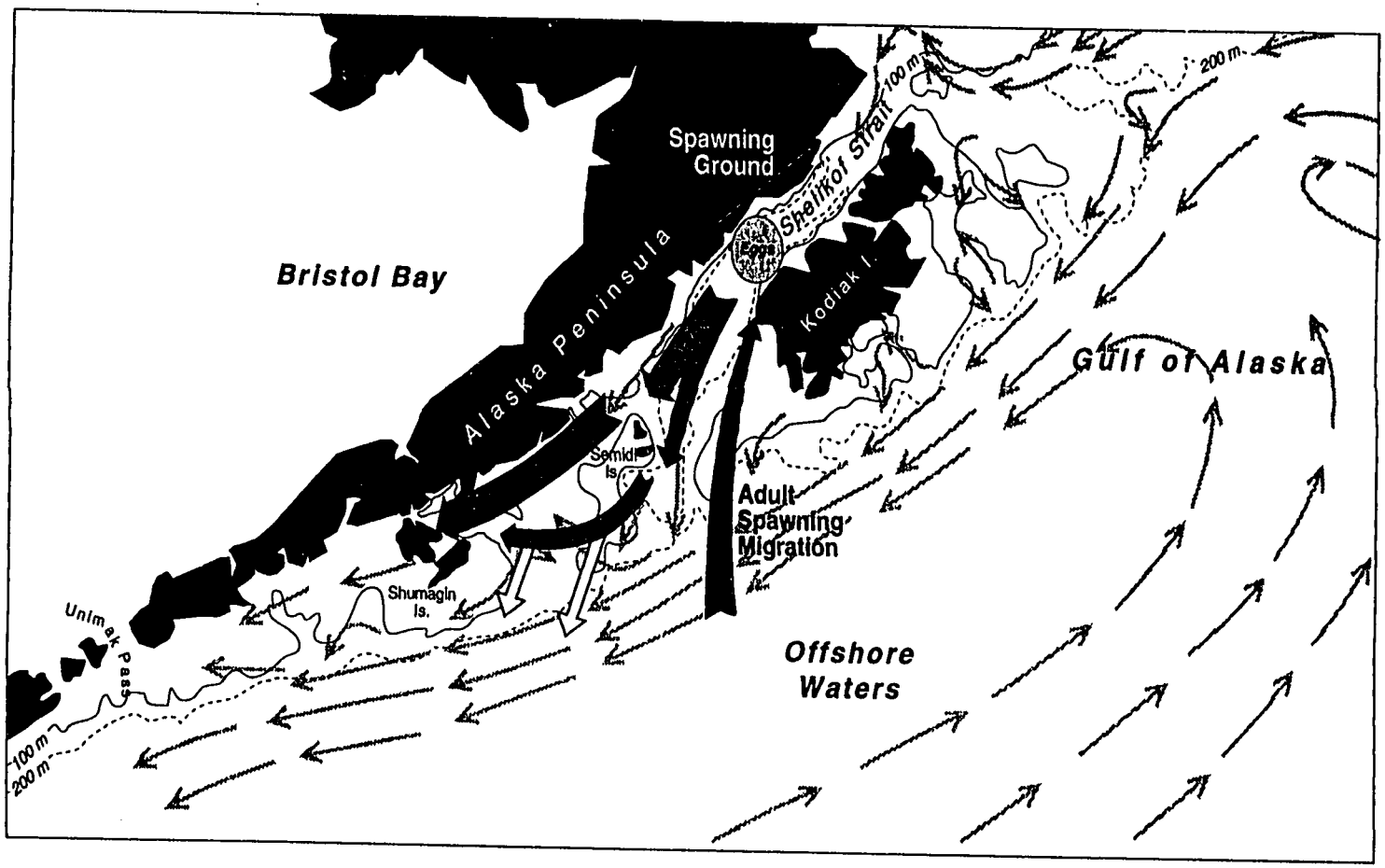

Figure 1.3. Conceptual life history of Gulf of Alaska walleye pollock showing the spawning area in Shelikof Strait, the downstream movement of eggs, larvae and juveniles, and the return migration of spawning adults.

10^6 m^3s^{-1} (Schumacher et al. 1989, Stabeno et al. 1995b). The maximum of the relative volume transport (> 1 x $10^6 m^3 s^{-1}$) is associated with the accumulation of freshwater in autumn, however the greatest monthly transports occurred in the winter, associated with wind-driven perturbations (Schumacher et al. 1989). Flow shoreward of the ACC in Shelikof Strait is relatively weak, stagnating near Sutwik Island. Current speeds between the Semidi Islands and the Shumagin Islands are also sluggish, averaging less than 10 cm s^{-1}. There is a high degree of vertical and horizontal variability in the currents over time at many different time scales. We are especially interested in variability over the time scales critical to young pollock, ie. those occurring over periods of days to months (Incze et al., 1989, Kendall et al., 1996, Vastano et al. 1992, Napp et al. 1996).

In the attempt to understand recruitment of pollock in the western Gulf of Alaska, several hypotheses have been developed. The initial hypothesis has been that the best survival and subsequent recruitment occurs when young pollock are transported along the coast of the Alaska Peninsula, rather than offshore into the Gulf of Alaska. Part of the water flowing through Shelikof Strait flows along the Alaska Peninsula towards the Shumagin Islands, and the rest flows down the sea valley into the Gulf of Alaska. There is interannual variability in the amount of water going along the Peninsula versus offshore. Of the water which heads offshore, some returns to the continental shelf, and some is entrained by the Alaskan Stream.

Larvae which are advected out of the sea valley into the Gulf of Alaska and into the Alaskan Stream are thought to starve or be lost to the population. Larvae which are initially advected out of the sea valley may be returned to the shelf and recruit to the juvenile nursery areas around the Shumagin Islands. Conditions for growth and survival are thought to be better in the more productive coastal waters. For these reasons, the process of advection from spawning areas to nursery areas, or conversely, out of the region altogether, must be examined.

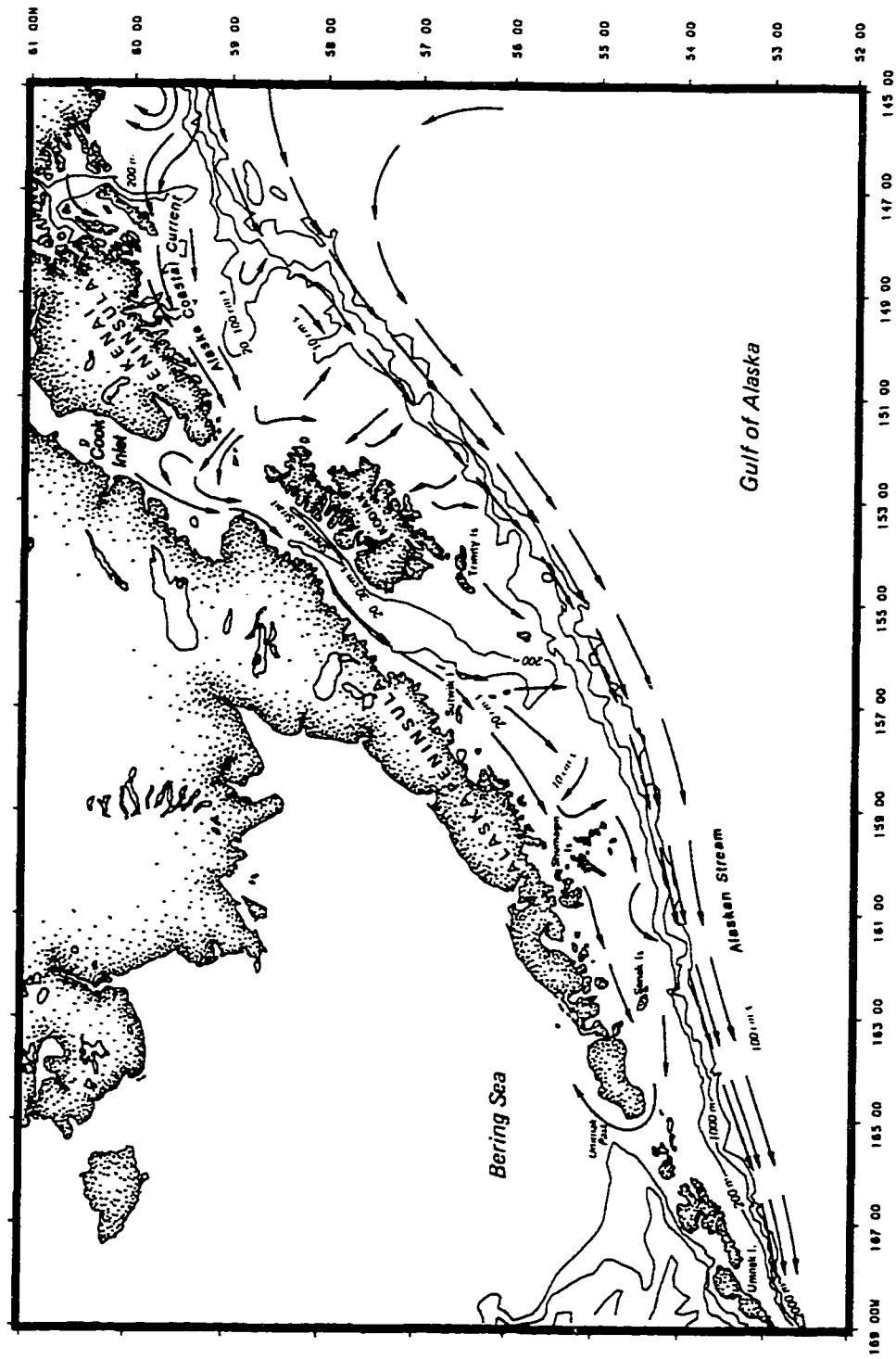

Figure 1.4. Gulf of Alaska, showing the major current systems.

The timing and location of spawning are integral components of the adaptation of marine fish life cycles to their environments. Maintenance of a population is dependent on successful recruitment of young fish to juvenile nursery areas and from nursery areas back to the parent populations. This is facilitated by the choice of spawning time and location, as these are likely to optimize either the transport of planktonic early life stages to the juvenile nursery areas, or the conditions experienced by the young fish along the way, or both. In highly advective systems, this location and timing may be chosen based on the necessity to avoid excessive transport (ie. that which carries them past or away from the nursery areas) and the need for retention in areas conducive to survival.

In Shelikof Strait, walleye pollock are known to spawn in a limited region at predictable times (Kendall et al. 1987, Schumacher and Kendall 1991). Although eggs and larvae deriving from the Shelikof Strait spawning aggregation drift generally to the southwest, it does not appear that drift continues indefinitely. Surface currents of only 10 cm s^{-1} could transport larvae as much as 1200 to 1800 km downstream and out of the Gulf before they become large enough to resist the flow (Strickland and Sibley 1989). The nursery area in the Shumagin Islands is only 350-400 km downstream of the spawning location in Shelikof Strait. Currents in the ACC range from 25 to 100 cm s^{-1} (Stabeno et al. 1995b). Some mechanisms must therefore exist to prevent loss of eggs and larvae.

Several retention mechanisms have been proposed. One is alongshore or onshore transport. About 25% of the water in the ACC flows along the Alaska Peninsula after it leaves the Strait (Fig. 1.5). Current speeds in the nearshore area, especially to the west of the Semidi Islands , are slow, averaging less than 10 cm s^{-1}. The other 75% of the ACC water heads offshore, although part of this water does return to coastal areas (Schumacher et al. 1989). If larvae were to remain in the ACC water which stays along the coast, or in that which eventually returns to coastal waters, they would most likely be transported to the Shumagin Islands region.

The flow through Shelikof Strait usually contains a high degree of mesoscale variability (Fig. 1.6). Some of this variability may aid in retention. For example, pollock larvae have been observed in higher concentrations is mesoscale eddies (Schumacher et al. 1993, Bailey et al.1995), and some observations suggest that feeding and survival conditions may be better in these eddies (Canino et al. 1991). It has been proposed (Stabeno et al. 1996) that as many as half of the eggs spawned in Shelikof may end up in eddies for some portion of their early life. It has also been hypothesized that retention in eddies, which generally translate downstream at slower rates than the mean currents (Bograd et al. 1994), aids in delivering larvae to the juvenile nursery areas. Meanders and areas of weaker flow or reversal of flow (for example due to wind events) may also aid in retention. In years such as 1991, when high winds and runoff forced extremely strong currents with little mesoscale variability through Shelikof Strait, larvae appear to be carried out into offshore areas and into the Alaskan Stream (Bailey et al. 1995).

Although an important nursery area for juvenile pollock is located around the Shumagin Islands, large numbers of juveniles are found in some years in bays and coastal areas around Kodiak Island (Spring and Bailey 1991). The source of these juveniles is not clear, although Smith et al. (1984) concluded that it was unlikely that they originated in Shelikof Strait.

The majority of surveys done for eggs and spawning adults indicate that Shelikof Strait is the most important pollock spawning region in the western Gulf of Alaska. Alton and Deriso (1983) found no evidence for any major spawning aggregation east of Kodiak Island, nor did Kendall et al. (1987). There is some debate, however, about the relationship of small amounts of spawning fish seen in other times and areas to the Shelikof stock. It is not clear whether pollock in the Gulf of Alaska constitute a single stock, dominated by the spawning aggregation in Shelikof Strait, or whether separate spawning stocks exist. Although smaller spawning aggregations have been observed at different times of the year in other parts of the Gulf of Alaska, such as near Chirikof Island and the Shumagin Islands, the importance of these spawning aggregations to the overall stock biomass in the

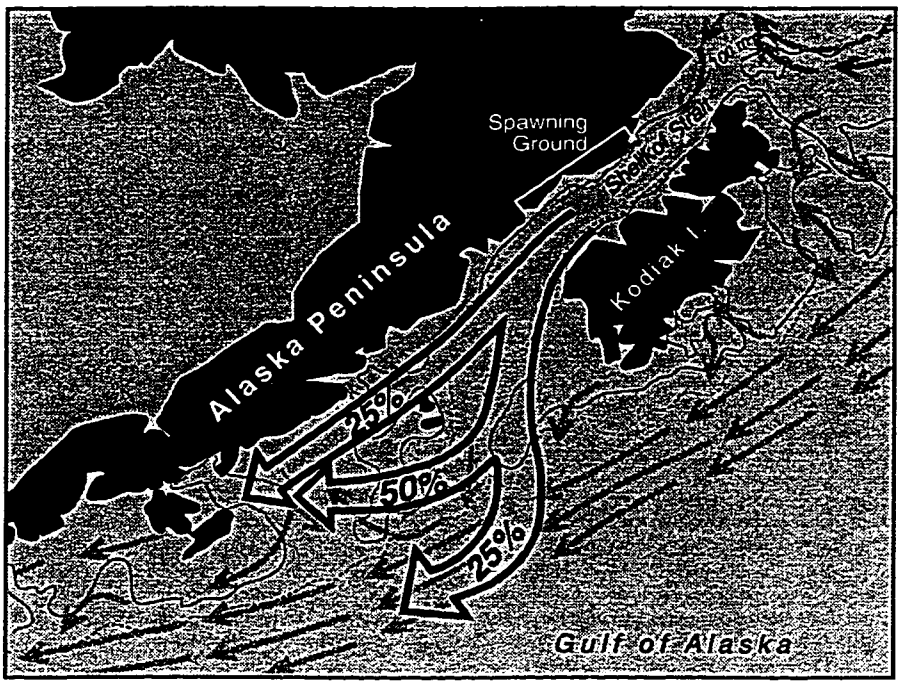

Figure 1.5. Approximately 75% of the Alaska Coastal Current (ACC) water flowing through Shelikof Strait in 1987 stayed in coastal areas near the Alaska Peninsula, and 25% moved offshore to join waters of the Alaskan Stream.

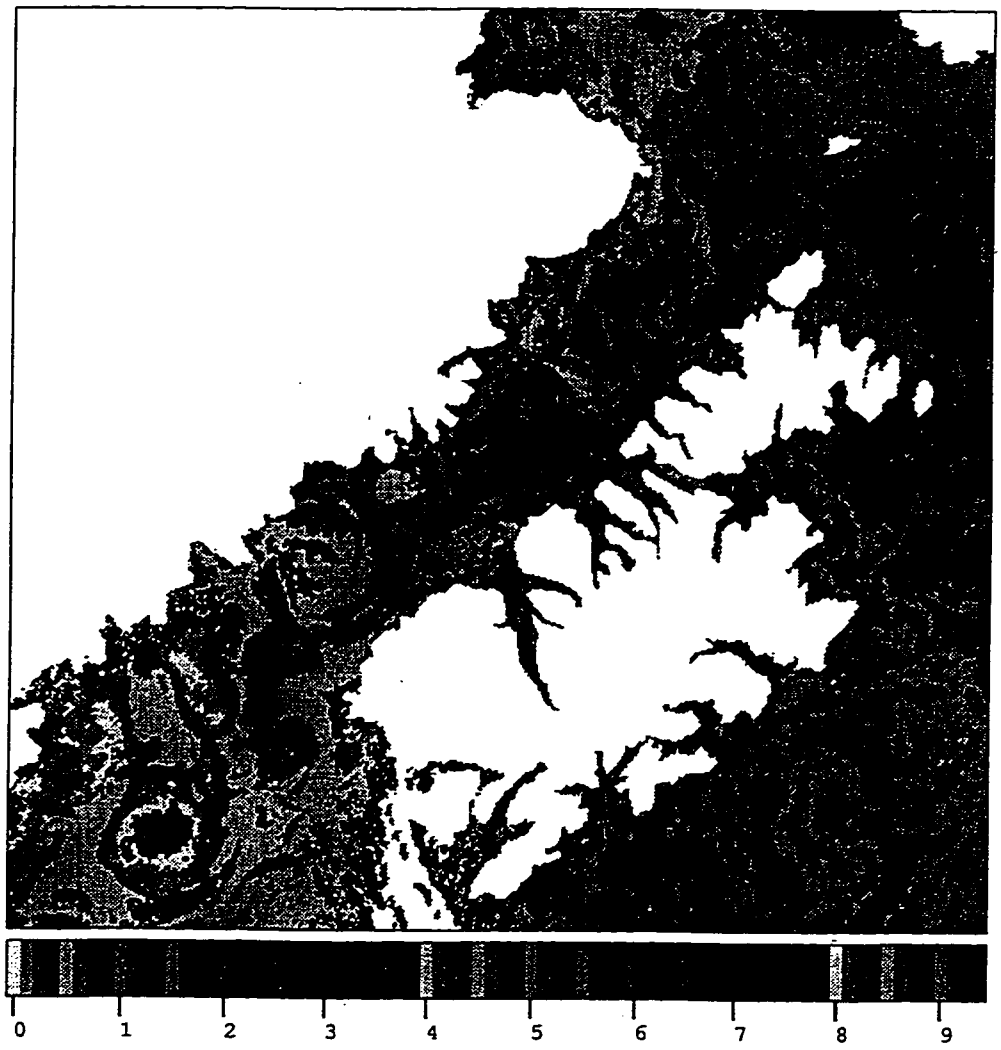

Figure 1.6. Sea surface temperature (°C) as measured by AVHRR in the vicinity of Shelikof Strait on 11 May, 1987, indicating mesoscale features of the circulation. Figure from Hermann and Stabeno (1996).

Gulf is unclear. Nor is it clear where the juvenile nursery areas for these spawning groups are located.

During the course of the FOCI studies, several observations have emerged which are thought to reflect processes significantly affecting the survival and growth of early life stages of pollock during their transport to the juvenile nursery areas. As mentioned earlier, higher abundances of larvae and their prey are often found in association with mesoscale eddies (Fig. 1.7), with associate higher growth rates for early larvae (as evidenced by RNA/DNA ratios, Canino et al. 1991). This has led to the hypothesis that entrainment and retention of larvae in eddies may positively affect growth, survival and transport to suitable nursery areas. This may be (1) because eddies may cause enhanced advection to juvenile nursery areas around the Shumagin Islands instead of offshore into the Alaskan Stream, (possibly by translating to the southwest more slowly than the mean current, or by delivering larval to coastal areas where transport to the Shumagin Islands is more likely); (2) because eddies may retain larvae in the lower Shelikof Strait area where prey availability is higher, instead of moving them too early to the relatively prey-depauperate areas just west of the Semidi Islands (Incze et al. 1997, Napp et al. 1996); (3) because prey levels are sometimes seen to be higher in eddies (due to entrainment or in situ production) causing higher larval growth rates; or (4) because eddies may be less affected by wind stress, ie. storm-induced mixing events (which may negatively affect larval feeding rates, Bailey and Macklin 1994) due to stronger stratification in some eddies. The hypothesis that eddies positively affect larval growth, survival or transport also implies that a significant portion of the larvae are entrained into eddies, that prey in eddies does not become depleted over the life-span of the eddy, and that predators do not accumulate in eddies (or if they do, that the increased growth rates of larvae due to higher prey levels causes a decrease in predation due to the increase in larval size which may overcome the effect of an increased population of predators). Megrey et al. (1995) also found that there is a high correlation between recruitment strength of pollock in the Gulf of Alaska and the amount of fresh water input to the system in the first year of life. The input of freshwater is strongly related to the number of eddies produced, as increased freshwater input increases

the density gradient between water types in Shelikof Strait, supporting baroclinic instabilities which lead to more eddies. Eddies occur most frequently in the spring (March - May) and fall, with the fall peak more pronounced than the spring peak.

Another important observation (Bailey and Macklin 1994) from first-feeding distributions derived from otolith analysis, is that there is higher survival of larvae through the first-feeding period if winds are calm at that time. Periods of higher than average winds are correlated with low survival of larvae through first-feeding. Megrey et al.'s (1995) analysis also indicated a high correlation between recruitment strength and the North-East Pacific Pressure Index (NEPPI), an index related to transport through Shelikof Strait (Roach and Schumacher 1991) and to storminess in the western Gulf of Alaska. NEPPI is a scalar index of the large scale, sea-level pressure gradient between Reno, Nevada, and the area south of Amukta Pass in the Aleutian Islands. This index tracks the intensity and location of the Aleutian Low, which dominates the variability of the atmospheric circulation in the Gulf of Alaska, as well as strongly affecting oceanographic circulation (Neibauer 1988). Mantua et al. (1997) state that interdecadal variations in the dominant pattern of North Pacific sea level pressure have closely paralleled those seen in North Pacific sea surface temperature, an indicator of what is now termed the Pacific Decadal Oscillation. The Pacific Decadal Oscillation, describing climate changes in the Pacific over periods of decades, as described by Mantua et al. (1997) and others, has implications for coastal circulation in the Gulf of Alaska. When the Pacific Decadal Oscillation is in its positive polarity, indicating warmer sea surface temperatures and intensification of the Aleutian Low, the coastal areas experience enhanced cyclonic flow of warm, moist air, indicating higher levels of precipitation.

There are several possible mechanisms by which wind-induced turbulence may affect larval growth and survival. Storms may dilute patches of prey, or retard stratification of the water column thereby reducing or delaying production of prey, negatively affecting growth and survival rates. Larvae may avoid turbulence by going deeper in the water column (Olla and Davis 1990, Kendall et al. 1994), where prey are in lower abundance.

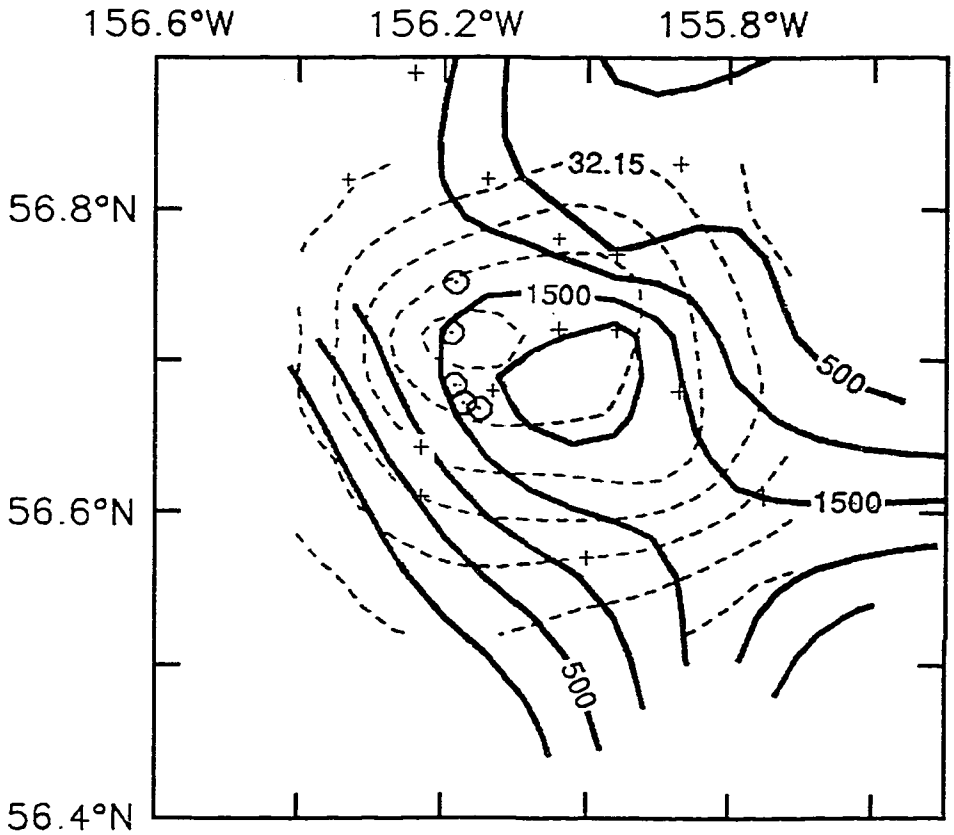

Figure 1.7. Contours of salinity (dotted lines) in a counterclockwise rotating eddy, overlaid by densities of larval pollock (no. m^{-2}, solid lines). Figure from Schumacher et al. (1993).

Changes in turbulent energy due to wind stress may affect the consumption rates of larvae, by altering encounter rates or the probability that the larva will successfully capture its prey. At low rates of turbulence, consumption may increase due to increased encounter rates (Rothschild and Osborn 1988). At high rates of turbulence, decreased consumption may result from decreased rates of capture of prey by larvae (MacKenzie et al. 1994, MacKenzie and Kiørboe 1995). These effects of turbulence may also affect mortality by affecting the consumption rates of predators on larvae, however this has not been examined. Changes in wind stress may also affect mesoscale circulation or advection in ways that affect larval growth, survival or transport by affecting retention in eddies or advection to the juvenile nursery areas.

1.2 Objectives

A spatially explicit biophysical model has been developed which describes the dynamics of survival and growth of the early life stages of walleye pollock. We have used this model to examine hypotheses about survival and growth of young walleye pollock, and their implications for recruitment. This biophysical model consists of three components: a three-dimensional hydrodynamics model (SPEM), an individual-based model of the early life stages of pollock, and a nutrient-phytoplankton-zooplankton (NPZ) model which provides a spatially and temporally explicit food supply for larval pollock.

The hydrodynamic model is capable of reproducing mesoscale and larger circulation features, of advecting individuals through space in a reasonably accurate manner using daily velocity fields along with self-directed vertical movements appropriate to each life stage, and of providing spatial distributions of important physical factors such as temperature and salinity. The Lagrangian biological IBM follows individuals from spawning through the fall of the 0-age juvenile year, modeling each individual's interactions with the biotic and abiotic environment and preserving each individual's unique trajectory through space, while recording important characteristics such as length, weight, stage, etc. as these change. The Eulerian NPZ model, run over a subset of the larger SPEM grid, contains a

stage-structured representation of the zooplankton species which is the major food source of larval pollock, and allows for examination of the overlap of larvae with the correct sizes of prey.

Research such as that of Megrey et al. (1995) and Bailey and Macklin (1994) have correlated aspects of the physical environment with survival or recruitment. These aspects, as mentioned earlier, include a negative relationship of survival through the first feeding larval stage with wind mixing, a positive relationship of recruitment with the input of fresh water (and therefore the creation of eddies), a negative relationship of recruitment with wind mixing at specific locations in spring months and with the NEPPI Index, which correlates to volume transport through Shelikof Strait. As stated by Megrey et al. (1995), however, we know little about the specific mechanisms that underlie these correlations. How do eddies and wind mixing affect larvae? How do changes in transport affect young pollock?

We use this model to examine possible mechanisms underlying some of the hypotheses that have been proposed as controlling the survival and growth of pollock through the early life stages and their delivery to appropriate nursery areas. This work allows us to test our knowledge of the system, and perhaps point out areas which would be benefited by further study.

Hypotheses

Much of our work with this model to date has focused on examination of the mechanisms and implications of the process of advection between spawning and nursery areas, and how this process is influenced by physical forcing, the presence of eddies, and features of the wind field. The specific hypotheses addressed by the present work include:

(1) The survival of early life stages of walleye pollock is enhanced by transport along the Alaska Peninsula. Larvae which are advected out of the sea valley into the Gulf of Alaska and are entrained in the Alaskan Stream are lost to the population. Larvae which are initially advected out of the sea valley may be returned to the shelf and eventually recruit to

the juvenile nursery areas around the Shumagin Islands. Recruitment to the juvenile nursery area (and thereby, by implication, to the year class) is enhanced when there is a low percentage of flow which goes offshore and joins the Alaskan Stream.

(2) The choice of spawning time and location of adult walleye pollock in the western Gulf of Alaska is controlled mainly by the necessity to optimize transport of eggs and larvae to the juvenile nursery areas, versus the necessity to optimize conditions of feeding, growth and survival along the way.

(3) Entrainment of eggs and larvae in mesoscale eddies in Shelikof Strait enhances advection to appropriate juvenile nursery areas around the Shumagin Islands, and aids in larval growth and survival by retaining larvae in areas of higher prey.

(4) The depth of an individual, which varies by life stage and time, is an important life history trait which strongly affects their chance of survival.

Data from the FOCI program on various aspects of the early life stages of pollock in the western Gulf of Alaska are used to compare against model results. These include surveys for the abundance and distribution of the egg, larval and juvenile life stages, and measurements of survival and growth of larval and juvenile stages. Data on the abundance and distributions phytoplankton chlorophyll-a and of the main prey sources of larval pollock, also collected by the FOCI program have also been used. These data have been collected every year since 1985.

First, we deal with some of the issues raised during the process of model development, such as those concerned with the effect of added spatial complexity. We test the effect on larval growth of adding a realistic Lagrangian time series of temperature over simplistic (nonspatial) ways of dealing with temperature to a simplified version of the IBM. We also test the effect of the addition of realistic representations of vertical location and migration on the horizontal advection of individuals, by examining the difference in individual trajectories through space.

Next, we show how the IBM performs in hindcasting the spatial distributions of various life stages over the first six months of life (April-September) for different years (1978, 1987, 1988, 1989, 1991 and 1994), and whether the modeled transport between spawning and nursery areas is realistic. We also compare the modeled growth rates to those derived from FOCI data on larval and juvenile growth from otolith analyses. Modeled primary production and populations of pollock prey are described and compared to data on the distributions and abundances of phytoplankton chlorophyll-a and various life stages of *Pseudocalanus*,spp. the major food item of larval pollock in this region.

The advection of young pollock between the spawning area and the nursery area is examined in some detail. We have used the coupled model to examine the question of whether the stability in timing and spatial location of spawning in Shelikof Strait pollock is primarily an adaptive strategy to optimize transport to the nursery area, or to conditions of growth and survival along the way. Interannual comparisons in transport are made, with examination of how these are forced by different physical scenarios of wind and freshwater runoff which drive the circulation model. The possible consequences of these interannual differences to recruitment are considered. We also look at smaller scale patterns in modeled distributions and growth, such as the patchiness of different life stages, retention in eddies, effects of different wind and eddy patterns on growth, and how turbulence in the larval stage can affect population attributes.

Finally, we examine one hypothesis of how wind-induced turbulence affects larval fish consumption rates and integrative parameters such as growth by performing a sensitivity analysis of this mechanism. We end with a discussion of the utility of complex spatially and temporally dynamic biophysical models for studies of recruitment processes, and what this modeling effort has taught us about the Shelikof Strait population of pollock.

Chapter 2. The Models and Simulation Experiments

2.1 The Physical Model

The hydrodynamic model used in this biophysical modeling effort (described fully in Hermann and Stabeno 1996) is a three-dimensional, prognostic, rigid-lid, eddy-resolving model of velocity and salinity fields in the northern Gulf of Alaska. The model domain encompasses the northern Gulf of Alaska, from east of Shelikof Strait to west of the Shumagin Islands (Fig. 2.1). The model solves the hydrostatic, primitive hydrodynamic equations, with wind forcing distributed over the top 20 m of the water column, and buoyancy forcing (due to runoff) along the coastline of Alaska. The hydrodynamic model is forced by winds and fresh-water runoff. The wind field used to force the model is time-variable (12-hourly), and derived from Fleet Numerical Oceanographic Center modeled geostrophic winds. A monthly runoff time series is used. Runoff forcing the model is a line source along the coastline of the Gulf of Alaska, for the modelled period. The model code is based on the Semispectral Primitive Equation Model (SPEM) of Haidvogel et al. (1991) modified for this region. The model employs a curvilinear-orthogonal horizontal coordinate system which follows the irregular coastline. Mean grid spacing in the area between Kodiak and the Shumagin Islands is 4 km. Beyond this region, the grid is expanded to broader spacing, to allow for a large recirculation region. The vertical dimension is treated using a depth-following ('sigma') coordinate system, with nine vertical levels.

Currents generated by the model have been compared with those measured by moored current meters and satellite-tracked drifting buoys (Stabeno and Hermann 1996). The model reproduces dominant circulation features including the Alaska Coastal Current and the Alaskan Stream, with appropriate cross-shelf structure, vertical shear, and mean transport. Floats tracked at 40 m (the depth of mean larval pollock abundance) using filtered model velocity fields compared favorably with observed drifter tracks at that depth (Sta-

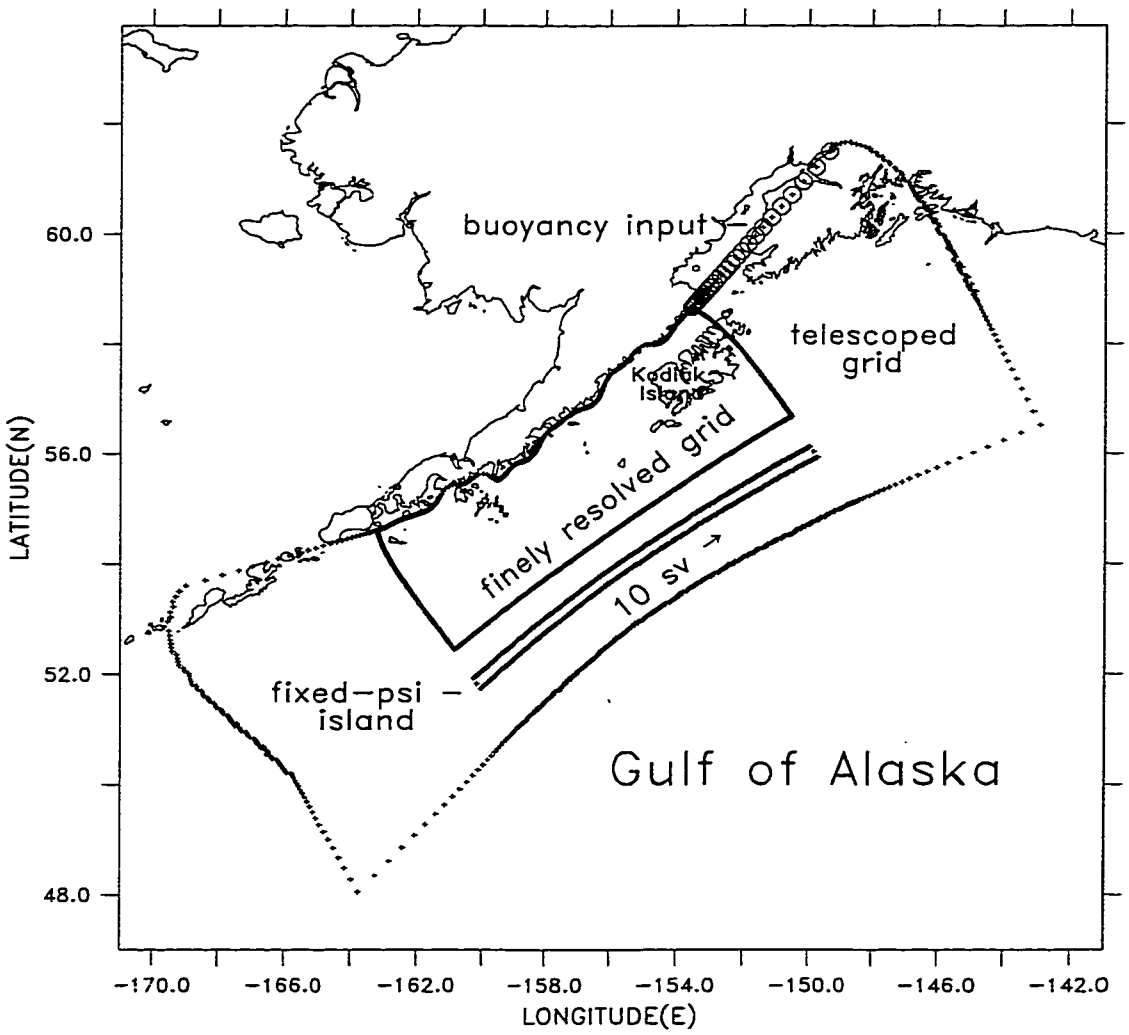

Figure 2.1. Boundary of the SPEM model grid, shown with the true coastline of Alaska. Note telescoping of the grid at the southeastern, northeastern, and southwestern edges of the finely resolved domain. The "island" of fixed stream function is also shown; barotropic flow is specified at 10 Sv around this island. Circled grid points indicate locations of buoyancy input.

beno and Hermann 1996, Fig. 11). Discrepancies between the model and data were generally due to the formation of mesoscale eddies in the model at different times than those observed, although eddy statistics (e.g. rate of eddy formation, location) were similar for both.

For the longer (through September) simulations, additions to the model described in Stabeno and Hermann (1996) were made. Mean vertical profiles of salinity and temperature for March and October were obtained from the data of Reed et al. (1987). These profiles were linearly interpolated in time, to provide a climatological background for the advective-diffusive evolution of salinity and temperature. The calculation of advective and diffusive terms then proceeds as outlined for salinity in Hermann and Stabeno (1996). In both that model and this one, density is a function of salinity only.

Further details of the model configuration and validation may be found in Stabeno et al. (1995a), Hermann and Stabeno (1996), and Stabeno and Hermann (1996).

2.2 The Individual-based Model

The IBM is divided into four life stages between spawning and the fall of the 0-age juvenile year: the egg stage, the yolk-sac larval stage, the feeding larval stage, and the juvenile stage (Fig. 2.2). Processes such as mortality and growth for each life stage are described in the following sections. These processes and the parameters associated with them are based, for the most part, on a wide variety of field and laboratory observations on this population. Based on these processes, population size, length and weight and other characteristics of individuals are updated once per day ($\Delta t_{IBM} = 24$ hr). Positions of individuals are updated more frequently, as described in the section on "Biophysical Coupling". A summary of parameter values is presented in Table 2.1.

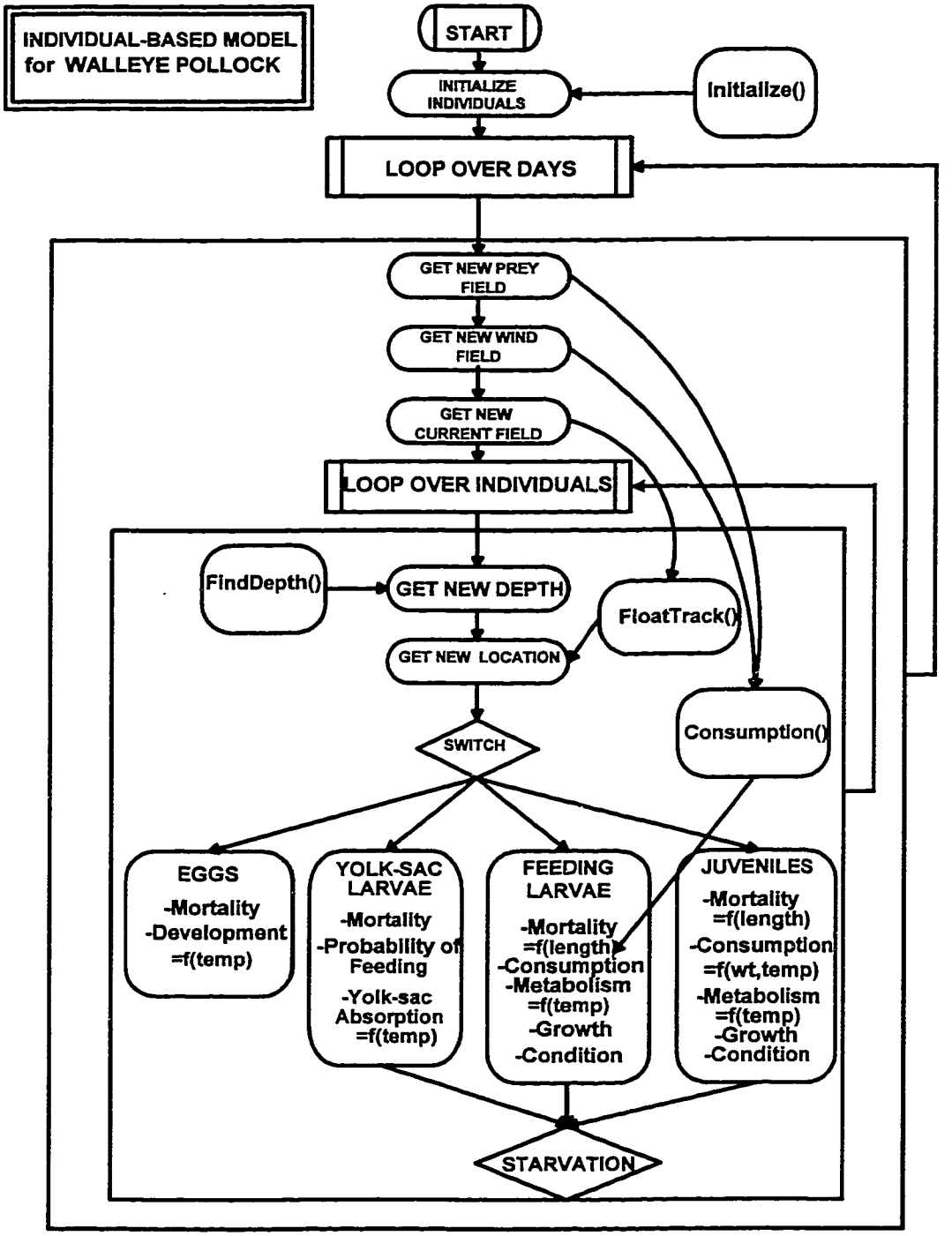

Figure 2.2. Flow chart of the individual-based model (IBM) of the early life stages of walleye pollock.

Table 2.1. Parameters for the Individual-based model

	Parameter	Value	Source
spd	Spawning date used in Simulations 2 and 3	90	
sdmn	Mean spawning date (DOY) used in Simulations 4 and 6	97	Picquelle & Megrey 1993
sdmin	Minimum spawning date (DOY) used in Simulations 4 and 6	73	Picquelle & Megrey 1993
sdmax	Maximum spawning date (DOY) used in Simulations 4 and 6	121	Picquelle & Megrey 1993
es	Mean egg diameter at start of simulation (mm)	1.314	Hinckley 1990
es_{min}	Minimum egg diameter (mm)	1.2786	Hinckley 1990
es_{max}	Maximum egg diameter (mm)	1.3494	Hinckley 1990
es^2	Variance of initial egg diameter	0.0002	Hinckley 1990
z_e	Mean instantaneous daily mortality of eggs (d^{-1}) used in Simulation 2	0.25	Brodeur et al. 1996
$minz_e$	Minimum daily egg mortality (d^{-1})	0.15[1]	Brodeur et al. 1996
$maxz_e$	Maximum daily egg mortality (d^{-1})	0.35	Brodeur et al. 1996
dep_e	Mean depth of eggs used in Simulation 3 (m)	200	
z_y	Mean instantaneous daily mortality of yolk-sac larvae (d^{-1}) used in Simulations 2, 5 and 6	0.15[1]	Bailey et al. 1996b
$minz_y$	Minimum daily yolk-sac larval mortality (d^{-1})	0.0	
$maxz_y$	Maximum daily yolk-sac larval mortality (d^{-1})	0.30	
δ_{FFR}	Degree days to first feeding readiness	18.0	Theilacker, pers. comm.

Table 2.1. Parameters for the Individual-based model

	Parameter	Value	Source
δ_{PNR}	Degree days to point of no return	67.5	Theilacker, pers. comm.
ss_{ysl}	Swimming speed of yolk sac larval (body lengths per second)	0.3	Olla, pers. comm.
dep_{ysl}	Mean depth of yolk-sac larvae used in Simulation 3 (m)	100	
z_f	Instantaneous daily mortality of feeding larvae (d^{-1}) used in Simulation 2	0.05[1]	Bailey et al. 1996b
z_{fsm}	Instantaneous daily mortality of small feeding larvae (d^{-1}) used in Simulations 2, 5 and 6	0.10[1]	Bailey et al. 1996b
$minz_f$	Minimum daily mortality rate for feeding larvae (d^{-1})	0.0	Bailey et al. 1996b
$maxz_f$	Maximum daily mortality rate for feeding larvae (d^{-1})	2.0* *nmort*	
Q_{10}	Q_{10} for consumption, feeding metabolism and routine metabolism	2.0	
T_{init}	Initial temperature for temperature effect on consumption, feeding metabolism and routine metabolism (°C)	4.5	Bailey, pers. comm.
s_c^2	Variance of consumption (µg dry wt $d^{-1})^2$	25.0	
γ	Oxycaloric equivalent (cal µl O_2)	0.00463	Brett & Groves 1979
β	Calorie to microgram conversion (µg cal^{-1})	227.0	Theilacker & Kimball 1984
α_l	Assimilation efficiency for feeding larvae	0.8	Webb 1978 Houde 1989
k_{cl}	Critical condition factor for feeding larvae	0.4	Bailey, pers. comm. Seifert, pers. comm.

Table 2.1. Parameters for the Individual-based model

	Parameter	Value	Source
S_M	Size at metamorphosis from larva to juvenile (mm)	25.0	Dunn & Matarese 1987
$ss1_{fdl}$	Mean swimming speed of feeding larvae less than 6 mm SL (body lengths s^{-1})	0.1	Olla, pers. comm.
$ss2_{fdl}$	Mean swimming speed of feeding larvae larger than 6 mm SL (body lengths s^{-1})	0.8	Olla, pers. comm.
s^2_{ssfdl}	Variance of swimming speed of feeding larvae	0.28	
S_{dm}	Size at which feeding larvae begin diel migration (mm)	6.0	Kendall et al. 1994
Lmin	Minimum preferred light level (μmol m^{-2} s^{-1})	6.0	Kendall et al. 1994
Lmax	Minimum preferred light level (μmol m^{-2} s^{-1})	13.0	Kendall et al. 1994
k	Extinction coefficient	0.16	R.Davis, pers. comm.
sd	Standard deviation of nighttime feeding larval depth distribution (m)	3.65	Kendall et al. 1994
zpmin	Minimum depth of feeding larvae (m)	10.0	Kendall et al. 1994
zpmax	Maximum depth of feeding larvae (m)	60.0	Kendall et al. 1994
dep_{fdl}	Mean depth of feeding larvae used in Simulation 3 (m)	40	Kendall et al. 1994
ht	Handling time (s)	1.7	MacKenzie & Kiørboe 1995
PF	Pause frequency (s^{-1})	0.52	Spring 1996
z_j	Mean instantaneous daily mortality of juveniles (d^{-1}) used in Simulation 5	0.02[1]	Yoklavich & Bailey 1990
$minz_j$	Minimum daily mortality of juveniles (d^{-1})	0.0	
$maxz_j$	Maximum daily mortality of juveniles (d^{-1})	0.04	

Table 2.1. Parameters for the Individual-based model

	Parameter	Value	Source
dep_j	Mean depth of juveniles (m)	17.0	
$mindep_j$	Minimum depth of juveniles (m)	10.0	
$maxdep_j$	Maximum depth of juveniles (m)	70.0	
k_{cj}	Critical condition factor for juveniles	0.42	Harris 1985
α_j	Assimilation efficiency for juveniles	0.7	Winberg 1956, Harris et al. 1986
sda	Specific dynamic action for juveniles	0.12	Buckley & Livingston 1994
jact	Activity multiplier for juvenile metabolism	2.0	Brett & Groves 1979, Houde 1989
hd	Hours of darkness	8.0	
hl	Hours of light	16.0	
Δt_c	Time step for depth algorithm in biophysical coupling (hr)	1.0	
Δt_{fta}	Time step for float tracking algorithm (hr)	0.2	
Δt_{fta}	Time step for float tracking algorithm (hr)	0.2	
Δt_{IBM}	Time step for individual-based model (hr)	24.0	

[1]Mortalities set to 0.0 for Simulations 3 and 4. For Simulations 5 and 6 the superindividual method was used, and for feeding larvae greater than 7.0 mm SL, an age-mortalily function was used.

2.2.1 The Egg Stage

Eggs are released in the model on a fixed date for early simulations, day of year (DOY) 90. Later, a normal or triangular distribution of spawning dates was added (Table 2.1). A triangular distribution is often used because all it requires is a mean, miminum and maximum values, ie. no estimate of variance (which is often difficult to find). Also, triangular

distributions may be asymmetrical. Eggs are randomly assigned an egg diameter (from a normal distribution in early simulations, from a triangular distribution in later simulations). Eggs are assigned an initial spawning depth of 200 m. Actual spawning depth probably varies, however there is little data to parameterize this. The egg stage lasts about 2 weeks at 5°C (Haynes and Ignell 1983).

Mortality

For early simulations, the daily probability of survival for an individual egg is

$$s_{ej} = e^{-z_e}, \qquad \text{(EQ 2.1)}$$

where,

s_{ej} = the probability of survival of the egg on day j, and
z_e = the instantaneous daily mortality rate of eggs (a constant over j).

A random number (from a uniform distribution) between 0 and 1 is generated, and if this number is larger than the probability of survival on day j, the egg dies. If the random number is smaller, the egg survives.

For later simulations, we have used a more detailed scheme to calculate mortality. One problem of using stochastic individual-based models to study processes affecting early life stages is that of how to model enough individuals to result in sufficient fish remaining at the end of the simulation, especially in a spatial context. Extremely high mortality rates in the egg, yolk-sac and feeding larval stages mean that number of individuals is quickly reduced. Computational limitations limit the number of individuals that can be reasonably modeled.

Several ways of dealing with this problem have been devised. One, a reseeding algorithm (Rose et al. 1993) replaces individuals lost due to mortality with a randomly chosen surviving member of the population. This method will not work with spatially-explicit modeling, as individuals from different locations will vary due to differences in the environment experienced over time, and it is these differences that we are interested in.

Random choice of one of the surviving individuals would bias the spatial information contained in the model.

A second way of dealing with this problem has been called the "superindividual" method (Scheffer et al. 1995). A modified version of this method has been implemented in this model. In this method, "individuals", each represented as a point in space or "float", actually becomes a "superindividual" or cohort, which experiences the same velocity, temperature, salinity, and prey conditions. Feeding, metabolism and growth within each cohort are assumed to be the same. This is an assumptions which we feel is appropriate, given the goals of this modeling. We are mainly interested in differences at the mesoscale spatial level, and this method preserves these differences by assuming that the individuals located at the same place experience the same conditions.

A variable called "*value*" is defined for each individual (we will continue to use the term "individual" when referring to superindividuals). This variable is set at the beginning of the simulation to a number representing the initial number in the cohort. This initial *value* is then reduced each day by mortality. The variable *value* is updated each day using the equation:

$$V_{t+1} = V_t e^{-nmort} \qquad \text{(EQ 2.2)}$$

where,

V_{t+1} = *value* on day $t + 1$,
V_t = *value* on day t.

The calculated parameter, *nmort*, represents an estimate of the total daily mortality rate, a random deviate from a triangular distribution with the mean being the year-specific constant (e.g. z_e) or length-specific mortality rate for larger feeding larvae, and minimum and maximum specific to each life stage also (Table 2.1). The mean egg mortality rates are year-specific:

If year = 1978, mean $z_e = 0.2091$;

If year = 1987, mean $z_e = 0.2262$;

If year = 1988, mean $z_e = 0.3005$;

If year = 1989, mean $z_e = 0.1739$;

If year = 1991, mean $z_e = 0.2215$;

If year = 1994, mean $z_e = 0.2091$ (average over years, as data not available);

Else, mean $z_e = 0.2091$ (average over years).

These data are from Brodeur et al. (1996). The number that die each day from each "individual" is also recorded.

Development

The egg development process is divided into 21 stages (Blood et al. 1994) in order to compute the development rate (from age and temperature) and the egg density from available data. This part of the model (the depth finding algorithm) is updated hourly as is the float-tracking algorithm (where depth is an argument). The egg stage is a function of age and temperature:

(if egg age is less than 20 hr)

$$e = -2.9935 + 3.0438\sqrt[3]{a} + 0.0172aT \qquad \text{(EQ 2.3)}$$

(if egg age is greater than or equal to 20 hr)

$$e = -4.8019 + 1.0851\sqrt{a} + 0.0051aT + 0.1595T\sqrt{a} \qquad \text{(EQ 2.4)}$$

where,

e = egg stage,
a = egg age (hr), and
T = temperature (°C)

To calculate density (in order to estimate depth, see next section), eggs are separated into seven groups based on their stage of development (Kendall and Kim 1989), as follows:

Group 1 = Stages 1-6 (cell stages)
Group 2 = Stages 7-8 (early germ ring stages)
Group 3 = Stages 9-12 (germ ring stages)
Group 4 - Stages 13-15 (middle stages)
Group 5 = Stages 16-18 (early late stages)
Group 6 = Stages 19-21 (late stages)
Group 7 = Hatching.

Absolute changes in density of eggs with development, corrected for the depth of spawning, are calculated from laboratory studies reported in Kendall and Kim (1989) for Type II eggs. (Type II eggs are the most common class of pollock eggs and are heavier in the early developmental stages than are Type I eggs.) Egg density increases with developmental stage until just before hatch, when density drops. When the egg reaches stage 21 (group 7), it hatches, and the individual passes into the yolk-sac larval stage. Egg specific gravities are used to calculate the depth of each individual egg at each time step, as discussed in the next section.

Depth

Changes in egg depth occur due to changes in density with development Initial egg density is set equal to the water density at the depth of spawning (which is a function of salinity; see Eq. 2.5) (Craik and Harvey 1987, Coombs et al. 1985, Kändler and Tan 1965, Solemdal 1967, 1973). The output files from the SPEM run are called at the beginning of the simulation, and a salinity at the location of each individual on the day of spawning is obtained. Water density is then calculated as in the physical model (Hermann and Stabeno 1996):

$$\rho_w = [0.824S + 999.843]10^{-3} \qquad \text{(EQ 2.5)}$$

where,

ρ_w = water density (g cm^{-3}), and
S = salinity (ppt).

During the spring and summer seasons in this region, salinity is the most important factor determining density; temperature has only a very small effect.

The density of an individual egg is assigned depending on its group (see Section 2.2.1. Development) which changes with development. As in Kendall and Kim (1989), the terminal velocity of an egg in the vertical direction is calculated from the equation used by Sundby (1983) for Reynolds number (Re) < 0.5:

$$w = gd^2\frac{(\rho_e - \rho_w)}{18.0v} \qquad \text{(EQ 2.6)}$$

where,

w = terminal vertical velocity (cm s^{-1}),
g = gravitational constant (g = 980.0 cm s^{-2}),
d = egg diameter (cm),
ρ_w = the density of water (g cm^{-3}, see Eq. 2.5),
ρ_e = egg density (g cm^{-3}),
v = the molecular viscosity of water (v = 0.161 g cm^{-1} s^{-1}), and
Re = the Reynolds number (Re = wv/d).

The new depth of the egg after each time step is calculated as:

$$z_{t+1} = z_t + w\Delta t_c \qquad \text{(EQ 2.7)}$$

where,

z_{t+1} = depth of egg at new time step (m),
z_t = depth of egg at last time step (m),
w = terminal vertical velocity of egg (cm s^{-1}), and
Δt_c = time step (Δt_c = 1 hr).

2.2.2 The Yolk-sac Larval Stage

The size at hatch of an individual is determined by the egg size (Hinckley 1990):

$$l = 0.483 + 2.613d \qquad \text{(EQ 2.8)}$$

where,

l = larval standard length (SL, mm), and

d = egg diameter (mm).

Larval dry weight at hatch is a function of standard length (Yamashita and Bailey 1989):

$$W = 0.1754 l^{3.615} \quad \text{(EQ 2.9)}$$

where,

W = larval dry weight (μg), and
l = larval SL (mm).

Mortality

The daily probability of survival of yolk-sac larvae is determined in the same way as described in Section 2.2.1 ("The Egg Stage"), with mean daily mortality rate $z_y = 0.15$. If a yolk-sac larva reaches the point of no return (see below), it is removed from the model.

Development

Degree days are used to determine when the yolk-sac larva reaches first-feeding readiness and the point of no return (the time at which starvation is irreversible, ie. death from starvation is inevitable). Degree days are accumulated for every day after hatch using temperature information from the physical model for each location and time step. If degree days are less than the number of degree days to first-feeding readiness (δ_{FFR}=18.0), yolk-sac larval age is incremented one day. The parameter, δ_{FFR}, was adjusted to produce an age at first-feeding readiness comparable to laboratory studies (G. Theilacker, Alaska Fisheries Science Center, 7600 Sand Point Way NE, Seattle, WA 98115, pers. commun.). The parameter value used was less than what would be indicated by the laboratory studies for degree days, indicating a possibly nonlinear relationship between degree days and yolk-sac larval development times.

Once the larva is ready to feed, the probability of feeding on each day, a linearly increasing function of degree days: ($prfeed = 0.0238 ddays$), is compared with a random number from a uniform distribution. If the random number is greater than the probability of feeding, the larva does not feed. In this case, a new length is calculated which reflects a percent decline in size each day (Bailey and Stehr 1986):

$$l_{j+1} = l_j - (0.015 l_j) \qquad \text{(EQ 2.10)}$$

where,

l_{j+1} = larval standard length on day $j+1$ (mm), and
l_j = larval standard length on day j (mm).

Shrinkage in length of yolk-sac larvae is possible because the notochord, being cartilaginous, is somewhat flexible. Larval dry weight is calculated based on length as in Eq. 2.9, above.

If the random number is less than or equal to the probability of feeding, the larvae feeds and makes the transition to the feeding larval stage. Length and weight changes are then calculated based on the procedures discussed below (in Section 2.2.3 on "The Feeding Larval Stage") for the day of transition. If the larva passes the point of no return (δ_{PNR}=67.5 degree days, Bailey and Stehr 1986) without feeding, it dies, and the individual (float) is removed from the model.

The use of a linearly increasing function of degree days to calculate the probability of feeding is based on data which shows a higher proportion of larvae feeding with age and temperature, ie. a population estimate. It may be said that this is counterintuitive as far as individuals are concerned, that an individual would be *less* likely to feed as time goes on, due to the effects of starvation. It should be noted, however, that yolk-sac absorption has not yet taken place at the time of first-feeding readiness, and that the larva is not starving until this occurs. Yolk-sac absorption will occur sometime before the point of no return, and then the effects of starvation would probably operate. This is a difficult problem to

parameterize properly, and for this preliminary model the effect is simplified through the use of the linearly increasing function.

Depth

Yolk-sac larvae remain deep in the water column until first-feeding readiness, when they move upward in the water column at a speed of approximately $ss_{ysl} = 0.3$ body lengths per second (B. Olla, M. O. Hatfield Marine Science Center, Newport, Oregon, 97365, pers. commun.), to a location in the upper 20 to 60 m of the water column.

2.2.3 The Feeding Larval Stage

Mortality

For initial simulations, the probability of survival each day for feeding larvae is calculated in the same manner as described in Section 2.2.1 ("The Egg Stage"), with mean daily mortality rate $z_f = 0.05$. For later simulations, for larvae smaller than 7.0 mm, a constant daily rate is also used (Table 2.1), but the mean mortality rate for feeding larvae greater than or equal to 7.0 mm is a function of length and year, as fit to data (algorithms represent the best fit statistical models):

If year = 1987,

$$mortality = e^{(1.7007 - 2.0312\log(length))} \quad \text{(EQ 2.11)}$$

If year = 1988,

$$mortality = e^{(7.7095 - 5.2913\log(length))} \quad \text{(EQ 2.12)}$$

If year = 1989,

$$mortality = 0.7015 - 0.0674length \quad \text{(EQ 2.13)}$$

If year = 1990,

$$mortality = 0.3942 - 0.0373 length \quad \text{(EQ 2.14)}$$

If year = 1991,

$$mortality = e^{(7.3297 - 4.8768 \log(length))} \quad \text{(EQ 2.15)}$$

Otherwise,

$$mortality = e^{(7.4323 - 4.9738 \log(length))} \quad \text{(EQ 2.16)}$$

This relationship was derived from age-mortality information (Bailey et al. 1996b) and length-at-age information (Bailey et al. 1996a) derived from larvae sampled at the same locations and times. If the calculated mortality is less than 0.02, the mortality rate is set to 0.02. If a larva is greater than 25 d old, the mortality rate is also set to 0.02.

Starvation mortality is calculated in the model by using a critical condition factor k_{cl}. The critical condition factor was set equal to the minimum condition factor seen in larval length-weight data (K. Bailey, Alaska Fisheries Science Center, 7600 Sand Point Way, NE, Seattle, WA 98115, pers. comm., D. Seifert, Alaska Fisheries Science Center, 7600 Sand Point Way, NE, Seattle, WA 98115, pers. comm.). This is similar to the approach as used by Werner et al. 1995, whose "death barrier" consisted of a minimum dry weight at age. The critical condition factor used, $k_{cl} = 0.4$ is slightly smaller than that calculated for juvenile walleye pollock by Harris (1985) ($k_{cj} = 0.42$). We use the difference between the total mortality and the starvation mortality as an estimate of predation mortality. Other possible causes of mortality (for example, disease or the failure of egg fertilization) are not considered due to a lack of information.

Depth

In this model, feeding larvae begin diel migrations when they reach a length of 6 mm standard length (Kendall et al. 1994). If larvae are less than 6 mm, the change in depth is a function of swimming speed, which is a function of larval size. Mean swimming speed (ssl_{fdl} = 0.1 body lengths per second, B. Olla, M. O. Hatfield Marine Science Center, Newport, Oregon, 97365, pers. commun.) is used to generate a random deviate from a normal or triangular distribution. The direction of swimming (up or down) is also random for the smaller feeding larvae. Note that horizontal swimming movement is not modeled here for feeding larvae.

We modeled the pattern of vertical migration of feeding larvae greater than 6 mm based on the results of field studies (Kendall et al. 1987, Pritchett and Haldorson 1989, Kendall et al. 1994). Larvae are found deepest during midday and are shallowest at dusk. They are found somewhat deeper at night than at dusk or at dawn. Diel migrations are assumed to be a response to light levels (Kendall et al. 1994), with movement toward a range of preferred light levels between $Lmin$ = 6.0 and $Lmax$ = 13.0 µmol m^{-2} s^{-1}. The minimum preferred light level was adjusted from that cited by Kendall et al. (1994; 0.1 µmol m^{-2} s^{-1}) to produce a reasonable maximum depth of feeding larvae. Preferred light levels are used to calculate a preferred depth zone using Eq. 2.17 and Eq. 2.18:

$$zp_{min} = \frac{ln(Lmax) - ln(R_t)}{-k} \quad \text{(EQ 2.17)}$$

$$zp_{max} = \frac{ln(Lmin) - ln(R_t)}{-k} \quad \text{(EQ 2.18)}$$

where,

zp_{min} = minimum preferred depth (m),
zp_{max} = maximum preferred depth (m),
$Lmin$ = minimum preferred light level (6.0 µmol m^{-2} s^{-1}),

$Lmax$ = maximum preferred light level (13.0 μmol m^{-2} s^{-1}),
R_t = incident light at time t (μmol m^{-2} s^{-1}),
k = extinction coefficient ($k = 0.16$).

We assume an exponential decline in irradiance with depth, with incident light an average (sine function) dependent on time of day, measured just below the surface (i.e. not including reflected light). K is here considered a constant (R. Davis, Dalhousie Univ. Halifax, Nova Scotia, pers. comm.).

At each time step, the larva is moved in the vertical direction, with the distance travelled a function of swimming speed and time step size. The actual larval swimming speed during any one time step is a random variable with mean, $ss2_{fdl} = 0.08$ body lengths per second (B. Olla, M. O. Hatfield Marine Science Center, Oregon State University, Newport, OR 97365, pers. commun.), and variance, $s^2_{ssfdl} = 0.28$. The new position of the larva after each time step is checked to be sure that it is between zp_{min} and zp_{max}. If the larva's depth is less than zp_{min}, it's depth is reset to zp_{min}. If it's depth is greater than zp_{max}, the depth is reset to zp_{max}. This resetting is meant to reflect the probable behavioral response of larvae to light levels. As light levels decrease toward dusk, the larva will move up in the water column. If zp_{min} and zp_{max} become less than 10 m at night, zp_{min} is set to 10 m and zp_{max} is reset to 10 m plus a random deviate from a normal or triangular distribution which has a mean equal to the standard deviation of the nighttime larval distribution (sd = 3.65 m, A. Kendall, pers. commun., Alaska Fisheries Science Center, 7600 Sand Point Way, NE, Seattle, WA 98115). The larvae are thus distributed slightly deeper at night, as is seen in the field. As light levels increase at dawn, and the depth of the preferred light level deepens to below 10 m, the larva again changes depth in response to light.

Note that since swimming speed increases with body size (Neilson and Perry 1990), the distance moved during each time step increases and therefore the amplitude of the diel cycle increases for an individual as it grows. The model successfully reproduced the pat-

tern of depth distribution that is observed in the egg, yolk-sac, and feeding larval period. The general pattern of depth by life history stage is shown in Fig 2.3.

Consumption, Metabolism and Growth

For early simulations, a consumption-larval weight function slightly modified from MacKenzie et al. (1990), further modified with a Q_{10} function to account for the effect of temperature, was used:

$$C = [10^{(0.894\log_{10})(W)-0.27}][e^{(\log Q_{10}/10.0)(T-T_{init})}] \quad \text{(EQ 2.19)}$$

where,

C = daily consumption (µg dry wt. d^{-1}),
W = larval dry weight (µg),
Q_{10} = 2.0,
T = temperature (°C),
T_{init} = 4.5 °C.

A random deviate from a normal or triangular distribution with mean C and variance s^2_c = 25.0 µg dry wt. d^{-1} was used as the daily consumption for an individual. The variance of the consumption rate was somewhat arbitrary, as there was no information on this parameter.

Consumption in later simulations was modified to be a deterministic function of prey density, wind-generated turbulence, and larval body size. Rothschild and Osborn (1988) proposed the idea that contact rates between predators and prey may be enhanced by turbulence in the ocean. This idea has been explored further by MacKenzie and Leggett (1991), Sundby and Fossum (1990), and others. MacKenzie et al. (1994) has added a model of the potential negative effects of higher rates of turbulent energy on the larval feeding process, specifically on the post-encounter components of consumption (pursuit, attack and capture). The combination of these two conceptual models results in a dome-shaped consumption versus turbulence curve.

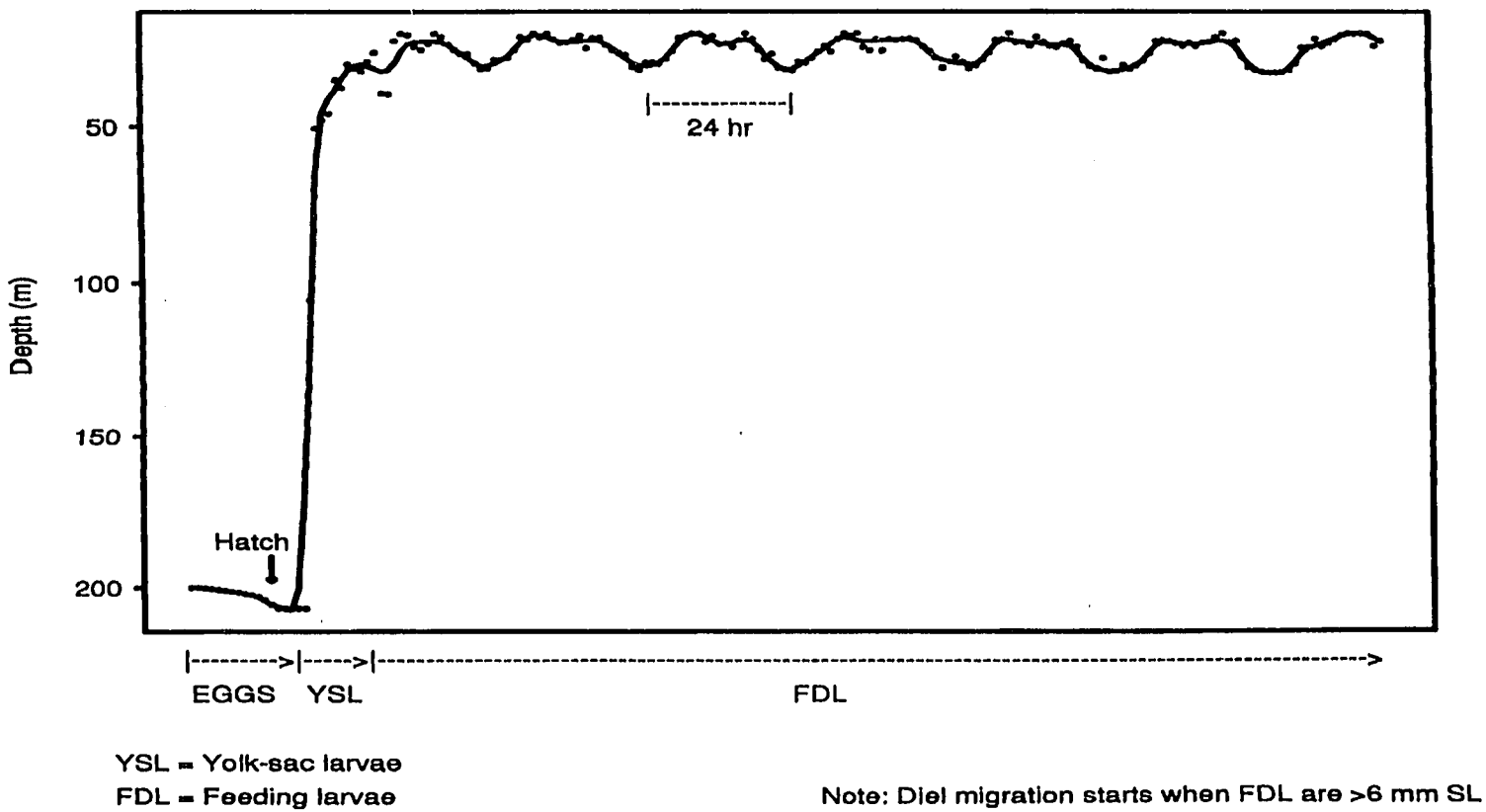

Figure 2.3. Depth of a representative individual from spawning through the feeding larval stage. Note: Egg stage duration is about 2 weeks, yolk-sac larval stage duration is about 1 week. Diel cycle shown for feeding larvae. The dots show the daily position for the egg and yolk-sac stages and hourly positions for the feeding larval stage. The line represents a smoothed average. Diel migration starts when FDL are > 6 mm SL.

In this model we have used the MacKenzie et al. (1994) formulation modified by the fact that larval pollock are pause-travel predators (MacKenzie and Kiørboe 1995), not cruise predators as proposed in MacKenzie et al. (1994). The encounter probability is therefore modified to reflect the fact that larvae only search for food when motionless.

Consumption, in μg dry weight consumed per day for an individual fish, is the product of the number of prey encountered per day, and the probability of successful pursuit. The number encountered per day is

$$E_s = \left(\frac{2\pi R^3}{3} N \cdot PF\right) + \pi R^2 N (u^2 + 2\Omega^2)^{0.5} \cdot PF \cdot PD \qquad \text{(EQ 2.20)}$$

(MacKenzie and Kiørboe 1995, Eq. 1b)

where,

E_s = encounter rate (prey s^{-1}),
R = reactive distance (m),
N = prey density (no m^{-3}),
u = prey velocity (m s^{-1}),
Ω = turbulent velocity (m s^{-1}),
PF = pause frequency (no s^{-1}),
PD = pause duration (s).

This assumes that the larva scans the half sphere directly in front of it, with a radius equal to its detection range. Also included is the added rate of encounter with prey that are advected or that swim into this half sphere. Each volume of water scanned during a pause is assumed to be independent of the last volume of water scanned. Then,

$$E_d = E_s(86,400)H \qquad \text{(EQ 2.21)}$$

where,

E_d = encounter rate (prey d^{-1}),
H = fraction of day when feeding occurs.

The constant, 86,400 is the number of seconds in a day. Feeding is assumed to occur for all daylight hours, which is about 16 hours per day (M. Canino, K. Bailey, Alaska Fisheries Science Center, 7600 Sand Point Way, NE, Seattle, WA 98115, pers. comm.) in this region.

The turbulent velocity, Ω, is a function of the dissipation rate, ε, and a length scale. Here, as in MacKenzie and Kiørboe (1995), the larval reactive distance, R, is assumed to be the proper length scale.

$$\Omega^2 = 3.615(\varepsilon R)^{0.667} \quad \text{(Rothschild and Osborn 1988)} \qquad \text{(EQ 2.22)}$$

where,

ε = the dissipation rate of turbulent kinetic energy (m s^{-3}).

The dissipation rate at any depth is derived from the wind speed:

$$\varepsilon_z = \frac{5.82 \times 10^{-9} W^3}{z} \quad \text{(MacKenzie and Leggett 1991)} \qquad \text{(EQ 2.23)}$$

where,

z = depth (m),
W = wind speed (m s^{-1}).

This assumes that the larva is in a well-mixed layer, and so may overestimate turbulent levels below the model mixed layer.

Development of the model for the probability of successful pursuit is detailed in MacKenzie et al. (1994). Briefly, the model assumes that the probability of successful pursuit (the prey approach and fixation time) is the most sensitive of the post-encounter processes to the negative effects of turbulence. A coordinate system centered on the larval eye is defined, with the larva considered fixed in space (with only relative motion between larva and prey considered important). Turbulence is assumed to be locally isotropic within the

larval encounter distance. The distance that the prey can be moved by turbulent motion, once it has been spotted by the larva, is ωt (turbulent velocity times minimum pursuit time), which defines a sphere of this radius. This sphere is termed the prey encounter sphere.

The model defines the likelihood that the prey will remain within the larval encounter sphere once it has been spotted (given that it is in a turbulent regime) for at least the minimum pursuit time. This probability is given by the ratio of the volume of overlap of the two spheres, the prey excursion sphere and the larval encounter sphere, over the total volume of the prey excursion sphere:

$$P(sp) = \frac{V_{over}}{V_{prey}} \qquad \text{MacKenzie et al. (1994), Eq. 2} \qquad \text{(EQ 2.24)}$$

where,

$P(sp)$ = probability of successful pursuit,
V_{over} = volume of overlap,
V_{prey} = volume of the prey excursion sphere.

Eq. 2.24 is solved for all values of a, the encounter distance between a larva and a prey item. The resultant solution is:

$$P(sp) = -\frac{3}{4}\frac{a}{\omega t}\left(\frac{r^2-(\omega t)^2+a^2}{2a\omega t}\right)^2-\left(\frac{3}{4}\frac{a}{\omega t}\right)+ \qquad \text{(EQ 2.25)}$$

$$\frac{1}{4}\left(\frac{2r^3}{(\omega t)^3}+2+\frac{a^3}{(\omega t)^3}\right)$$

(MacKenzie et al. 1994, Eq. 6)

There are three valid domains to this solution:

(1) $$\overline{P(sp)}_{\omega t<r} = \frac{1}{r}\left[\int_0^{r-\omega t} 1\,da+\int_{r-\omega t}^{r} P(sp)da\right] \qquad \text{(EQ 2.26)}$$

(2) $$\overline{P(sp)}_{r<\omega t<2r} = \frac{1}{r}\left[\int_0^{\omega t-r} \frac{r^3}{(\omega t)^3} da + \int_{\omega t-r}^{r} P(sp)da\right] \quad \text{(EQ 2.27)}$$

(3) $$\overline{P(sp)}_{\omega t>2r} = \frac{1}{r}\int_0^r \frac{r^3}{(\omega t)^3} da \quad \text{(EQ 2.28)}$$

where,

$\overline{P(sp)}$ = the expected probability of successful pursuit,
a = distance of prey from the larval eye (mm),
ω = turbulent velocity (mm s^{-1}),
r = reactive distance (mm),
t = minimum pursuit time (s).

The solutions for each domain, dependent on the walues of ω and t, are as follows:

$$\overline{P(sp)}_{\omega t<r} = [(12r^3t\omega) + (6r^2t^2\omega^2) + (44rt^3\omega^3) - (21t^4\omega^4) - (12r^4\log r) + (24r^2t^2\omega^2\log r) - (12t^4\omega^4\log r) + (12r^4\log(r-t\omega)) - (24r^2t^2\omega^2\log(r-t\omega)) + (12t^4\omega^4\log(r-t\omega))]/[64rt^3\omega^3] \quad \text{(EQ 2.29)}$$

$$\overline{P(sp)}_{r<\omega t<2r} = [(12r^3t\omega) + (6r^2t^2\omega^2) + (44rt^3\omega^3) - (21t^4\omega^4) - (12r^4\log r) + (24r^2t^2\omega^2\log r) - (12t^4\omega^4\log r) + (12r^4\log(-r+t\omega)) - (24r^2t^2\omega^2\log(-r+t\omega)) + (12t^4\omega^4\log(-r+t\omega))]/[64rt^3\omega^3] \quad \text{(EQ 2.30)}$$

$$\overline{P(sp)}_{\omega t>2\cdot r} = \frac{R^3}{(\omega t)^3} \quad \text{(EQ 2.31)}$$

Prey swimming speeds are calculated using Sundby and Fossum's (1990) estimate of 0.5 body lengths per second for *Euphausia pacifica* and applied to *Calanus finmarchicus*; and the median body length for the naupliar group and the copepodite group. Eggs are assumed to be motionless.

Larval reactive distance (r, mm) is a function of larval length, according to the formula

$$r = 0.679l \; . \quad \text{(EQ 2.32)}$$

This is derived from data for Arcto-Norwegian cod in MacKenzie and Kiørboe (1995) and Tilseth (1984). Pause frequency (*PF*) and pause duration (*PD*) are derived from labora-

tory experiments on larval feeding and swimming patterns at different food densities, and turbulence levels. Pause frequency is a constant, based on the work of Spring (1996) (PF = 0.52 s^{-1}). Pause duration is a function of larval length, prey density and turbulence, after the work of MacKenzie and Kiørboe (1995) on Arcto-Norwegian cod, as follows:

If ($\varepsilon < 7.4e^{-8}$),

If (Prey density < 35,000 per m^3),

PD = 2.522 + 0.111(length)

Else if (Prey density > 35,000),

PD = 24.267 - 3.667(length).

If (length>(24.267/3.667))

PD = 0.1.

If ($\varepsilon > 7.4e^{-8}$)

If (Prey density < 35,000),

PD = 5.189 - 0.556(length).

If (length>(5.189/0.556))

PD = 0.1.

Else if (Prey density > 35,000),

PD = 10.111 - 1.444(length).

If (length>(10.111/1.444))

PD = 0.1.

Values of wind speed are input to the model for each larval location using the same data set used by the SPEM model for each year (Stabeno et al. 1995a). This data set consists of geotriptic winds computed from 12-hr atmospheric surface pressure contributed by the Fleet Numerical Oceanographic Center. These geostrophic winds were rotated 15° counterclockwise, the speeds were reduced by 30%, and the results interpolated to the hydrodynamic grid (Macklin et al. 1993). For a specified range of wind directions, these geotriptic winds must be modified to account for ageostrophic winds which can be common in Shelikof Strait (Lackmann and Overland 1989, Macklin et al. 1993). An algorithm

which has been developed from observations is applied to the geotriptic winds to account for the channeling and enhancement of winds within the Strait.

Prey densities are read into the model using the output (average daily numbers m^{-3} of each *Pseudocalanus* stage at the larval depth) from the NPZ model (see Section 2.3, Nutrient-Phytoplankton-Zooplankton Model). The data in the wind and prey field data sets uses the same 20 x 20 Eulerian grid that is used by the NPZ model, a subset of the SPEM grid The wind speed or prey density at each larval location is linearly interpolated to the larval locations using values from nearby grid points. If the larval location is beyond the boundaries of the NPZ grid, the prey value at the nearest boundary grid point is used.

The maximum size of prey items (*maxprey*) taken for a larva of length l is given by the equation

$$maxprey = 0.115e^{(0.235l)} \quad \text{(Nishiyama, Hirano and Haryu, 1983)} \qquad \text{(EQ 2.33)}$$

The maximum size of prey items taken is converted into the maximum stage of *Pseudocalanus* (*maxstage*) taken using a maximum carapace length for each stage (J. Napp, Alaska Fisheries Science Center, 7600 Sand Point Way, NE, Seattle, WA 98115, pers. comm.). Prey of the size taken by the larva are aggregated into three groups (eggs, nauplii and copepodites). The probability of a larva of length l taking prey that are eggs, nauplii or copepodites are determined using data from Kendall et al. (1987).

The encounter rate of a larva with eggs, naupliiar and copepodite stages are calculated separately. Then the probability of successful pursuit is determined, using one of Eq. 2.29-2.31. The appropriate equation used will be dependent on larval length (as t and r are dependent on larval length) and larval location (as ω is dependent on location). The number consumed of eggs, nauplii and copepodites is calculated as:

$$C_i = E_i P(sp) P(eat)_i \qquad \text{(EQ 2.34)}$$

where,

C_i = number of prey items eaten d^{-1} for group i = eggs, nauplii, or copepodites,
E_i = number of prey items encountered of i = eggs, nauplii, or copepodites,
$P(sp)$ = probability of successful pursuit,
$P(eat)_i$ = probability of larva eating group i = eggs, nauplii, or copepodites.

The dry weight of prey items in each group (egg, nauplii or copepodite) is calculated using the dry weight of each individual stage, and by assuming that the consumption in numbers of each group is divided equally between all stages in that group. The total consumption (dry weight d^{-1}) for the larva is the sum of the dry weights of each group consumed. This consumption is used in the energetics equation (Eq. 2.39). Feeding larval metabolic rates are based on the laboratory studies of Yamashita and Bailey (1989), with a Q_{10} modifier. Feeding metabolism (which includes resting metabolism plus the cost for specific dynamic action) is calculated as

$$M_{fn} = [0.00308\,W^{0.9059}][e^{(\log Q_{10}/10.0)(T-T_{init})}] \qquad \text{(EQ 2.35)}$$

Routine metabolism (which includes resting metabolism plus a cost for light-generated activity) is calculated as

$$M_{ro} = [0.00253\,W^{0.9699}][e^{(\log Q_{10}/10.0)(T-T_{init})}]. \qquad \text{(EQ 2.36)}$$

Total daily metabolic cost is calculated as

$$M_{24} = (2.0M_{ro}hl) + (M_{fn}hd) \quad , \qquad \text{(EQ 2.37)}$$

where,

M_{fn} = feeding metabolism ($\mu l\ O_2\ h^{-1}$),
M_{ro} = routine metabolism ($\mu l\ O_2\ h^{-1}$),
M_{24} = 24-hour metabolic cost ($\mu l\ O_2\ d^{-1}$),
W = larval dry weight (μg),
Q_{10} = 2.0,
hl = hours of daylight (hl = 16.0),
hd = hours of darkness (hd = 8.0),

T = temperature (°C), and
T_{init} = 4.5 °C.

This assumes that the cost of active swimming while feeding is twice that of routine metabolism (Brett and Groves 1979, Houde 1989). As mentioned by Houde (1989), this multiplier is commonly used , but may be conservative. It is also assumed that there are 16 hr of daylight and 8 hr of darkness (at 57 °N latitude). Daily metabolic cost in µl O_2 d^{-1} is converted to µg d^{-1} as follows:

$$R_{tot} = M_{24}\gamma\beta_l \qquad \text{(EQ 2.38)}$$

where,

R_{tot} = daily respiration rate (µg dry weight d^{-1}),
γ = oxycaloric equivalent,
β_l = calorie to µg conversion factor.

This uses the oxycaloric equivalent (γ) of 0.00463 cal µl O_2 (Brett and Groves 1979), and a calorie to microgram conversion factor (β_l) of 227.0 µg cal^{-1} (Theilacker and Kimball 1984). Assimilation efficiency (α_l) is set equal to 0.8, which is within the range of values cited by Webb (1978) and by Houde (1989) for marine fish larvae (when the temperature was extrapolated to 6.5°C). Houde and Shekter (1981), Checkley (1984) and Kiørboe et al. (1987) present evidence that both growth efficiency and assimilation efficiency varies with ration, however this factor has been neglected here for simplification and due to the lack of information on this subject for pollock.

The daily weight change of a larva is then calculated as

$$W_{j+1} = W_j + \alpha_l C - R_{tot} \qquad \text{(EQ 2.39)}$$

where,

W_{j+1} = larval dry weight on day $j+1$ (µg),
W_j = larval dry weight on day j,
α_l = assimilation efficiency for larvae,

C = daily consumption (µg dry wt. d^{-1}), and
R_{tot} = daily respiration rate (µg dry weight d^{-1}).

If there is a net gain in dry weight (i.e. if $\alpha_l C > R_{tot}$), then the increase in standard length (SL) is calculated as follows:

(if SL is less than 7.0 mm)

$$l = 10^{(\log_{10}(W) + 0.756)/3.615} \quad \text{(Yamashita and Bailey 1989)} \quad \text{(EQ 2.40)}$$

(if SL is greater than or equal to 7.0 mm)

$$l = 10^{(\log_{10}(W) + 0.486)/3.395} \quad \text{(Bailey and Stehr 1986).} \quad \text{(EQ 2.41)}$$

If there is no net gain in dry weight (i.e. if $\alpha C \leq R_{tot}$), then SL stays the same. Note that feeding larvae cannot shrink in length, as can yolk-sac larvae. This is because ossification of the vertebral column prevents shrinkage. The depth of a feeding larva at each time step is predicted from the algorithms described in the next section. When the larva reaches the size at metamorphosis, S_M = 25 mm SL, it is considered a juvenile (Dunn and Matarese 1987).

2.2.4 The Juvenile Stage

Mortality

The probability of mortality each day for juvenile pollock, and the *value* of each individual is calculated in the same manner as described in Section 2.2.1. ("The Egg Stage"). Starvation mortality for juveniles is calculated (in the later simulations) the same way as was done for feeding larvae (Section 2.2.3.), with a critical condition factor, k_{cj} = 0.42 (Harris 1985). As for feeding larvae, we use the difference between total mortality and

starvation mortality as an estimate of predation mortality, ignoring other possible causes of death due to lack of knowledge.

Depth

At the time of developement of the juvenile stage section of the IBM, little was known about the depth distribution of juvenile pollock. Since that time, more information has been obtained (Brodeur and Wilson 1996a, 1996b), and an updated version of the IBM adapted for the Bering Sea includes this new knowledge.

For this version of the model, two simple schemes are used to determine the depth of an individual juvenile. Most simply, a random deviate from a normal or triangular distribution was used. In the second scheme, the average depth of an individual increased linearly with length, and a random deviate using this mean was generated.

Consumption, Metabolism and Growth

There is little information on the processes of consumption and metabolism for the summer months of the 0-age year (ages 2 to 6 months), although research has been done on later stages of juveniles (Paul 1986, Smith et al. 1986, Harris et al. 1986, Paul et al. 1990). The mean daily consumption is modeled as a function of weight. Note that this is a developmental response only, as there was a complete lack of information to parameterize a functional response (consumption as a function of prey density). Different formulations were used for fish less than or greater than 70 d old, as follows:

If ($age \leq 70$ d)

$$C = (10^{0.898(\log W) - 0.27})\left(e^{\left(\frac{\log Q10}{10}\right)(T-4.5)}\right) \qquad \text{(EQ 2.42)}$$

If ($age > 70$ d)

$$C = 63.70 W^{0.61} \left(e^{\left(\frac{\log Q10}{10}\right)(T-4.5)} \right) \quad \text{(EQ 2.43)}$$

where,

C = mean daily consumption (µg dry weight d^{-1}),
W = weight (µg dry weight),
T = temperature (°C).

Actual daily consumption is a random deviate obtained using C as the mean of a triangular distribution with minimum and maximum set at the 95% confidence limits for the mean. The parameters in the mean consumption functions were fit by adjusting consumption levels to produce the growth curve described by Brown and Bailey (1992). Seventy days is the location of the inflexion point in Bailey and Browns' growth curve.

Larval metabolic rates (resting metabolism), as described by Yamashita and Bailey (1989) produced a reasonable fit to the same growth curve for fish less than 70 d old:

$$M_{re} = 0.00276 W^{0.8707} \quad \text{(EQ 2.44)}$$

where,

M_{re} = resting metabolism (µl O_2 hr^{-1}).

For fish older than 70 d, resting metabolic rates from Paul (1986) were used:

$$M_{re} = 0.141872 W^{0.755} \quad \text{(EQ 2.45)}$$

Total oxygen used in metabolism was

$$M24 = hd \cdot M_{re} + jact \cdot hl \cdot M_{re} \quad \text{(EQ 2.46)}$$

where,

$M24$ = total oxygen consumed in 24 hours (µl),
$jact$ = activity multiplier ($jact = 2.0$).

Total daily respiration, in units of dry weight, was derived as follows:

$$R_{tot} = M24\gamma\beta_j \quad \text{(EQ 2.47)}$$

where,

R_{tot} = total daily respiration (µg dry weight d^{-1}).

The constant, γ, represents the conversion from µl oxygen to calories (Brett and Groves 1979). The constant, β_j, is the conversion from calories to µg dry weight of juvenile pollock (Harris 1985).

The new weight for an individual on day t+1 is then:

$$W_{t+1} = W_t - \alpha_j C - Rtot + sdaC \quad \text{(EQ 2.48)}$$

where,

α_j = assimilation efficiency,
sda = specific dynamic action.

The assimilation efficiency is set at 0.7 (Winberg 1956, Harris et al. 1986). The loss due to specific dynamic action is set at 0.12 times the daily consumption (Buckley and Livingston 1994).

2.3 Nutrient-Phytoplankton-Zooplankton Model

A nutrient-phytoplankton-zooplankton (NPZ) model was developed in order to include the effects of a temporally and spatially varying food source on young pollock (Fig. 2.4). This NPZ model is similar to the ecosystems process models of Frost (1987, 1993), however we are modeling a coastal area, not the open ocean as does Frost. *Neocalanus* spp. (*N. plumchrus and N. flemingerii*), the biomass-dominant copepod in the western coastal Gulf of Alaska and Shelikof Strait, is the primary grazer in the model. *Pseudocalanus*

spp. is included, as its egg, naupliar and copepodite stages form a major portion of the diet of larval pollock (Dagg et al. 1984, Kendall et al. 1987, Canino et al. 1991). Each *Pseudocalanus* stage (egg, naupliar or copepodite) is modeled with a separate equation. The NPZ model runs from DOY 70 to 165, through the spring transition period (the period when the strong winter winds which deepen the mixed layer subside, and this decrease in wind mixing energy and the increase in buoyancy due to the increase in heat and fresh water lead to increased stratification of the upper water column), and covering the time period when pollock are in the larval stage. The time step is 0.1 d. Smaller time steps were examined, and not found to change system dynamics. Parameter values for the NPZ model are shown in Table 2.2.

2.3.1 Vertical Structure

Vertically, the NPZ model has a 3-layered structure, similar to that described in Frost (1993). Three layers are (1) the homogeneously mixed layer, which varies in depth daily, (2) a vertically stratified layer extending from the bottom of the mixed layer to 100 m depth, and (3) a "bottom" layer, where the values of state variables are assumed to be fixed. A simple 2-layer model (as in Frost, 1987) with a upper mixed layer, and fixed values of nitrogen, phytoplankton and zooplankton in the lower layer, was not adequate for our purposes. Larval pollock are sometimes found below the mixed layer (Kendall et al. 1994), and the variability in vertical stratification in food, as well as currents, temperature, etc. below the mixed layer may contribute to individual differences in larval transport, growth and survival.

Calculations are done on each meter of a water column which is 100 m deep. This is necessary as the depth of the mixed layer can change each day. The upper layer in the NPZ model is homogeneously mixed. It extends from the surface to the mixed layer depth. Calculations are done on the top meter and the values at each meter of the mixed layer are set equal to that value, with all updated values mixed at the end of each time step. The second layer extends from the mixed layer depth to 100 m and is vertically stratified, ie. calculations are done and values are allowed to vary at each meter. The bottom layer, rep-

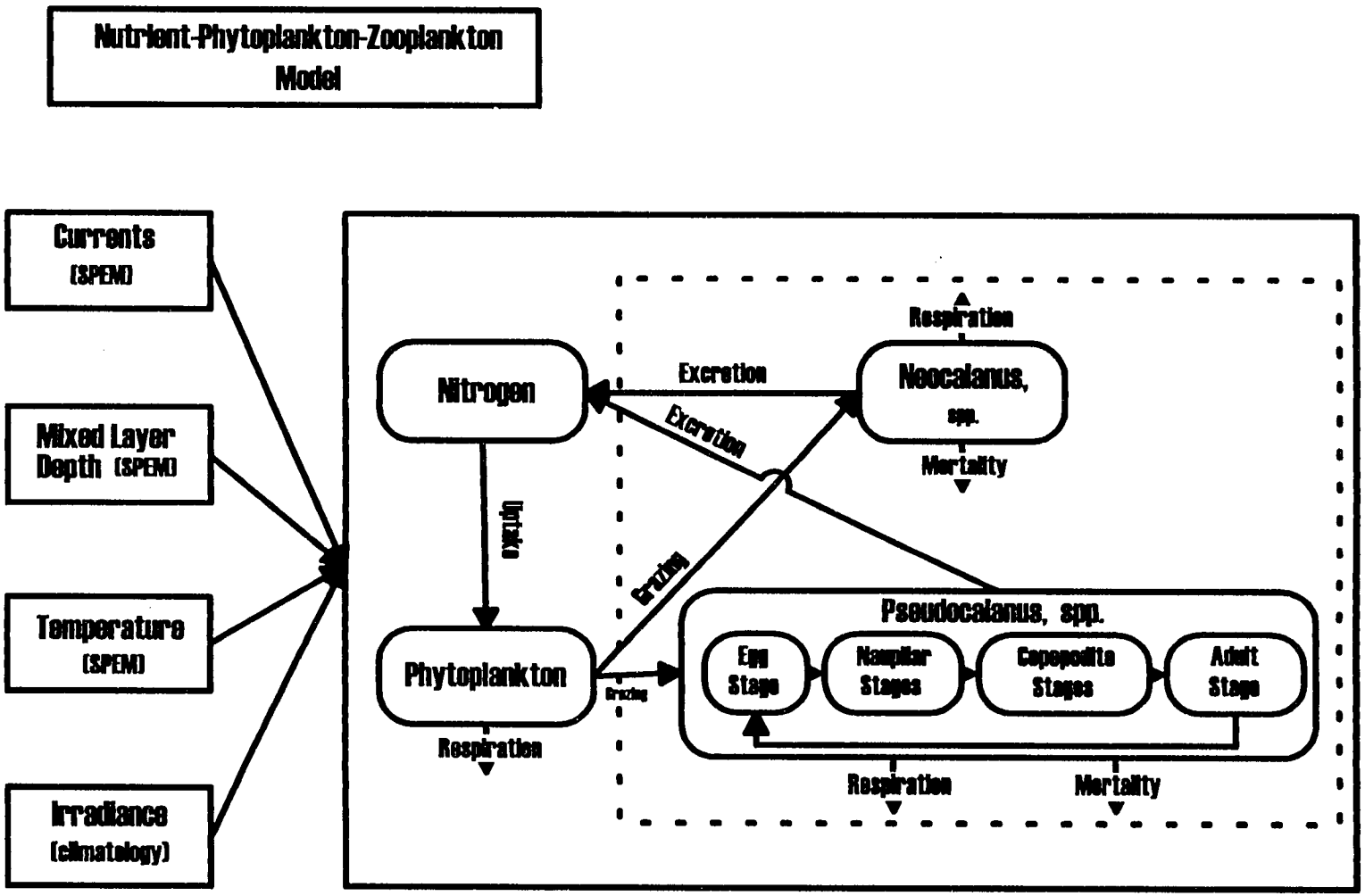

Figure 2.4. Flow chart of the nutrient-phytoplankton-zooplankton (NPZ) model. *Pseudocalanus*, spp. stages modeled are one egg stage, six naupliar stages, five copepodite stages and one adult stage.

Table 2.2. Parameters for the Nutrient-Phytoplankton-Zooplankton model.

	Parameters	Value	Source
Δt	Time step (d^{-1})	0.1	
k_{deep}	Light extinction coefficient below 70 m	0.7	Herman & Platt 1983
ξ	Nitrogen:carbon ratio (mmol N (mg C)$^{-1}$)	0.0126	Redfield et al. 1963
α	Photosynthetic efficiency (mg C(mg chl-a)$^{-1}$(Em^{-2})$^{-1}$	21.0	Frost 1993
d	Half-saturation constant for nitrogen uptake (mmol N m^{-3}) by phytoplankton	1.0	Frost 1987
γ_1	Growth efficiency for *Neocalanus*	0.522	Frost 1987[1]
m_1	Mortality rate for *Neocalanus* (d^{-1})	0.0048	1
a	Proportion of female *Pseudocalanus*	0.667	Seifert & Incze 1989
emax	Maximum number of eggs produced d^{-1} female^{-1} *Pseudocalanus*	5.0	Corkett & McLaren 1978
kv	Vertical eddy diffusivity (m^2d^{-1})	1.0	Hermann & Stabeno 1996
conv	Dryweight:carbon conversion factor	0.4	Parsons et al. 1977
c	Phytoplankton carbon:chlorophyll-a ratio	55.0	Frost 1993
e_1	*Neocalanus* maximum specific ingestion rate (mg C(mg C)$^{-1}d^{-1}$)	0.166	1
f_1	*Neocalanus* half-saturation constant for ingestion (mg C(m^3)$^{-1}$)	45.69	1
e_i $(i=5...8)$	*Pseudocalanus* naupliar maximum specific ingestion rate (mg C(mg C)$^{-1}d^{-1}$) for stage i	3.645	1
$f_i(i=5...8)$	*Pseudocalanus* naupliar half-saturation constant for ingestion (mg C(m^3)$^{-1}$)	67.31	1

Table 2.2 (cont.). Parameters for the Nutrient-Phytoplankton-Zooplankton model.

	Parameter	Value	Source
e_i $(i=9...13)$	*Pseudocalanus* copepodite maximum specific ingestion rate (mg C(mg C)$^{-1}$d^{-1})	3.478	1
f_i $(i=9...13)$	*Pseudocalanus* copepodite half-saturation constant for ingestion (mg C(m^3)$^{-1}$)	28.285	1
e_{14}	*Pseudocalanus* adult maximum specific ingestion rate (mg C(mg C)$^{-1}$d^{-1})	2.526	1
f_{14}	*Pseudocalanus* adult half-saturation constant for ingestion (mg C(m^3)$^{-1}$)	57.425	1
γ_i $(i=3...14)$	*Pseudocalanus* growth efficiency	0.192	1
m_1	*Neocalanus* mortality (d^{-1})	0.0048	1
m_2	*Pseudocalanus* egg mortality (d^{-1})	0.58	1
m_3	*Pseudocalanus* Naupliar I mortality (d^{-1})	0.545	1
m_4	*Pseudocalanus* Naupliar II mortality (d^{-1})	0.455	1
m_5	*Pseudocalanus* Naupliar III mortality (d^{-1})	0.453	1
m_6	*Pseudocalanus* Naupliar IV mortality (d^{-1})	0.313	1
m_7	*Pseudocalanus* Naupliar V mortality (d^{-1})	0.516	1
m_8	*Pseudocalanus* Naupliar VI mortality (d^{-1})	0.483	1
m_9	*Pseucalanus* Copepodite I mortality (d^{-1})	0.536	1
m_{10}	*Pseudocalanus* Copepodite II mortality (d^{-1})	0.382	1
m_{11}	*Pseudocalanus* Copepodite III mortality (d^{-1})	0.451	1
m_{12}	*Pseudocalanus* Copepodite IV mortality (d^{-1})	0.435	1
m_{13}	*Pseudocalanus* Copepodite V mortality (d^{-1})	0.543	1
m_{14}	*Pseudocalanus* Copepodite VI mortality (d^{-1})	0.59	1

[1] Optimized parameter.

resenting depths greater than 100 m, contains fixed values of nitrogen, phytoplankton and zooplankton.

Vertical exchange between layers is assumed to be a result of turbulent diffusion and the change in position of the mixed layer. As in Frost (1993), diffusion is a simple Fickian process:

$$F_z = k_v \frac{\partial C_z}{\partial z} \qquad \text{(EQ 2.49)}$$

where,

F_z = the vertical flux of a property,
k_v = vertical eddy diffusivity,
C_z = concentration of a property,
z = depth.

Changes in the concentration of a property in the mixed layer caused by vertical mixing was described using a finite approximation (forward-in-time, central-in-space):

$$\frac{\Delta C}{\Delta t} = \frac{k_v}{z_m}(C_{z_m+1} - C) \qquad \text{(EQ 2.50)}$$

where,

C = concentration in the mixed layer,
z_m = mixed layer depth (m),
C_{z_m+1} = concentration 1 m below the mixed layer.

The change in concentration for each meter of the stratified layer was calculated as:

$$\frac{\Delta C_z}{\Delta t} = k_v[C_{z-1} + C_{z+1} - (2C_z)] \qquad \text{(EQ 2.51)}$$

where,

C_z = concentration at depth z.

Eddy diffusivity (k_v) is assumed to be vertically isotropic in the stratified layer and spatially constant, and is set to a constant value, which is the same value as that used by the SPEM model (Hermann and Stabeno 1996).

2.3.2 Horizontal Structure

A horizontal (20 x 20) Eulerian grid was laid out over the area where the majority of larval pollock are usually found (Fig. 2.5). This grid is a subset of the SPEM grid. Grid points were 20 km apart. See Section 2.4.2 for a discussion of the rationale behind the choice of grid spacing.

2.3.3 Solar Radiation

Incident solar radiation, which strongly affects the production rate of phytoplankton, was derived from a climatological time series (R. Davis, Dalhousie University, Canada, pers. comm.) obtained from the National Weather Service's Kodiak, Alaska weather station (SOLMET 1979, National Renewable Energy Laboratory 1992). This time series was input to the model as a mean daily value (I_0, E m^{-2} d^{-1}).

Irradiation at depth (I_z) is calculated as:

$$I_z = I_0 e^{-kz} \qquad \text{(EQ 2.52)}$$

where,

k = attenuation coefficient (m^{-1}).

The attenuation coefficient is a linear function of chlorophyl-a concentration, as well as of the absorption by water:

$$k = 0.07 + 0.12 P_{chl-a} \qquad \text{(EQ 2.53)}$$

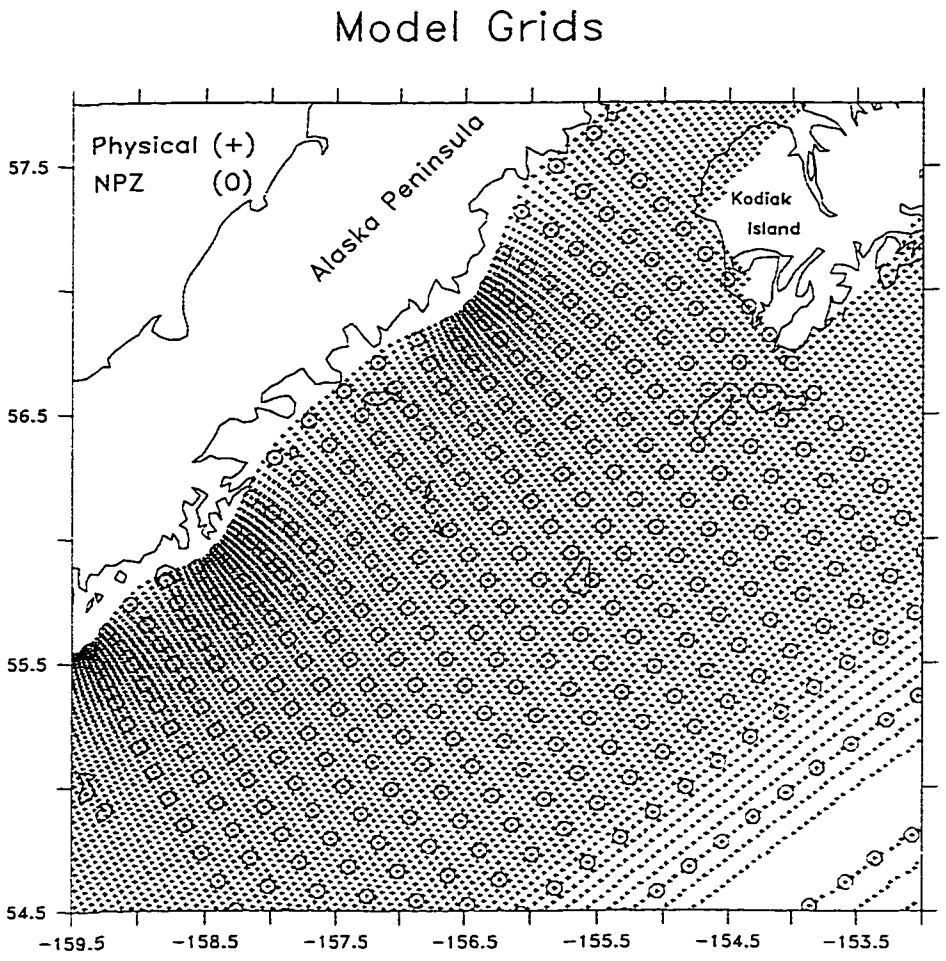

Figure 2.5. Overlay of SPEM (+) and NPZ (o) model grids. Horizontal spacing of the NPZ grid is 5x larger than the SPEM grid.

where,

$P_{chl\text{-}a}$ = chlorophyll-a concentration (mg m^{-3}).

The intercept (0.07) represents the attenuation due to absorption by seawater and other suspended particles. This formulation is taken from Herman and Platt (1983), who derived this function for a coastal shelf area similar to our study region (the Scotian Shelf). The value of k below 70 m is set to a constant ($k_{deep} = 0.07$), as levels of phytoplankton below this depth are minimal.

Photosynthetically-available solar radiation (PAR_z) is taken to be 0.5 times the irradiation at depth (Frost 1987):

$$PAR_z = 0.5 I_z \qquad \text{(EQ 2.54)}$$

No correction for cloudiness was made to PAR, as this factor has already been included in the observational time series of incident solar radiation used to drive the model.

2.3.4 Mixed Layer Depth

Dynamics of the model are significantly affected by the mixed layer depth (z_m). Mixed layer depth (MLD) for the model is derived from the vertical profile of density produced by the SPEM model for each year, day and location in the Eulerian grid. A simple algorithm is employed, where MLD is defined as that depth where the salinity field (the primary determinant of density in this region during spring) assumes a value 0.05 psu (Practical Salinity Units) greater than the surface value. This is a crude parameterization, so future circulation modeling in this region will include explicit mixed layer physics.

2.3.5 Temperature

The temperature time series was derived by horizontally averaging all CTD casts performed in the vicinity of Shelikof Strait and the Alaskan Stream during extensive hydrographic surveys conducted in March and October of 1985 (Reed et al., 1987). A time

series of runoff for 1974–1992 (T. Royer, Inst. of Mar. Sci., Univ. Alaska, Fairbanks, pers. comm.) indicates that 1985 was an average year for spring runoff . We used the horizontally averaged depth profiles for March and October as endpoints for linear interoplation according to date, to obtain the mean temperature by time and depth. Advection and diffusion of temperature proceeds over this background temperature as described for salinity in Hermann and Stabeno (1996). Mixed layer temperature was derived by averaging over the depth of the mixed layer.

2.3.6 Initial Conditions

Initial conditions for the NPZ model are derived from data collected by the FOCI program (J. Napp, Alaska Fisheries Science Center, 7600 Sand Point Way, NE, Seattle, WA 98115, pers. comm., Incze and Ainaire 1994). Most of the observations are from stations in the exit region of Shelikof Strait in April, averaged across years and stations. Information was available for all state variables, nitrogen, phytoplankton chlorophyll-a, *Neocalanus*, spp. and *Pseudocalanus*, spp. (Incze et al. 1997, Napp et al. 1996). In some cases the data were depth-integrated over the depth of sampling. In these cases, the total biomass was divided by the depth sampled, so that concentrations at all depth were set to equal values.

2.3.7 Nitrogen Equations

The equation for nitrogen in the mixed layer is:

$$N_{t+\Delta t} = N_t + \frac{\Delta N}{\Delta t} \qquad \text{(EQ 2.55)}$$

where,

$$\frac{\Delta N}{\Delta t} = -\frac{\xi}{z_m}\left[\sum_{z=0}^{z_m} P \cdot PMAX \cdot \tanh\left(\frac{\alpha PAR_z}{PMAX}\right)\left(\frac{N}{d+N}\right)\right] \qquad \text{(EQ 2.56)}$$

$$+ 0.3\sum_i\left(\frac{e_i PH_i}{f_i + P}\right) + \frac{k_v}{z_m}(N_{z_m+1} - N)$$

In the stratified layer,

$$N_{z,\,t+\Delta t} = N_{z,\,t} + \frac{\Delta N_z}{\Delta t} \qquad \text{(EQ 2.57)}$$

where,

$$\frac{\Delta N_z}{\Delta t} = -\xi\left[P_z \cdot PMAX \cdot \tanh\left(\frac{\alpha PAR_z}{PMAX'}\right)\left(\frac{N_z}{d+N_z}\right)\right] + 0.3\sum_i\left(\frac{e_i P_z H_{i,z}}{f_i + P_z}\right) \qquad \text{(EQ 2.58)}$$

$$+ k_v[N_{z-1} + N_{z+1} - (2N_z)]$$

where,

N = concentration of nitrogen (mg m^{-3}),
P = concentration of phytoplankton (mg C m^{-3}),
H_i = concentration of herbivore of species or stage i (mg C m^{-3}),
ξ = nitrogen:carbon ratio (mmol N (mg C)$^{-1}$),
z_m = mixed layer depth (m),
$PMAX$ = maximum carbon-specific growth rate (mg C (mg C)$^{-1}$ d^{-1}),
α = initial slop of photosynthesis vs. irradiance curve, photosynthetic efficiency (mg C (mg chl-a)$^{-1}$ (E m^{-2})$^{-1}$
$PMAX'$ = maximum chlorophyll-a specific growth rate (mg C (mg chl-a)$^{-1}$ d^{-1}),
d = half-saturation constant for N uptake by P (mmol N m^{-3}),
e_i = maximum specific ingestion rate (mg C (m C)$^{-1}d^{-1}$) for herbivore species or stage i,
f_i = half-saturation constant for ingestion of herbivore species or stage i (mg m^{-3}).

Values of parameters for the NPZ model are specified in Table 2.2. Nitrogen uptake by phytoplankton (photosynthetic rate) is a function of light and nutrients, and is described in the section 'Phytoplankton' (below). Regeneration of nitrogen via excretion by herbivores was taken to be 30% of the phytoplankton nitrogen ingested, described in the Zooplankton section (below). No distinction was made between the various forms of nitrogen (e.g. ammonia vs. nitrate) available.

2.3.8 Phytoplankton Equations

In the mixed layer,

$$P_{t+\Delta t} = P_t + \frac{\Delta P}{\Delta t} \qquad \text{(EQ 2.59)}$$

where,

$$\frac{\Delta P}{\Delta t} = \frac{1}{z_m}\left[\sum_{z=0}^{z_m} P \cdot PMAX \cdot \tanh\left(\frac{\alpha PAR_z}{PMAX'}\right)\left(\frac{N}{d+N}\right)\right] - \sum_i \left(\frac{e_i P H_i}{f_i + P}\right) + \qquad \text{(EQ 2.60)}$$

$$\frac{k_v}{z_m}(P_{z_m+1} - P)$$

In the stratified layer,

$$P_{z,\,t+\Delta t} = P_{z,\,t} + \frac{\Delta P_z}{\Delta t} \qquad \text{(EQ 2.61)}$$

where,

$$\frac{\Delta P_z}{\Delta t} = \left[P_z \cdot PMAX \cdot \tanh\left(\frac{\alpha \cdot PAR_z}{PMAX'}\right)\left(\frac{N_z}{d+N_z}\right)\right] - \sum_i \left(\frac{e_i P_z H_{i,z}}{f_i + P_z}\right) \qquad \text{(EQ 2.62)}$$

$$+ k_v[P_{z-1} + P_{z+1} - (2P_z)]$$

Chlorophyll-a specific photosynthetic rate as a function of photosynthetically active radiation (PAR) and temperature was derived as follows:

$$mgC(mgchl-a)^{-1}d^{-1} = PMAX\tanh\left(\frac{\alpha PAR_z}{PMAX'}\right) \qquad \text{(EQ 2.63)}$$

$PMAX'$ is derived from $PMAX$, the maximum carbon-specific photosynthetic rate:

$$PMAX' = cPMAX \qquad \text{(EQ 2.64)}$$

where c = phytoplankton C: chl-a ratio.

PMAX uses the temperature-dependent doubling rate of phytoplankton:

$$D = 0.851(10)^{0.0275\theta} \quad \text{(Eppley 1972)} \qquad \text{(EQ 2.65)}$$

where,

D = doublings d^{-1},
θ = temperature (°C).

This was adjusted for the number of hours of daylight (*DL*) and related to D as:

$$PMAX = (e^{D\ln 2} - 1.0)\frac{DL}{24} \qquad \text{(EQ 2.66)}$$

where, $DL = f(latitude, DOY)$.

The effect of nutrient (nitrogen) limitation on the photosynthetic rate is modeled simply as $\frac{N}{d+N}$. Ingestion by all grazers (*Neocalanus*, spp. and all stages of *Pseudocalanus*, spp.) is modeled as a Michaelis-Menton type functional feeding response.

2.3.9 *Neocalanus* Equations

The dynamics of populations of the biomass-dominant grazer, *Neocalanus*, spp., (representing the species *N. plumchrus* and *N. flemingerii*, Seifert and Incze 1989), is aggregated, with no stage structure included (ie. the total population biomass is modelled). In the mixed layer,

$$H_{1,\,t+\Delta t} = H_{1,\,t} + \frac{\Delta H_1}{\Delta t} \qquad \text{(EQ 2.67)}$$

where,

$$\frac{\Delta H_1}{\Delta t} = H_1\left(\frac{\gamma_1 e_1 P}{f_1 + P} - m_1\right) + \frac{k_v}{z_m}(H_{1,z_m+1} - H_1) \qquad \text{(EQ 2.68)}$$

In the stratified layer,

$$H_{1,z,t+\Delta t} = H_{1,z,t} + \frac{\Delta H_{1,z}}{\Delta t} \qquad \text{(EQ 2.69)}$$

where,

$$\frac{\Delta H_{1,z}}{\Delta t} = H_{1,z}\left(\frac{\gamma_1 e_1 P_z}{f_1 + P_z} - m_1\right) + k_v[H_{1,z-1} + H_{1,z+1} - (2H_{1,z})] \qquad \text{(EQ 2.70)}$$

where,

γ_1 = growth efficiency for *Neocalanus*,
m_1 = mortality rate for *Neocalanus* (d^{-1}).

A Michaelis-Menton type functional feeding response is assumed for *Neocalanus*.

2.3.10 *Pseudocalanus* Equations

Pseudocalanus, spp. in this model represents the species *P. newmanii, P. mimus* and *P. minutus*, all members of the springtime zooplankton community in Shelikof Strait (Seifert 1994). Eggs, nauplii and copepodites of *Pseudocalanus*, spp. form the basis of the diet of larval pollock. The proportion of each stage eaten by a larval pollock varies with larval length (Kendall 1987). For that reason, the dynamics of the thirteen stages of *Pseudocalanus* (the egg stage, 6 naupliar stages, and 6 copepodite stages) were modeled separately. H_2 is the egg stage, H_3 - H_8 are the naupliar stages, and H_9 - H_{14} are the copepodite stages, with the last copepodite stage (C_6) representing adults.

The Egg Stage

In the mixed layer,

$$H_{2,\,t+\Delta t} = H_{2,\,t} + \frac{\Delta H_2}{\Delta t} \qquad \text{(EQ 2.71)}$$

where,

$$\frac{\Delta H_2}{\Delta t} = aEH_{14}\frac{dwt_2}{dwt_{14}} - H_2(-t_2 + -m_2H_2) + \frac{k_v}{z_m}(H_{2,\,z_m+1} - H_2) \qquad \text{(EQ 2.72)}$$

In the stratified layer,

$$H_{2,\,z,\,t+\Delta t} = H_{2,\,z,\,t} + \frac{\Delta H_{2,\,z}}{\Delta t} \qquad \text{(EQ 2.73)}$$

where,

$$\frac{\Delta H_{2,\,z}}{\Delta t} = aEH_{14,\,z}\frac{dwt_2}{dwt_{14}} - H_{2,\,z}(-t_2 + m_2H_{2,\,z}) + k_v[H_{2,\,z-1} - H_{2,\,z+1} - (2H_{2,\,z})] \qquad \text{(EQ 2.74)}$$

where,

a = proportion of females,
E = number of eggs produced female^{-1} d^{-1},
dwt_2 = dry weight egg^{-1} (µg),
dwt_{14} = dry weight adult^{-1} (µg),
t_2 = hatching rate of eggs (d^{-1}).

The percent females in the adult population (a) is set at 0.667. This is estimated from springtime data in Shelikof Strait, for example as described in Siefert and Incze (1989). E is a function relating daily egg production by a female to food density as follows. The maximum daily egg production for a female, *emax*, is set at 5 eggs d^{-1} (Corkett and McLaren 1978). When phytoplankton carbon is greater than 200.0 mg m^{-3}; *er*, the frac-

tion of *emax* produced per day is set equal to 1.0. If phytoplankton carbon is less than 200.0 mg m^{-3},

$$er = 0.005P \qquad \text{(EQ 2.75)}$$

Then,

$$E = er \cdot emax \qquad \text{(EQ 2.76)}$$

The conversion factor between carbon and dry weight, *conv* = 0.4 mg C(mg dry weight)$^{-1}$ (Parsons et al. 1977). The hatch rate of eggs, t_2, is set equal to the inverse of the incubation period (dur_2), ie. the proportion transferring out of the egg stage per day.

$$dur_2 = 1845.0(\theta + 11.45)^{-2.05} \qquad \text{Corkett and McLaren 1978} \qquad \text{(EQ 2.77)}$$

Hatching, as an approximation, is assumed to occur continuously, rather than in discreet events for each individual.

Nonfeeding Stages

The naupliar stages N1 (H_3) and N2 (H_4) do not feed. The equations for these stages are as follows. For these stages in the mixed layer,

$$H_{i,\,t+\Delta t} = H_{i,\,t} + \frac{\Delta H_i}{\Delta t} \qquad \text{(EQ 2.78)}$$

where,

$$\frac{\Delta H_i}{\Delta t} = (t_{i-1}H_{i-1}) - H_i(t_i + m_iH_i) + \frac{k_v}{z_m}(H_{i,\,z_m+1} - H_i) \qquad \text{for } (i = 3, 4). \qquad \text{(EQ 2.79)}$$

In the stratified layer,

$$H_{i,\,z,\,t+\Delta t} = H_{i,\,z,\,t} + \frac{\Delta H_{i,\,z}}{\Delta t} \qquad \text{(EQ 2.80)}$$

where,

$$\frac{\Delta H_{i,z}}{\Delta t} = (t_{i-1}H_{i-1,z}) - H_{i,z}(t_i + m_i H_{i,z}) + k_v(H_{i,z+1} - H_{i,z-1} + 2H_{i,z}) \quad \text{(EQ 2.81)}$$

for ($i = 3, 4$).

where, H_i = concentration of stage i in the mixed layer.

The transfer coefficient, t_i is set equal to the inverse of the stage duration (dur_i), which is a multiple of the incubation period (Corkett and McLaren 1978):

$$dur_3 = 0.18(dur_2) \quad \text{(EQ 2.82)}$$

$$dur_4 = 0.37(dur_2) \quad \text{(EQ 2.83)}$$

Feeding Stages

Naupliar stages N3 - N5 (H_5 - H_8) and the copepodite stages C1 - C6 (H_9 - H_{14}) include a feeding function. In the mixed layer,

$$H_{i,t+\Delta t} = H_{i,t} + \frac{\Delta H_i}{\Delta t} \quad \text{(EQ 2.84)}$$

where,

$$\frac{\Delta H_i}{\Delta t} = (t_{i-1}H_{i-1}) + H_i\left(\frac{\gamma_i e_i P}{f_i + P} - m_i H_i - t_i\right) + \frac{k_v}{z_m}(H_{i,z_m+1} - H_i) \quad \text{(EQ 2.85)}$$

for ($i = 5...14$).

In the stratified layer,

$$H_{i,z,t+\Delta t} = H_{i,z,t} + \frac{\Delta H_{i,z}}{\Delta t} \quad \text{(EQ 2.86)}$$

where,

$$\frac{\Delta H_{i,z}}{\Delta t} = (t_{i-1}H_{i-1,z}) + H_{i,z}\left(\frac{\gamma_i e_i P_z}{f_i + P_z} - m_i H_{i,z} - t_i\right) + \quad \text{(EQ 2.87)}$$

$$k_v(H_{i,z+1} - H_{i,z-1} + 2H_{i,z})$$

A Michaelis-Menton type functional feeding response is assumed for *Pseudocalanus*. As before, the transfer coeffient, t_i, is set to the inverse of the stage duration, which is calculated as follows:

$$dur_5 = 1.46(dur_2) \quad \text{(EQ 2.88)}$$

$$dur_6 = 0.81(dur_2) \quad \text{(EQ 2.89)}$$

$$dur_7 = 0.69(dur_2) \quad \text{(EQ 2.90)}$$

$$dur_8 = 0.4(dur_2) \quad \text{(EQ 2.91)}$$

$$dur_9 = 1.23(dur_2) \quad \text{(EQ 2.92)}$$

$$dur_{10} = 1.0(dur_2) \quad \text{(EQ 2.93)}$$

$$dur_{11} = 0.98(dur_2) \quad \text{(EQ 2.94)}$$

$$dur_{12} = 1.02(dur_2) \quad \text{(EQ 2.95)}$$

$$dur_{13} = 1.32(dur_2) \quad \text{(EQ 2.96)}$$

$$dur_{14} = 8.0(dur_2) \quad \text{(EQ 2.97)}$$

2.3.11 Parameter Optimization

Some of the least well known parameters in the NPZ model were optimized (Table 2.2), using the first two steps of the Monte Carlo procedure described in Section 2.5.6. (Sensitivity Analysis) on a one-dimensional version of the NPZ model (which included the vertical dimension, but not the horizontal). In the optimization, first, a specified number of random sets (n = 1000) of model input parameters are drawn from a triangular distribution using the Latin Hypercube technique (McKay et al. 1979), and second, each set is used for a single model run generating a set of output variables (Table 2.3). Acceptable sets of parameters were defined as those which resulted in model output variables which fell within the range of observed data. Other sets of parameters were discarded. Of the acceptable sets of parameters, the best-fitting was chosen as the optimized parameter.

2.4 Model Coupling

In this section we describe possible methods of coupling the SPEM, IBM and NPZ models. Since models are not run concurrently (see below and Fig. 2.6 and Fig. 2.7), we describe the pairwise coupling methods considered and those we chose. To reiterate briefly, the SPEM model is deterministic, the IBM is stochastic and the NPZ model is deterministic. The method of coupling which was finally decided on, was to run the SPEM model first and store the results; then to run the NPZ model with SPEM velocity, mixed layer depth and temperature as driving variables; then, lastly, to run the IBM, perhaps multiple times, using output from the SPEM and NPZ models. Following are justifications for this method.

2.4.1 IBM-SPEM Coupling

Several possibilities exist for coupling a circulation model with a stochastic IBM:

Table 2.3. Output of NPZ model used in optimization

Name	Description	Min. Value	Max. Value
Pchlorapr17	Phytoplankton chlorophyll-a (mg m^{-3}) on 4/17	0.5	3.0
Pchlormay8	Phytoplankton chlorophyll-a (mg m^{-3}) on 5/8	5.0	20.0
Pchlormay30	Phytoplankton chlorophyll-a (mg m^{-3}) on 4/17	3.0	6.0
NCapr16	*Neocalanus*, spp. density (mg m^{-3}) on 4/16	0.5	10.0
NCapr26	*Neocalanus*, spp. density (mg m^{-3}) on 4/26	0.5	10.0
NCmay3	*Neocalanus*, spp. density (mg m^{-3}) on 5/3	0.5	15.0
NCmay10	*Neocalanus*, spp. density (mg m^{-3}) on 5/10	1.0	35.0
NCmay19	*Neocalanus*, spp. density (mg m^{-3}) on 5/19	15.0	85.0
naupapr16	*Pseudocalanus* naupliar density (no. m^{-3}) on 4/16	3000	15000
naupmay3	*Pseudocalanus* naupliar density (no. m^{-3}) on 5/3	12000	30000
naupmay10	*Pseudocalanus* naupliar density (no. m^{-3}) on 5/10	20000	50000
adapr16	*Pseudocalanus* adult density (no. m^{-3}) on 4/16	15	150
admay3	*Pseudocalanus* adult density (no. m^{-3}) on 5/3	50	250
admay10	*Pseudocalanus* adult density (no. m^{-3}) on 5/10	30	300
admay19	*Pseudocalanus* adult density (no. m-3) on 5/19	100	650

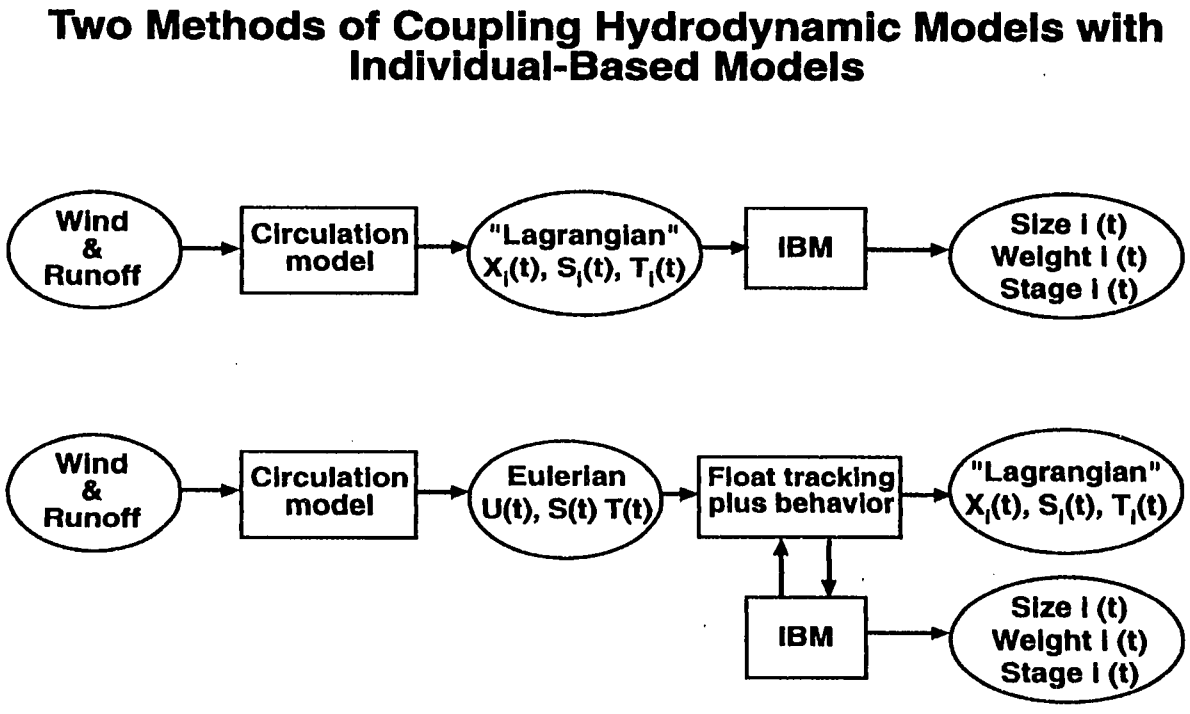

Figure 2.6. Two schemes for implementing a probabilistic Lagrangian biophysical model of the early life stages of marine fish. The upper diagram represents scheme (iii) described in the text. The lower diagram represents scheme (iv) described in the text. $[.]_i(t)$ refers to the value of some physical or biological quantity associated with individual i.

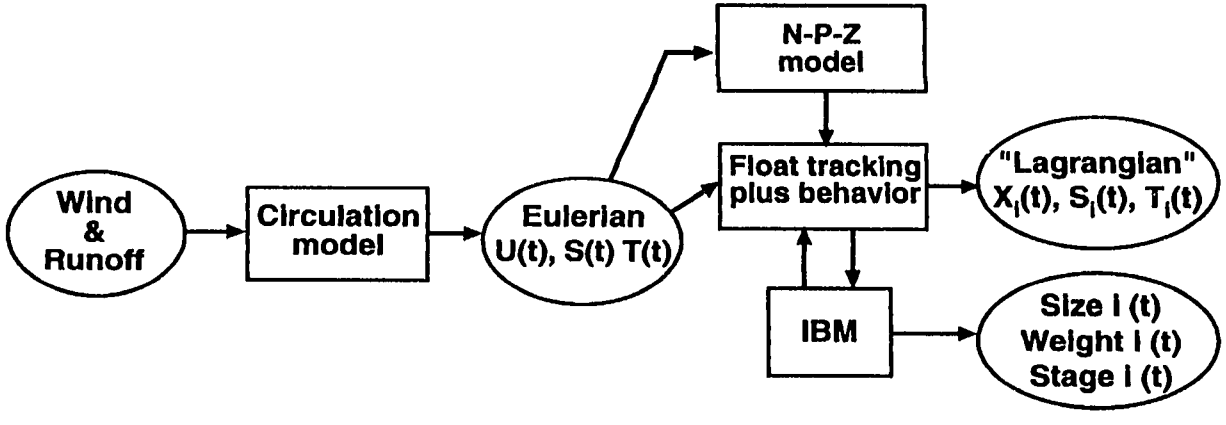

Figure 2.7. Summary of coupling between SPEM, NPZ and IBM models.

(i) Run the hydrodynamic and individual-based models in parallel, updating individual positions in the IBM at each new time step of the hydrodynamic model. Run the combined SPEM-IBM model many times, one for each realization of the IBM.

(ii) Run the hydrodynamic and individual-based models in parallel just once, computing all realizations of the IBM simultaneously.

(iii) Run the hydrodynamic model once, tracking a number of passive floats whose initial position correspond to initial organism concentrations in the model domain. Store the resulting Lagrangian series of position, temperature, salinity, etc. for later use by an IBM without any further spatial tracking (Fig 2.6, top).

(iv) Run the hydrodynamic model once, storing all relevant gridded velocity, temperature and salinity fields at each model gridpoint and time step, for subsequent use by an IBM which performs its own spatial tracking (Fig. 2.6, bottom).

All approaches have both advantages and drawbacks. Method (i) is at present computationally prohibitive for most three-dimensional hydrodynamic models, as it requires a potentially large number of runs. Method (ii) reduces computation of the physical model, but requires huge amounts of computer memory to keep track of all the biological realizations simultaneously. Method (iii) is efficient and allows for many individuals, but eliminates the possibility of adding individual behaviors (in particular, vertical locomotion) which vary as a function of the individual's unique, partly random life history. In other words, any realization of the IBM in Method (iii) cannot feed back on the float tracks, which are determined by the hydrodynamic model alone. Method (iv) offers the possibility of feedback, but requires potentially huge amounts of data storage to accomodate the three-dimensional circulation model output. Hence we propose a modification of Method (iv):

(iv-a) Run the hydrodynamic model once, storing suitably low-pass filtered (high-frequencies removed), decimated time series of all relevant gridded velocity, temperature,

and salinity fields at each model gridpoint, for subsequent use by an IBM which performs its own spatial tracking.

The characteristics of the filter used in Method (iv-a), and the interval for subsampling depend on what portion of the full spectrum of fluid motion is considered "expendable" for purposes of spatial tracking. For example, time-filtering would introduce a bias if locomotion of individuals were somehow correlated with higher frequency current fluctuations (for example, swimming in response to tides or internal waves), that had been removed. In general, primitive equation hydrodynamic model output contains far less energy at superinertial frequencies than is observed in real oceanographic measurements, and such fluctuations that do exist in the model are poorly correlated with the real data. Nevertheless, subsampling without filtering, while partially adequate for spatial tracking, could lead to serious aliasing errors when much high frequency energy is present. We suggest filtering be done to eliminate this poorly correlated high frequency energy band, but retain signifigantly correlated subinertial motions. The significance of tides is context-dependant, and needs to be considered carefully.

Consider how spatial tracking in Method (iv-a) might be efficiently accomplished with the filtered fields, and whether any of the information lost in the filtering process might be added back in by the tracking algorithm. Neutrally buoyant floats have been tracked in many numerical ocean models. Instantaneous float velocities are generally derived by interpolating between gridpoints to the current location of each float. Generally, the floats are advanced in time using the same time step as is used for solving the governing hydrodynamic equations, but this need not be the case, and especially not in our situation where previously stored, filtered velocity fields are used. How, then, to choose a time step for float tracking which is sufficiently short but not computationally prohibitive? One requirement for successful float tracking is that the Lagrangian decorrelation time, T_L, be much longer than the time step, dt, used for float tracking:

$$T_L >> \Delta t \qquad \text{(EQ 2.98)}$$

The property T_L is defined as follows. When moving within a turbulent flow field, particle velocities eventually become decorrelated from their starting velocities. This loss of "memory" can be characterized by the integral of the lagged correlation function:

$$T_L = \int_0^\infty R(\tau)d\tau \qquad \text{(EQ 2.99)}$$

where,

$$R(t) = \frac{1}{\overline{u'u'}}\left[\frac{1}{Tmax}\int_0^{Tmax} u_i'(t)u_i'(t+\tau)d\tau\right] \qquad \text{(EQ 2.100)}$$

Here $u'u'$ is the mean turbulent kinetic energy of the flow, $u'_i(t)$ is the velocity of the particle i at time t, $Tmax$ is a suitably long time used for averaging, and [] denotes an ensemble mean over all particles.

When Eq. 2.98 is satisfied, the moving float (individual) can be reasonably approximated to travel at constant velocity for a period of time which is longer than the time between updates of the velocity field used for tracking. When this is not the case, float tracks will diverge from "true" particle paths. Haidvogel (1982) has also demonstrated that adequate spatial resolution is crucial for accurate float tracking. With overly coarse resolution, nonlinear interactions present in the hydrodynamic equations will be improperly represented and floats will diverge from their true path as a result.

We generally expect time-filtering of velocities to increase T_L. This is helpful in allowing a longer time step for tracking, as well as reducing the size of the velocity file, if the higher-frequency variability can be reasonably sacrificed. If tides are a critical aspect of the individual's life history, there may be no easy way to avoid using unfiltered velocities, and a short tracking time step. However, some information about tides could be stored in compact form (amplitude and phase) for later use. Such reconstructed tidal velocities could be added to filtered (subtidal) velocity fields directly in the tracking algorithm, potentially reducing storage requirements.

With these considerations in mind, our scheme for coupling the models has evolved. Simulation 1 (Section 2.5.1) used only the physical model, and in it, we compare float trajectories using "direct" float tracking, with filtered and decimated velocities, in order to assess the proper time step and performance of this method, for use when coupling the biological and physical models. In Simulation 2 (Section 2.5.2), an early simulation, the biological and the physical models are run separately, with Lagrangian output from the hydrodynamic model driving processes in the biological model, as described in Method (iii). For the rest of the simulations, a dynamic coupling was implemented, as described in Method (iv-a). The dynamic approach allowed the addition of individual fish behavior which could affect the movement of the floats. This dynamic coupling operates in the following manner (Fig. 2.6, bottom). First, the SPEM model is run with a particular physical forcing scenario (winds, fresh-water input and boundary conditions). The model generates output once per day which includes low-pass filtered (half-power point = 36 hr) velocity vectors and environmental variables (e.g. temperature and salinity) at each grid point. (Low-pass filtering removes the highest frequencies; the half-power point is the frequency at which only half of the energy of the signal is returned.) The IBM is then run. Individual fish (or groups of fish) are assigned to "floats" inserted into the physical model domain at the time and place where each egg is spawned. Once per hour (Δt_c = 1 hr), the location, temperature and salinity are updated for each individual. Locations are based on both vertical and horizontal histories. Individual depth histories are required as current shear in the water column means that water at one depth may be moving in a different direction than water at another depth. This means that individuals (floats) at different depths may travel in significantly different directions. Furthermore, water properties such as temperature or salinity vary with depth, so that the vertical, as well as the horizontal path taken by an individual will determine the physical environment that it has been exposed to. This history will be integrated by an individual, resulting in a particular pattern of, for example, growth. The method of determination of the depth of an individual depends on its life stage, as vertical distribution or migration patterns differ depending on whether it is an egg, yolk-sac larva, feeding larva, or juvenile.

2.4.2 NPZ-SPEM Coupling

The characteristic length and time scales of biological properties are strongly influenced by the corresponding scales of their physical environment, but are not always identical to them. Ideally, we would like to resolve both fields so finely in space and time that all relevant scales are included, but this is rarely possible due to the computer cost involved. As a compromise, we chose different horizontal and vertical scales for the Eulerian physical and biological (NPZ) models. For NPZ dynamics, we generally require a finer vertical scale than for the physical model, due to the sensitivity of primary production to changes in mixed layer depth. This entails a sacrifice of horizontal resolution. The characteristic size of mesoscale eddies (which are features we believe affects larval survival and growth) in the vicinity of Shelikof Strait suggests a horizontal spacing of ~12 km as a desirable goal, as this is the average radius of an eddy. We should note, however, that the useful resolution for our NPZ model is fundamentally dependant on the characteristic scales of the *modeled* circulation, rather than the characteristic (and typically finer) scales of the circulation itself. As a first attempt, we chose to use a grid for the NPZ model with 1 meter resolution in the vertical, and 20 km resolution (5x the physical model) in the horizontal (Fig. 2.5), as mesoscale features in the modeled circulation tend to be somewhat larger than in the actual circulation. Vertical coverage is from 0 to 100 m depth. Background vertical diffusivities in the NPZ model were set at 10^{-5} m^2s^{-1}.

As with the IBM, we used time-filtered, stored output from the physical model as input to the NPZ model (Fig. 2.7). Time-filtered barotropic streamfunction output from the physical model is subsampled to the grid of the NPZ model. The horizontal gradients of the barotropic streamfunction, divided by the water column depth (or by 100 m in regions of deeper bathymetry), yields averaged velocities at each horizontal location. These are used to calculate the horizontal divergence and, subsequently, the vertical velocities. This approximation distorts the true vertical shear and vertical velocities, but avoids spurious (and potentially very large) convergence which typically results from subsampling a full three-dimensional velocity field. Errors in the computed vertical velocity field are likely

not too significant for the present case. Vertical upwelling of nutrients strongly affects production in some parts of the ocean, but in the Gulf of Alaska, downwelling predominates during most of the year. Horizontal advection and mixed layer deepening are hence the more significant sources of nutrients to feed production in this area.

Since we have used stored, time-filtered and decimated streamfunction fields to drive the NPZ model, we must consider the effects of that filtering on the prey dynamics. Float tracking experiments suggest an acceptable loss of temporal information for our rigid lid circulation model with no tides (see Results, Simulation 1). The effect of varying spatial resolution on the NPZ fields depends on the magnitude of the advection terms, relative to the local nonconservative (biological) dynamics. If biological dynamics predominate over advective change, then coarse resolution of the advective terms is a permissible compromise. We may ultimately be able to invoke spatially dependent diffusivities, to partially compensate for the loss of spatial resolution. In Shelikof Strait, biological components with the fastest turnover times (phytoplankton in our NPZ model) will be the least sucepitible to aliasing from the choice of a coarse spatial grid, while those with longer turnover times will be most affected. Napp et al. (1996) have demonstrated that advection may play a large role in determining the spatial patterns of phytoplankton and zooplankton observed in Shelikof Strait. Future iterations of our coupled SPEM-NPZ models will examine the consequences of decreasing the spatial scale.

The NPZ model domain is a subset of the physical model, and needs boundary conditions for each of its biological variables. In the interior, the balance of Eq. 1.1 holds, and separating out the spatial terms yields:

$$B_t[x, y, z, t] = -u^h \bullet \nabla^h B + \nabla^h \bullet (k^h \nabla^h B) - wB_z + (k^z \nabla B)_z + f_{biol}[B, x, y, z, t] \qquad \text{(EQ 2.101)}$$

where B is an NPZ model variable (e.g. Phytoplankton), ∇^h is the horizontal gradient operator, u^h, v^h, and k^h are the horizontal velocities and eddy diffusivity, w is the vertical velocity, k^z is the vertical eddy diffusivity and f_{biol} represents all nonconservative biologi-

cal dynamics. Perfect knowledge of upstream values would permit direct specification of B at the upstream boundary; instead, we are limited to several springtime measurements per year taken 7 km apart along a transect across the lower exit region of Shelikof Strait (Napp et al. 1996, Incze and Ainaire 1994, Incze et al. 1997). We therefore provide values at the upstream end by running the model in one-dimensional mode (no advection or horizontal diffusion) at those locations:

$$B_t[x, y, z, t] = -wB_z + (k^z \nabla B)_z + f_{biol}[B, x, y, z, t] \qquad \text{(EQ 2.102)}$$

Boundary values computed using Eq. 2.102, above are advected into the interior, driven by the velocity field and the horizontal gradient term of Eq. 2.101. Eq. 2.102 may be thought of as a dynamically consistent interpolator of boundary values. At the downstream boundary, a zero gradient was imposed for all biological variables:

$$B_x[x, y, z, t] = 0 \qquad \text{(EQ 2.103)}$$

2.4.3 IBM-NPZ Coupling

Some of the issues discussed above for the proper application of stored circulation fields to the IBM hold for the application of the Eulerian biological NPZ fields as well. Ideally, we could interpolate perfectly accurate Eulerian prey values onto the location and time of the tracked individuals of the Lagrangian IBM. In practice, we must settle for statistically correct prey fields, driven in part by the statistically correct velocity fields from the physical model. The mapping of prey values to individual fish locations is straightforward, and is performed in the IBM using simple linear interpolation of NPZ model output in time and space.

It should be noted that the coupling between the IBM and the NPZ models, in this scheme, is unidirectional. There is no density-dependant effect of larval fish on their prey. This was rationalized based on the idea that larval fish in the ocean are probably too dilute to substantially affect the abundance of their prey. Future versions of the model will probably test this assumption by implementing a bidirectional coupling.

Boundary conditions for the IBM are presently as follows: (1) When an individual is located outside the NPZ model domain, we apply the prey values of the NPZ boundary point nearest that individual's present location. (2) When an individual is advected outside the finely resolved circulation model domain, it is removed from the population. We also trap individuals at the downstream (southwestern) end of the physical domain, to prevent their re-entrance at the upstream end.

2.5 Simulation Experiments

The following section describes six simulation model experiments which were conducted with several objectives in mind. Some of the simulations (1, 2 and 3) were initially done to test aspects of model development and issues that arose therein. Simulation 2 (Lagrangian factors) was done to assess the effect of the modelled variation in physical factors on biological outcomes. Simulation 4, (Hindcasts) was done to both compare model output with data and assess its performance, and assess the impact of physical driving variables such as wind and freshwater runoff on biological state variables. Simulation 5, the spawning experiment, was designed to examine specific questions about the timing and location of spawning. Simulation 6, the sensitivity analysis, was done to assess the performance and importance of our formulation of the effects of turbulence on growth and survival of the early life stages.

2.5.1 Simulation 1. Float-tracking experiments.

This simulation compared float-tracking with pre-stored, filtered and decimated (subsampled in time) velocity fields, versus "direct" tracking with the unfiltered field, using modeled 1987 currents. Details of SPEM forcing for 1987 are described in Hermann et al. (1996b). Ten floats are tracked using the instantaneous velocity produced by the SPEM model at each time step with a 4th-order Runge-Kutta scheme. The time step in the SPEM model is 0.0375 hr. We refer to this as case (a). Interpolation of velocities between model gridpoints is performed as described in Hofmann et al. (1991). This entails linear interpo-

lation in the horizontal, and spectral (here, Chebyshev) expansion in the vertical. Initial positions span a northwest-southeast line between the Alaska Peninsula and the northwest corner of Kodiak Island, and 40 m depth.

We then show tracks of floats from the same initial positions tracked with pre-stored, filtered and decimated velocity fields. These experiments would correspond to case (iv-a) described in Section 2.4.1. The velocity fields are produced by applying a 30-hour low-pass filter to the original model time series during execution of the run, and storing the filtered result once per day. This filtering process eliminates all of the near-inertial, internal wave oscillations. **We would like to see if accurate float tracking can be achieved with time steps longer than the 0.0375 hr of the "direct", unfiltered method, and whether the resulting tracks compare favorably with those derived using the unfiltered method.** Float tracking is done using three different values of the time step: (b) dt = 1 hr, (c) dt = 0.2 hr, and (d) dt = 0.04 hr. Linear interpolation in time is used to provide velocity values in between the stored daily values. Spatial interpolation is performed as described above. In each case, floats are seeded at the same locations and depths as in case (a).

2.5.2 Simulation 2. The importance of Lagrangian factors.

The goal of this simulation was to examine how the addition of spatial information, in the form of a Lagrangian time series of abiotic factors, affects the outcome of the IBM. In this simulation, the hydrodynamic model was run once, with float tracking occurring simultaneously. The floats, whose initial positions correspond to initial organism concentrations in the model domain, were completely passive in this simulation. An array of 50 floats was tracked for 45 d (DOY 105 to 150) directly within the hydrodynamic model run (case (iii) in Section 2.4.1). Lagrangian time series of salinity are recorded for each float. These salinity values were converted to temperatures using a linear temperature-salinity relationship appropriate to the upper ocean at this locale and time.

An ensemble of 80,000 individuals was divided equally among the floats, thus, 1600 individuals utilize each of the 50 Lagrangian time series ("Lagrangian T" experiment). This is

equivalent to 1600 independent runs of the biological model, each starting with the same spatial array of 50 individuals and a different random number seed (the hydrodynamic model is deterministic). In the biological IBM, all 80,000 individuals are tracked separately through the larval stage, until such time as each becomes a juvenile. This version of the IBM used constant mortality rates for each life stage and no "superindividual" scheme. Consumption was a function of weight and temperature as described in Eq. 2.19, ie. the model included no effect of spatially varying prey density. In this version of the IBM, temperature affects egg development rate, yolk-sac stage duration, and the consumption and metabolic rates in the feeding larval stage. The simulation begins on DOY 90; temperatures and locations at DOY 105 are used for the period of DOY 90 to 105 as the physical model output begins at DOY 105 to allow more time for proper spinup of the wind- and buoyancy-driven velocity field (the physical spinup begins on DOY 1). Individuals which are still larvae beyond DOY 150 continue to utilize the temperature at DOY 150 until they reach the juvenile stage. Both length and weight of all individuals are updated at each time step in the simulation.

In contrast to the "Lagrangian" experiment, a second set of 80,000 individuals is subjected in the IBM to temperatures held constant at T = 3°C ("Constant T" experiment). A third set of 80,000 individuals is subjected to temperatures which increase linearly from 3°C to 6°C over the 45 d simulation period ("Linear T" experiment), as a proxy for seasonal warming in a spatially homogenous environment.

2.5.3 Simulation 3. The importance of vertical location.

The goal of the third simulation was to test whether the addition of complex algorithms to predict the depth of individual fish (ie. those described in Sections 2.2.1, 2.2.2. and 2.2.3., "Depth") cause significant changes in the horizontal trajectories of individuals when compared to the trajectories derived via the use of a simpler scheme to predict depth (an average depth for each stage for all individuals). These complex depth prediction algorithms are a major component of the method that we have used to couple the biological and physical models. We also examine whether the trajecto-

ries for particular individuals resulting from changes in vertical location yielded significantly different growth histories, due to the different histories of exposure to temperature or salinity, versus those resulting from use of an average depth for each life stage. The version of the IBM used in this simulation was the same as that used for Simulation 2, described above. In this simulation, temperature affects egg development rate, yolk-sac stage duration, and the consumption and metabolic rates in the feeding larval stage, and salinity affects egg density and vertical movement. Again, prey is considered spatially uniform.

Two IBM model runs were done. For both simulations, the hydrodynamic model was run once, and the velocity, temperature and salinity output at each model gridpoint was stored every 15 d. In this early simulation, we had not yet developed the use of filtered velocity fields. The consequence of using velocity fields stored at 15 d intervals would be to underestimate the difference between the trajectories of floats for the two IBM runs. This is due to the fact that we are missing the time variability of the vertical shear, which itself varies horizontally. A 10 x 10 grid representing spawning locations was set up (Fig. 2.8) and used for both runs. Thirty floats (individuals) were released from each grid point on DOY 90 at 200 m depth for a total of 3000 individuals per run. The duration of this simulation was 140 d. The two model runs differed as follows. For the "null" model, eggs were constrained to remain at 200 m, yolk-sac larvae at 100 m, and feeding larvae at 40 m. These are average depths for each life stage derived from field observations (Kendall et al. 1994). For the "alternative" model, vertical location in the water column at each time step varied as described in Sections 2.2.1., 2.2.2., and 2.2.3, "Depth". Mortalities for these runs were set to zero so that the smaller numbers of floats could be followed (the superindividual scheme was not used here).

2.5.4 Simulation 4. Hindcasts.

A series of IBM model runs was done for different years (1978, 1987, 1988, 1989 and 1991) with the goal of comparing model output versus FOCI field data for the distributions of the different life stages, and size distributions of larvae. As these years dif-

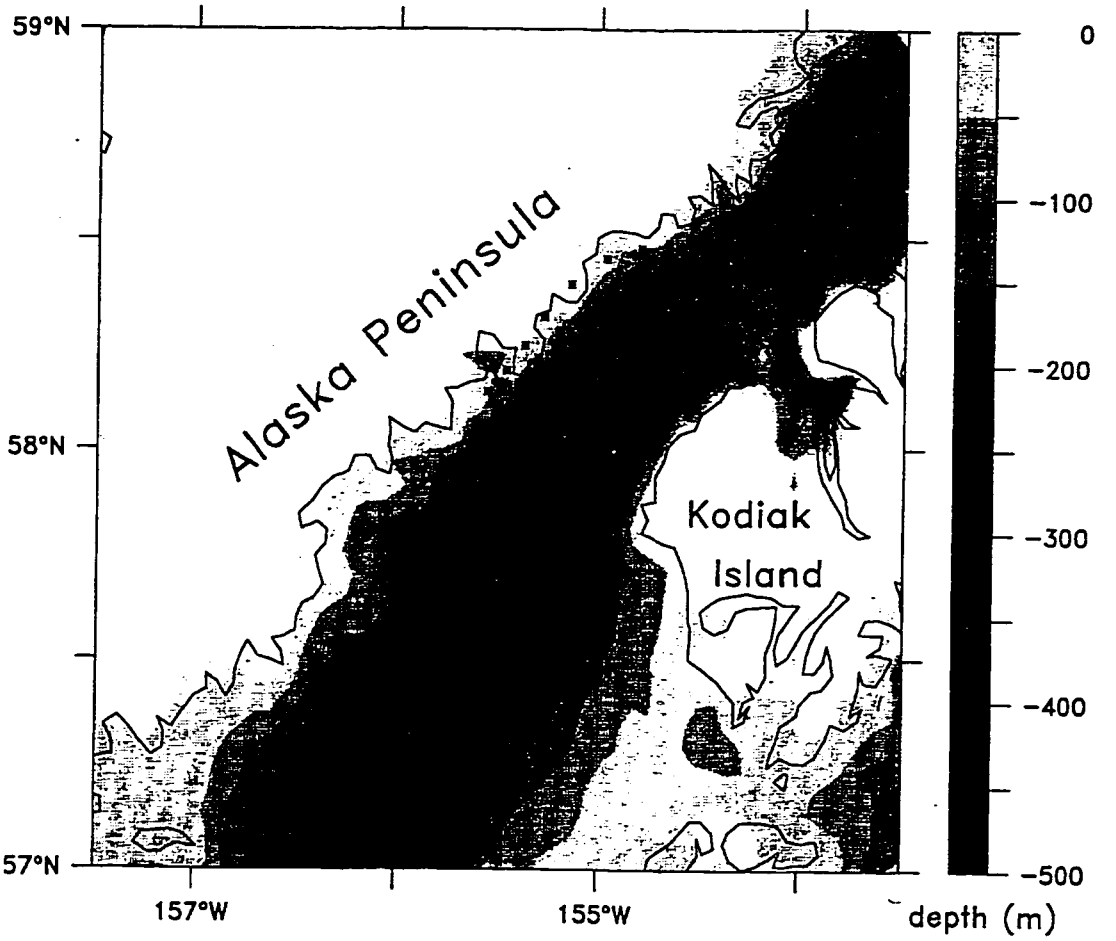

Figure 2.8. Grid of spawning locations for Simulation 3 and later model runs. The location of the points closest to land are offshore of landward boundary of the numerical model, which is smoothed compared to the actual coastline shown in this figure.

fered significantly in physical forcing, we can also make interannual comparisons of the effects of the physical forcing on the distributions of young pollock. Data from years 1987-1989 are used to validate the model, by comparing larval and juvenile locations predicted from the simulations with measurements for those years. Results from all simulations done are presented, ie. best-fit examples were not specifically chosen. Rigorous statistical procedures were not used to compare modelled vs. sampled distributions, as models never exactly predict the real world, ie. summary statistics are probably most appropriate. We use Lloyds patchiness index (see below) as our summary statistic.

The five years chosen span a wide range of system conditions (winds, runoff, and recruitment success). These attributes are summarized in Table 2.4. Months are classified as weak, moderate or strong based on levels of runoff or downstream (Shelikof Strait) wind stress. Computational resources limit the number of years simulated; primarily we chose to focus on years when data had been collected (1985-present), plus a year of exceptional recruitment (1978).

The years analysed may be considered as natural experiments involving two fundamentally different 'treatments': runoff and winds (Fig. 2.9). We focus especially on : a dry year with strong winds (1978), a wet year with average winds (1987), a wet, windy year (1988), and a dry, calm year (1989).

The SPEM model was forced with wind and freshwater input appropriate for each year. Royer (1982, and pers. comm.) has computed the monthly mean runoff for the eastern and northern Gulf of Alaska, using rainfall and temperature time series for the period 1930-1994. He reported a seasonal pattern with minimum runoff values in March and maximum values in October. The series exhibit considerable variation from year to year. Time series for January through September, the period of the simulations are shown in Fig. 2.10a. Note in particular how the integrated flux for March varies over an order of magnitude, with some years (e.g. 1987, 1988) especially 'wet' and others (e.g. 1989) especially 'dry'. Overall runoff is largest in the fall in this region, but it is high in March, and

Table 2.4. Interannual variability in runoff, winds and recruitment. Recruitment estimates from Megrey et al. 1996.

Year	Month	Runoff	Winds	Recruitment of year class
1978	March	weak	moderate	strong
	April	moderate	weak	
	May	strong	moderate	
1987	March	strong	strong	weak
	April	moderate	moderate	
	May	strong	moderate	
1988	March	moderate	strong	moderate
	April	strong	strong	
	May	moderate	moderate	
1989	March	weak	moderate	weak
	April	weak	moderate	
	May	moderate	weak	
1991	March	weak	weak	weak
	April	moderate	moderate	
	May	strong	moderate	
1994	March	weak	moderate	strong
	April	moderate	weak	
	May	strong	moderate	

most notably, this is the time of year in which the most variability in runoff is seen; we think this variability plays an important role in the survival of young pollock.

Time series of winds (dt = 12 h) have been computed as mentioned previously, using Fleet Numerical Oceanographic Center surface pressure analyses, corrected for local ageo-

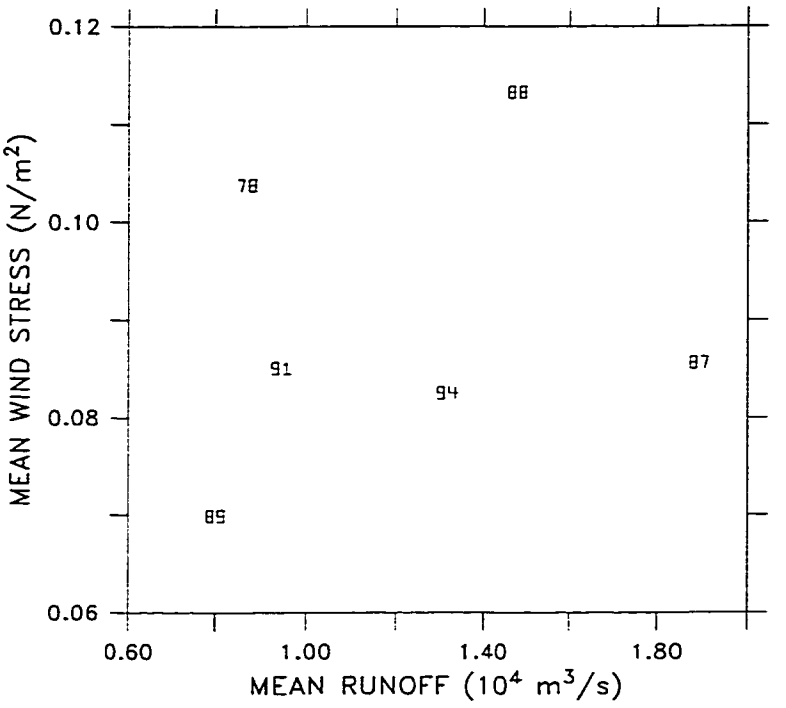

Figure 2.9. Scatterplot of downstream winds vs. runoff for the 6 years. Values are averages for the period January-May of each year.

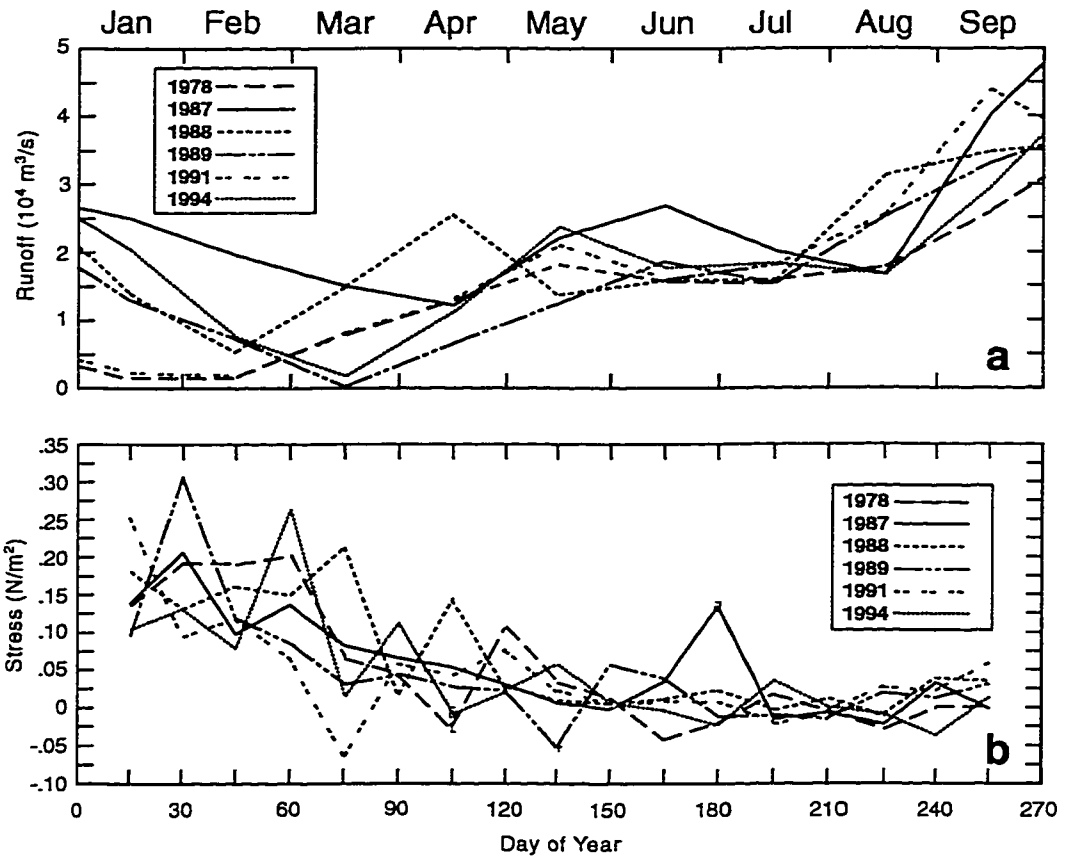

Figure 2.10. (a) Monthly averaged freshwater runoff into the Gulf of Alaska (in m^3 s^{-1}) for 6 years: 1=1978, 2=1987, 3=1988, 4=1989, 5=1991, 6=1994.

(b) Monthly averaged wind stress (N m^{-2}) at the southwestern exit of Shelikof Strait. Time axes are labelled by month and day of year.

strophic effects (Stabeno et al. 1995a), which have been noted by Lackmann and Overland (1989) and Macklin et al. (1993). Variability is present at daily, weekly, and monthly time scales in all years. Figure 2.10b illustrates the average magnitude of the north-easterly ('downstrait') wind at the exit of Shelikof Strait, as a function of month for the 5 years. The mean pattern exhibits greatest downstrait winds in February, with steadily decreasing values through July. As with the runoff time series, there is considerable variability from year to year for any particular month. Overall, 1988 exhibited the strongest downstrait winds during January-May, while 1989 exhibited the weakest downstrait winds during that period (Fig. 2.10b). It must be noted, however, that winds were quite weak in late April of 1988, and this weakness may have contributed to recruitment success for that year class (Bailey and Macklin 1994).

The version of the IBM used for these hindcasts carried fish through the end of September of the 0-age juvenile year, contained no mortality (so that fewer floats had to be followed), contained the simplified feeding function (Eq. 2.19, implying that mean prey density is uniform in space and time, but that variable levels are encountered or captured by an individual on any particular day) and contained the complex depth algorithms as described in Sections 2.2.1., 2.2.2., and 2.2.3., "Depth". In these simulations, we neglect the effects of spatial history on mortality, instead focusing on those changes in the local population resulting from advective loss and temperature history.

For these simulations, eggs were 'spawned' in a rectangular pattern near the exit of Shelikof Strait (Fig. 2.8), in a grid which overlies the observed distribution of spawning (Kendall et al. 1987, Kendall and Picquelle 1990). The modeled spawning dates are normally distributed around DOY 96.75 with a range of 72-122.

A second set of simulations using the NPZ model was done for the years 1978, 1987, 1988, 1989, 1991 and 1994. Physical forcing for these years was the same as described above. The NPZ model was parameterized using optimized parameter values. The simulation was run from DOY 70 through DOY 165. Values for state variables were compared to data for the Shelikof Strait exit region ("Line 8") only. The purpose of these simula-

tions was to examine differences in prey distribution and abundance for the modelled years.

2.5.5 Simulation 5. The importance of spawning location and timing

This model experiment was conducted to examine the hypothesis that the spatial and temporal specificity of spawning of pollock in Shelikof Strait evolved to optimize physical transport to the juvenile nursery areas near the Shumagin Islands. The version of the IBM used in this simulation follows individuals through the fall of their 0-age juvenile year. The "superindividual" method is used to account for mortality, and the feeding function which relates consumption of any individual on a particular day to prey density and the level of turbulence is used. Prey densities are provided via the NPZ model.

A balanced factorial design was used in this model experiment (Table 2.5). The first factor was YEAR, with two levels (1978 and 1994). We chose two years of good recruitment which varied significantly in physical forcing. The second factor was REGION. Five 4 x 4 grids were set up in different regions (Fig. 2.11). The regions were chosen to be as far apart as possible within the SPEM grid. Region (1), central Shelikof Strait, represents the observed spawning area. Five individuals were released from each grid point for each combination of factors. The third factor was spawning time (SPTIME). This was set to four levels, each representing a mean spawning date in the IBM. The spawning times ranged from mid-February to mid-July. The observed spawning time is early April. The fourth factor was spawning depth (SPDEPTH), with two levels, on-bottom (defined as 1 m off bottom), and off-bottom (defined as 50 m off bottom, but not less than 20 m). This variable was thought to be important as the vertical location in the water column strongly affects the direction of horizontal advection. The true vertical distribution of spawning is not well known. The last variable (IN/OUT), was derived from the location (latitude, longitude) of each fish on DOY 244 (September 1st), and indicated whether the fish was inside or outside of the polygon defining the Shumagin nursery area (Fig. 2.11). The "ray crossings" method (O'Rourke 1993) was used to determine whether the point lay inside or

outside the polygon. In this method, a ray is drawn from the point, in an arbitrary direction (for example, the +x direction), and the number of crossings with the boundary of the polygon are counted. The point is inside the polygon if the number of crossings is odd, and outside if the number of crossings is even. This factor was represented by a 1, if inside, or a 0, if outside the nursery area. The polygon represents the region downstream of Shelikof Strait where most juveniles are found in early fall (Walters et al. 1985, Spring and Bailey 1991, Wilson et al. 1996).

Table 2.5. Factors in spawning location and timing simulation - loglinear model.

Factor	Levels
Year	1. 1978 (~30% windier)
	2. 1994 (~50% wetter)
Spawning Region	1. Central Shelikof Strait[1]
	2. Northern Shelikof Strait
	3. Outside Kodiak Island
	4. Northwest Shelikof Sea Valley
	5. Southeast Shelikof Sea Valley
Spawning Time	1. Early ($\bar{x}$ = February 16)
	2. Middle ($\bar{x}$ = April 7)[1]
	3. Late ($\bar{x}$ = May 27)
	4. Very Late ($\bar{x}$ = July 16)
Spawning Depth	1. Near-bottom
	2. Off-bottom

[1] Observed

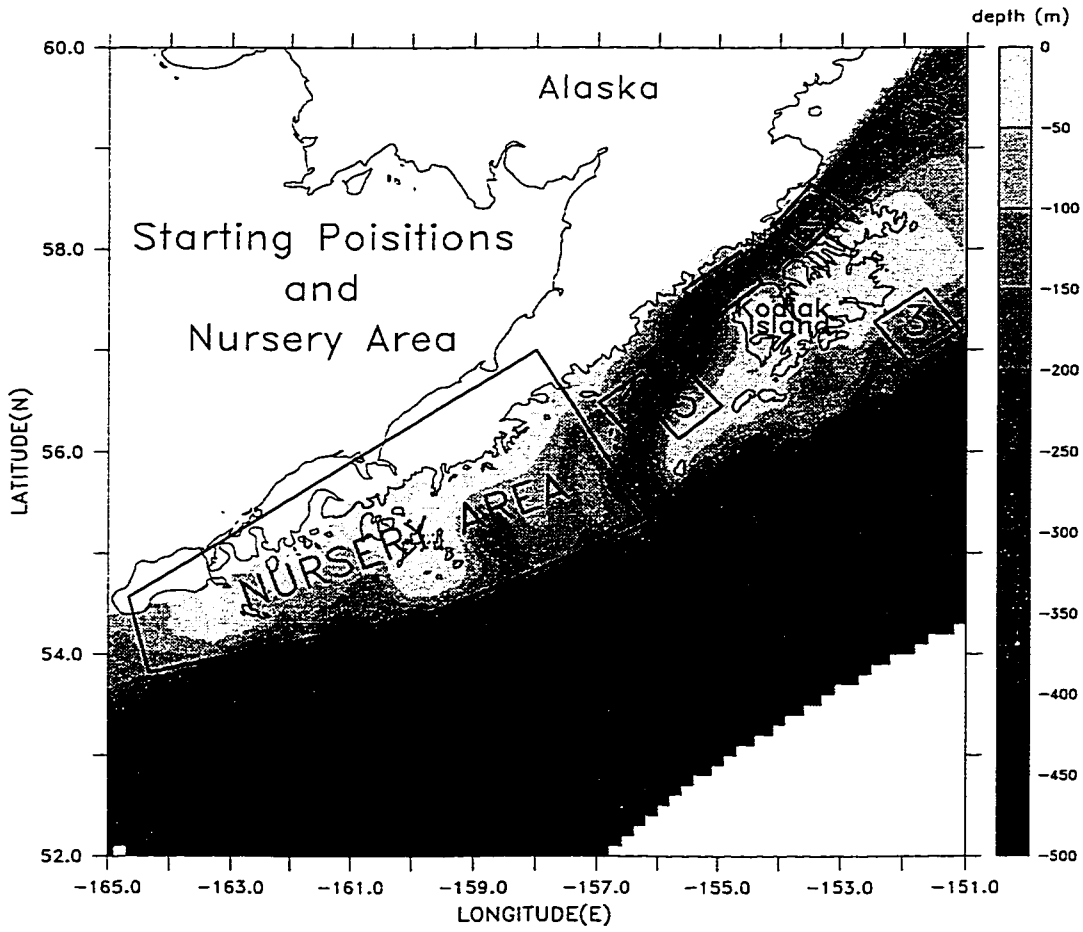

Figure 2.11. Spawning regions and juvenile nursery area as specified in the model experiment. 1. Central Shelikof Strait, 2. Northern Shelikof Strait, 3. Outside Kodiak Island, 4. Northwest Shelikof Sea Valley, 5. Southeast Shelikof Sea Valley.

In the primary analysis, to understand the effects of region, spawning time, and depth on the success of reaching the nursery area, 2 four-dimensional contingency tables were created, one for the year 1978 and one for 1994. The factors used to create the tables were REGION, SPTIME, DEPTH and IN/OUT. It is common for researchers to look at all possible two-way tables among all factors but this would ignore the possibility of three and four-factor interactions and does not allow for the simultaneous expression of all factors in one model. Therefore, a loglinear model was determined to be the best way to test relationships among the factors (Fienberg 1980). This was preferred to the classic analysis of variance model for three reasons: (1) the data is multinomially distributed (for each combination of factors, a fixed sample size of 80 was taken and classified according to whether it succeeded in reaching the nursery area or not), which means the observed cells were not independent, a violation of the basic assumption of ANOVA, (2) although a logarithmic transformation applied to the data would linearize the model, the variances would still be unequal, another violation of the ANOVA assumptions, and (3) if a square root transformation were applied to the proportional data (number of successes over total number of trials for each combination of factors), the transformed observations would have equal variances, but linear models in the square root scale are difficult to interpret in terms of contingency table data (Fienberg 1980).

A loglinear model makes use of the formula for the estimated expected value of the frequency of a particular cell in a contingency table under the hypothesis of independence. In a two-dimensional table, the expected value of the (i,j) cell would be:

$$\hat{e}_{ij} = \frac{r_{i+} \; + c \; _{+j}}{N} \qquad \text{(EQ 2.104)}$$

where,

$\hat{e}_{ij}$ = expected value of the (i,j) cell,
r_{i+} = row counts,
c_{+j} = column counts,
N = total frequencies,

and + indicates summing over levels of that particular factor.

Taking the natural logarithm of both sides yields:

$$\ln e_{ij} = \ln r_{i+} + \ln c_{+j} - \ln N \qquad \text{(EQ 2.105)}$$

The model can then be expressed in terms similar to that of classical ANOVA:

$$\ln e_{ij} = \mu + \alpha_i + \beta_j \qquad \text{(EQ 2.106)}$$

The full loglinear model used in this paper is:

$$\ln \hat{f} = \mu + \alpha_i + \beta_j + \gamma_k + \lambda_l + \alpha\beta_{ij} + \alpha\gamma_{ik} + \alpha\lambda_{il} + \beta\gamma_{jk} + \beta\lambda_{jl} + \gamma\lambda_{kl} + \alpha\beta\gamma_{ijk} + \alpha\beta\lambda_{ijl} + \alpha\gamma\lambda_{ikl} + \beta\gamma\lambda_{jkl} + \alpha\beta\gamma\lambda_{ijkl} \qquad \text{(EQ 2.107)}$$

where,

$\hat{f}$ = the predicted cell frequency,
μ = the mean of the expected frequencies,
α_i = the effect of spawning region (i=1,...,5),
β_j = the effect of spawning time (j=1,...,4),
γ_k = the effect of spawning depth (k=1,2),
λ_l = in or out of the nursery area (0 or 1).

The loglinear model differs from the ANOVA in that one is more interested in testing the independence of factors rather than the significance of main effects, therefore one is primarily looking at interaction terms. First, a likelihood ratio (LR) goodness of fit chi-square test is made after fitting the saturated model (i.e. one with all possible effects and interactions). Subsequent LR chi-square tests are made by (1) testing the fit of the model without each term and (2) testing the significance of the difference between the two chi-square statistics (that of the full model and that of the model with the term removed). Since six models were used in screening effects before ending up with the most appropriate model, and alpha level of .05/6=.008 was used in order to prevent inflation of the overall type I error (Bonferroni method, p. 240 in Sokal and Rohlf (1995). If both tests are insignificant, (that is, the model with the term removed fits (p>.008)) and the difference in the 2 chi-square statistics is small enough (p>.008), then the term can be removed from

the model. In this way, terms in the model are screened and one ends up with the most parsimonius model. Beginning with the highest order interaction term, in this case the four-way interaction term, the tests are performed and if the term can be removed, then all three-way interaction terms are tested, and then the two-way interactions are tested. In this way one can determine which factors are totally independent, which are independent given a particular level of a third (conditionally independent), and which variables are independent of two other variables jointly.

A second loglinear analysis was applied to the data to determine the effects of region, spawning time, and depth on success of reaching the juvenile stage by September 1st.

2.5.6 Simulation 6. The effect of turbulence on feeding.

The goal of this simulation was to test the sensitivity of larval growth and mortality to the effects of turbulence. The IBM, in this simulation, followed individuals through the egg, yolk-sac larval and feeding larval stages. The "superindividual" mortality scheme was used, as was the consumption function which included the effects of prey density and turbulence. Prey densities for each larval location are read into the model using the output (average daily numbers m^{-3} of each *Pseudocalanus* stage at the larval depth) from the one-dimensional NPZ model. Note that the IBM, for this simulation, was not spatially explicit, ie. was run as though no advective effects were operational.

Sensitivity Analysis

The sensitivity analysis was conducted using Monte Carlo error analysis (Gardner et al. 1983) wherein model input parameters are drawn from a random distribution in each model run (one complete execution of the simulation model for a given set of random input parameters is referred to hereafter as a run).

The Monte Carlo error analysis was implemented using Latin Hypercube Sampling (LHS, McKay et al. 1979) in a three-step procedure. The first step involved generating a suite of random input parameter values for the simulation model, the second was running the sim-

ulation model to generate a set of output variables. The simulation model was executed numerous times to generate a set of replicated model input parameter and output variable observations. Finally, the third step involved the statistical analysis of the model input parameters and the output variables. Partitioning the variance of an ouput variable into contributions from all input parameters suggest which input variables have the largest influence on the output variable.

LHS, a random sampling approach, was selected as the method to perform the sensitivity analysis. This relatively obscure but powerful method is based on a type of stratified sampling scheme. A LHS error analysis differs from the individual parameter perturbation because all model input parameters are modified simultaneously during each run instead of increasing or decreasing one parameter at a time by a fixed amount. In LHS error analysis, a set of simulation model input parameters, typically considered fixed in value, are represented as random variates drawn from an assumed probability distribution. It is also important to point out that (as did Letcher et al. 1996) we adjusted model variables (e.g. prey size), results of computations (e.g. probability of successful pursuit), as well as equation parameters (e.g. slope and intercept) of purely empirical relationships.

If simple random sampling was used, model parameter values could cluster, or there could be regions in the random parameter space from which no parameter values were sampled. The result would be redundancy or gaps in the information of the model runs. A stratified sampling method was used to avoid this problem. Stratified sampling ensures more even coverage of the parameter space by dividing the parameter space into sections and sampling from each section with a certain probability. In LHS, the number of runs made is determined by the number of intervals forming the probability distributions, regardless of the size of the model. In each run, every input parameter distribution is sampled. LHS has the useful property that the number of model runs required for an analysis is independent of the number of model parameters.

Sensitivity is evaluated with rank correlation or simple correlation depending on whether covariance exists between the input parameters. The premise underlying the use of this

statistic is that the greater the correlation between the parameter and the output variable (percent variance explained in the output variable by the parameter), the more influence the parameter has in controlling model behavior (Rose et al. 1991). Figure 2.12 shows a theoretical schematic of a LHS sensitivity analysis made up of six Monte Carlo runs of the simulation model using three input parameters and one output variable. Input parameters are described by the normal, uniform and triangular probability distributions. Each input parameter distribution, P_j, is divided into six intervals, I_{jk}, k=1,...,6. All intervals contain an equal area under the assumed probability density function. Intervals are randomly assigned to model simulations so that each interval appears in only one model run. Within an input parameter distribution, a single value is randomly sampled from each interval, assuming a uniform distribution over the interval. The assumption of uniformity is valid, since the intervals forming the distribution were constructed so that all contain equal area under the distribution. In the schematic, the sensitivity analysis resulted in six replicate runs describing the response of simulation model output variables to a random suite of three input parameters. We used simple correlation statistics (Pearson's R) to analyze results of the sensitivity analysis. The premise underlying the use of a Pearson's R is that the greater the correlation between the output variable and the input parameter, the more influence the parameter has in controlling model behavior. Sensitivity is measured in terms of magnitude (values of the correlation coefficient) and the direction of the influence (sign of the correlation coefficient). No covariance relationship among the input parameters was specified, therefore the parametric R^2 could be used.

Simulation Process

The sensitivity analysis of the IBM model examined the importance of 119 model parameters (Table 2.6) describing the feeding dynamics (the consumption-turbulence process), growth, mortality and depth distribution of the larval stage only. Eleven parameters dealt with growth and bioenergetic calculations such as descriptions of bioenergetic processes and energy transfer efficiencies and weight-length conversions. Fifteen parameters described the mortality process including larval mortality-size functions, base mortality,

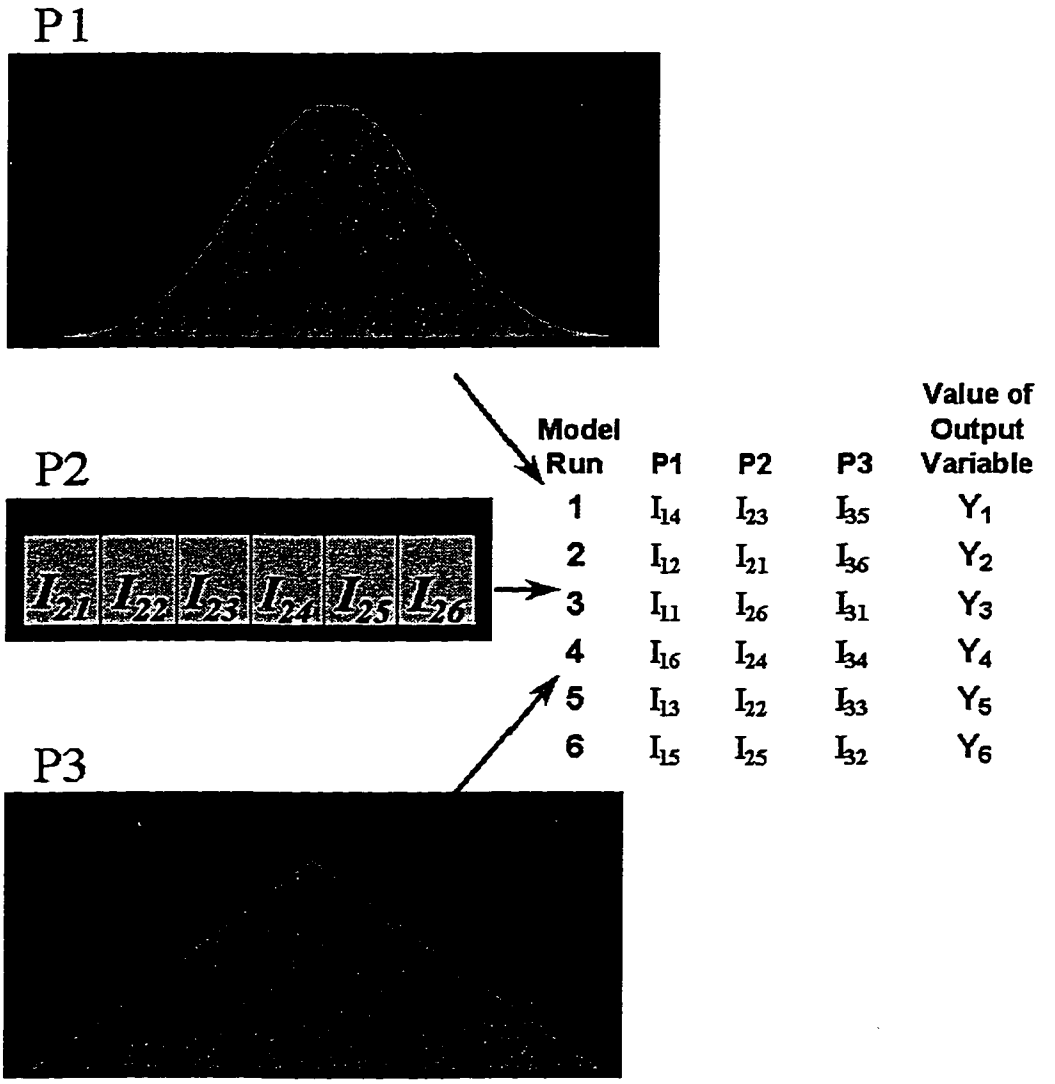

Figure 2.12. Theoretical schematic of a LHS sensitivity analysis made up of six Monte Carlo runs of the simulation model using three input parameters and one output variable. See text for explanation.

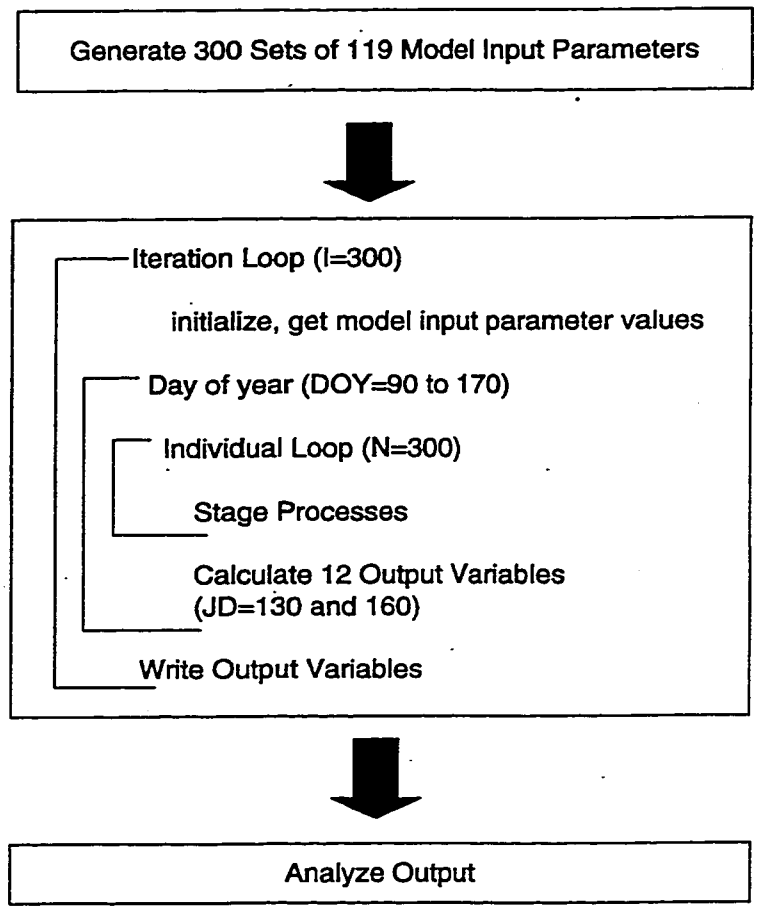

Figure 2.13. Summary of simulation process for sensitivity analysis. See text for explanation.

and starvation and predation mortality. The consumption-turbulence formulation needed 83 parameters to describe the probability of eating eggs, nauplii, and copepodite stages of *Pseudocalanus* (14 stages), larval pause duration (prey density, turbulence and size dependent), prey weight, diel larval migration, turbulent diffusion and velocity, prey speed, and encounter probability.

The complete simulation process is described schematically in Figure 2.13. Three hundred data sets consisting of 119 model input parameters were generated. Within each set, random variates for each input parameter were drawn from a triangular distribution. A triangular distribution was used because it closely approximates a normal distribution yet does not require an estimate of variance. This was an important consideration since variance estimates for most of the input parameters were not well known. It was easier to provide a mean, minimum, and maximum value; the minimum information requirements for describing triangular probability density functions. Also note that a triangular probability density function is not required to be symmetric. Random variates for each input parameter were independent among the 300 data sets. Input parameters and their nominal values are given in Table 2.6.

Input variables were subjective and somewhat arbitrarily selected so as to maxmize the ability to ascertain any time dependence of the sensitivity conclusions, determine important aspects of model behavior, provide information for judging parameter importance, and to evaluate overall model response to changes in the input parameters. Output variables were calculated for two days of the year, DOY 130 (May 10) and DOY 160 (June 10). On these two days, 24 output variables, described in Table 2.7, were computed. Two output variables, cumulative consumption and average probability of successful pursuit, were also calculated for two larval sizes, small and large. Small larvae were defined as those having sizes less than the average larvae, while large larvae were defined as those having sizes greater or equal to the average size. Average size computed on DOY 130 and 160 were used as the basis for this calculation.

The IBM simulation model was executed 300 times in three main loops. The innermost loop tracked 300 individuals and controlled all stage processes. The middle loop controlled the day of the year. The IBM was configured to execute a simulation running from DOY 90 (April 1) to DOY 170 (June 20). Within this loop, output variables were calculated on DOY 130 and 160. The outer loop iterated through the 300 input parameter sets. Within this loop all model variables were initialized, input parameter values assigned, and input parameters and output variables were written to an output file. Finally results contained in the output file were analyzed.

Several external inputs to the IBM were required in addition to the input parameter file. Input files of driving variables from 1987 included the prey field derived from the dynamic (NPZ) prey model resolved over time and depth. A wind field file was required to drive the turbulence equations. A temperature and salinity file, derived from the circulation model of the region (SPEM), was required to drive temperature dependent biological processes.

Table 2.6. Input parameters for the individual-based model (IBM) and nominal values used to generate random variates from a triangular probability distribution.

Input Parameter	Description	Mean	Minimum	Maximum
AELARV	Larval assimilation efficiency	0.8	0.6	0.9
BIGPD	Pause duration (s) for larvae > 25 days old	0.1	0.05	0.15
CALM	Turbulent velocity definition that deliniates calm vs turbulent conditions (m2/s3)	7.40E-08	3.70E-08	1.11E-07
COPSPEED	Swimming speed of *Pseudocalanus* spp. copepodites (m/s)	0.0004503	0.0002252	0.0006755
CRITKFDL	Critical condition factor defining the onset of starvation in feeding larvae	0.4	0.25	0.5
DWTC1	Dry weight of 1st *Pseudocalanus* spp. copepodite stage (mg)	7.20E-04	0.00036	0.00108
DWTC2	Dry weight of 2nd *Pseudocalanus* spp. copepodite stage (mg)	1.20E-03	0.0006	0.0018
DWTC3	Dry weight of 2nd *Pseudocalanus* spp. copepodite stage (mg)	2.00E-03	0.001	0.003
DWTC4	Dry weight of 2nd Pseudocalanus spp. copepodite stage (mg)	3.40E-03	0.0017	0.0051
DWTC5	Dry weight of 2nd *Pseudocalanus* spp. copepodite stage (mg)	6.00E-03	0.003	0.009
DWTC6	Dry weight of 2nd *Pseudocalanus* spp. copepodite stage (mg)	8.00E-03	0.004	0.012

Table 2.6. Input parameters for the individual-based model (IBM) and nominal values used to generate random variates from a triangular probability distribution.

Input Parameter	Description	Mean	Minimum	Maximum
DWTEGG	Dry weight of *Pseudocalanus* spp. egg (mg)	7.00E-05	0.000035	0.000105
DWTN1	Dry weight of 1st *Pseudocalanus* spp. naupliar stage (mg)	8.00E-05	0.00004	0.00012
DWTN2	Dry weight of 2nd *Pseudocalanus* spp. naupliar stage (mg)	8.00E-05	0.00004	0.00012
DWTN3	Dry weight of 3rd *Pseudocalanus* spp. naupliar stage (mg)	1.80E-04	0.00009	0.00027
DWTN4	Dry weight of 4th *Pseudocalanus* spp. naupliar stage (mg)	2.70E-04	0.000135	0.000405
DWTN5	Dry weight of 5th *Pseudocalanus* spp. naupliar stage (mg)	4.00E-04	0.0002	0.0006
DWTN6	Dry weight of 6th *Pseudocalanus* spp. naupliar stage (mg)	6.40E-04	0.00032	0.00096
ENDFEED	Hour of day when feeding ends (h)	22	11	33
ETAA	Proportional coefficient in turbulence dissipation rate function	5.82E-09	2.91E-09	8.73E-09
FDEPTHG	Depth of feeding larvae (m)	25	15	50
FDLACT-MULT	Activity multiplier (see equation 10 in Hinckley et al. 1996b)	2	1.5	3
HRLIGHT	Hours of daylight (h)	16	6	18

Table 2.6. Input parameters for the individual-based model (IBM) and nominal values used to generate random variates from a triangular probability distribution.

Input Parameter	Description	Mean	Minimum	Maximum
LOWPREY	Low prey density definition (no/m3)	35000	5000	40000
LWBSA	Length-weight conversion function parameter (see equation 10 in Hinckley et al. 1996b)	0.3266	0.1633	0.4899
LWBSB	Length-weight conversion function parameter (see equation 10 in Hinckley et al. 1996b)	3.395	1.6975	5.0925
LWYBA	Length-weight conversion function parameter (see equation 13 in Hinckley et al. 1996b)	0.1754	0.0877	0.2631
LWYBB	Length-weight conversion function parameter (see equation 13 in Hinckley et al. 1996b)	3.615	1.8075	5.4225
MAXPREYA	Proportional coefficient of larval length-maximum prey size function	0.115	0.0575	0.1725
MAXPREYB	Slope coefficient of larval length-maximum prey size function	0.235	0.1175	0.3525
MFDLSM	Base mortality when larval length < 7.0mm (per day)	0.1	0.05	0.2
MFNFDLA	Proportional coefficient in feeding metabolism-weight function (see equation 8 in Hinckley et al. 1996b)	0.00308	0.00154	0.00462

Table 2.6. Input parameters for the individual-based model (IBM) and nominal values used to generate random variates from a triangular probability distribution.

Input Parameter	Description	Mean	Minimum	Maximum
MFNFDLB	Power coefficient in feeding metabolism-weight function (see equation 8 in Hinckley et al. 1996b)	0.9059	0.45295	1.35885
MINMORT	Minimum mortality (per day)	0.02	0.001	0.05
MROFDLA	Proportional coefficient in routine metabolism-weight function (see equation 9 in Hinckley et al. 1996b)	0.00253	0.001265	0.003795
MROFDLB	Power coefficient in routine metabolism-weight function (see equation 9 in Hinckley et al. 1996b)	0.9699	0.48495	1.45485
MSIZEA1	Proportional coefficient in mortality-length function for 1987	1.7007	0.85035	2.55105
MSIZEA2	Proportional coefficient in mortality-length function for 1988	7.7095	3.85475	11.56425
MSIZEA3	Proportional coefficient in mortality-length function for 1989	0.7015	0.35075	1.05225
MSIZEA4	Proportional coefficient in mortality-length function for 1990	0.3942	0.1971	0.5913
MSIZEA5	Proportional coefficient in mortality-length function for 1991	7.3297	3.66485	10.99455
MSIZEA6	Proportional coefficient in mortality-length function for average year	7.4323	3.71615	11.14845

Table 2.6. Input parameters for the individual-based model (IBM) and nominal values used to generate random variates from a triangular probability distribution.

Input Parameter	Description	Mean	Minimum	Maximum
MSIZEB1	Slope coefficient in mortality-length function for 1987	2.0312	1.0156	3.0468
MSIZEB2	Slope coefficient in mortality-length function for 1988	5.2913	2.64565	7.93695
MSIZEB3	Slope coefficient in mortality-length function for 1989	0.0674	0.0337	0.1011
MSIZEB4	Slope coefficient in mortality-length function for 1990	0.0373	0.01865	0.05595
MSIZEB5	Slope coefficient in mortality-length function for 1991	4.8768	2.4384	7.3152
MSIZEB6	Slope coefficient in mortality-length function for average year	4.9738	2.4869	7.4607
NAUPSPEED	Swimming speed of Pseudocalanas spp. nauplii (m/s)	0.0001054	0.0000527	0.0001581
OLDMORT	Mortality when age is greater than 25 days old (per day)	0.02	0.001	0.05
PCOP1	Probability of a pollock larvae less than 6mm eating a *Pseudocalanus* spp. copepodite	0.015	0.00075	0.01575
PCOP10	Probability of a pollock larvae between 14 and 15mm eating a *Pseudocalanus* spp. copepodite	0.217	0.20615	0.22785
PCOP11	Probability of a pollock larvae between 15 and 16mm eating a *Pseudocalanus* spp. copepodite	0.337	0.32015	0.35385

Table 2.6. Input parameters for the individual-based model (IBM) and nominal values used to generate random variates from a triangular probability distribution.

Input Parameter	Description	Mean	Minimum	Maximum
PCOP12	Probability of a pollock larvae between 16 and 17mm eating a *Pseudocalanus* spp. copepodite	0.348	0.3306	0.3654
PCOP13	Probability of a pollock larvae between 17 and 19mm eating a *Pseudocalanus* spp. copepodite	0.875	0.83125	0.91875
PCOP14	Probability of a pollock larvae greater than 19mm eating a *Pseudocalanus* spp. copepodite	0.873	0.82935	0.91665
PCOP2	Probability of a pollock larvae between 6 and 7mm eating a *Pseudocalanus* spp. copepodite	0.02	0.001	0.021
PCOP3	Probability of a pollock larvae between 7 and 8mm eating a *Pseudocalanus* spp. copepodite	0.015	0.00075	0.01575
PCOP4	Probability of a pollock larvae between 8 and 9mm eating a *Pseudocalanus* spp. copepodite	0.008	0.0004	0.0084
PCOP5	Probability of a pollock larvae between 9 and 10mm eating a *Pseudocalanus* spp. copepodite	0.025	0.00125	0.02625
PCOP6	Probability of a pollock larvae between 10 and 11mm eating a *Pseudocalanus* spp. copepodite	0.048	0.0024	0.0504

Table 2.6. Input parameters for the individual-based model (IBM) and nominal values used to generate random variates from a triangular probability distribution.

Input Parameter	Description	Mean	Minimum	Maximum
PCOP7	Probability of a pollock larvae between 11 and 12mm eating a *Pseudocalanus* spp. copepodite	0.099	0.00495	0.10395
PCOP8	Probability of a pollock larvae between 12 and 13mm eating a *Pseudocalanus* spp. copepodite	0.192	0.1824	0.2016
PCOP9	Probability of a pollock larvae between 13 and 14mm eating a *Pseudocalanus* spp. copepodite	0.236	0.2242	0.2478
PD1A	Proportional coefficient in prey density-larval length function for calm conditions and low prey density	2.522	1.261	3.783
PD1B	Slope coefficient in prey density-larval length function for calm conditions and low prey density	0.111	0.0555	0.1665
PD2A	Proportional coefficient in prey density-larval length function for calm conditions and high prey density	24.267	12.1335	36.4005
PD2B	Slope coefficient in prey density-larval length function for calm conditions and high prey density	3.667	1.8335	5.5005
PD3A	Proportional coefficient in prey density-larval length function for turbulent conditions and low prey density	5.189	2.5945	7.7835

Table 2.6. Input parameters for the individual-based model (IBM) and nominal values used to generate random variates from a triangular probability distribution.

Input Parameter	Description	Mean	Minimum	Maximum
PD3B	Slope coefficient in prey density-larval length function for turbulent conditions and low prey density	0.556	0.278	0.834
PD4A	Proportional coefficient in prey density-larval length function for turbulent conditions and high prey density	10.111	5.0555	15.1665
PD4B	Slope coefficient in prey density-larval length function for turbulent conditions and high prey density	1.444	0.722	2.166
PEGGS1	Probability of a pollock larvae less than 6mm eating a *Pseudocalanus* spp. egg	0.015	0.00075	0.01575
PEGGS10	Probability of a pollock larvae between 14 and 15mm eating a *Pseudocalanus* spp. egg	0.624	0.5928	0.6552
PEGGS11	Probability of a pollock larvae between 15 and 16mm eating a *Pseudocalanus* spp. egg	0.382	0.3629	0.4011
PEGGS12	Probability of a pollock larvae between 16 and 17mm eating a *Pseudocalanus* spp. egg	0.01	0.0005	0.0105
PEGGS13	Probability of a pollock larvae between 17 and 19mm eating a *Pseudocalanus* spp. egg	0.01	0.0005	0.0105

Table 2.6. Input parameters for the individual-based model (IBM) and nominal values used to generate random variates from a triangular probability distribution.

Input Parameter	Description	Mean	Minimum	Maximum
PEGGS14	Probability of a pollock larvae greater than 19mm eating a *Pseudocalanus* spp. egg	0.01	0.0005	0.0105
PEGGS2	Probability of a pollock larvae between 6 and 7mm eating a *Pseudocalanus* spp. egg	0.02	0.001	0.021
PEGGS3	Probability of a pollock larvae between 7 and 8mm eating a *Pseudocalanus* spp. egg	0.015	0.00075	0.01575
PEGGS4	Probability of a pollock larvae between 8 and 9mm eating a *Pseudocalanus* spp. egg	0.03	0.0015	0.0315
PEGGS5	Probability of a pollock larvae between 9 and 10mm eating a *Pseudocalanus* spp. egg	0.015	0.00075	0.01575
PEGGS6	Probability of a pollock larvae between 10 and 11mm eating a *Pseudocalanus* spp. egg	0.053	0.00265	0.05565
PEGGS7	Probability of a pollock larvae between 11 and 12mm eating a *Pseudocalanus* spp. egg	0.156	0.1482	0.1638
PEGGS8	Probability of a pollock larvae between 12 and 13mm eating a *Pseudocalanus* spp. egg	0.327	0.31065	0.34335
PEGGS9	Probability of a pollock larvae between 13 and 14mm eating a *Pseudocalanus* spp. egg	0.35	0.3325	0.3675
PF	Pause frequency (s^{-1})	0.52	0.2	0.75

Table 2.6. Input parameters for the individual-based model (IBM) and nominal values used to generate random variates from a triangular probability distribution.

Input Parameter	Description	Mean	Minimum	Maximum
PNAUP1	Probability of a pollock larvae less than 6mm eating a Pseudocalanas spp. nauplii	0.97	0.9025	0.9975
PNAUP10	Probability of a pollock larvae between 14 and 15mm eating a Pseudocalanas spp. nauplii	0.159	0.15105	0.16695
PNAUP11	Probability of a pollock larvae between 15 and 16mm eating a Pseudocalanas spp. nauplii	0.281	0.26695	0.29505
PNAUP12	Probability of a pollock larvae between 16 and 17mm eating a Pseudocalanas spp. nauplii	0.642	0.6194	0.6846
PNAUP13	Probability of a pollock larvae between 17 and 19mm eating a Pseudocalanas spp. nauplii	0.115	0.11875	0.13125
PNAUP14	Probability of a pollock larvae greater than 19mm eating a Pseudocalanas spp. nauplii	0.117	0.12065	0.13335
PNAUP2	Probability of a pollock larvae between 6 and 7mm eating a Pseudocalanas spp. nauplii	0.96	0.9025	0.9975
PNAUP3	Probability of a pollock larvae between 7 and 8mm eating a Pseudocalanas spp. nauplii	0.97	0.9025	0.9975

Table 2.6. Input parameters for the individual-based model (IBM) and nominal values used to generate random variates from a triangular probability distribution.

Input Parameter	Description	Mean	Minimum	Maximum
PNAUP4	Probability of a pollock larvae between 8 and 9mm eating a Pseudocalanas spp. nauplii	0.96	0.9025	0.9975
PNAUP5	Probability of a pollock larvae between 9 and 10mm eating a Pseudocalanas spp. nauplii	0.95	0.9025	0.9975
PNAUP6	Probability of a pollock larvae between 10 and 11mm eating a Pseudocalanas spp. nauplii	0.899	0.85405	0.94395
PNAUP7	Probability of a pollock larvae between 11 and 12mm eating a Pseudocalanas spp. nauplii	0.745	0.70775	0.78225
PNAUP8	Probability of a pollock larvae between 12 and 13mm eating a Pseudocalanas spp. nauplii	0.481	0.45695	0.50505
PNAUP9	Probability of a pollock larvae between 13 and 14mm eating a Pseudocalanas spp. nauplii	0.414	0.3933	0.4347
PREYLENC1	Median carapace length of 2nd *Pseudocalanus* spp. naupliar stage (mm)	0.528725	0.2643625	0.7930875
PREYLENC2	Median carapace length of 2nd *Pseudocalanus* spp. naupliar stage (mm)	0.701531	0.3507655	1.0522965
PREYLENC3	Median carapace length of 2nd *Pseudocalanus* spp. naupliar stage (mm)	0.779336	0.389668	1.169004

Table 2.6. Input parameters for the individual-based model (IBM) and nominal values used to generate random variates from a triangular probability distribution.

Input Parameter	Description	Mean	Minimum	Maximum
PREYLENC4	Median carapace length of 2nd *Pseudocalanus* spp. naupliar stage (mm)	1.02197	0.510985	1.532955
PREYLENC5	Median carapace length of 2nd *Pseudocalanus* spp. naupliar stage (mm)	1.27041	0.635205	1.905615
PREYLENC6	Median carapace length of 2nd *Pseudocalanus* spp. naupliar stage (mm)	1.53912	0.76956	2.30868
PREY-LENEGG	Median Pseudocalanas spp. egg diameter (mm)	0.13	0.065	0.195
PREYLENN1	Median carapace length of 1st *Pseudocalanus* spp. naupliar stage (mm)	0.1419	0.07095	0.21285
PREYLENN2	Median carapace length of 2nd *Pseudocalanus* spp. naupliar stage (mm)	0.1506	0.0753	0.2259
PREYLENN3	Median carapace length of 2nd *Pseudocalanus* spp. naupliar stage (mm)	0.1868	0.0934	0.2802
PREYLENN4	Median carapace length of 2nd *Pseudocalanus* spp. naupliar stage (mm)	0.2347	0.11735	0.35205
PREYLENN5	Median carapace length of 2nd *Pseudocalanus* spp. naupliar stage (mm)	0.2728	0.1364	0.4092
PREYLENN6	Median carapace length of 2nd *Pseudocalanus* spp. naupliar stage (mm)	0.2888	0.1444	0.4332

Table 2.6. Input parameters for the individual-based model (IBM) and nominal values used to generate random variates from a triangular probability distribution.

Input Parameter	Description	Mean	Minimum	Maximum
Q10L	Q10 for consumption, feeding and routine metabolism of feeding larvae (see equations 7,8, and 9 in Hinckley et al. 1996b)	2	1.75	3
RDA	Slope coefficient of reactive distance-length relationship (mm)	0.769	0.3845	1.1535
STARTFEED	Hour of day when feeding starts (h)	5	2.5	7.5
t	Minimum pursuit time (s)	1.7	0.85	2.55
WA	Proportional coefficient in turbulent velocity function	3.615	1.8075	5.4225

Table 2.7. Description of IBM output variables for sensitivity analysis.

Output Variable	Description
MCFLL130	Mean cumulative feeding (μg dry wt/day), large larvae, DOY 130
MCFLL160	Mean cumulative feeding (μg dry wt/day), large larvae, DOY 160
MCFSL130	Mean cumulative feeding (μg dry wt/day), small larvae, DOY 130
MCFSL160	Mean cumulative feeding (μg dry wt/day), small larvae, DOY 160
MGR130	Mean instantaneous growth rate (per day), DOY 130
MGR160	Mean instantaneous growth rate (per day), DOY 160
MLEN130	Mean length (mm), DOY 130
MLEN160	Mean length (mm), DOY 160
MMD130	Mean number of fish reaching juvenile stage by DOY 130
MMD160	Mean number of fish reaching juvenile stage by DOY 160
MNO130	Mean number of surviving individuals (number), DOY 130
MNO160	Mean number of surviving individuals (number), DOY 160
MPSLL130	Mean probability of successful pursuit, large larvae, DOY 130
MPSLL160	Mean probability of successful pursuit, large larvae, DOY 160
MPSSL130	Mean probability of successful pursuit, small larvae, DOY 130
MPSSL160	Mean probability of successful pursuit, small larvae, DOY 160
MPZ130	Mean instantaneous predation mortality rate (per day), DOY 130
MPZ160	Mean instantaneous predation mortality rate (per day), DOY 160
MSZ130	Mean instantaneous starvation mortality rate (per day), DOY 130
MSZ160	Mean instantaneous starvation mortality rate (per day), DOY 160
MWT130	Mean weight (μg dry weight), DOY 130
MWT160	Mean weight (μg dry weight), DOY 160
MZ130	Mean instantaneous total mortality rate (per day), DOY 130
MZ160	Mean instantaneous total mortality rate (per day), DOY 160

Chapter 3. Results

3.1 Simulation 1. Float-tracking experiments.

To help address the accuracy of float tracking with pre-stored, filtered and decimated velocity fields, versus "direct" tracking with the unfiltered fields, we present results from a simulation of 1987 currents and float tracks in the Gulf of Alaska.

As seen in Fig. 3.1a, many of the floats circulate around and between a cyclonic-anticyclonic eddy pair, just downstream from the exit of Shelikof Strait. Note how some of the floats, released over deep regions, cross bathymetric contours to the shallower continental shelf. In Figs. 3.1b-3.1d we illustrate the same set of floats, this time tracked with pre-stored, filtered and decimated velocity fields. In case (b) (Fig. 3.1b), with a time step of 1 hour, the broadly defined paths of the float tracks from case (a) (Fig. 3.1a) are reasonably well reproduced, but the details of the paths differ as the floats are advected downstream. Case (c), with a time step of 0.2 hour, differs from case (b) primarily in the improved fit with features in the vicinity of the Shumagin Islands (55°N, -160°E). Case (d) (Fig. 3.1d), with a time step of 0.04 hour, exhibits no substantial difference from case (c).In (Fig. 3.2), we plot the root-mean-squared (rms) horizontal displacement of the floats in case (b) from their corresponding locations in case (a), the displacement of floats between cases (b) and (c), and the displacement between cases (c) and (d). During the first four days of simulation, case (b) generates float tracks within ~2 km of their locations in case (a). Thereafter, case (b) results diverge from case (a), to a mean displacement of ~40 km (the typical width of the deep strait and sea valley in this area). Near day 30 of the simulation, the mean displacement increases once more, ultimately achieving values of ~140 km. Cases (b) and (c) diverge significantly from each other after day 30 while cases (c) and (d) are essentially identical through day 60.

Apparently, by shortening the time unit from 1 hour to 0.2 hour, we sufficiently converge on the "true" solution for the filtered velocity field, that is, we have achieved a step suffi-

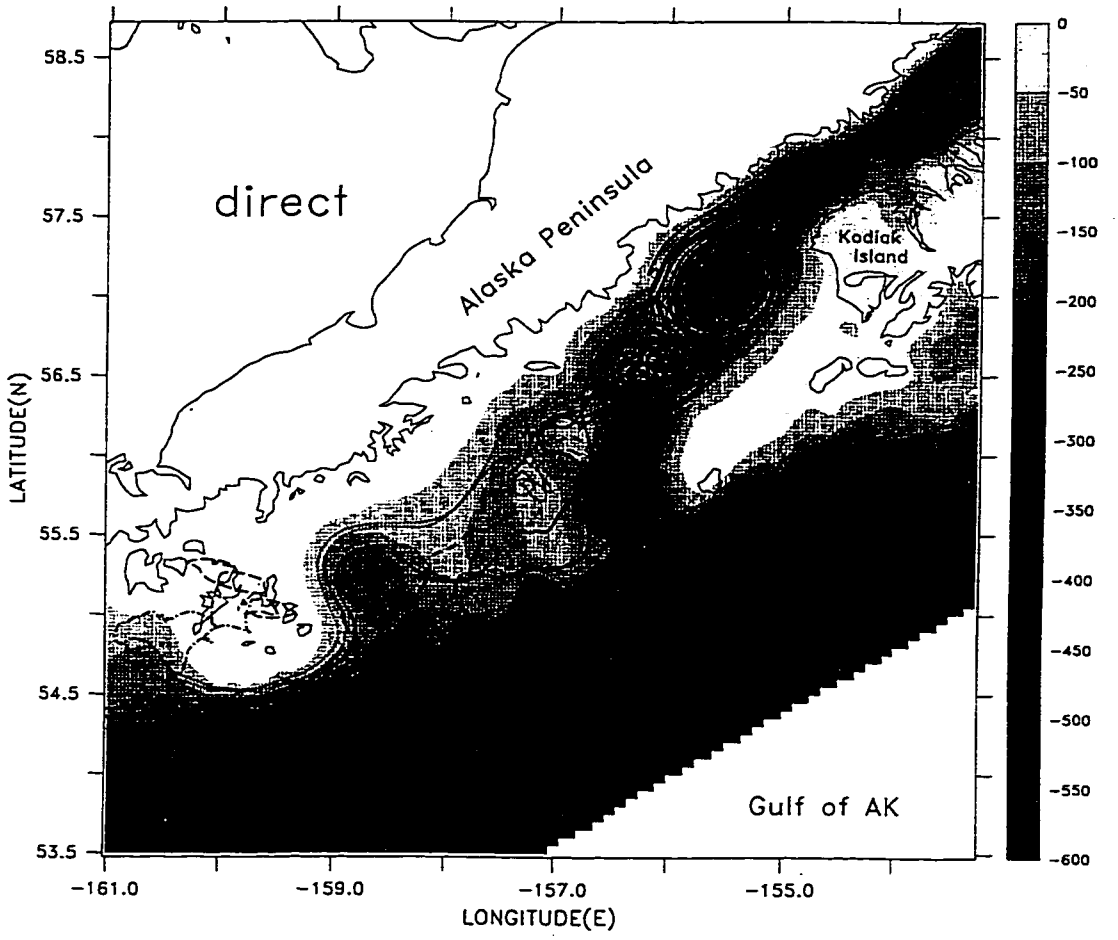

Figure 3.1a. Float tracks generated by directly updating float positions at each time step in a hydrodynamic model (SPEM) simulation of 1987. Ten floats, released along a cross-shelf line at 40m depth on DOY 135 are shown. Tracks are coded by time interval: DOY 135-165 (solid), DOY 165-195 (dashed), DOY 195-225 (dotted).

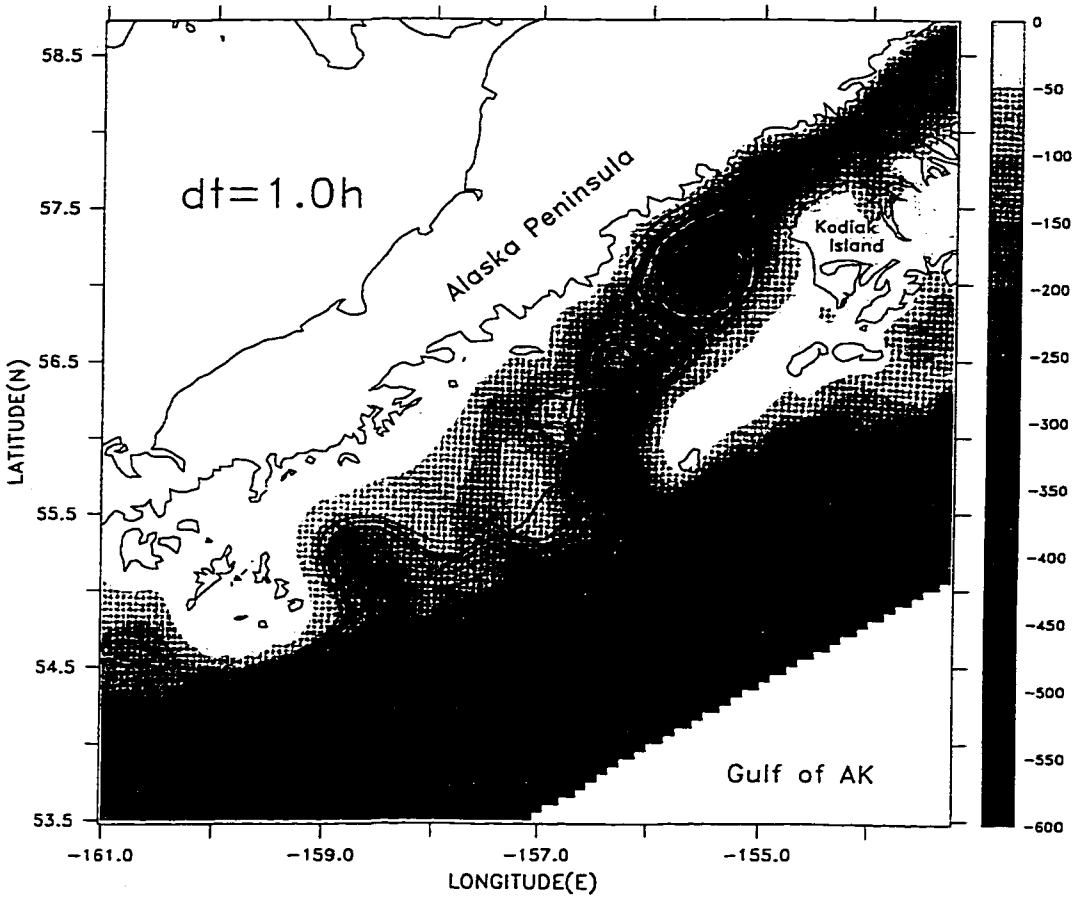

Figure 3.1b. Float tracks generated by updating float positions using previously stored, filtered, daily velocity fields, with dt = 1.0 hour for the float tracking algorithm.

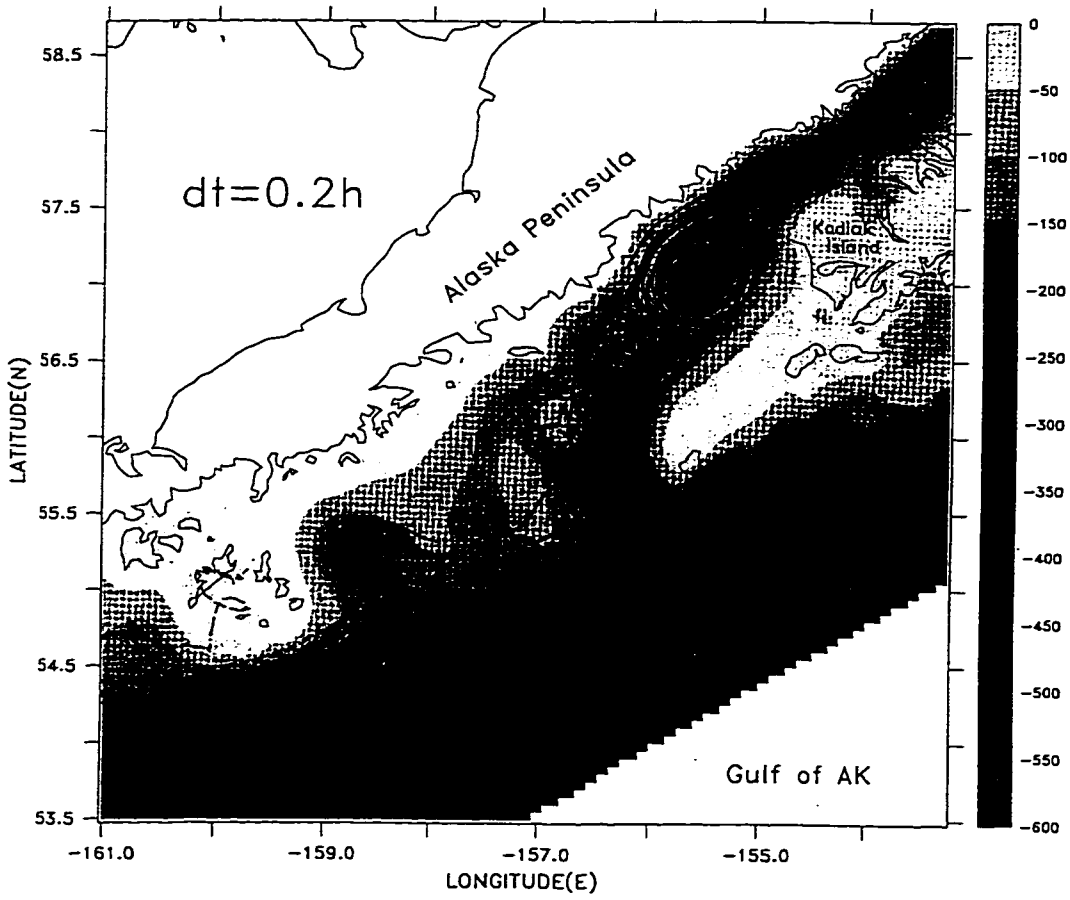

Figure 3.1c. Results as in (b) using dt = 0.2 hour for the float tracking algorithm.

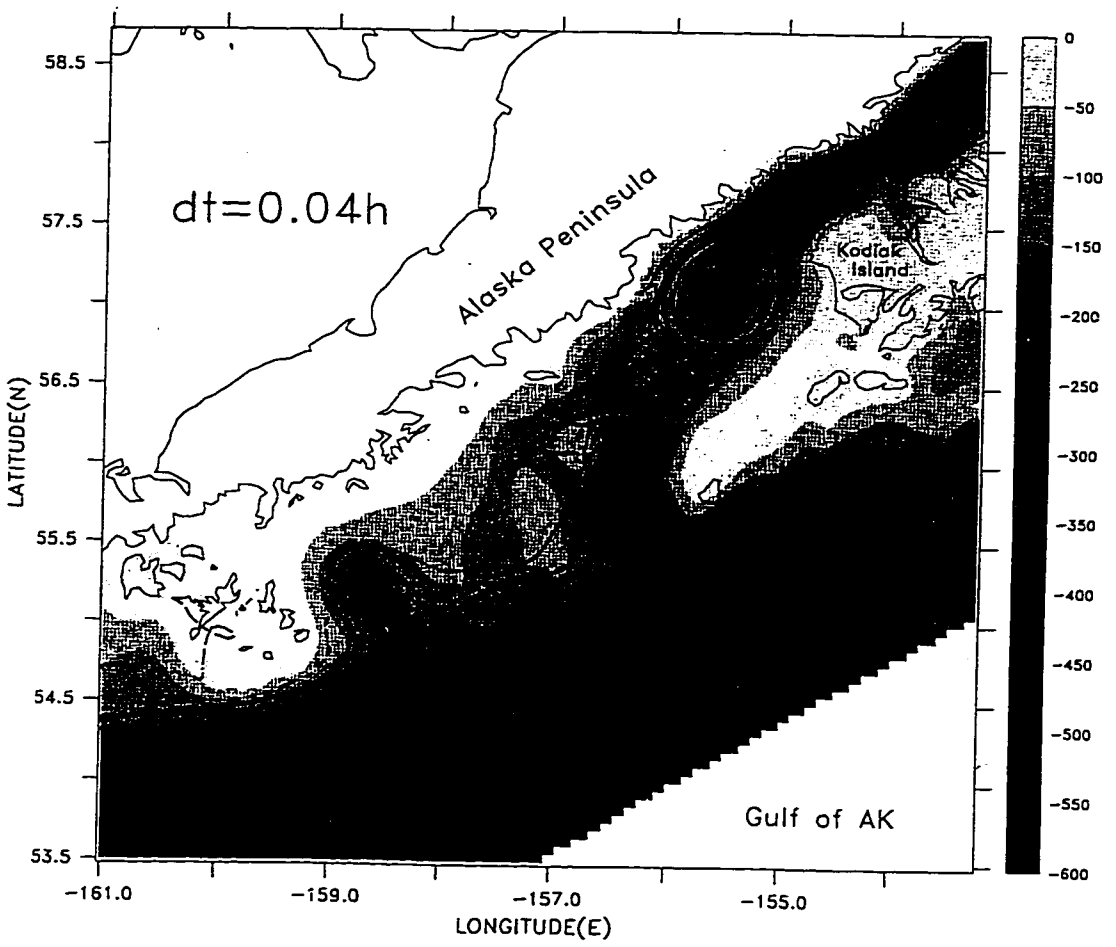

Figure 3.1d. Results as in (b) using dt = 0.04 hour for the float tracking algorithm.

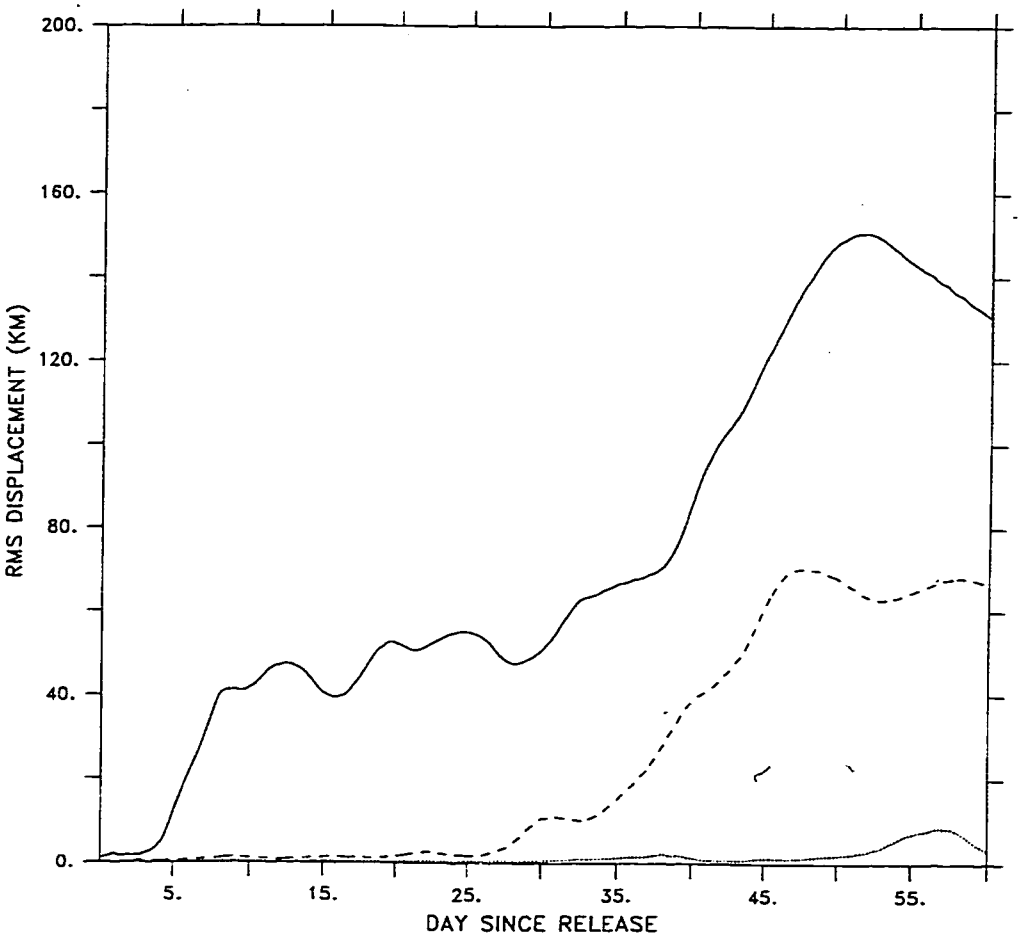

Figure 3.2. Root-mean-square relative displacement of float tracks among the various tracking experiments. Solid line = filtered velocities with dt = 1.0 hour (case b) versus "direct" tracking (case a). Dashed line = filtered velocities with dt = 1.0 hour (case b) versus dt = 0.2 hour (case c). Dotted line = filtered velocities with dt = 0.2 hour (case c) versus dt = 0.04 hour (case d). Mean relative displacement in each case is plotted as a function of time since the beginning of the experiment (DOY 105, 1987).

ciently shorter than the Lagrangian decorrelation time for the filtered velocities to yield an accurate result. This justifies the use of a time step of 0.2 hour in the float tracking algorithm. The same time step and spatial interpolation method is used to generate the results of the rest of the simulations.

Fewer of the float tracks cross into shallow shelf areas when the filtered velocities are used, compared to the unfiltered technique. In future studies, this deficiency could be addressed to some extent by adding a suitable random walk component to the tracked floats, an equivalence first noted by Taylor (1921). We caution, however, that the diffusivity lost by temporal filtering may be spatially dependent, and that spatial variabiton in the magnitude of a random walk can pose special difficulties (Hunter et al. 1993, Holloway 1994).

We discuss the importance of vertical position in Section 3.3. In Fig. 3.3 we underscore this importance by plotting float paths as in case (c), but with all floats constrained to remain at 40 m depth (the mean depth of feeding larvae, Kendall et al. 1994), rather than being free to follow the flow field in three dimensions. The influence of the eddy field is markedly reduced by this constraint; floats do not circulate around the eddy pair as they did in other cases.

3.2 Simulation 2. The importance of Lagrangian factors.

The goal of Simulation 2 was to examine how the addition of spatial information, in the form of a Lagrangian time series of abiotic factors, affects the outcome of the IBM. For the "constant T" case (Fig. 3.4a), individuals exhibit a normal distribution of lengths, with minor variations, at DOY 110, 140 and 160. Length increases exponentially through time as expected. Similarly, in the "linear T" case (Fig. 3.4b), the distribution is still quasi-normal, although the general rate of development is faster than the constant T case, and all individuals have either died or passed into the juvenile stage before DOY 160. In contrast, the "Lagrangian T" case (Fig. 3.4c) exhibits a significantly different pattern. By DOY

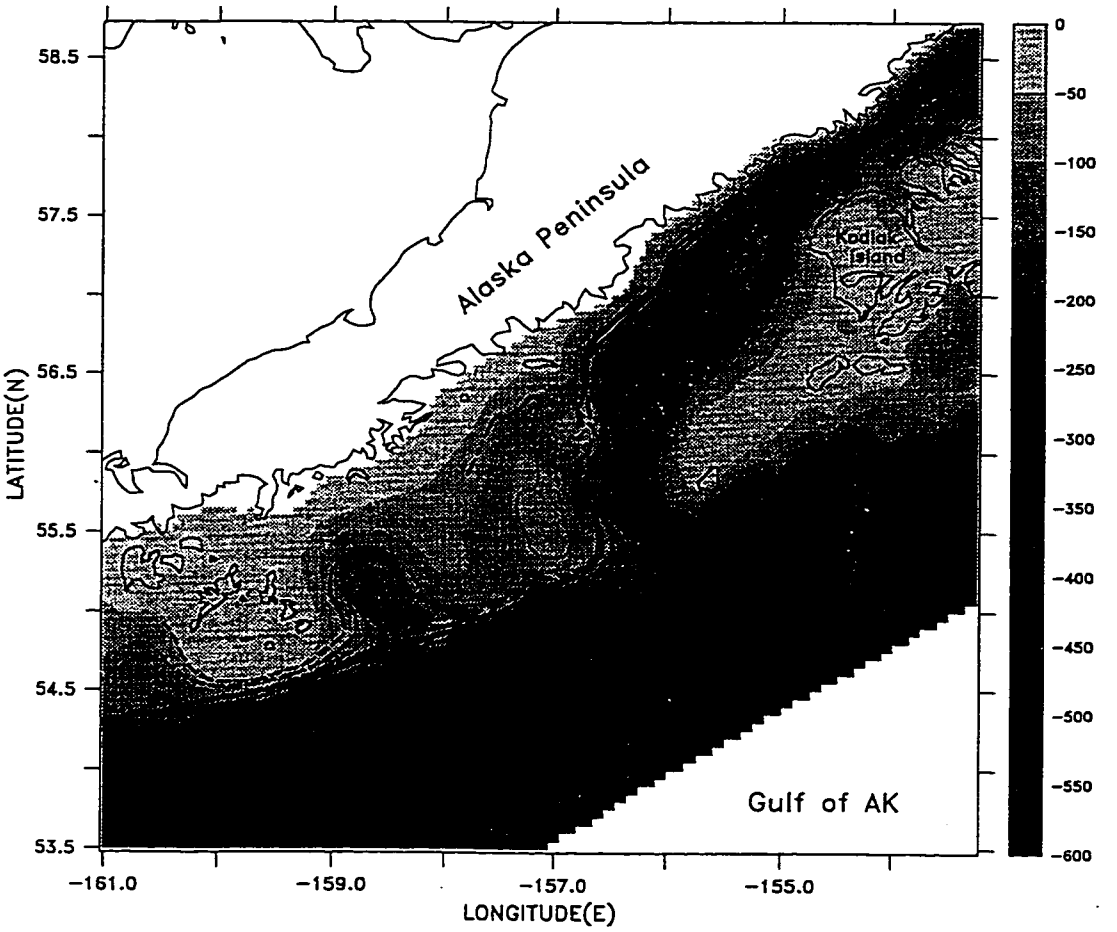

Figure 3.3. Float tracks generated by directly updating float positions at each time step in a hydrodynamic model (SPEM) simulation of 1987, where all floats are constrained to remain at 40m depth. Initial float positions and coding of tracks as in Fig. 3.1.

110, the initial normal distribution becomes skewed, with a preponderance of individuals at the low end of the range of lengths (Fig. 3.4c) and some individuals that have grown significantly faster than others. By DOY 140, lengths of survivors evolve into a bimodal distribution. By DOY 160, lengths of survivors are strikingly fragmented into 2 groups. Bimodal length distributions have been seen in young walleye pollock in the Gulf of Alaska (M. Wilson, Alaska Fisheries Science Center, 7600 Sand Point Way NE, Seattle, WA 98115, pers. comm.). In the model, these patterns arise from the variation in environmental conditions experienced by these individuals. Fig. 3.5 shows the Lagrangian time series of temperature for a subsample of the floats. Some of the records remain nearly constant at high or low temperatures, others exhibit trends to higher or lower values, and others vary in an erratic manner, possibly as a result of their being advected in and out of mesoscale features captured by the physical simulation. The bimodal length distribution could result if individuals get stuck in regions of colder or warmer temperature, or due to random life history processes.

The spatial tracking of individuals allows us to map weights, lengths and temperatures as a function of space and time. Fig. 3.6 illustrates the temperatures in regions of larval distribution on DOY 105. The larval habitat is coldest near the coast (due to the input of cold, fresh waters at the coast in the physical model, as is seen in the Gulf) and warmer further away from the coast. The absence of any individuals in the larval stage at this date near the coast (asterisks on figure) is due to the lower temperatures, and the resulting slower development times in the egg stage. High mortality rates in the egg stage have depleted the stock of potential larvae at this location, eliminating the stock of larvae there by DOY 105. The pattern of weights of surviving larvae shows generally heavier individuals in the eastern part of the sea valley and shelf, and lighter individuals to the north and west by DOY 150 (Fig. 3.7). Note, however, that considerable patchiness exists, with heavy individuals juxtaposed with much lighter ones at some locations. A number of individuals were advected to the south and east of the sea valley and Kodiak Island. This is not something which is commonly seen in field data and was determined to be an artifact of the initial crude bathymetric dataset employed by this early model. A finer bathymetric dataset

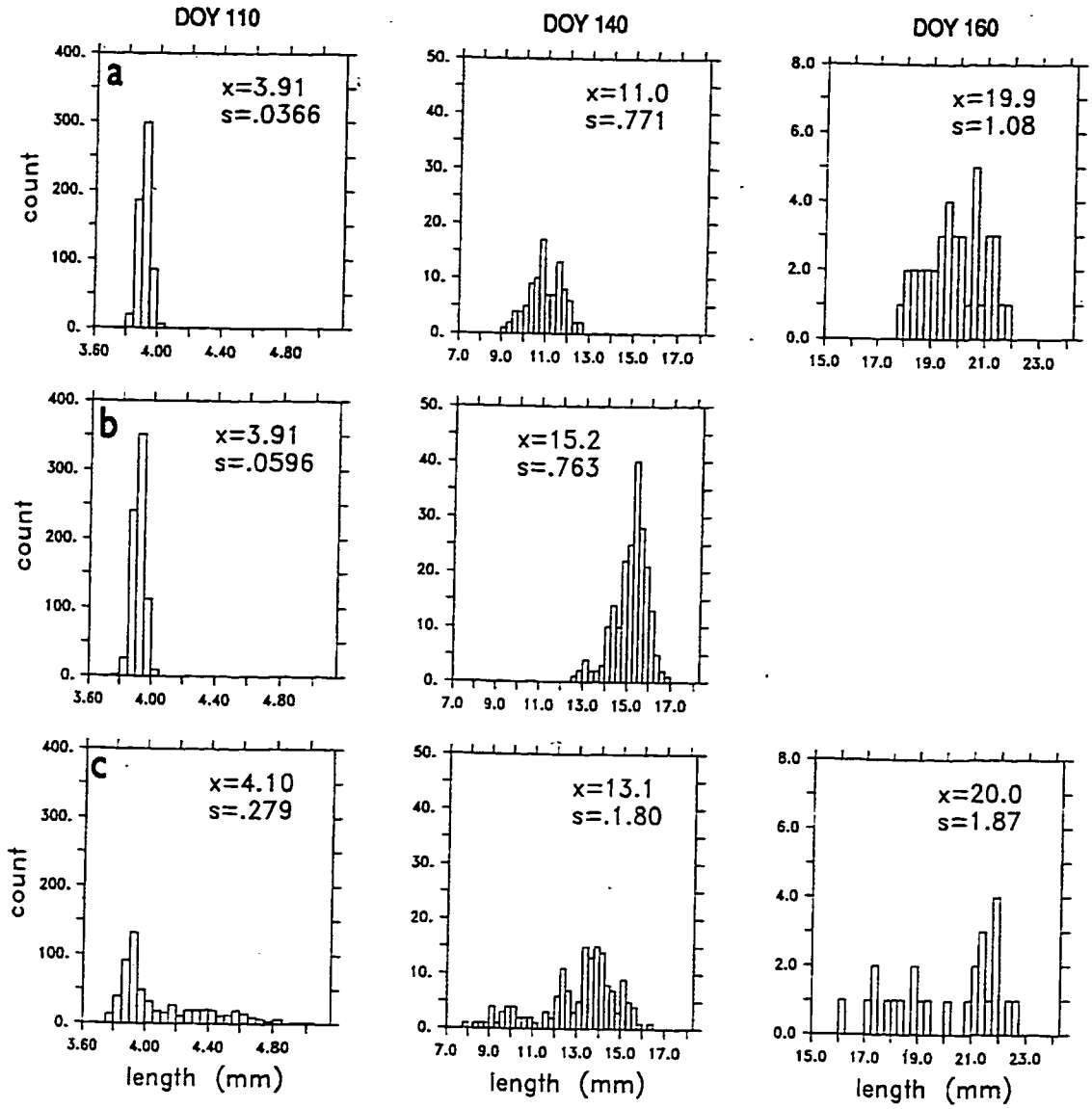

Figure 3.4. Length distributions of the larval stages from Simulation 2. 'Count' refers to the number of individuals represented by each bar. (a) 'Constant T' case, (b) 'Linear T' case, (c) 'Lagrangian T' case.

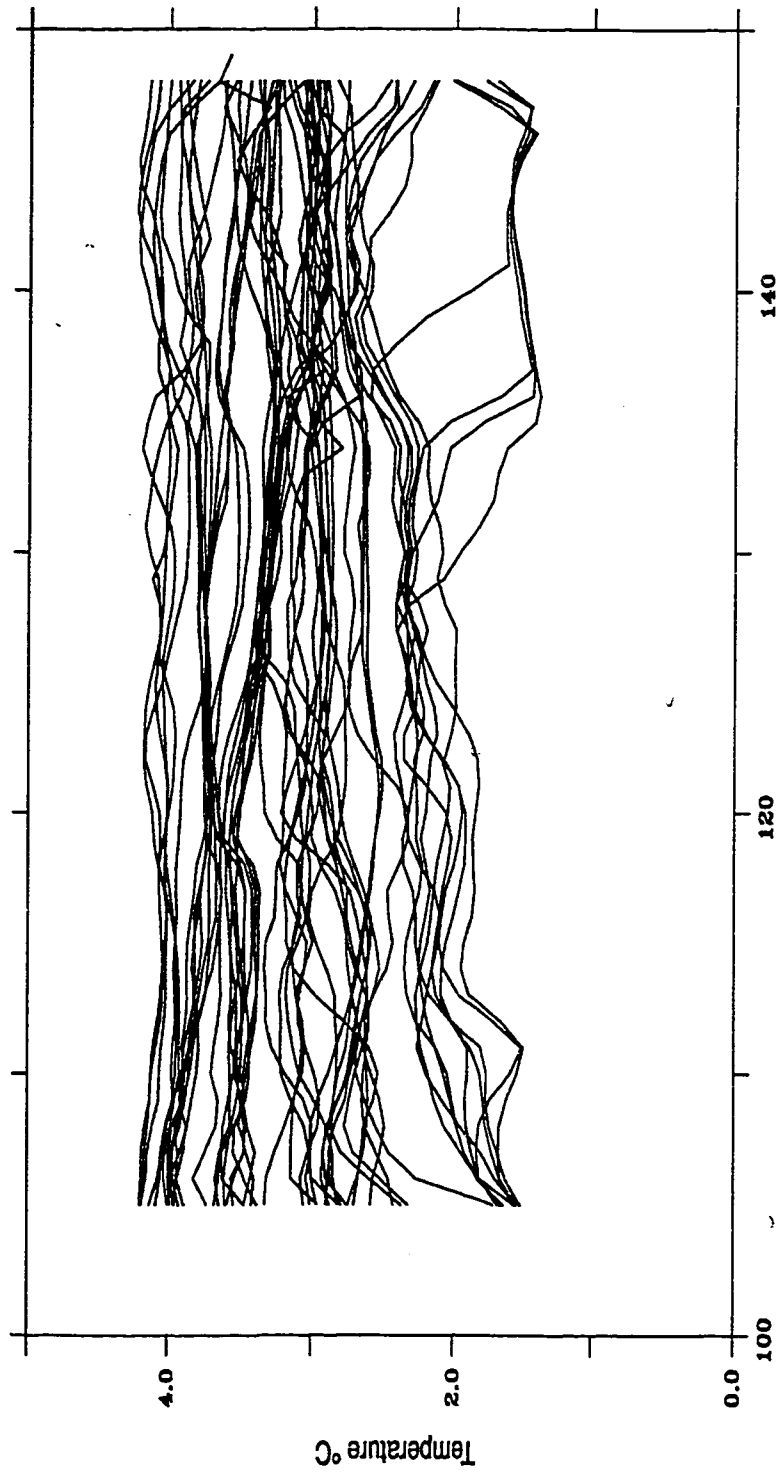

Figure 3.5. Lagrangian time series of temperature following 25 of the floats tracked by the hydrodynamic model in Simulation 2. Floats are initially released in a square pattern at 40 m depth, at the south western end of Shelikof Strait between Kodiak Island and mainland Alaska.

(Hermann and Stabeno 1996) was used for all subsequent simulations, to eliminate this bias.

A plot of larval weights versus accumulated degree days at DOY 150 (Fig. 3.8) reveals that (for this version of the IBM) much of the variance in weights among individuals can be explained by the integrated temperature history, due to the effects of temperature on development, consumption and respiration. Note that while the integrated Lagrangian temperatures exhibit a range of values, they do not exhibit a simple bimodal pattern of "warm" versus "cold" individuals. Hence, the ultimate bimodal pattern must be attributed to both the deterministic temperature factors and the random mortality, life-stage transitions and feeding in the probabilistic IBM.

3.3 Simulation 3. The importance of vertical location.

In this simulation, we examined the effect of adding complex algorithms that varied by life stage to determine the depth of an individual, over a simpler scheme where average depths by life stage were used. Fig. 3.9a and 3.9b show the trajectories of 2 floats, one released from either end of the southwestern-most row of the grid, for each run. The floats do not follow the same track between runs, and the endpoints of the float tracks are not in the same positions for the null and alternative models. In order to test whether the trajectories are different for each depth algorithm, we used latitude and longitude on DOY 149 as a representative bivariate measure. Location on DOY 149 was chosen because it is the day before the first larva metamorphosed into the juvenile stage (i.e. the last day in which all larvae are still in the model). A multivariate ANOVA (MANOVA) was done which included depth algorithm (null or alternative), initial position and the interaction between depth algorithm and initial position as factors, and latitude and longitude on DOY 149 as the dependent variables.

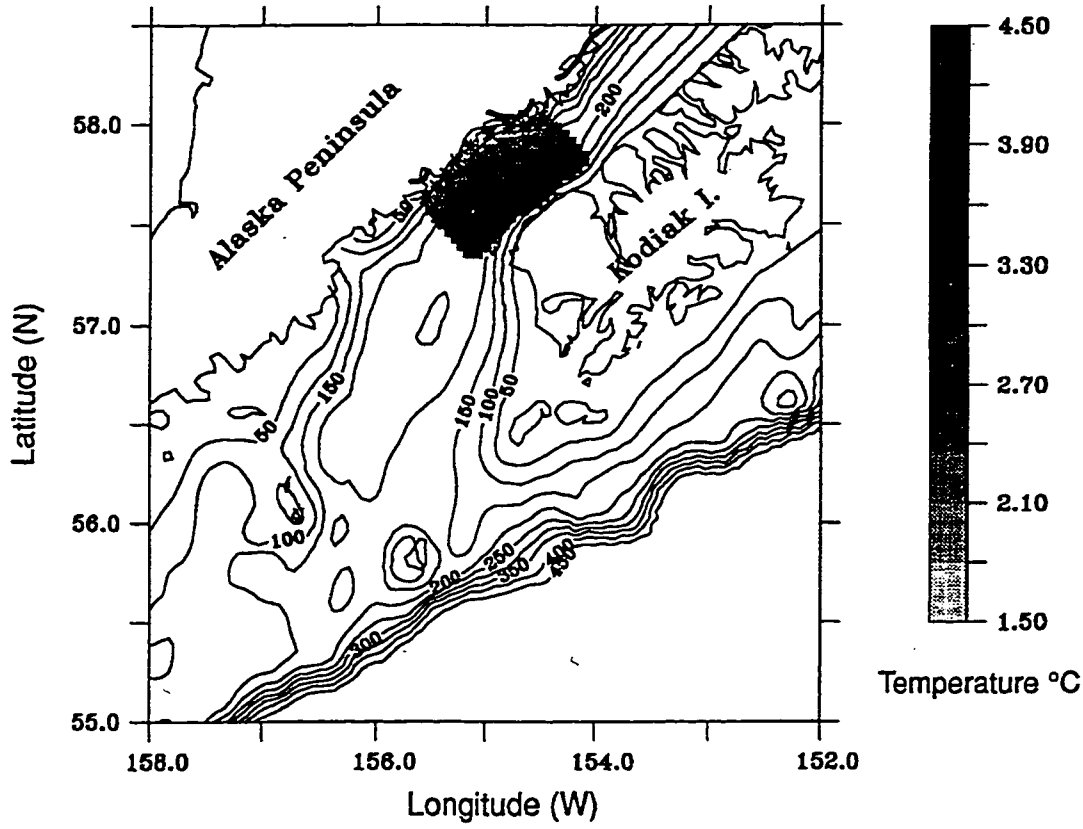

Figure 3.6. Temperatures of tracked floats at DOY 105. Temperatures are represented in greyscale; *: position of a float associated with no living individuals (that is, all individuals using temperature series from that float have died).

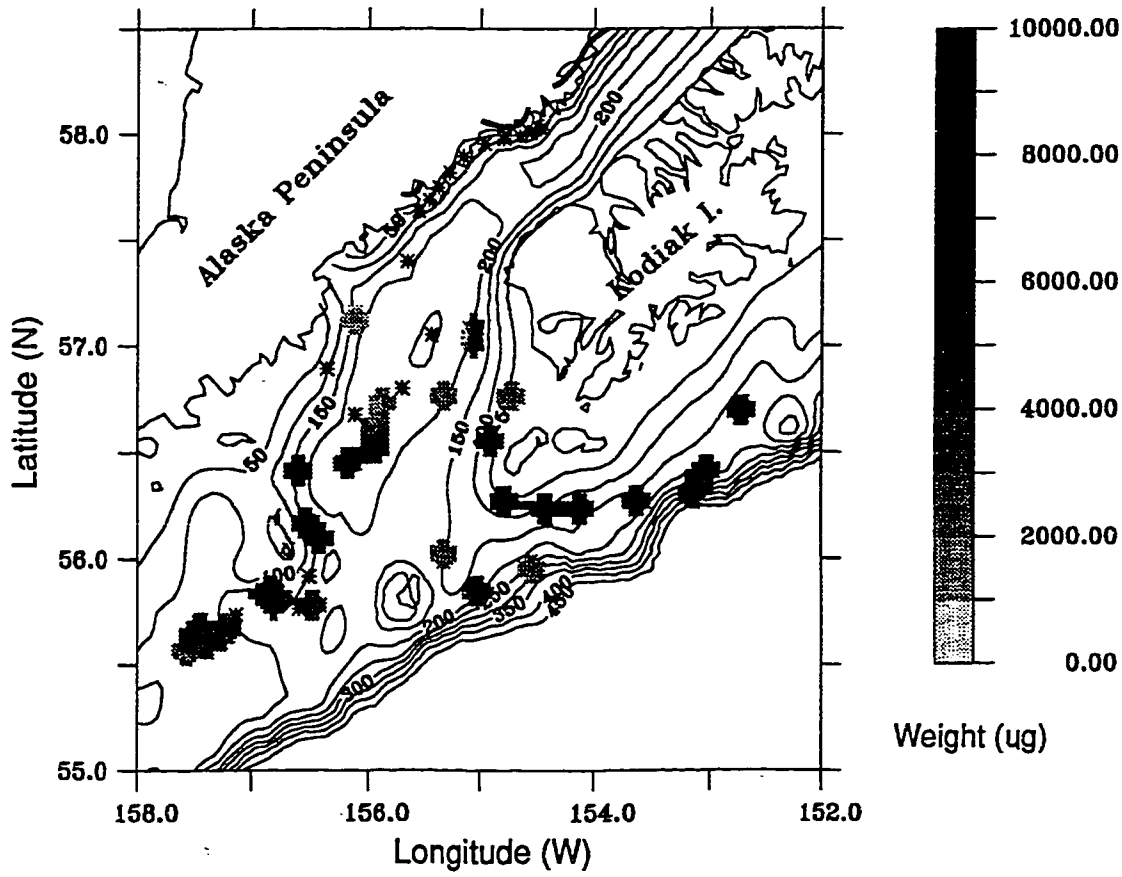

Figure 3.7. Average weights for living individuals associated with each of the tracked floats at DOY 150. Mean weights are represented in greyscale; *: all dead individuals.

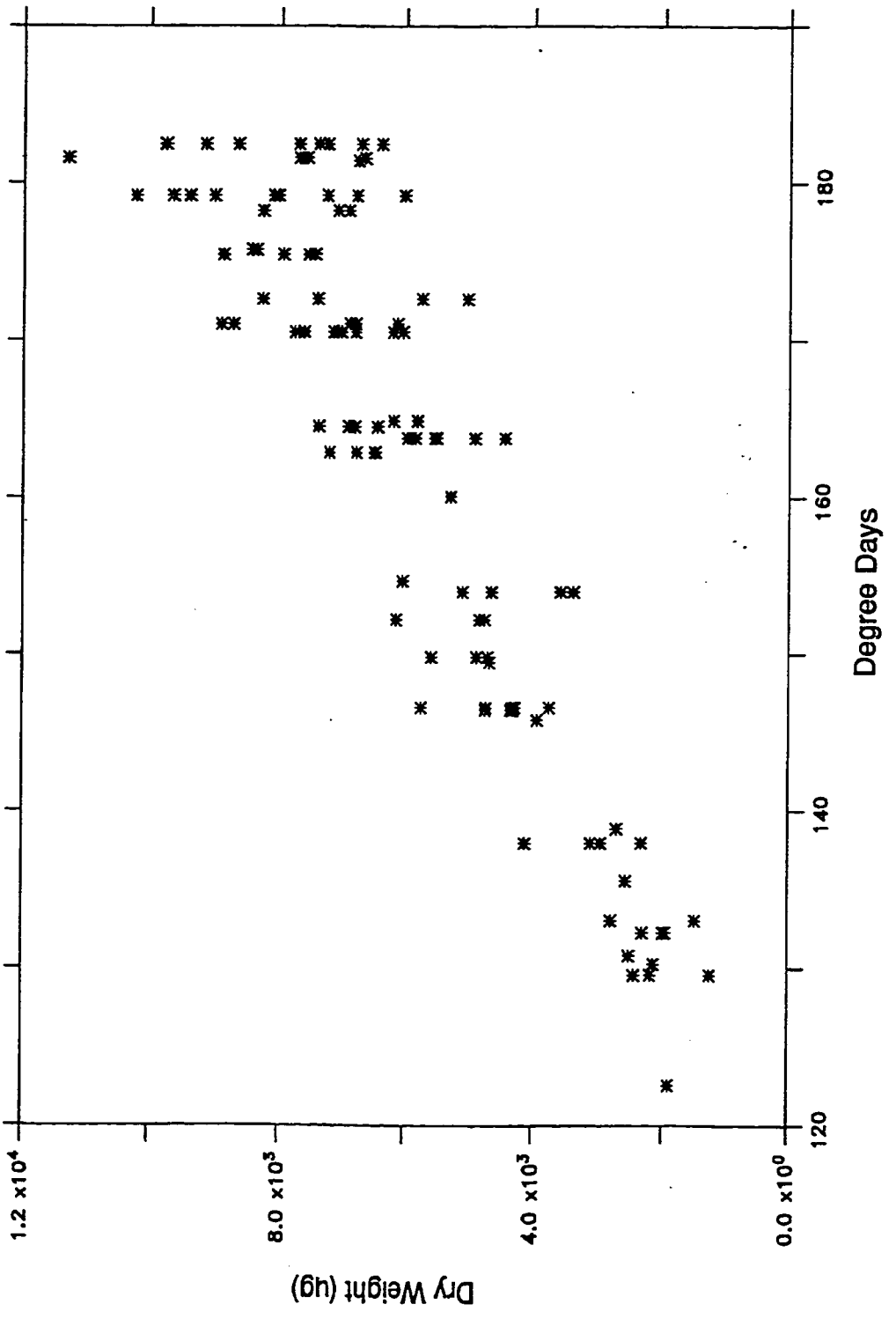

Figure 3.8. Scatter plot of individual weights at DOY 150, versus degree days accumulated by each individual at DOY 150.

$$(x, y)_{ijk} = \mu + a_i + b_j + ab_{ij} + \varepsilon_{ijk} \quad \text{(EQ 3.1)}$$

where,

μ = expected mean,
x = latitude on DOY 149 (°N),
y = longitude on DOY 149 (°W),
a = effect of depth algorithm (i = 1,2),
b = effect of starting location (j = 1,...,100),
ε = error term (k = 1,...,30).

This analysis indicated a significant interaction effect (MANOVA, $p < 0.001$). We therefore ran separate MANOVAs for each initial location, with the depth algorithm as the only factor. We found that the effect of the depth algorithm was significant for each initial position (MANOVA, $p < 0.001$) for all tests). We interpret this to mean that the divergence among trajectories of individuals due to the effect of the depth algorithm varies with the starting location, but that the effect of the difference due to the depth algorithm is significant overall.

It seems reasonable to conclude that varying vertical location has an important effect on the subsequent horizontal position of an individual, and that correct advection of individuals through space using this model is dependent on specification of the depth of individuals in a manner which reflects what is known about their true vertical distribution and migration rather than using a simplified scheme.

We examined whether the addition of vertical migration, as in the alternative model, resulted in any differences in growth rates, dates of transition or other individual attributes between the 2 model runs. Such differences would be due to different temperature histories resulting from the differing vertical and horizontal trajectories. When a linear model is fit to the length-age relationship (with length square-root transformed to linearize the data) for modeled larvae, there is a significant difference between the null model (Fig. 3.10a) and the alternative model (Fig. 3.10b) (ANCOVA, $p<0.001$). The mean length on DOY 149 was larger and the standard deviation of length on DOY 149 was less variable for the null model (Fig. 3.10c) than for the alternative model (Fig. 3.10d). The date on

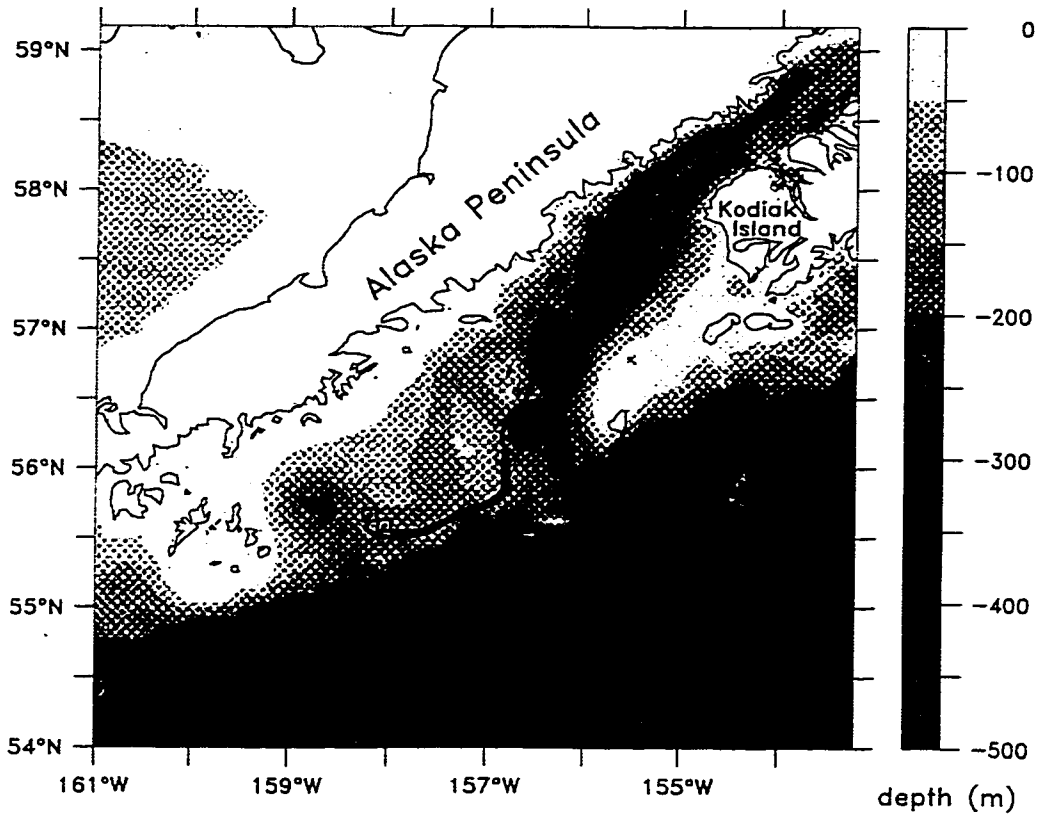

Figure 3.9a. Trajectories of 2 representative floats from the Simulation 3 model run which uses the null model (i.e. average depths for each life stage.

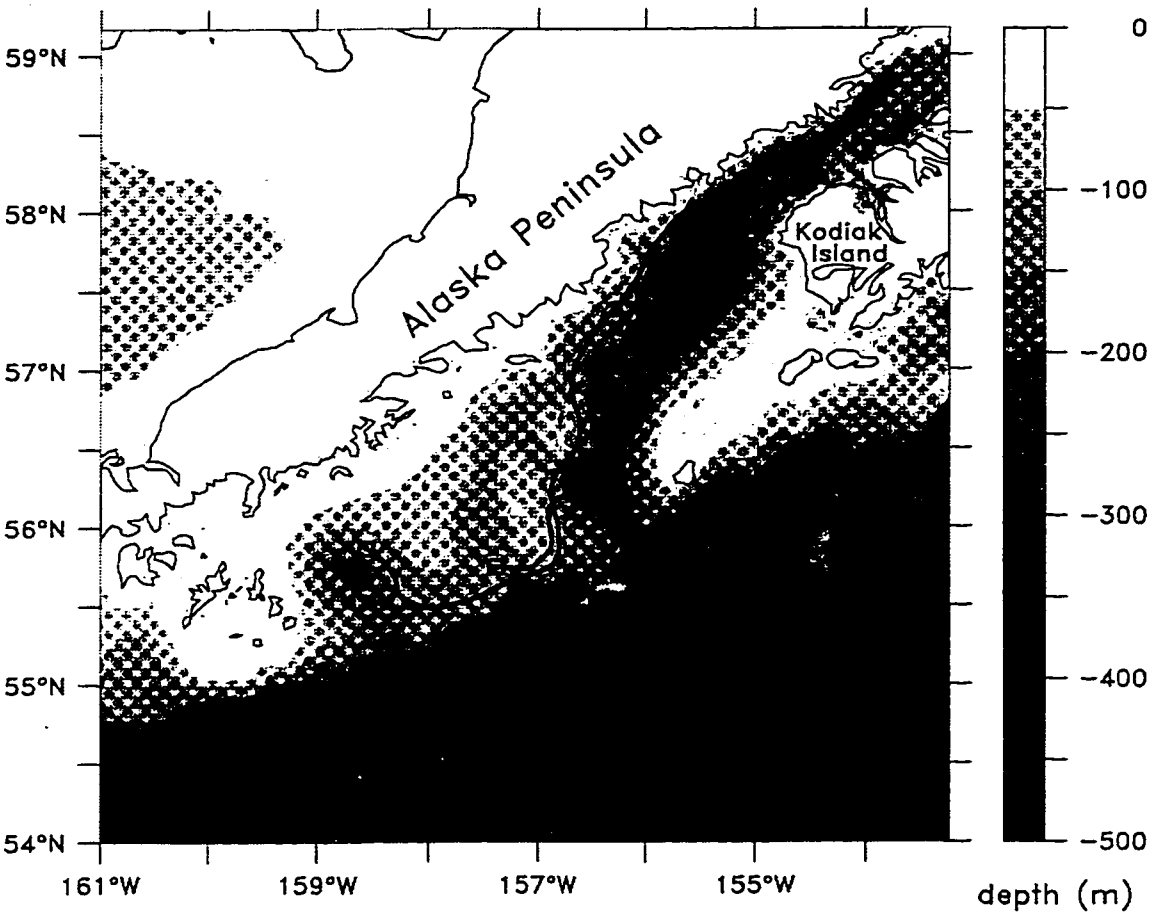

Figure 3.9b. Trajectories of 2 representative floats from the Simulation 3 model run which uses the alternative model; that is, the vertical movement and migration algorithm described in the text.

which first feeding occurred (i.e. the transition from the yolk-sac larval to the feeding larval stage) was earlier in the null model (t-test, $p<0.001$), as was the date at which metamorphosis from the feeding larval stage to the juvenile stage occurred (t-test, $p<0.01$). It is important to realize, also, that use of locations interpolated between velocity fields stored every 15 d would tend to underestimate the divergence betweed the null and the alternative models. It is apparent from these statistics that growth and other life history characteristics of young pollock were significantly affected by the choice of depth algorithm.

In an early simulation that ran through the 0-age juvenile stage, we also tested the difference in individual trajectories between two depth algorithms for the juvenile stage: (1) an average depth of 40 m, plus random noise, and (2) linearly increasing depth with length, plus random noise. Juveniles were treated as purely passive particles in the horizontal direction. The modelled distributions were compared to distributions of juveniles for September, 1990.

The actual distribution of juvenile pollock in September, 1990 was concentrated just east of the Shumagin Islands. The distribution was patchy, and the highest concentrations were inshore. The modeled distribution of juveniles using the depth algorithm which increased with size showed good agreement in degree of patchiness and the location of the highest concentration (east of the Shumagins), but the center of the modeled distribution was somewhat farther offshore. Advection along bottom contours significantly affected the distribution, as near-bottom flows tend to follow bathymetric contours. When an average depth was used, resulting in somewhat shallower distributions of individuals, the distribution of juveniles was significantly further inshore, but still a bit offshore of actual distributions. Their location, due to their shallower distribution, was less influenced by bottom topography. In spite of the fact that juvenile pollock have significant horizontal swimming capabilities by September of their 0-age year, it appears that advective processes may be more important than active, directed swimming behaviors in determining distributions (at scales larger than schooling) in September. Directed swimming behaviors

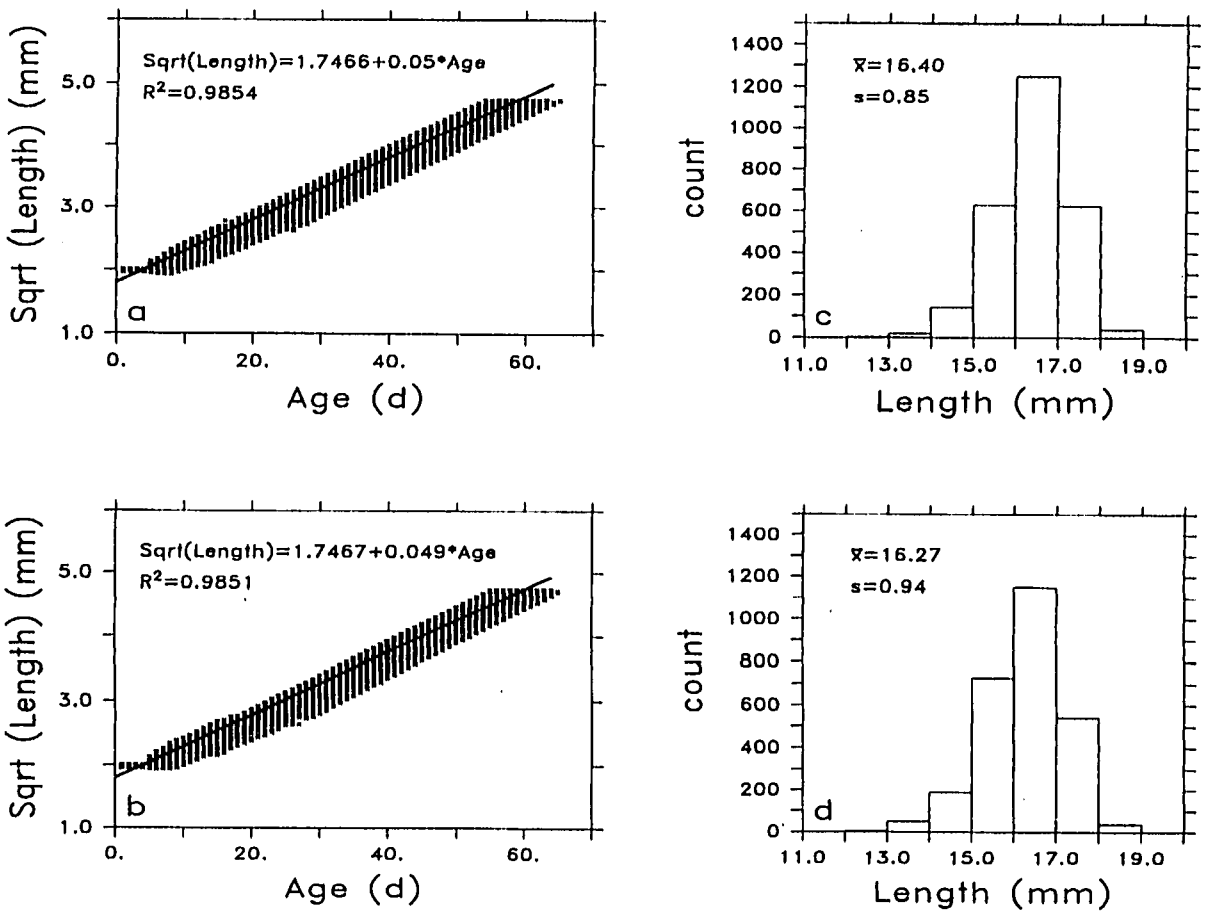

Figure 3.10. (a) Length-age relationship for larvae from the null model, Simulation 3. Line represents the fitted linear equation. (b) Length distribution of larvae from the alternative model, Simulation 3. (c) Length-age relationship for larvae from the null model, Simulation 3. Line represents the fitted linear equation. (d) Length distribution of larvae from the alternative model, Simulation 3.

that do exist appear to transport juveniles towards inshore areas to some degree, as well as contributing to schooling, and therefore to the patchiness of the distribution.

3.4 Simulation 4. Hindcasts

The results of Simulation 4 are presented in five major sections. Not all years were simulated for each part, these hindcast simulations were not all done at the same time. First we present and compare patterns of circulation (salinity and velocity) for four years: 1978, 1987, 1988 and 1989. Second, we examine modelled vs. measured larval density patterns for several dates in 1987, 1988 and 1989. For 1989, we look at the results of two slightly different versions of the IBM, using the same runs of SPEM. Third, we look at positions and lengths of individual fish for DOY 142, DOY 202 and DOY 262, for 1978, 1987, 1988 and 1989, using model output. Fourth, we examine output of the NPZ model for 1978, 1987, 1988, 1989, 1991 and 1994. We examine interannual variation of four state variables (chlorophyll, *Neocalanus*, spp., the sum of the *Pseudocalanus*, spp. naupliar stages, and the *Pseudocalanus*, spp. adult stage) over time for both Line 8, and averaged over the whole NPZ model domain. We also look at spatial patterns of the sum of *Pseudocalanus*, spp. naupliar stages in detail, (these stages are the most important food of larval pollock). We examine spatial patterns every 10 d from DOY 111 to DOY 161 for all years. We also examine output from a run of the 3-way (SPEM-NPZ-IBM) coupled model for mid-June, 1987. Fifth, we use two spatial statistics measures: the number of fish remaining in the region between Kodiak Island and the Shumagin Islands, and Lloyd's (1967) Index of Patchiness, to compare model output with data.

3.4.1 Salinity and velocity patterns

As a result of the interannual variability in wind and runoff inputs to the physical model, the different years exhibit significantly different salinity and velocity fields. Here we compare the physical results at 40 m for 1978 (strong wind, low runoff), 1987 (moderate wind, strong runoff), 1988 (strong but variable winds, strong runoff), and 1989 (weak

wind, weak runoff). First, consider the salinity fields on DOY 142 (22 May; Fig. 3.11). The 1978 run yielded smooth flow through most of the strait, with meandering and eddy-like structures further along in the sea valley. The 1987 run produced a prominent matched pair of counter-rotating eddies in the upper sea valley, with other eddy features present in the strait. The 1988 run produced a single prominent eddy at the head of the sea valley, while the 1989 run produced no prominent eddy features in the sea valley or shelf area.

By DOY 172 (21 June), the meanders present in the 1978 run had evolved into an eddy pair in the sea valley. The eddy pair present at DOY 142 of 1987 moved downstream, as a bolus of fresh water from the strait moved in to replace it. The singular eddy of 1988 was still present, along with an eddy pair near the exit of the sea valley. An eddy pair formed near the head of the sea valley in the 1989 output.

By DOY 202, (21 July), the eddy activity of 1978 had weakened. The 1987 field exhibited a variety of eddy structures, both in the sea valley and on the continental shelf. A new, powerful counter-rotating pair of eddies had formed in the center of the sea valley, while the pairs further to the southwest were less energetic remnants of formerly strong vortex structures. Year 1988 exhibited continued meandering in the sea valley, with one or two fresh-core structures lodged near the exit of the strait. Year 1989 exhibited two linked fresh-core eddies spanning the strait exit and the upper sea valley; the latter structure was found to be quite durable, persisting at that location from late June until it was washed down the sea valley and dissipated in early August.

For all years, low salinities occupied the northwestern half of the strait and higher salinities were generally found in the deeper areas off the continental shelf. The "wet" year of 1987 (mean runoff of ~1.9×10^4 m^3 s^{-1}) was the most eddy-rich year of the four compared here. Animations of the 1987 salinity field from March to September revealed how eddy pairs repeatedly formed at the head of the sea valley, then subsequently washed down the valley to be replaced by a new pair. Overall, the "dry" year of 1989 (mean runoff of ~ 0.8

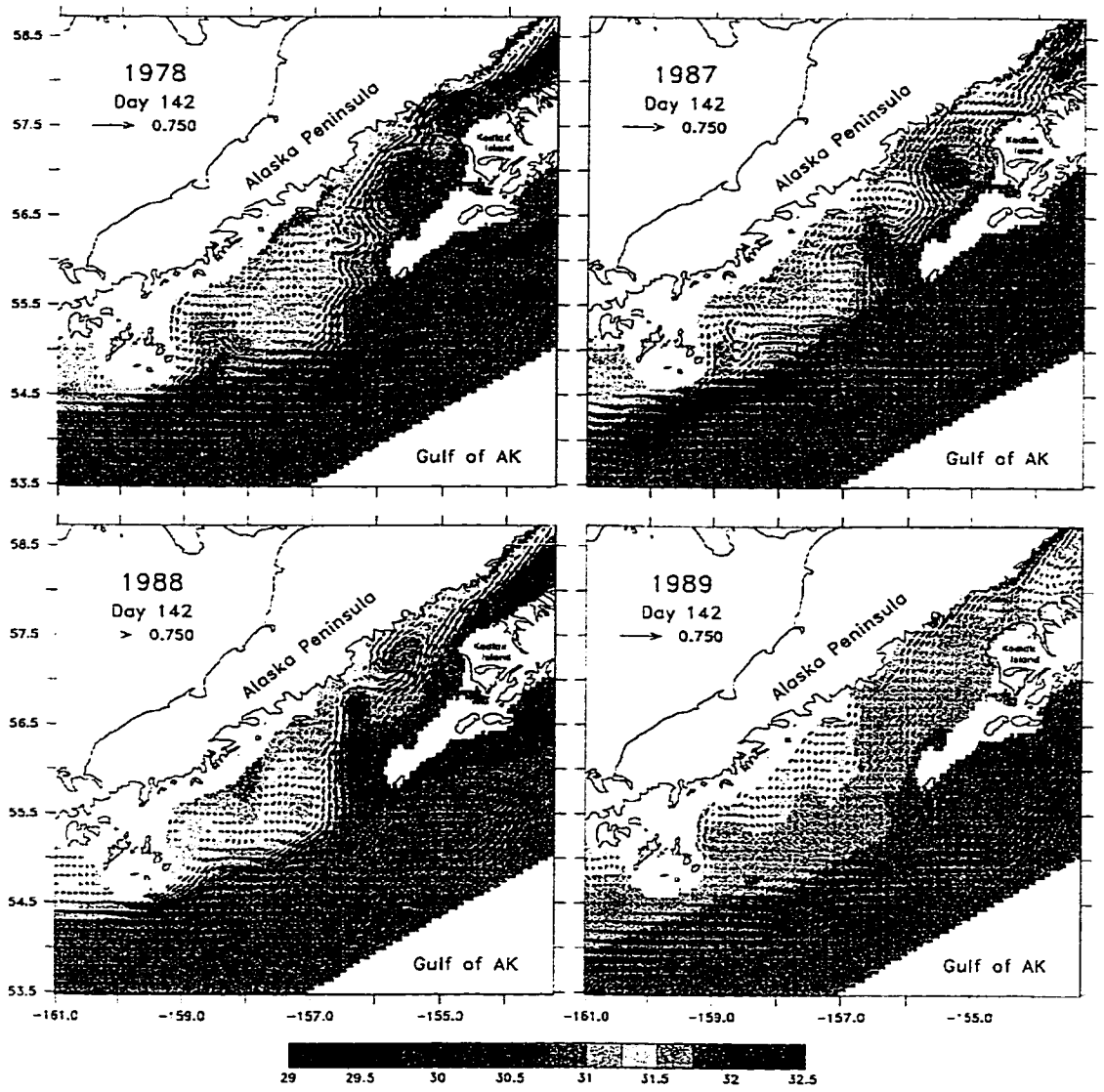

Figure 3.11. Comparison of modelled salinity (in psu) and velocity at 40 m depth on day 142 (22 May) for 1978, 1987, 1988 and 1989. Key indicates length of 0.75 m s^{-1} velocity vector.

x 10^4 m^3 s^{-1}) spawned far fewer eddies than was the case in 1987. We interpret these results as the natural consequence of enhanced runoff leading to enhanced available potential energy, which drives the eddy formation process. However, we note that abundant runoff by itself was not sufficient to form eddies downstream of the strait; strong winds appeared necessary to drive the fresh water through the strait. Indeed, it was a wind burst at the beginning of July 1989 which ultimately forced a large bolus of fresh water through the strait, and led to the large, persistent eddy observed on DOY 202.

Velocity fields in the 4 years are summarized using maps of mean velocity (Fig. 3.12) and eddy kinetic energy (Fig. 3.13) for the period covered by the biological runs (March - September). The mean velocity field for 1978 exhibits a strong flux through the strait, trapped against the coastal boundary and flowing out the exit of the sea valley, to join with the Alaskan Stream. In 1987, the mean flow is seen to meander significantly in the center of the sea valley; this reflects the repeated formation of vortex pairs in that area (~3-4 such pairs form, decay, and are swept downstream from this area over the course of the spring and summer). In 1988, the field is similar to that of 1978, but whereas 1978 exhibits a weak cyclonic tendency on the southern side of the ACC beyond the exit of the strait (~57.4°N, 155.5°W), 1988 exhibits an anticyclonic tendency at that location. Year 1991 (not shown) exhibited powerful currents similar to those of 1978 and 1988, and with fewer eddies than in 1987. In 1994 (not shown) was a relatively "normal" year, however it exhibits significant eddy activity, with several pairs forming and dissolving , especially between DOY 150-190. Before DOY 120, not much mesoscale activity is seen. 1994 is similar in its rate of eddy formation as 1988 except that the eddies in 1988 were somewhat larger and more persistent. In 1989, the mean flow is significantly weaker than in any of the other years, with a weak anticyclonic pattern at the head of the sea valley.

Maps of eddy kinetic energy at 40 m depth (Fig. 3.13) represent the mean squared deviation of north-south and east-west velocities from their mean values at each physical location. In each case the highest values are observed along the coastline near the exit of the strait, with high values penetrating into the sea valley proper. The year of strongest winds

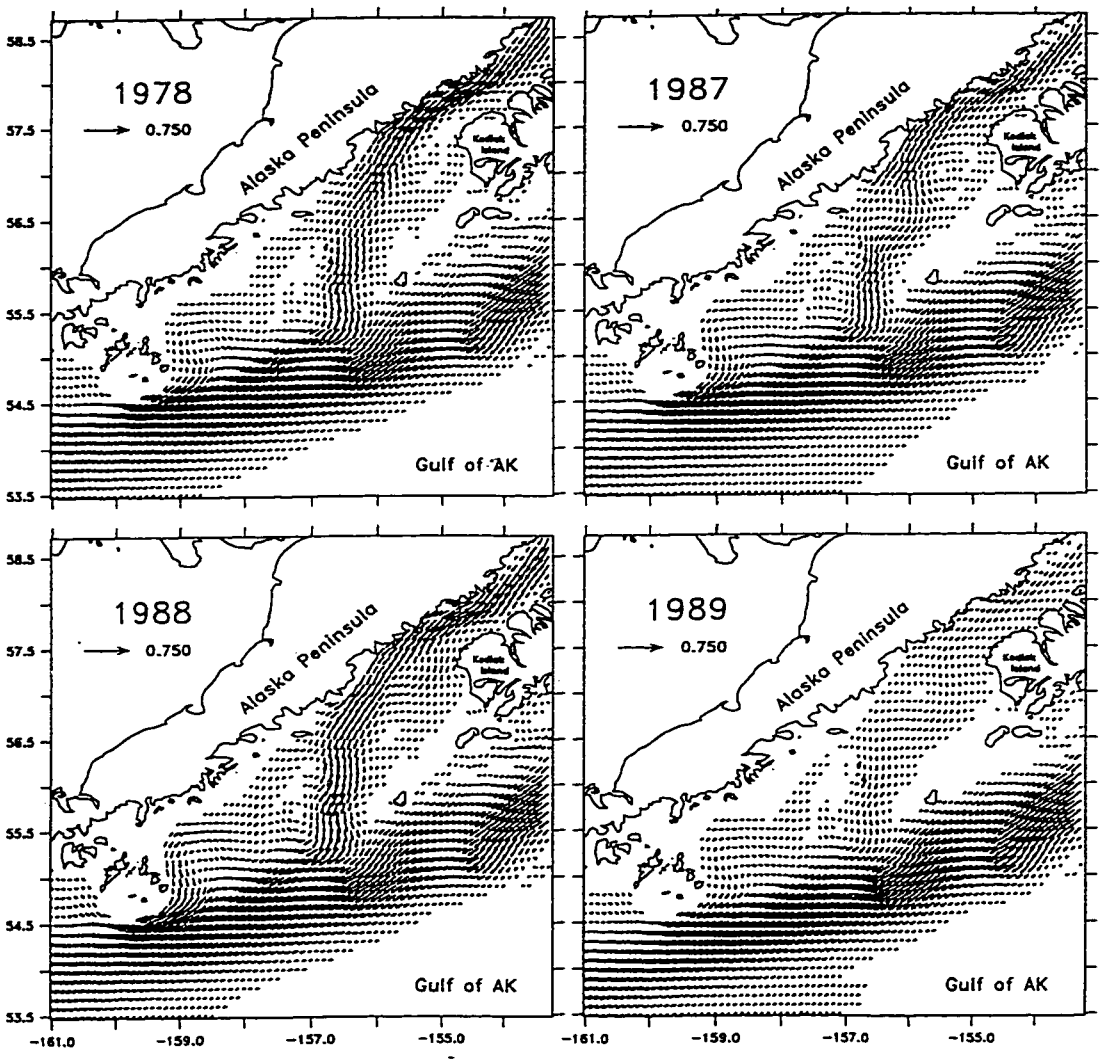

Figure 3.12. Comparison of average modelled velocity fields for DOY 60-269 at 40 m depth for 1978, 1987, 1988 and 1989. Key indicates length of 0.75 m s^{-1} velocity vector.

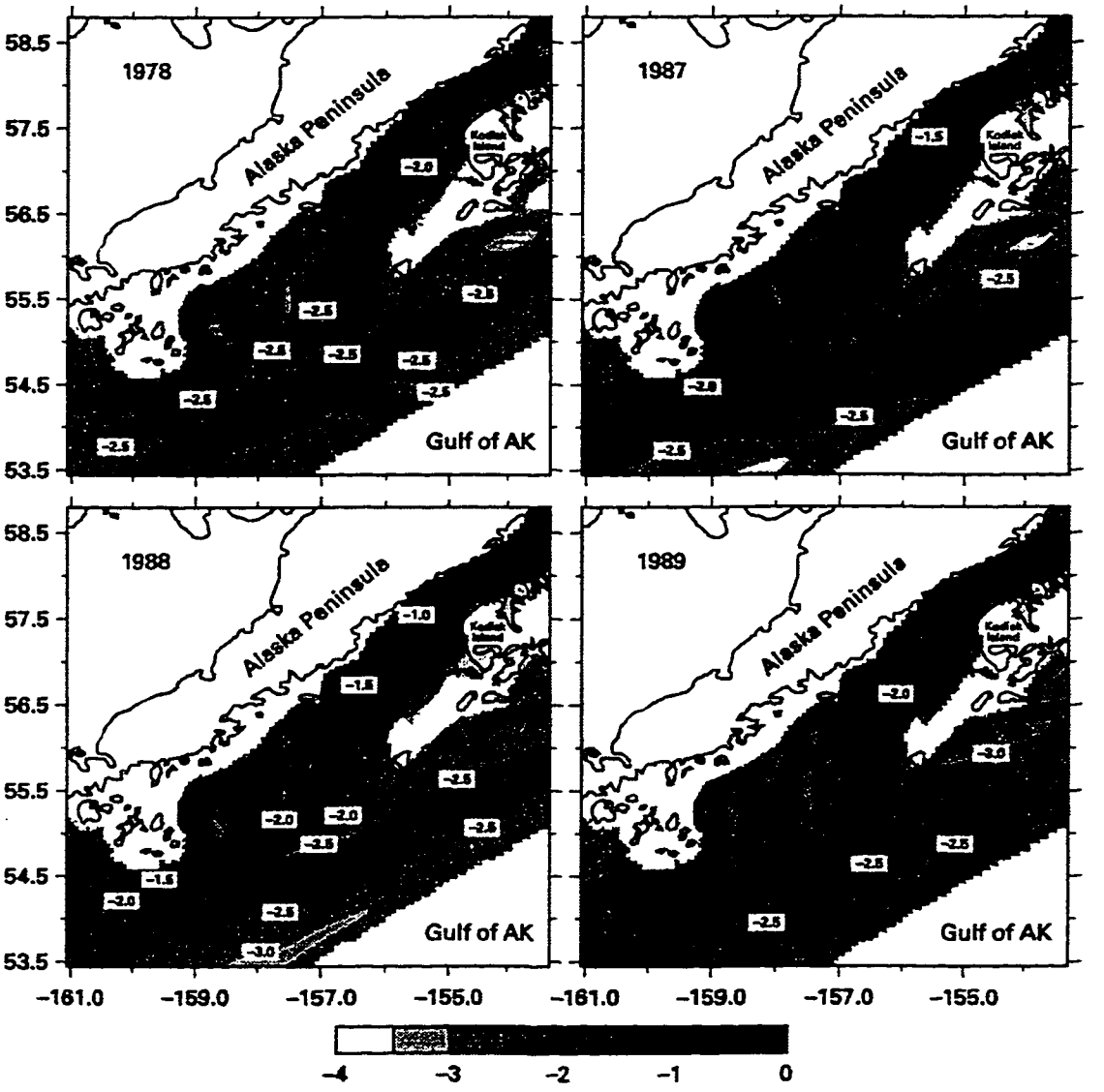

Figure 3.13. Comparison of eddy kinetic energy for DOY 60-269 at 40 m depth for 1978, 1987, 1988 and 1989. Units are $\log_{10}(m^2s^{-2})$.

and strong runoff (1988) exhibits the highest values. Year 1987 is next, reflecting the prevalence of mesoscale eddies driven by the powerful runoff that year. Year 1978 exhibits weaker values than 1987, with 1989 (a year of weak winds and runoff) exhibiting the lowest values overall.

3.4.2 Larval density patterns

Initial positions of the spawned individuals were shown in Fig. 2.8. It is necessary to demonstrate that the biophysical model places individuals in approximately the correct physical locations. To this end, we compare the concentration of modeled individuals at DOY 142 with the measured concentration of larvae during DOY 135-150 (15-31 May) for 1987, 1988 and 1989 (Fig. 3.14), and further comparisons for mid-May and late May, using a version of the IBM with slight differences. The aggregated field data, gleaned from earlier FOCI studies of larval advection, is discussed in Hermann et al. (1996a, see pp. 58-70).

Weaker shoreward concentrations were sometimes observed in model output, than were present in the data. This may indicate that the hydrodynamic model underestimates shelfward transport downstream of Shelikof Strait or that larvae and juveniles exhibit behaviors that transport them towards shore that are not described by the IBM. Despite this discrepancy, interannual differences observed in the data were reasonably reproduced by the model.

In late May of 1987, larvae were found concentrated to the west and south of Kodiak Island, with a large number centered near the coastline at ~57°N, 156.5°W. Modeled individuals at this time appear focused at the same latitude, but primarily in the sea valley, to the east of the measured concentration maximum. In both measured and (especially) modeled fields, lower concentrations were found to the southwest of the sea valley. In 1988, measured concentrations were greatest in a near-coastal band leading from the 1987 maximum to Semidi Island. As in 1987, the model tended to place individuals deeper in the sea valley, but at similar latitudes to the measurements. A long trail of individuals streams out

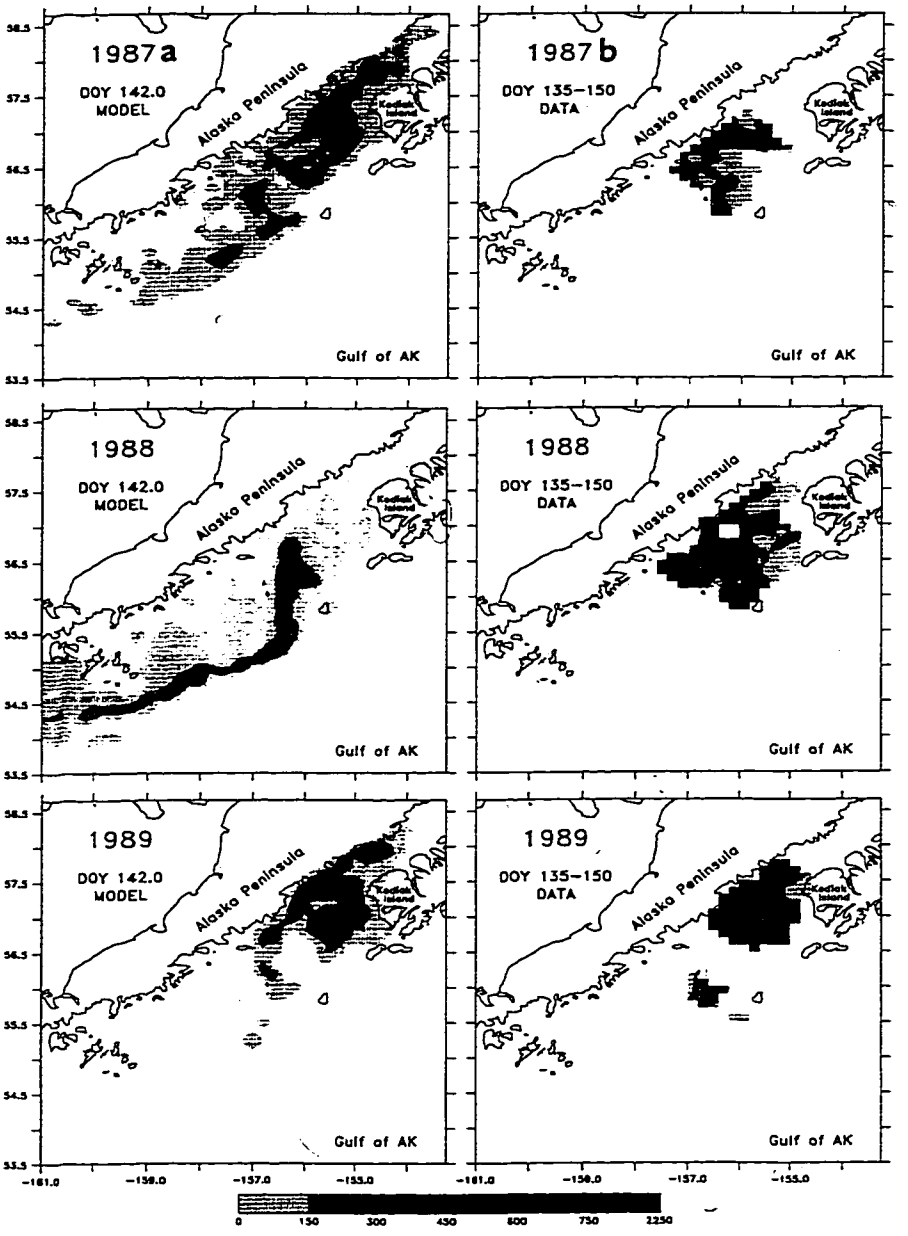

Figure 3.14. (a) Density of individuals in the IBM model runs on DOY 142 (22 May) for the 3 years. Values are number of individuals per spatial bin (0.1° latitude x 0.2° longitude), converted to larval density (number per 10 m^2). Only non-zero density areas are shaded. (b) Measured larval density for all individuals collected during 15-31 May in each of 3 years: 1987, 1988 and 1989. Shaded, contoured areas indicate the spatial extent of the collected data.

from that maximum in the model, following the inside edge of the Alaskan Stream out past the Shumagin Islands to the southwest. In 1989, two intense maxima of larval concentration were observed upstream of the 1987 and 1988 locations. One maximum lies against the coast just past the exit of the strait, while a larger maximum lies to the south in the middle of the sea valley. Smaller concentrations were found near the exit of the sea valley, between Chirikof and the Semidi Islands. The model reproduced this pattern extremely well. Most significantly, the enhanced concentrations of larvae found in the field in 1989, relative to 1988 and 1987, were faithfully reproduced by the model. The model suggests that some of the larvae in 1988 and 1987 were advected far downstream of the sampled area by late May. By DOY 172, 1978 and 1988 exhibited considerably lower concentrations overall in the model domain than 1987 and 1989. The maximum concentration of individuals in 1987 remained in the sea valley on this date, trapped within a cyclonic eddy there. A large portion of the larvae present near the exit of the strait on DOY 142 of 1989 had been advected onto the continental shelf to the southwest; the remainder had been flushed out the exit of the sea valley to join with the Alaskan Stream.

An additional run of the IBM with 1989 velocity fields was run, with the only difference from those described above being that the spawning date was fixed at DOY 90 (this was an earlier simulation). Fig. (3.15a) shows the observed larval distribution between May 9, 1989 and May 16, 1989, as measured by a FOCI ichthyoplankton survey (Savage 1990). Fig. (3.15b) shows the modeled distribution of larvae on May 10, 1989. Although details differ, these 2 plots appear similar in that the highest concentrations of larvae are found near Sutwik Island and in the middle of the sea valley in both, although the highest measured distributions were somewhat farther offshore. The modeled distribution also shows a similar degree of patchiness as the measured distribution. Fig. (3.16a,b) shows the measured versus modeled larval distributions near the end of May 1989. The distributions again appear similar, with high concentrations near both Sutwik and the Semidi Islands, and similar patchiness of distribution.

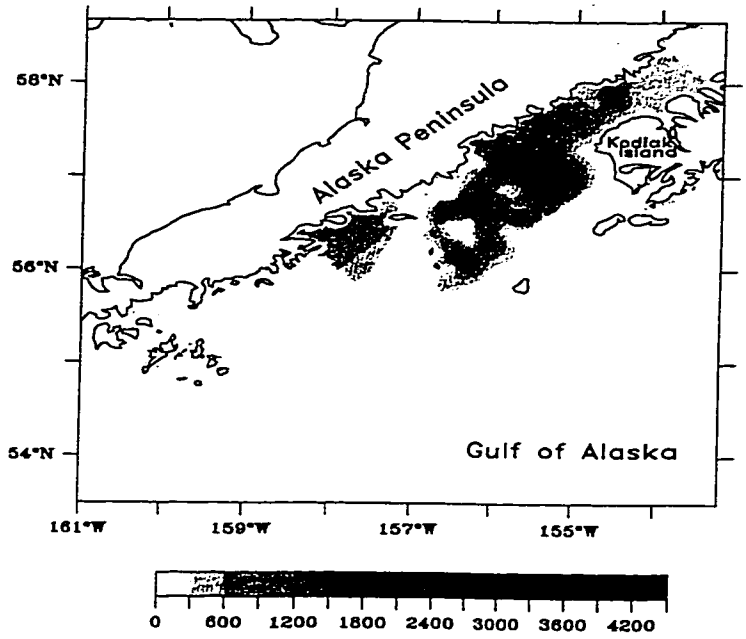

a.

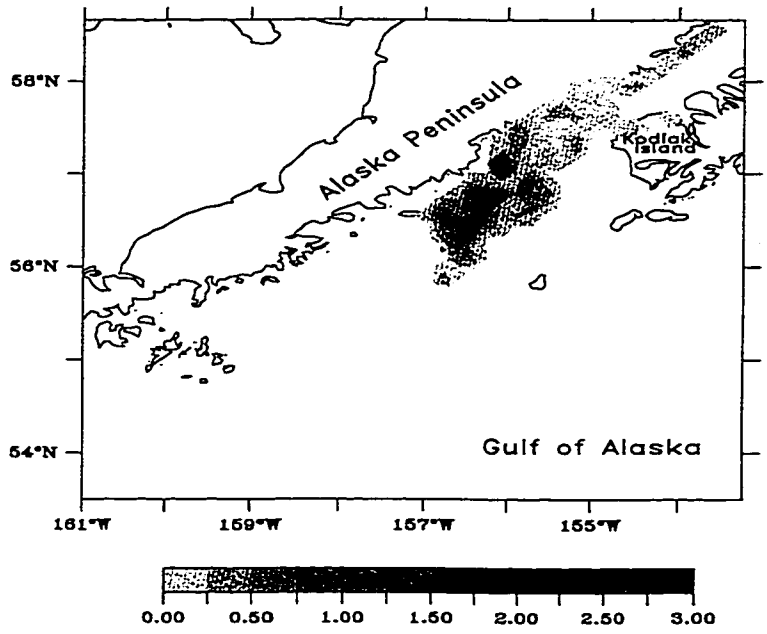

b.

Figure 3.15. (a) Measured abundance of larval walleye pollock between May 9 and 16, 1989. (b) Abundance of modelled larvae for May 10, 1989. Greyscale represents relative larval densities.

a.

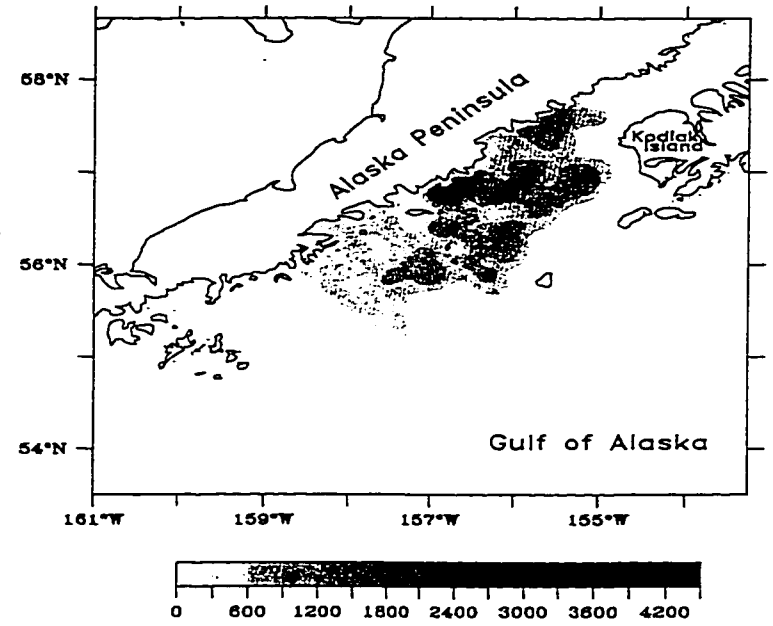

b.

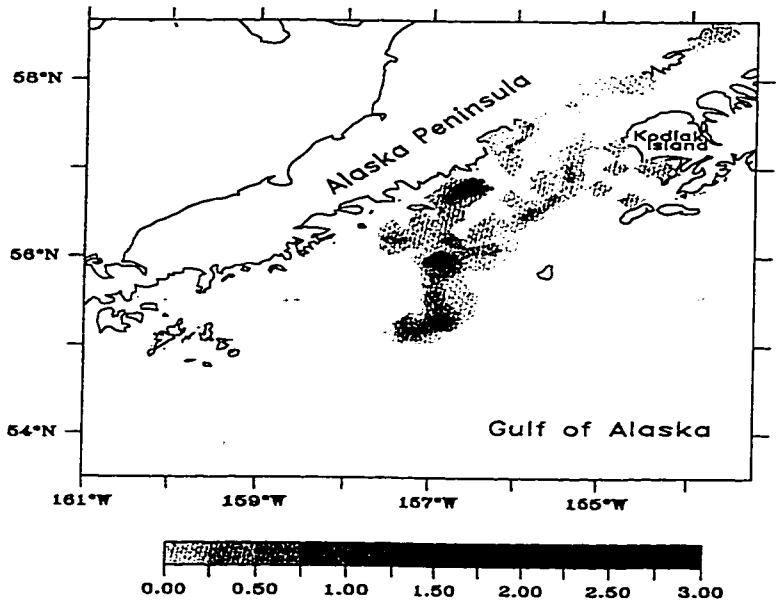

Figure 3.16. (a) Measured abundance of larval walleye pollock between May 29 and June 5, 1989. (b) Abundance of modelled larvae for May 30, 1989. Grey scale represents relative larval densities.

Animations of larval distributions for 1994 (not shown) indicate that many larvae travelled around the Semidi Islands and up onto the outer shelf area east of the Shumagins between DOY 160 and DOY 175. Significant numbers stayed in Shelikof Strait and the sea valley, while others remained close to the coastline near Sutwik Island. Few larvae had travelled past the Shumagins by DOY 145, as they did in 1988.

Fig. (3.17a-h) shows a series of output from the model through the feeding larval stage. These are plots of individual fish locations from the 1989 simulation for DOY 90 to 160 at 10 d intervals. At the beginning of the simulation on DOY 90 the eggs are released in Shelikof Strait. The egg mass follows the bottom topography and moves to the southwest (downstream). As they move downstream the eggs disperse, hatch into yolk-sac larvae and then feeding larvae. This series of distribution plots reproduces the conceptual model of egg and larval transport (Fig. 1.3) which has been derived from field observations.

3.4.3 Individual positions and lengths

We now compare larval positions and lengths among the modeled years. Raw positions are plotted to allow coding by length, and because the distribution of individuals becomes too sparse for contouring spatial density by the end of the simulation. Contours of barotropic stream function are superimposed on the plots, to illustrate the location of mesoscale circulation features (eddies and meanders).

As noted in the larval density maps, DOY 142 exhibits large differences among years (Fig. 3.18). For the 1989 run, individuals clustered near their release point. In the 1987 run, they were carried somewhat farther to the southwest, and a large number were entrained into an eddy pair in the center of the sea valley on that date. Few were carried as far as the Shumagin Islands. Conversely, in 1978, 1988 and 1991 (not shown), many of the individuals were swept into the Alaskan Stream and past the Shumagin Islands by DOY 142. In 1978 and 1991, large numbers collected on the shallow shelf northeast of the Shumagin Islands, due to the strong shelfward flows prior to DOY 142. Note the general tendency in

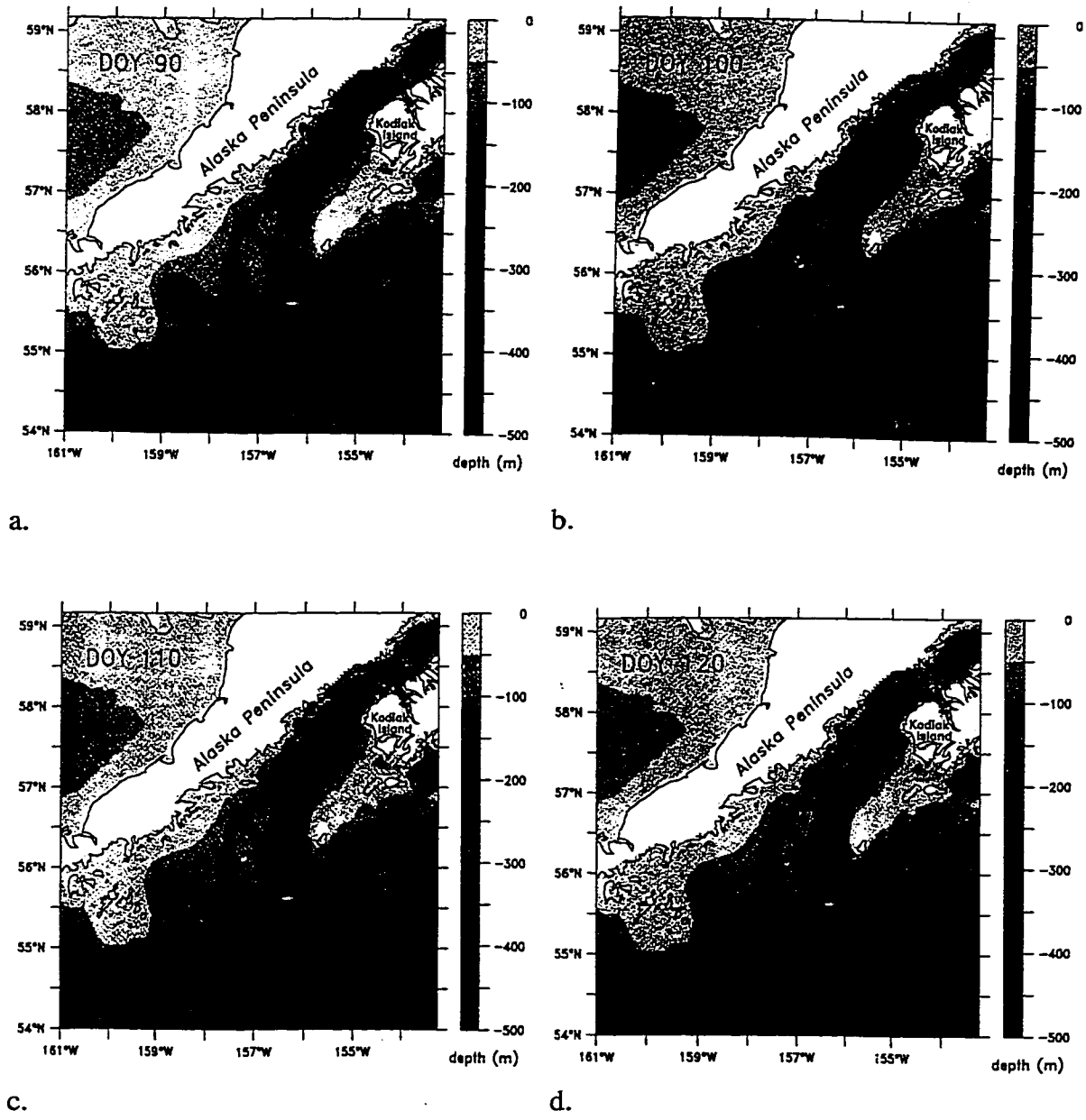

Figure 3.17. (a-h) Plots of modelled egg and larval walleye pollock distributions for DOY 90 (March 31) through DOY 160 (June 10) for 1989.

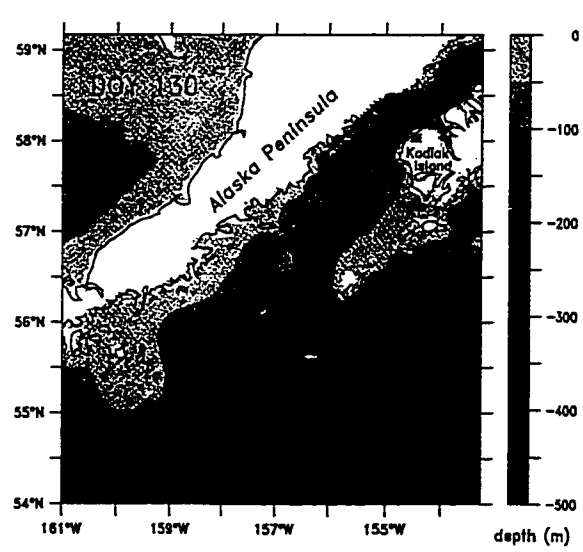

e.

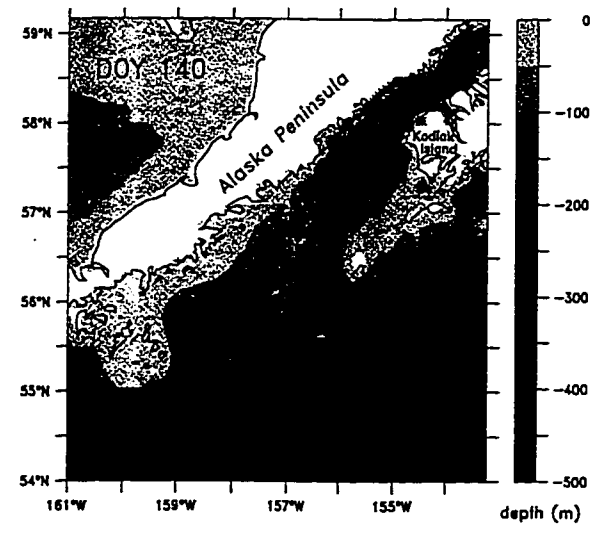

f.

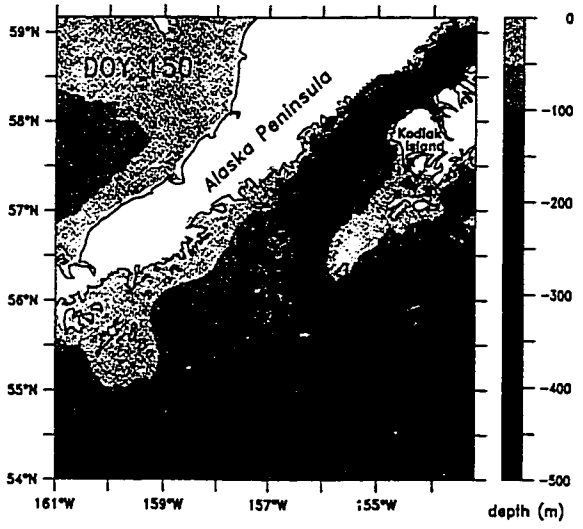

g.

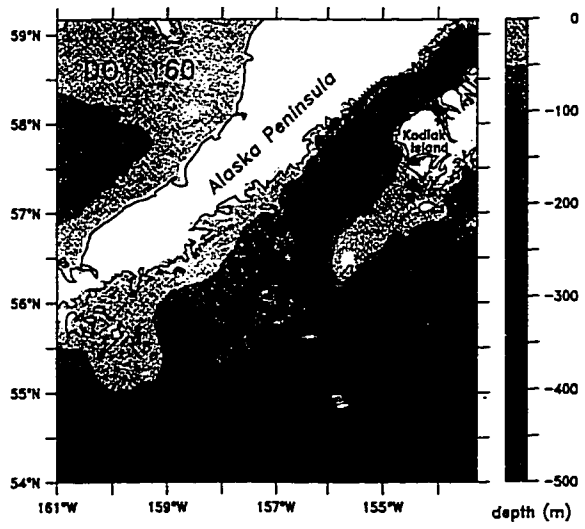

h.

Figure 3.17 (cont.)

the stronger forcing years (1978, 1987, 1988) for individuals to shear out along the streamlines of flow.

When eddy activity is weak (e.g. 1989), there is a tendency for the larger individuals to be located further downstream of the release point. The greater size of these downstream individuals is a consequence of their earlier birthdates. When eddy activity is strong (e.g. 1987), individuals of a particular size class can become trapped in closed circulation features. Note in particular how the individuals trapped in the cyclonic member of the 1987 eddy pair tended to be greater in length than the rest of the population, while those trapped in the anticyclonic member tended to be smaller. In 1978, a cluster of small individuals became trapped in the cyclonic eddy spanning the northeastern portion of the sea valley. Measured lengths for 1987 reveal spatial patchiness at similar scales, with patches of both short and long individuals (Fig. 3.19).

By DOY 202, all of the hindcasts exhibited transport of individuals further to the southwest of their positions at DOY 142 (Fig. 3.20). In 1978 and 1989, the bulk of the individuals hovered on the shelf to the northeast of the Shumagin Islands. In the 1988 run, most had already passed the Shumagin Islands; many were located to the west of the Islands by DOY 202. In each run, some individuals lingered in the sea valley or, as in 1987, even "upstream" of the release point. The spatial pattern obtained for 1987 - in particular, the aggregation of individuals on the shelf between the Shumagin Islands and the sea valley - corresponds to the observed late larval/early juvenile distributions for June/July of that year (Hinckley et al. 1991; their Figure 6). While strong mesoscale features are present in several of the years, none of the eddies contains significant numbers of individuals at this late date. The eddies present on DOY 142 have dissipated by DOY 202, releasing any trapped individuals to the surrounding waters.

There is no clear spatial pattern to the lengths on DOY 202; long and short individuals appear randomly juxtaposed. However, much of the length variance among individuals at this time is explained by their temperature history (Fig. 3.21). Individuals with early birthdates and/or "warm" histories exhibit greater lengths on average. Modeled growth curves

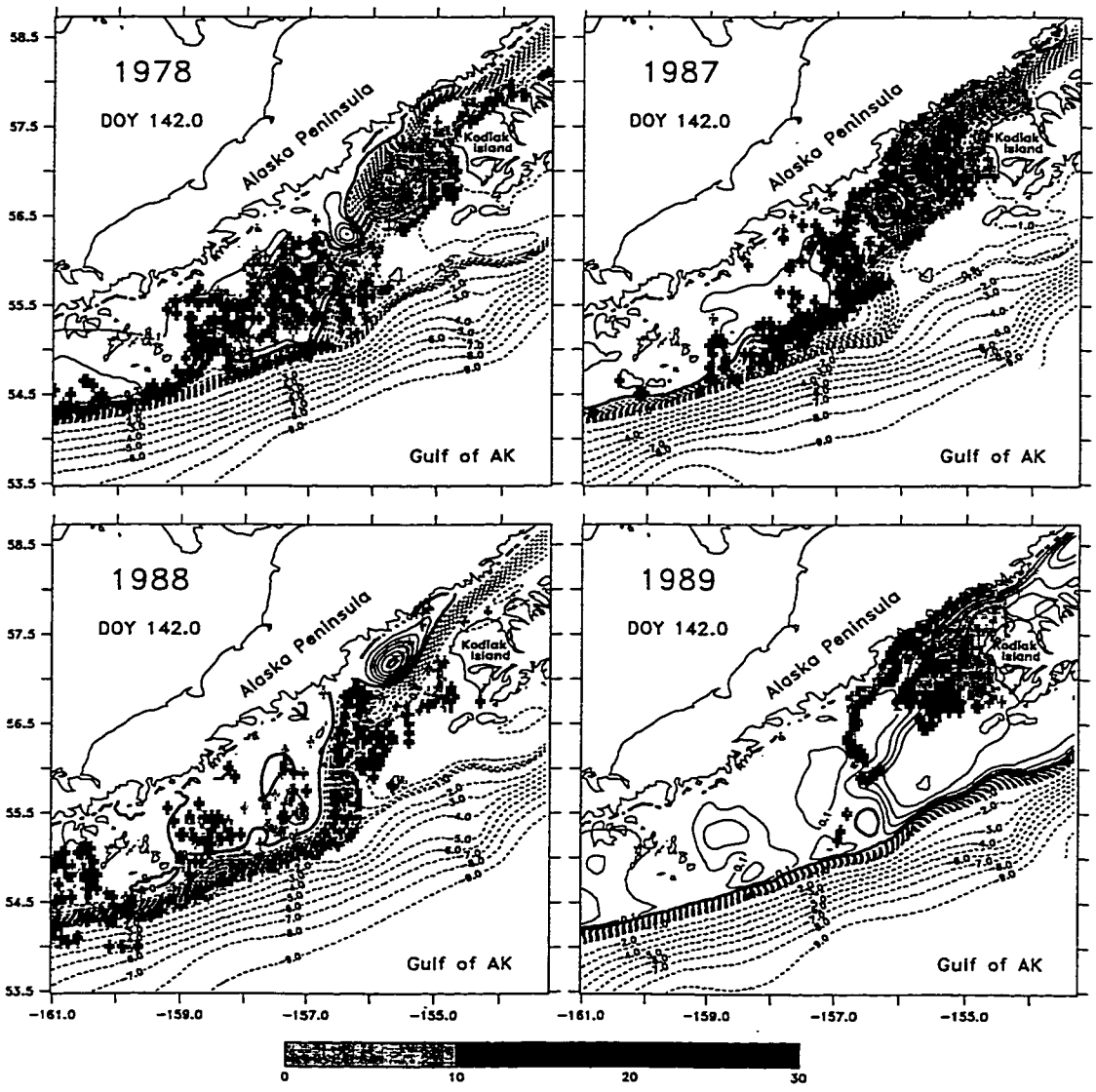

Figure 3.18. IBM results for DOY 142. Individual positions are greyscale-coded by the length of the individual (in mm). Where more than one individual fits into a single bin of the grid used for plotting, lengths are averaged prior to greyscale-coding. Contours of barotropic stream function (in 10^6 m^3 s^{-1}) are superimposed to indicate the circulation field. Contour interval for stream function is 0.1 for values between -1.0 and 1.0, and 1.0 for values less than -1.0.

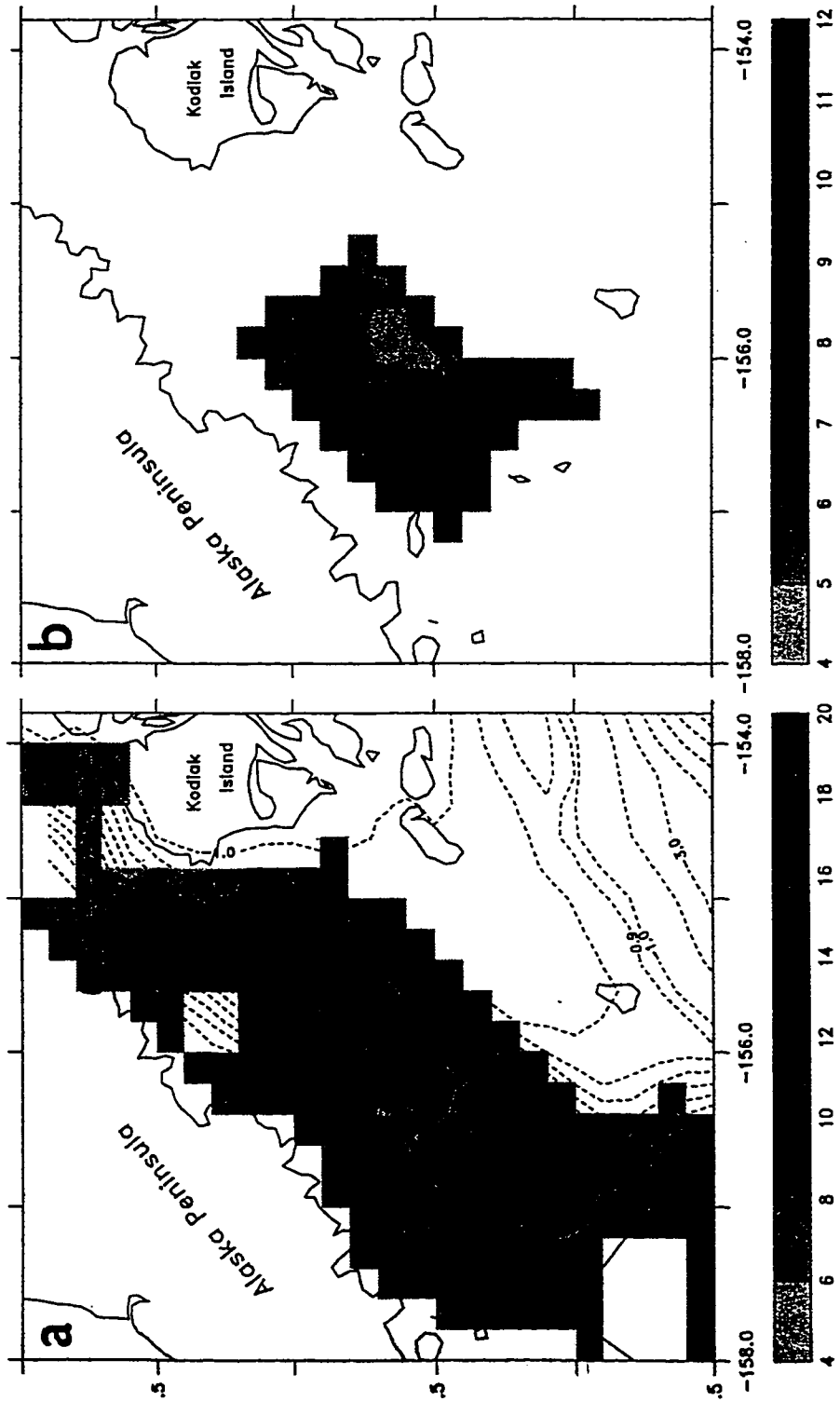

Figure 3.19. Close-up of length distribution near Shelikof Strait on DOY 142: (a) results from the model, (b) data from larval surveys. Lengths are in mm.

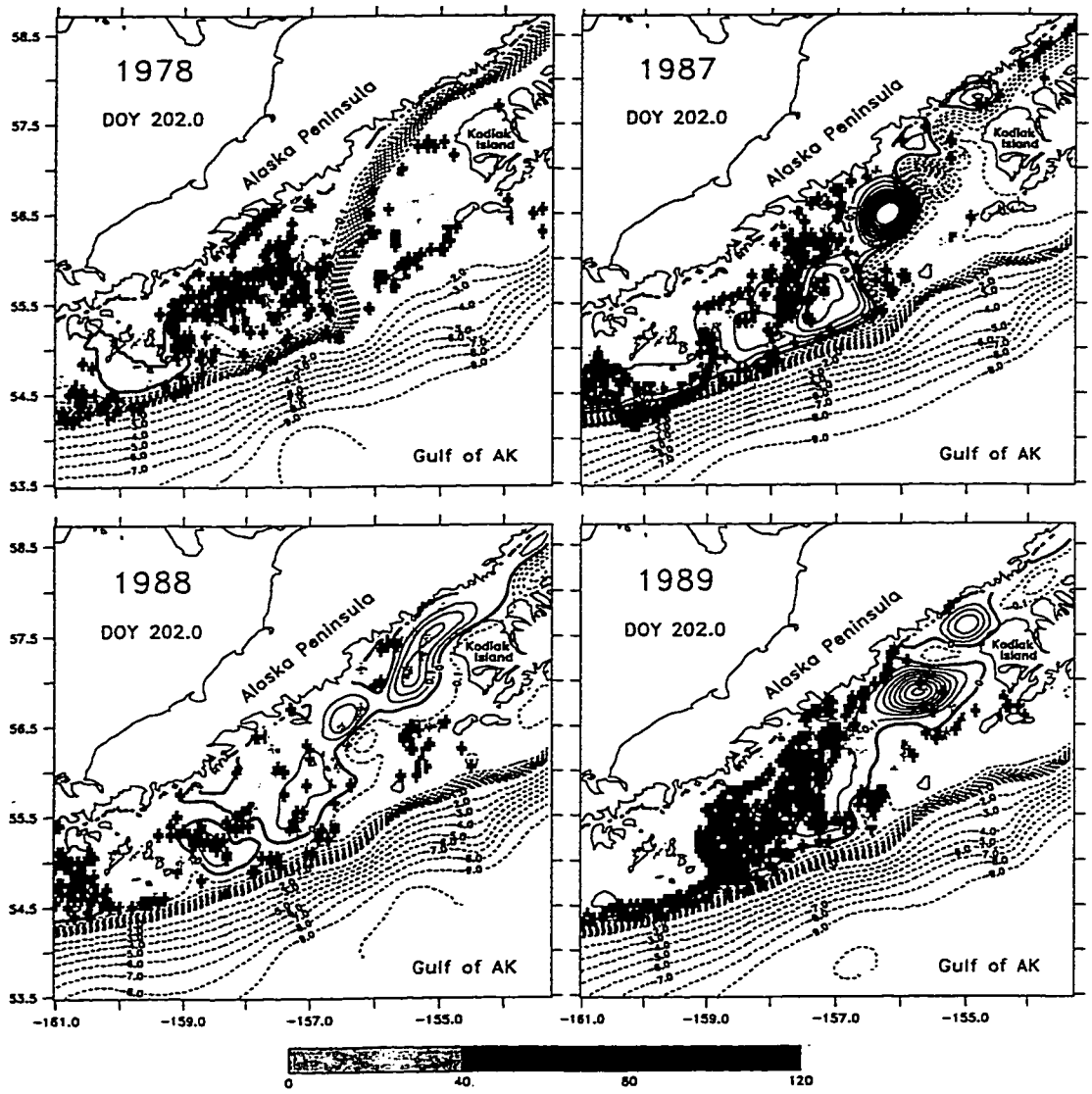

Figure 3.20. IBM results for DOY 202 (21 July). See Fig. 3.18 for details of symbols.

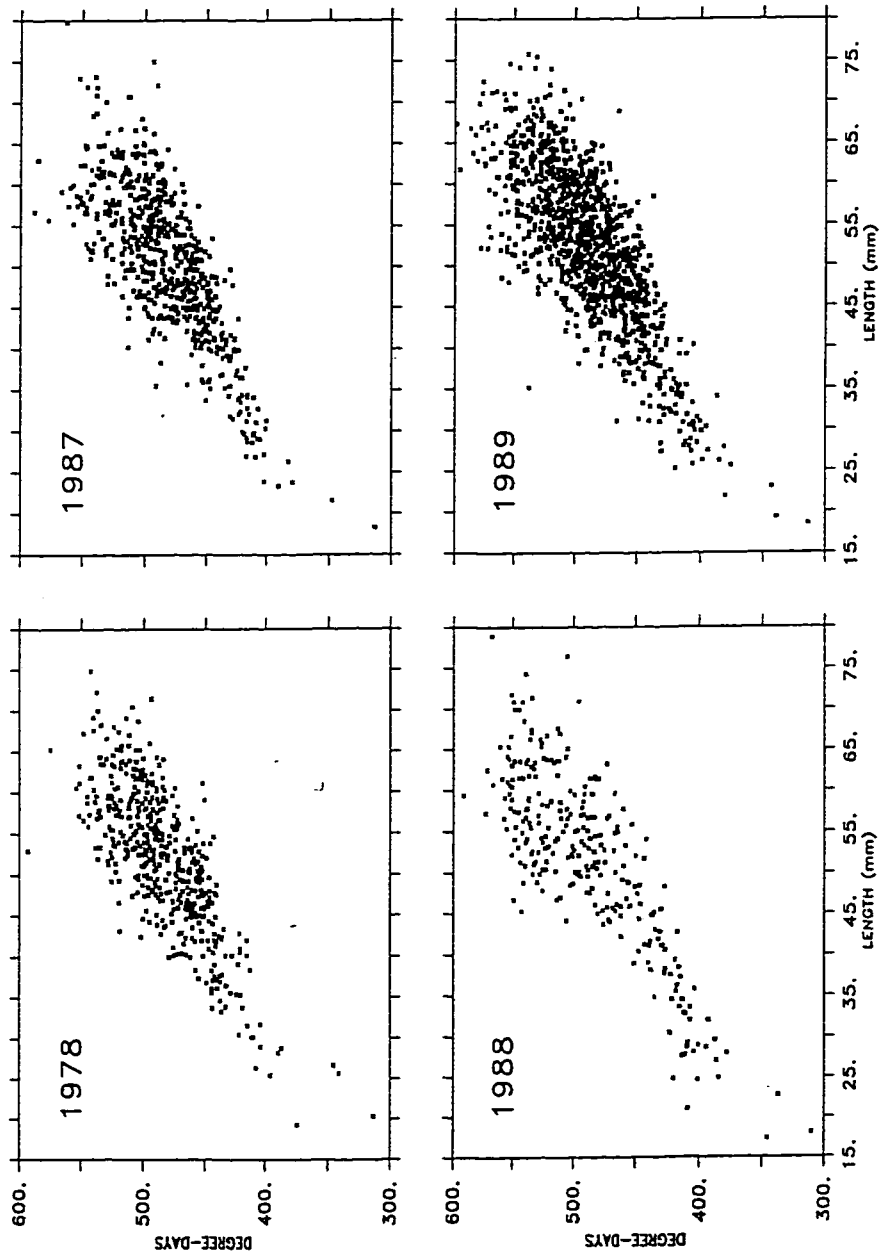

Figure 3.21. Scatterplot of individual length (mm) vs. integrated temperature history (degree-days) for individuals within the model domain on DOY 202.

(length vs. age) compare favorably with the measurements reported in Brown and Bailey (1992). By DOY 262, when all individuals had reached the juvenile life stage, few individuals remained in the sea valley (Fig. 3.22). The vast majority hovered on the shelf to the northeast of the Shumagin Islands in all hindcasts; a few accumulated to the south of Kodiak Island in each case. The 1989 run yielded the largest number of individuals on the shelf to the northeast of the Shumagin Islands on DOY 262, but appreciable numbers were also evident for 1978 and 1991. In the 1988 run, most of the individuals had left the model domain; some remained clustered around the Shumagin Islands however, especially on the southwestern side. In the 1987 run, individuals were uniformly dispersed on the shelf areas to the northeast of the Shumagins. Late juveniles surveys for August/September of that year found most individuals among and to the southwest of the Shumagin Islands (Hinckley et al. 1991). In other years, the distribution of modeled individuals was much patchier; note especially the strong aggregation of individuals along the coastline in 1978 and 1989. Histograms of final lengths (not shown) indicated a roughly normal distribution in each year. As at DOY 202, lengths of individuals appeared randomly distributed in space.

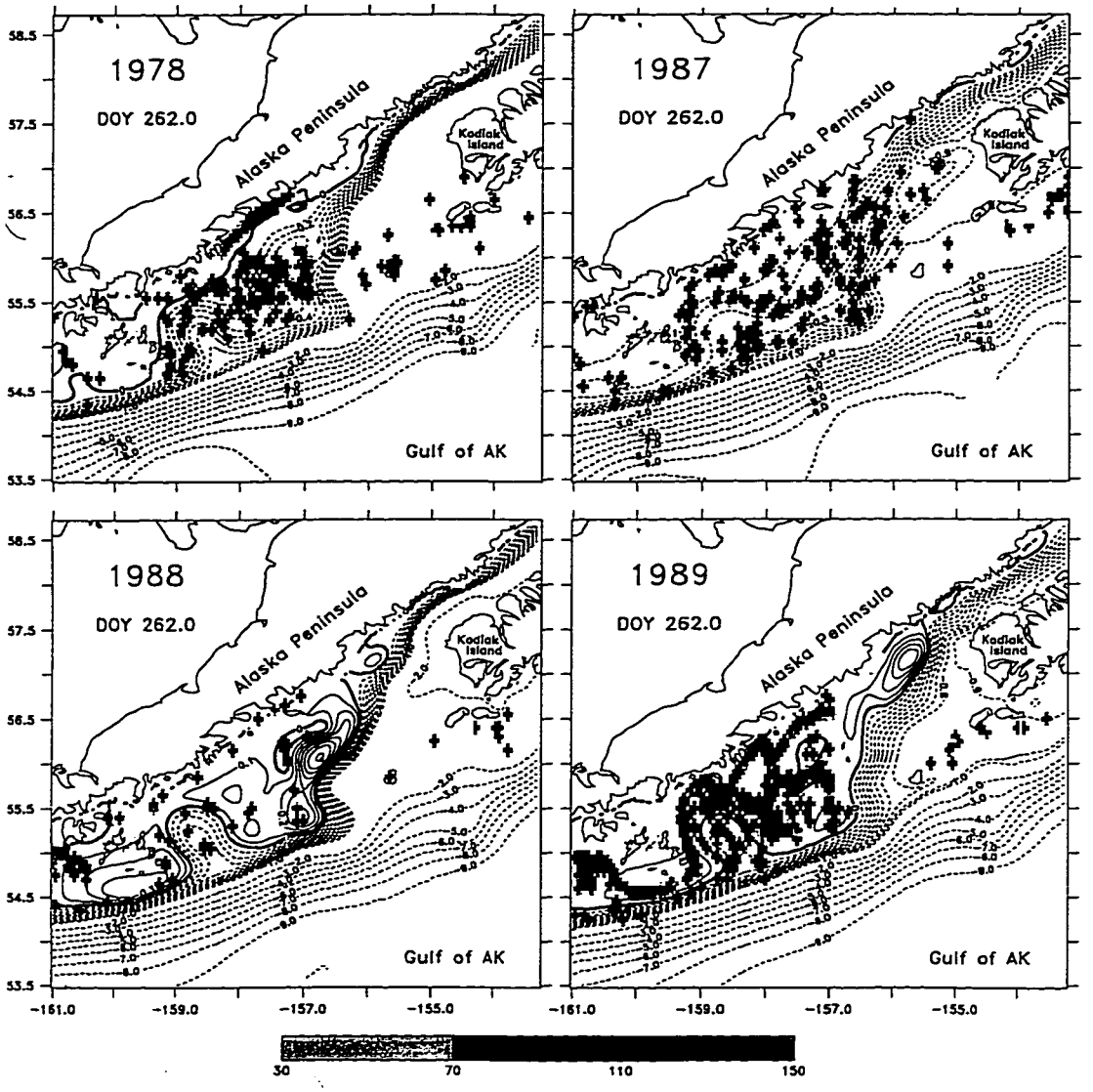

Figure 3.22. IBM results for DOY 262 (22 Sept.). See Fig. 3.18 for details of symbols.

3.4.4 NPZ and Coupled SPEM-NPZ-IBM Output

Interannual Variation

Figures 3.23-3.28 (a-d) show NPZ model output over the simulation period at Line 8 for the years 1978, 1987, 1988, 1989, 1991 and 1994, for phytoplankton chlorophyll-a (P, mg m^{-3}), *Neocalanus*, spp. biomass (H1, mg m^{-3}), the sum of *Pseudocalanus*, spp. naupliar I-VI stages (sumnauplii, no. m^{-3}), and *Pseudocalanus*, spp. adults (H14, no. m^{-3}). Figures 3.29-3.34 (a-d) show the same state variables averaged over the whole model domain (Fig. 2.5) for the simulation period.

Data for validation of the NPZ model were sparse. The model was able to capture the chlorophyll-a dynamics reasonably at Line 8 (Fig. 3.23-3.28, a) and over the whole area (Fig. 3.29-3.34 a), except for in 1989, where the model predicts a very late bloom, whereas the data showed higher concentrations earlier. *Neocalanus*, spp. biomass is captured well by the model both at Line 8 (Fig. 3.23-3.28 b) and over the whole domain (Fig. 3.29-3.34 b). Naupliar stage and adult *Pseudocalanus*, spp. numbers were slightly overestimated during their initial increase in most years for Line 8 (Fig. 3.23-3.28 c and d), but the model performed reasonably for the whole region averages (Fig. 3.29-3.34 c and d).

It may be seen from Fig. 3.23-3.28a that the spring bloom (defined as the time when chlorophyll-a biomass exceeds 2.0 mg m^{-3}) at Line 8 occurs at about the same time (about DOY 110) in all years except 1989, when chlorophyll-a levels do not reach this level until after DOY 140. This pattern is also seen in Figures 3.28-3.34a for the averaged values over the whole model domain. 1989 shows consistently lower values of chlorophyll-a until late in the spring.

At Line 8, the peak of the spring bloom is bimodal or trimodal in 1978, 1987, 1988, 1991 and 1994, but chlorophyll-a levels do not drop below bloom levels between peaks. At Line 8, the maximum chlorophyll-a level is about 13-20 mg m^{-3} in all modelled years. In 1989, the bloom occurs so late that the maximum level is not clear. The maximum chloro-

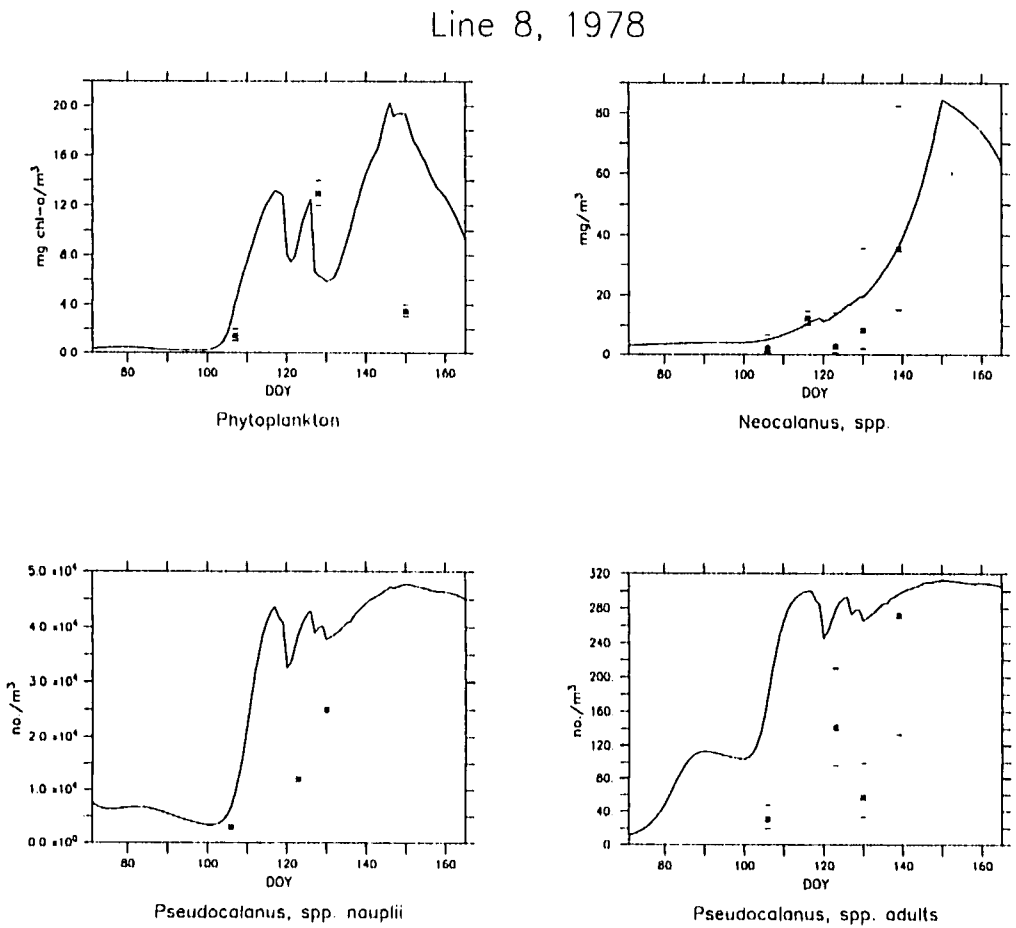

Figure 3.23. NPZ results for the mixed layer for 1978 at Line 8 (the exit region of Shelikof Strait). (a) Phytoplankton chlorophyll-a (mg m^{-3}), (b) *Neocalanus*, spp. biomass (mg C m^{-3}), (c) sum of NI-NVI naupliar stages of *Pseudocalanus*, spp. (no. m^{-3}), (d) *Pseudocalanus*, spp. adult (CVI) abundance (no. m^{-3}). *: data point from Line 8. (bars represent minimum and maximum data values).

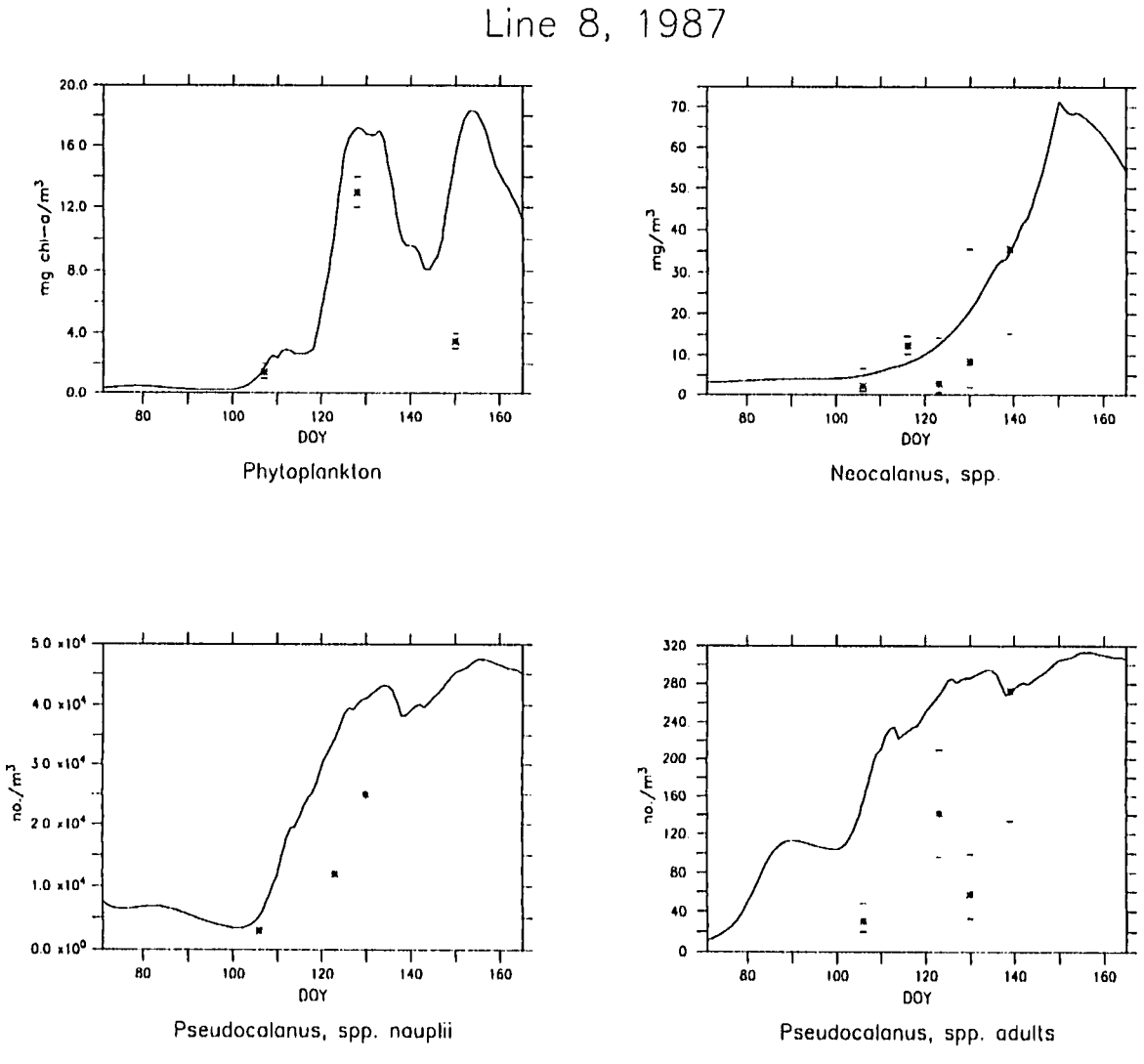

Figure 3.24. NPZ results for the mixed layer for 1987 at Line 8. a-d and symbols as described for Figure 3.23.

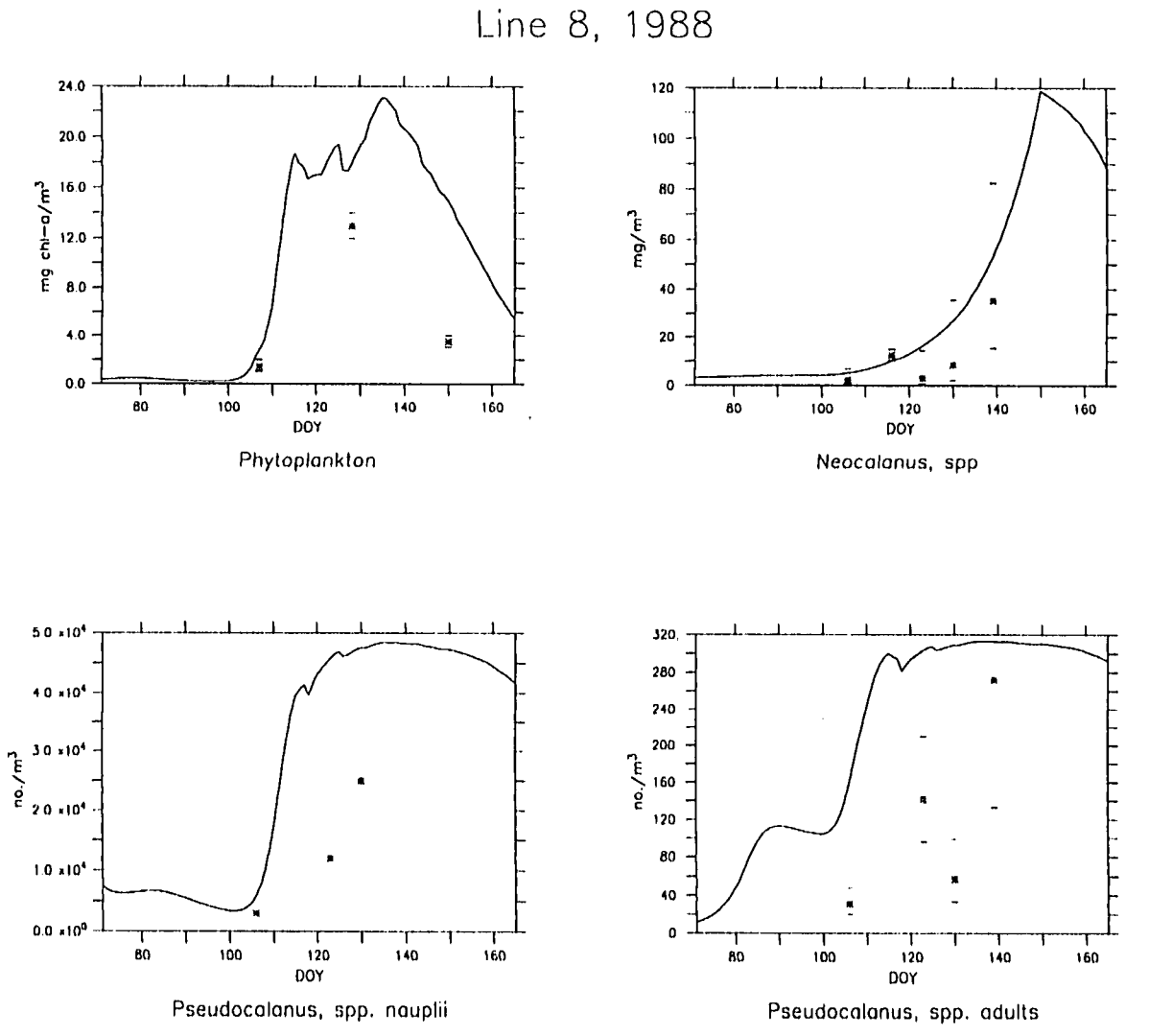

Figure 3.25. NPZ results for the mixed layer for 1988 at Line 8. a-d and symbols as described for Figure 3.23.

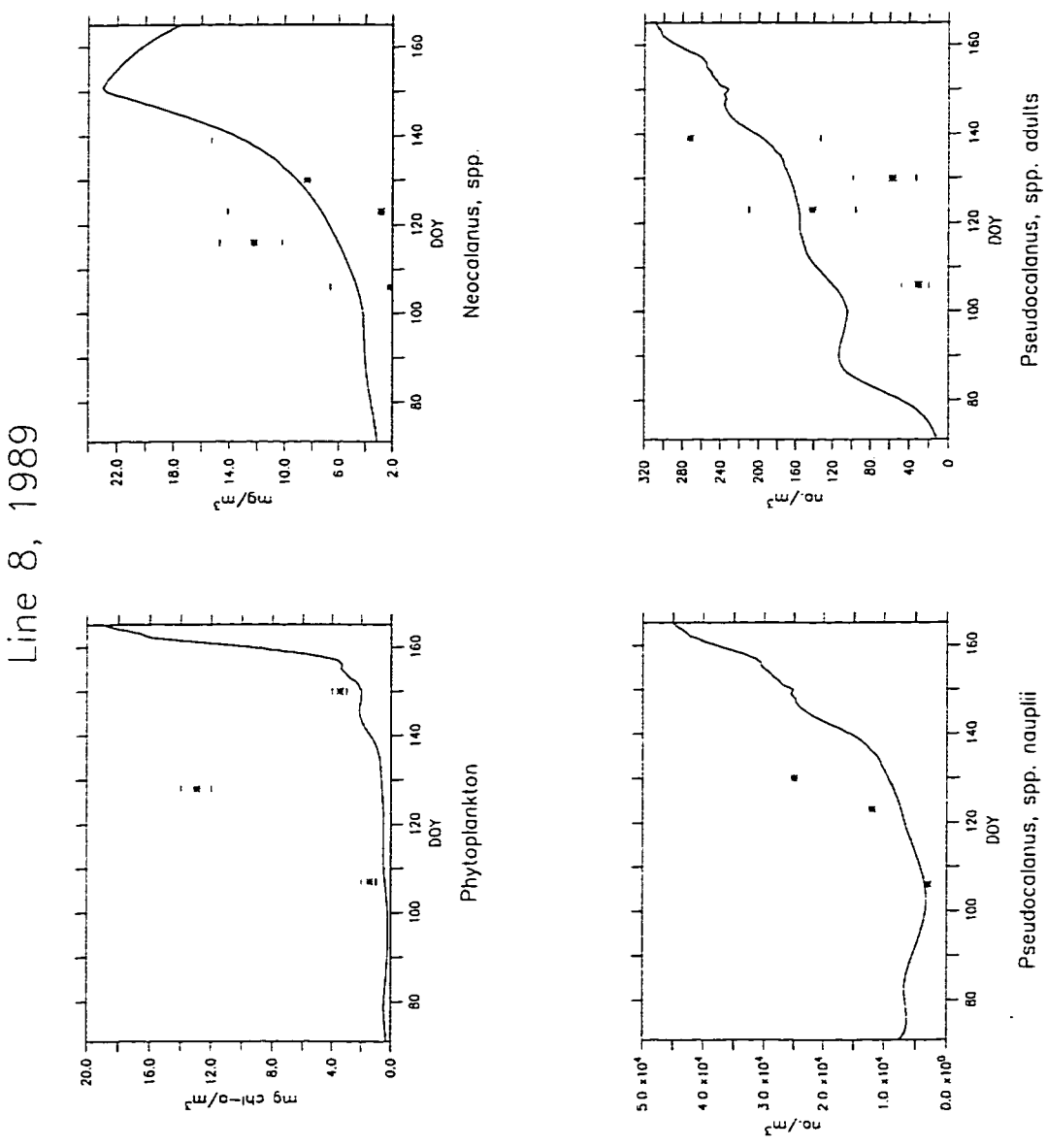

Figure 3.26. NPZ results for the mixed layer for 1989 at Line 8. a-d and symbols as described for Figure 3.23.

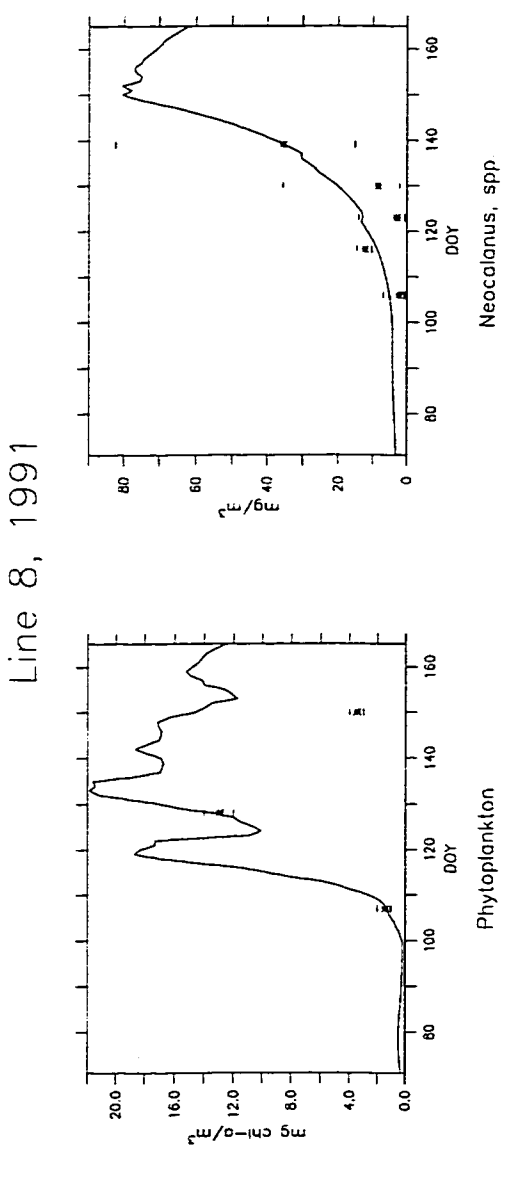

Figure 3.27. NPZ results for the mixed layer for 1991 at Line 8. a-d and symbols as described for Figure 3.23.

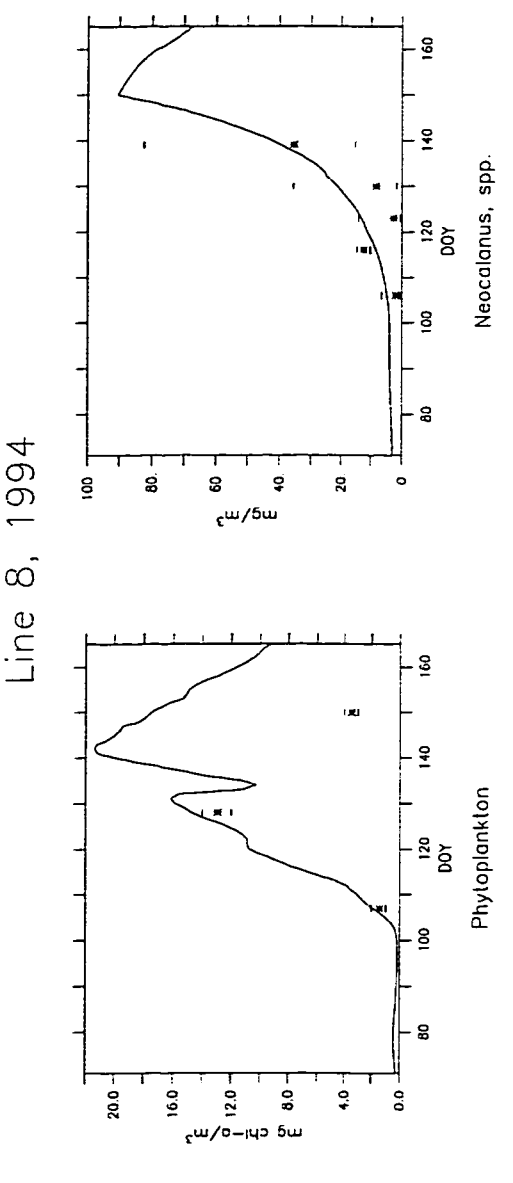

Figure 3.28. NPZ results for the mixed layer for 1994 at Line 8. a-d and symbols as described for Figure 3.23.

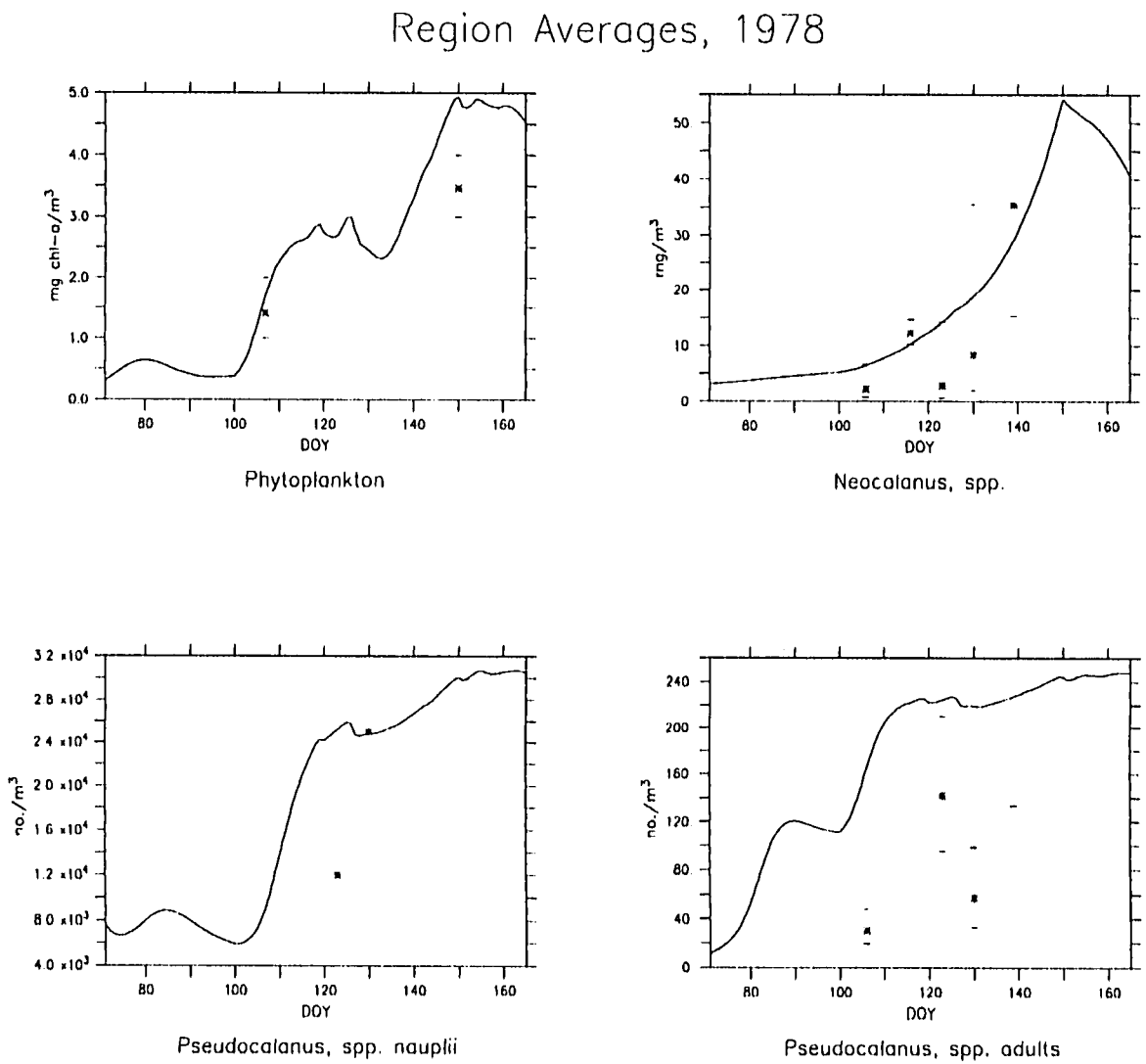

Figure 3.29. NPZ results for the mixed layer for 1978 averaged over the whole area. a-d and symbols as described for Figure 3.23.

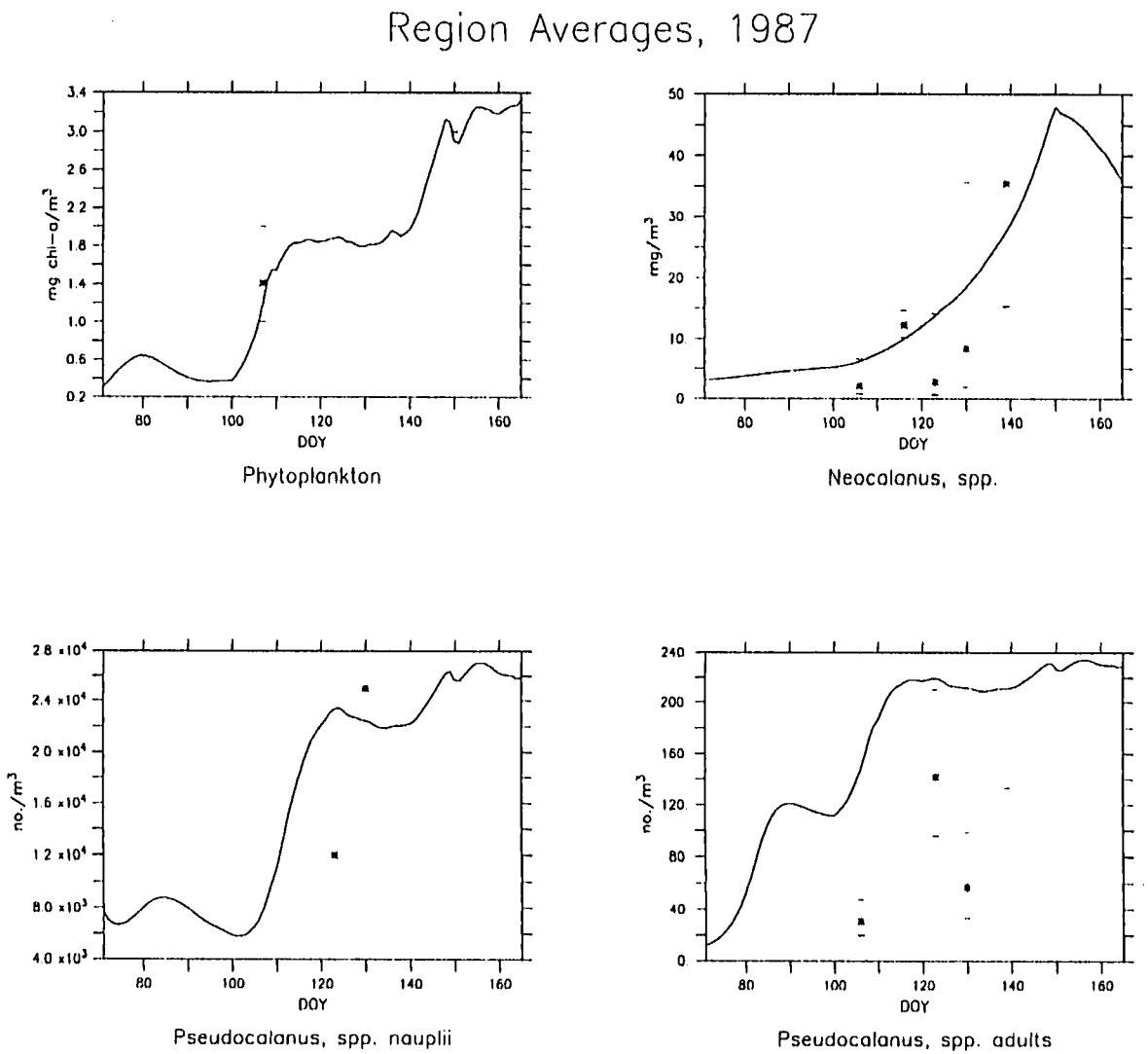

Figure 3.30. NPZ results for the mixed layer for 1987 averaged over the whole area. a-d and symbols as described for Figure 3.23.

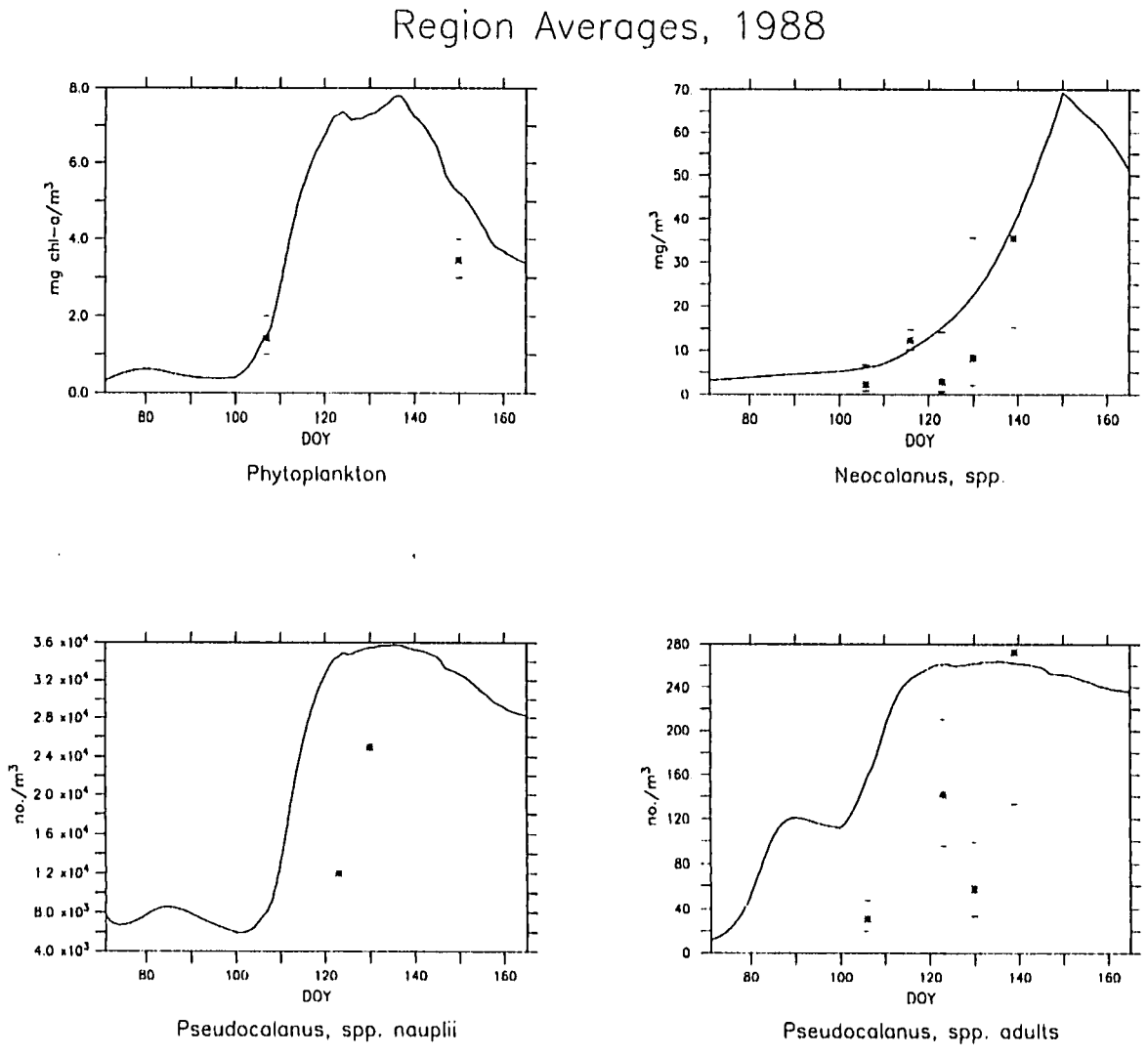

Figure 3.31. NPZ results for the mixed layer for 1988 averaged over the whole area. a-d and symbols as described for Figure 3.23.

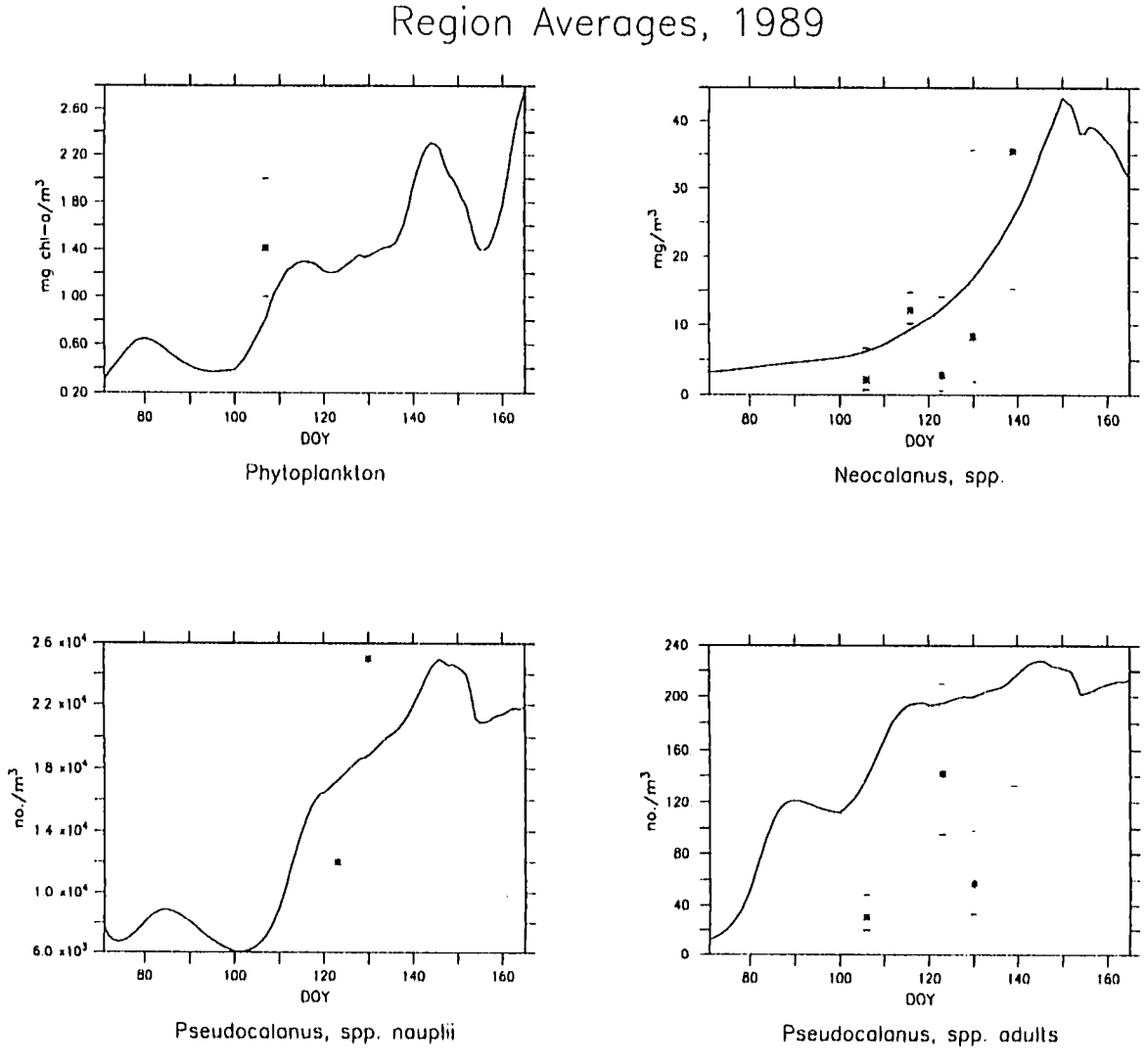

Figure 3.32. NPZ results for the mixed layer for 1989 averaged over the whole area. a-d and symbols as described for Figure 3.23.

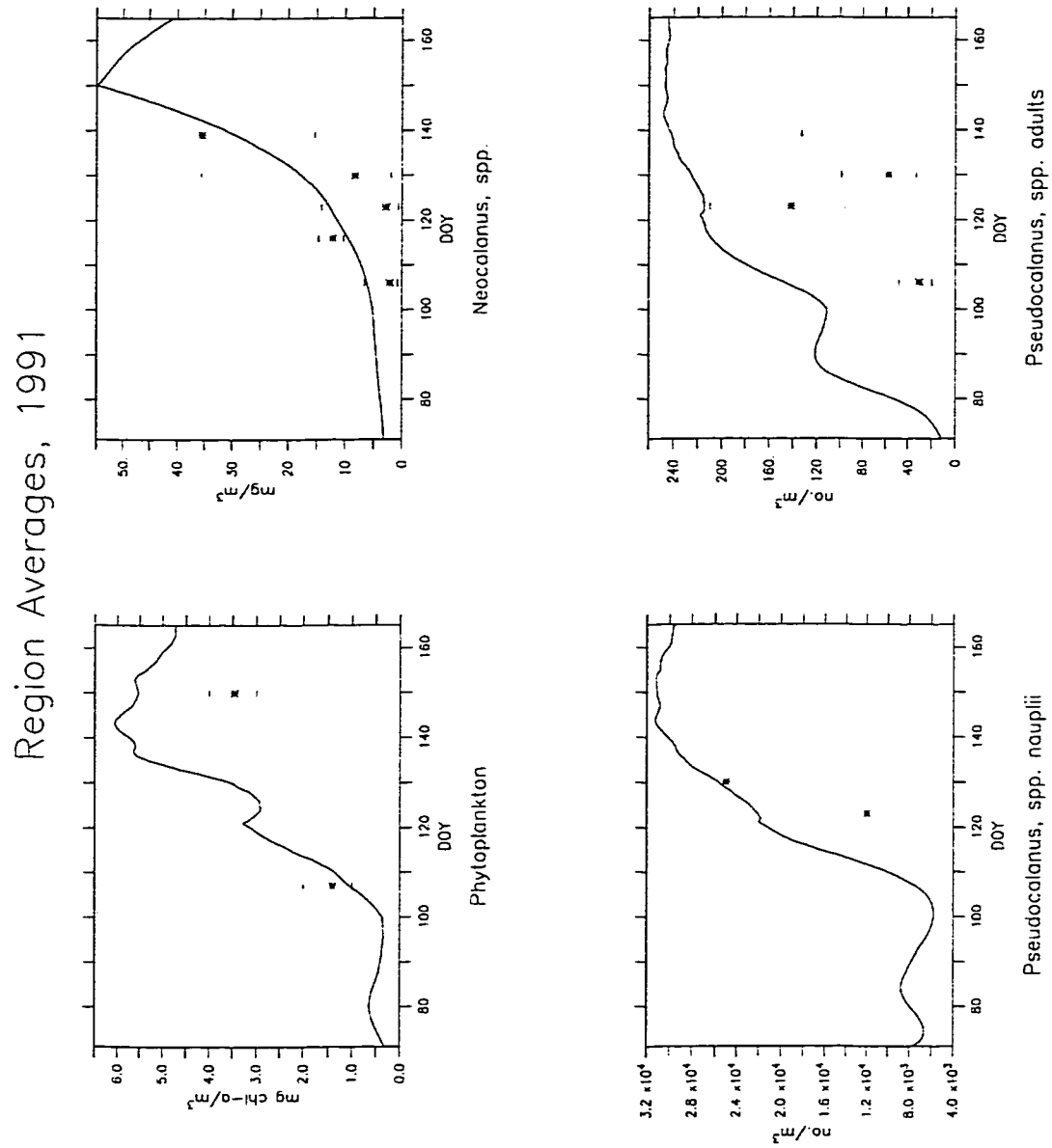

Figure 3.33. NPZ results for the mixed layer for 1991 averaged over the whole area. a-d and symbols as described for Figure 3.23.

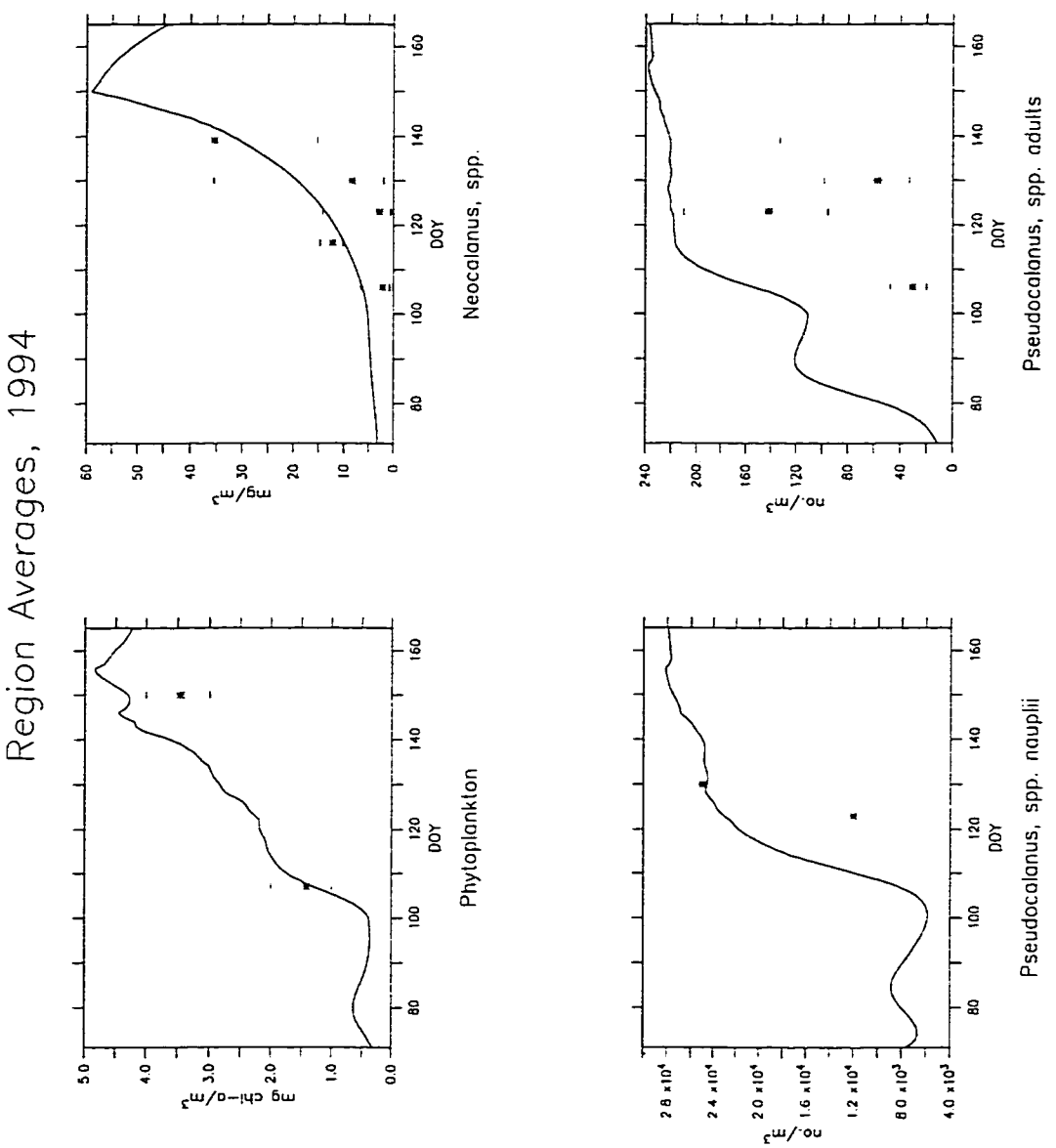

Figure 3.34. NPZ results for the mixed layer for 1994 averaged over the whole area. a-d and symbols as described for Figure 3.23.

phyll-a level averaged over the whole domain is, of course, lower as it integrates over areas of high and low production, whereas Line 8 is usually in the region of highest production. The whole area maximum varies from about 3.0-8.0 mg m^{-3}. The whole area average curves are unimodal in 1988, 1991 and 1994, and either a stepped curve or approximately bimodal in 1978, 1987 and 1989.

The sum of naupliar stages, which comprise the major part of the larval pollock diet, is shown in Part c of Figures 3.23-3.28 (Line 8) and 3.29-3.34 (the whole region). At Line 8, the first peak of naupliar numbers occurs at approximately DOY 110-120 for 1978, DOY 130-140 for 1987, DOY 120-140 for 1988, after DOY 160 for 1989, DOY 120-130 for 1991 and DOY 130-140 for 1994. The maximum numbers of nauplii on DOY 120 are seen in 1978 and 1988, with somewhat lesser numbers in 1994, and fewest in 1989. The patterns are similar over the whole area, with 1988 having the most nauplii on DOY 120, then 1978; and again, 1989 showing the least.

Spatial Patterns of Nauplii

In all simulated years, the region of the Trinity Banks, to the southwest of Kodiak Island, showed the earliest phytoplankton chlorophyll-a production, and subsequent increase of the naupliar stages. I will not describe the dynamics of this region in detail, as the young stages of pollock are rarely found in this region, due to the lack of exchange of water between this region and Shelikof Strait proper (due to its shallowness).

On DOY 111 in 1978 (Fig. 3.35), levels of naupliar stages are highest near Cape Kekurnoi at the exit region of Shelikof Strait (the Line 8 region). A series of anticyclonic (clockwise-rotating) eddies (as defined by solid red closed stream function coutours) are seen on the coastal side of the sea valley. The eddy nearest the exit region of Shelikof Strait has a tongue of higher naupliar abundance around its edge. Nauplii are patchy in the Strait itself, and lower (<10,000 per m^{-3}) between the Semidi Islands and the Shumagin Islands. On the same day in 1987 (Fig. 3.35), there are fewer nauplii at Line 8 than in 1978, and the distribution is less patchy. There is a large patch with slightly higher than

background levels near a large cyclonic (counterclockwise-rotating) eddy (as defined by the closed dotted red stream function contours) in the middle of the sea valley. Numbers are low to the west of the Semidi Islands. In 1988 on DOY 111 (Fig. 3.35), there are no strong eddies, but some patches in the sea valley and the coastal areas between Wide Bay and Sutwik Island, with up to 40,000 nauplii m^{-3}. A patch (which is seen in many of the other times and years) is seen near Mitrofania Island (between Sutwik and the Shumagin Islands). In 1989 on DOY 111 (Fig. 3.35), the background level is low (<15,000 m^{-3}) in the sea valley, with somewhat higher levels in coastal areas between Sutwik Island and the Shumagins. 1991 (Fig. 3.35) is somewhat patchier in the sea valley, with higher levels in the region near Mitrofania. Levels of nauplii are low to the west of the Semidi Islands otherwise. In 1994 (Fig. 3.35), a higher abundance patch is seen near Cape Kekurnoi. No eddies are seen in the sea valley at this time. Some areas of higher than background abundance are seen to the west of the Semidis. In 1978, 1987 and 1994, abundances in the region of the Shumagin Gully are higher than the background levels.

By DOY 121 (Fig. 3.36), some first feeding larvae are likely to be present. It is thought that densities of at least 20,000 nauplii m^{-3} (20 $liter^{-1}$) are necessary to ensure survival of early feeding larvae. Naupliar abundances at this time in 1978 (Fig. 3.36) are higher (to 50,000 m^{-3}) in a tongue down the southeast side of the sea valley, around the edge of a cyclonic eddy. A tongue of higher abundances of nauplii also extends out of the sea valley to the west along the shelf break. Mitrofania and the Shumagin Gully have patches of higher abundance. The abundances are patchy but fairly low to the west of the Semidi Islands. In 1987 (Fig. 3.36), an area of high (to 50,000 m^{-3}) abundance at Line 8, and a patch of high abundance around the edge of a cyclonic eddy, part of an eddy pair midway down the sea valley are seen. A small patch of low naupliar abundance is seen in the corresponding anticyclonic eddy. The background level in the sea valley is around 15-20,000 m^{-3}, with high patches along the coast, and patchy but lower abundances on the shelf to the west of the Semidis. In 1988 (Fig. 3363) abundances over the whole region are patchy but noticably higher than other years. A patch of up to 55,000 m^{-3} is seen near Cape

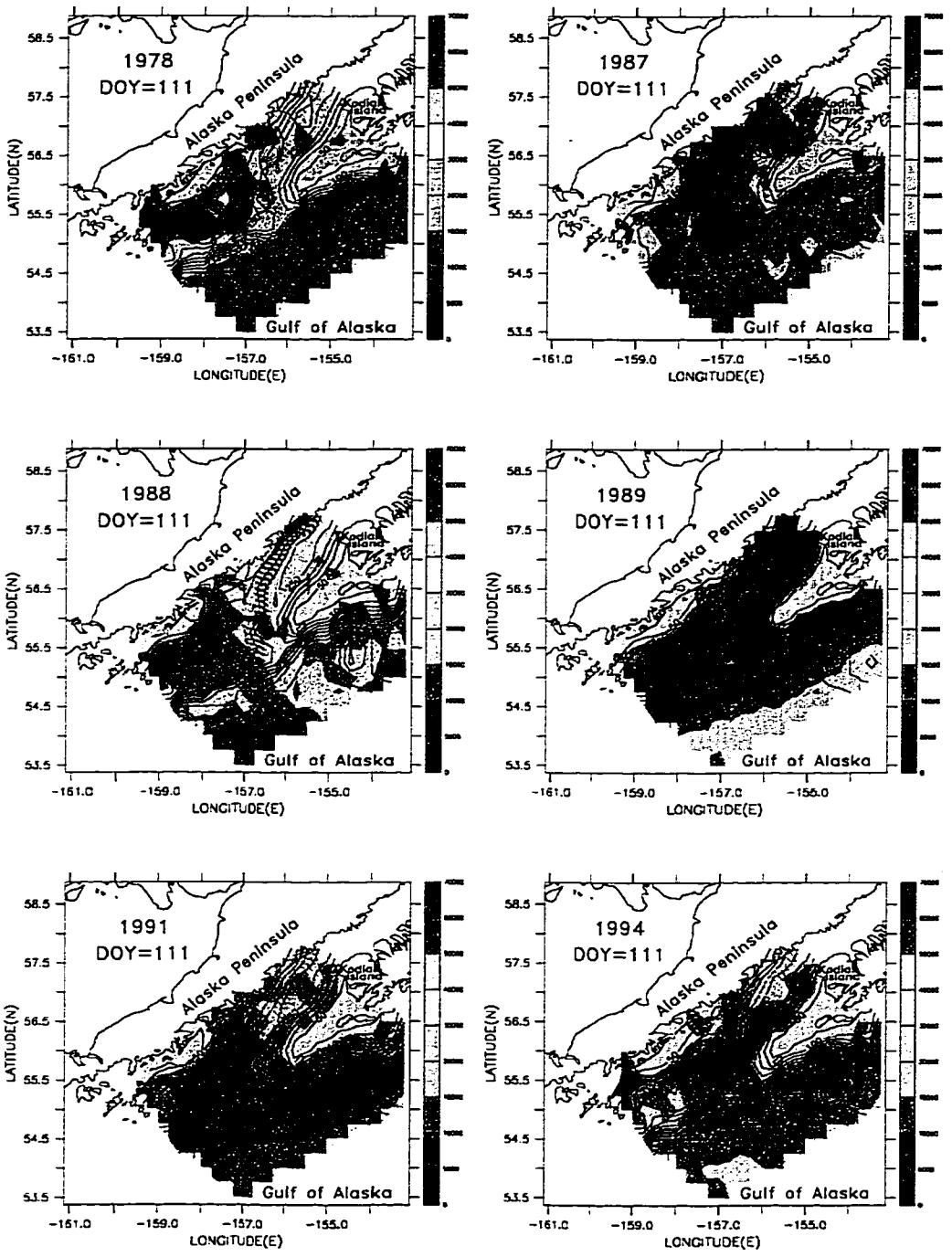

Figure 3.35. NPZ results for the mixed layer (the sum of naupliar stages of *Pseudocalanus*, spp.) over model domain on DOY 111 for all years. Color coded by no. m^{-3}. Red lines represent stream function. Black lines represent bottom contours (m).

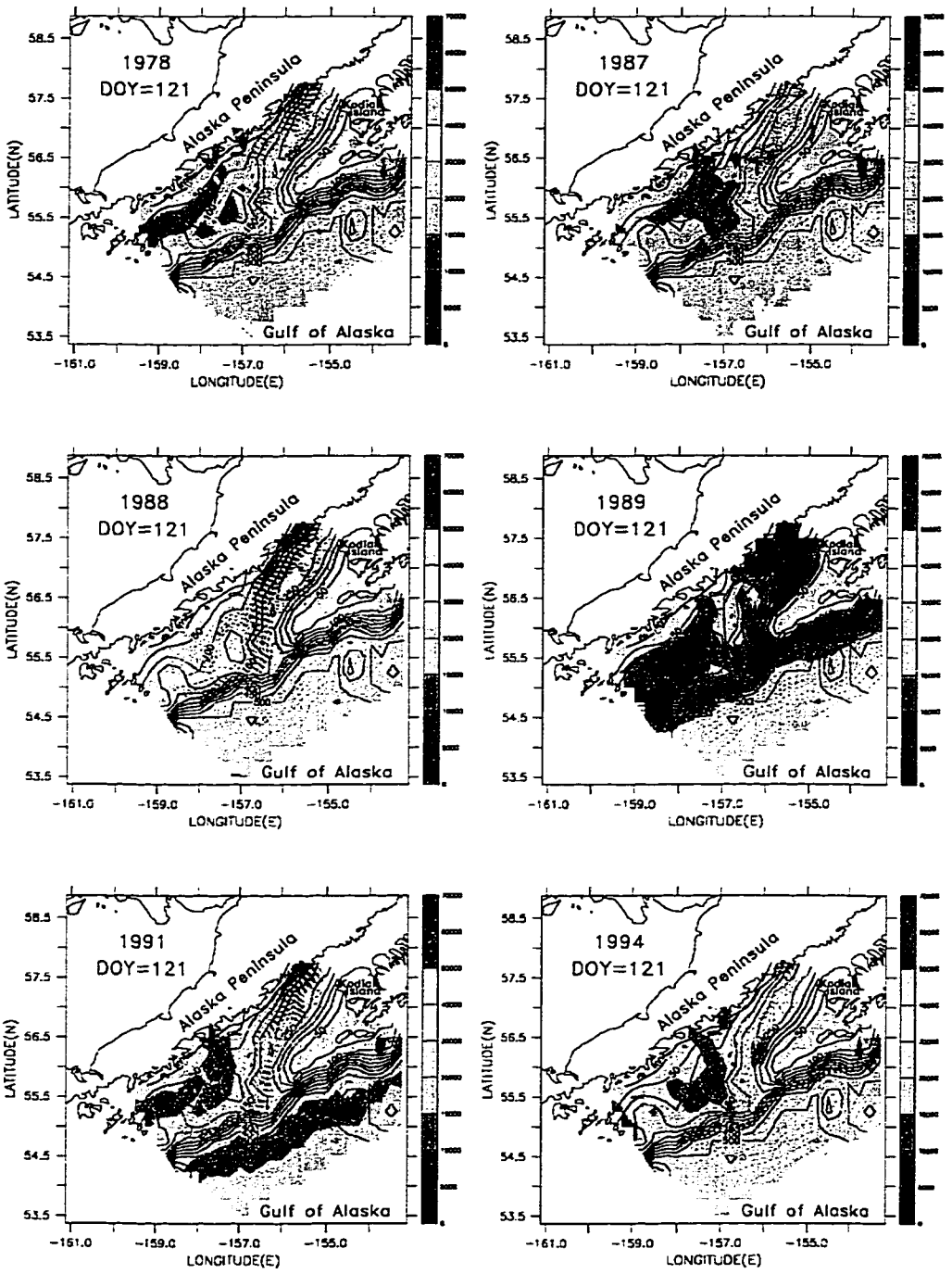

Figure 3.36. NPZ results for the mixed layer (the sum of naupliar stages of *Pseudocalanus*, spp.) over model domain on DOY 121 for all years. Color coded by no. m^{-3}. Red lines represent stream function. Black lines represent bottom contours (m).

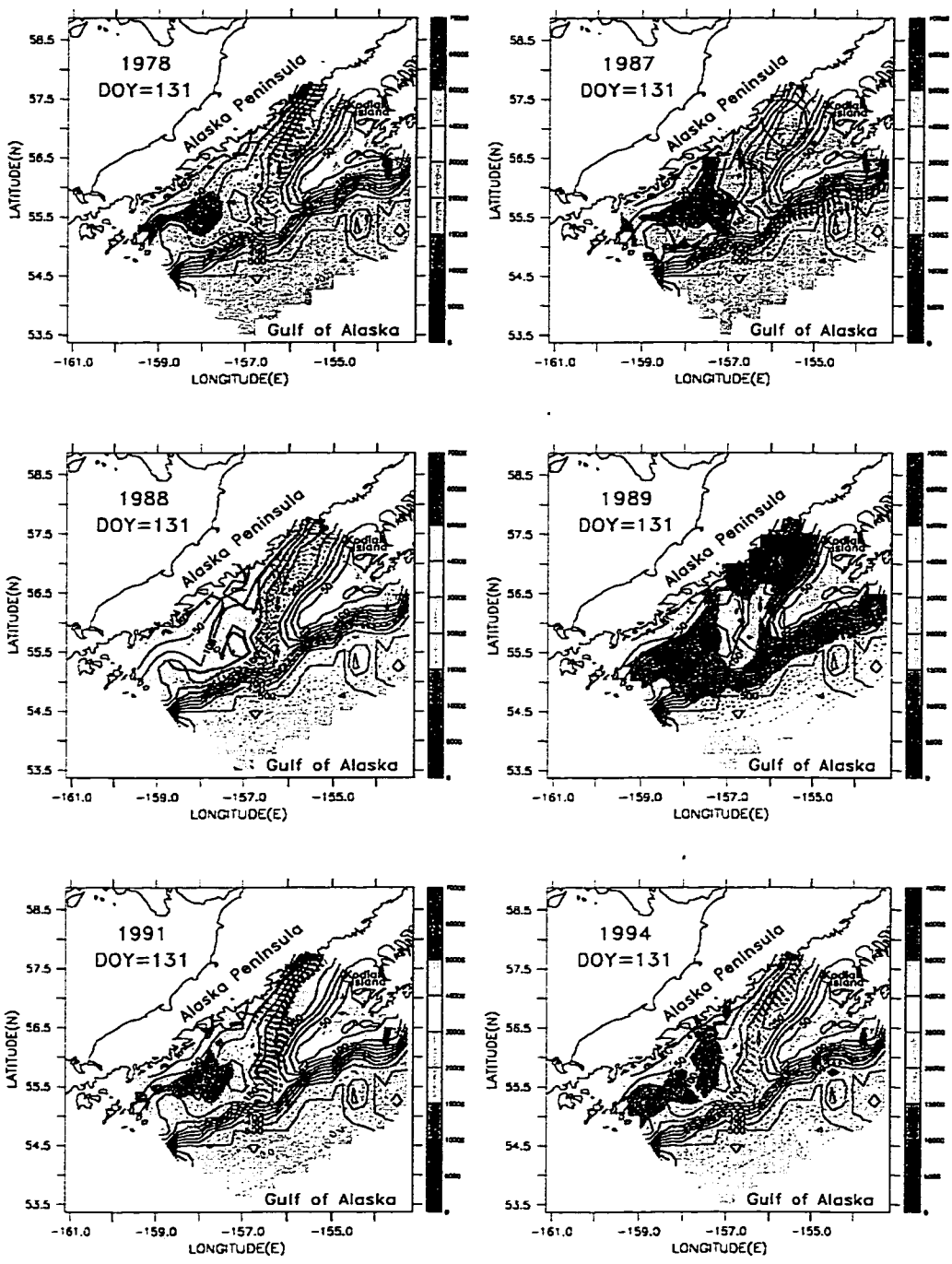

Figure 3.37. NPZ results for the mixed layer (the sum of naupliar stages of *Pseudocalanus*, spp.) over model domain on DOY 131 for all years. Color coded by no. m^{-3}. Red lines represent stream function. Black lines represent bottom contours (m).

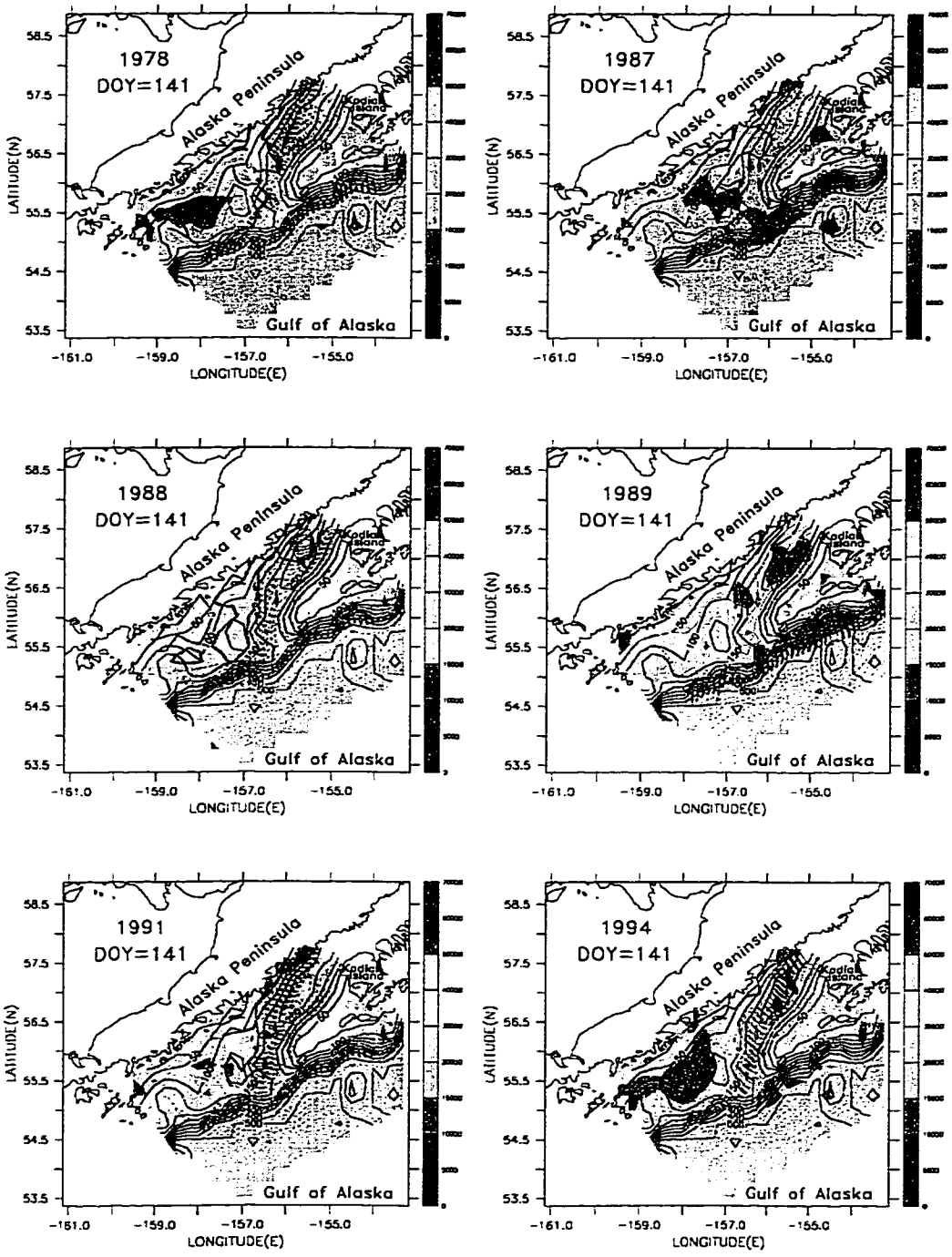

Figure 3.38. NPZ results for the mixed layer (the sum of naupliar stages of *Pseudocalanus*, spp.) over model domain on DOY 141 for all years. Color coded by no. m^{-3}. Red lines represent stream function. Black lines represent bottom contours (m).

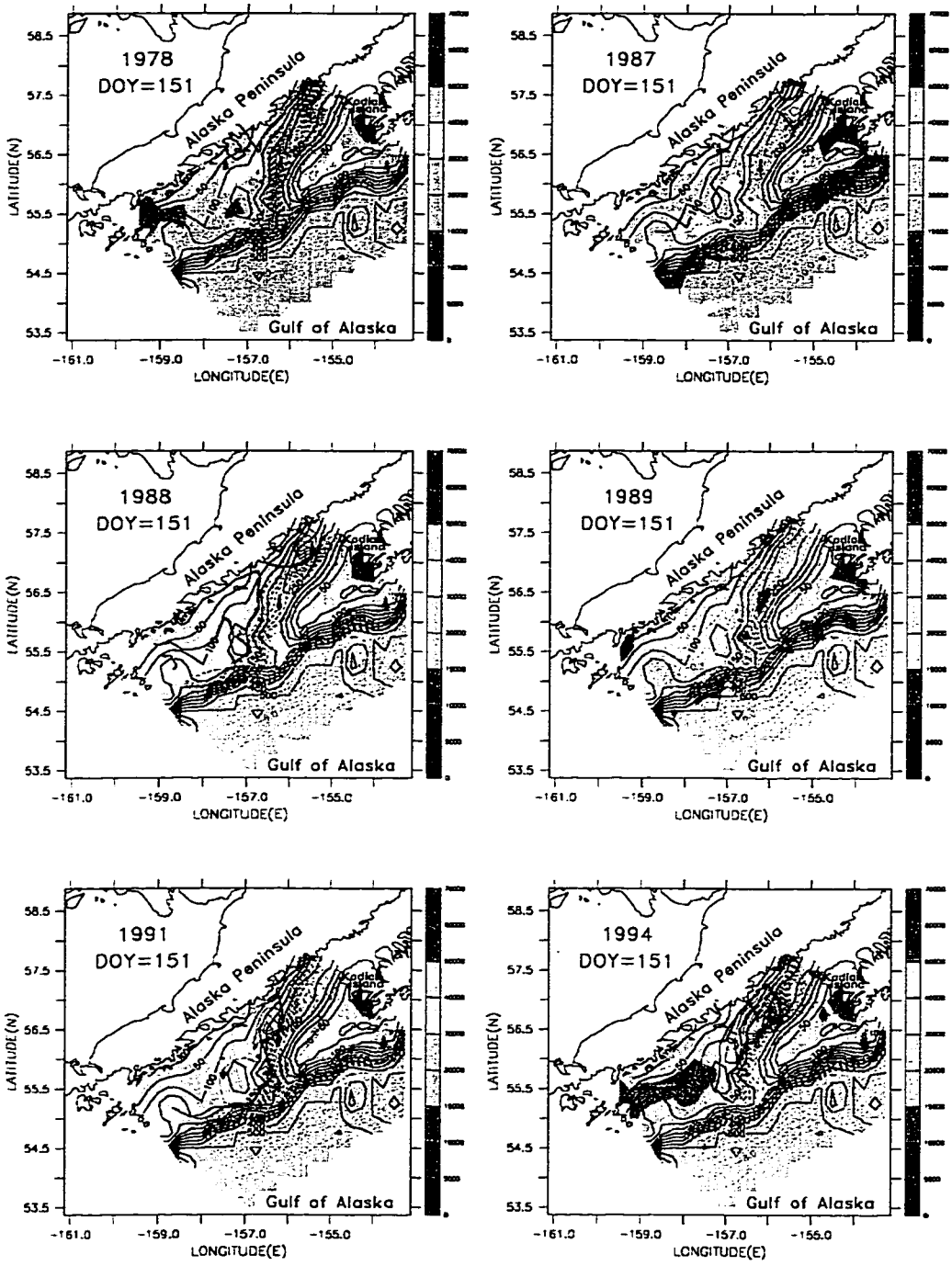

Figure 3.39. NPZ results for the mixed layer (the sum of naupliar stages of *Pseudocalanus*, spp.) over model domain on DOY 151 for all years. Color coded by no. m^{-3}. Red lines represent stream function. Black lines represent bottom contours (m).

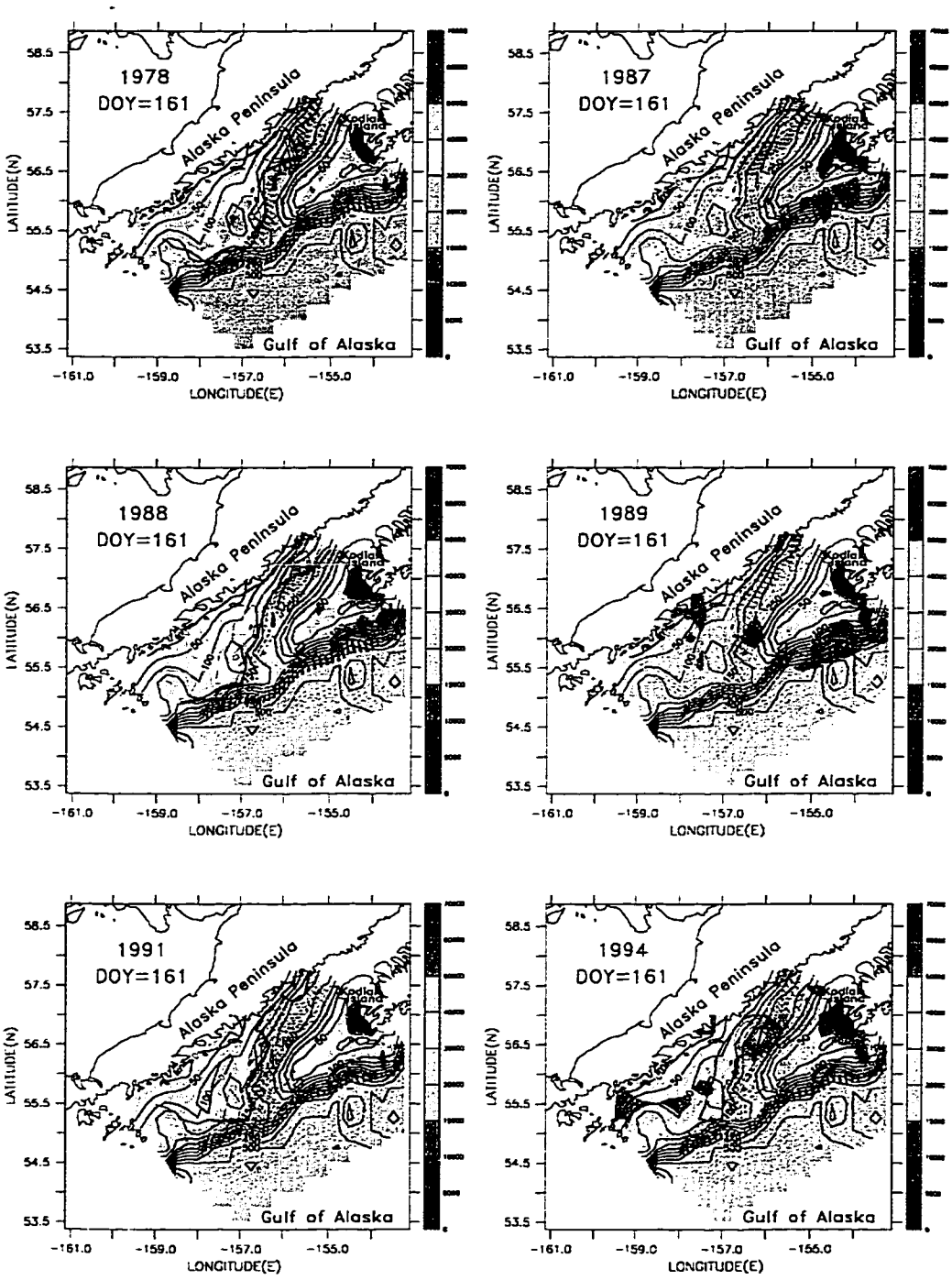

Figure 3.40. NPZ results for the mixed layer (the sum of naupliar stages of *Pseudocalanus*, spp.) over model domain on DOY 161 for all years. Color coded by no. m^{-3}. Red lines represent stream function. Black lines represent bottom contours (m).

Kekurnoi. A tongue of nauplii is advected down the sea valley (and around a cyclonic eddy) midstream, out along the shelf break to the west of the sea valley as far as the Shumagin Islands. The region of lowest abundance is in the coastal regions to the east of the Shumagin Islands. In 1989 (Fig. 3.36), the background levels are still very low (<15,000 m^{-3}) overall, and there is little patchiness. In 1991 (Fig. 3.36) on DOY 121, levels of nauplii are high in the upper sea valley, and a tongue of higher abundance follows the stream function down the sea valley, with a patch near the Semidi Islands, and along the shelf break to the west of the exit of the sea valley. In 1994 (Fig. 3.36), the background levels are almost all over 20,000 m^{-3}, with a higher spot (to 50,000 m^{-3}) near Cape Kekurnoi. High levels are seen on the coastal side of the upper sea valley, with a tongue emerging from Wide Bay. Levels are generally above 20,000 m^{-3} to the west of the Semidi Islands.

By DOY 131, in 1978 (Fig. 3.37), there is a patchy tongue down the sea valley, with especially high abundances (45-50,000 m^{-3}) on the southeast side of the upper sea valley and around the edge of a cyclonic eddy. A tongue of nauplii extends down the sea valley and out towards the west of the exit along the shelf break. Distributions are patchy to the west of the Semidis with higher levels at Mitrofania and in the Shumagin Gully. In 1987 on DOY 131 (Fig. 3.37), levels are generally lower, with a localized high (to 60,000 m^{-3}) at Line 8. There is also a patch of higher abundance extending between an eddy pair midway down the sea valley. Background levels in the sea valley are generally over 20,000 m^{-3}, and high patches are seen along the coast. An area of lower abundance is seen midshelf to the west of the Semidi Islands. In 1988 (Fig. 3.37), background levels are again very high (to 50,000 m^{-3}) throughout much of the sea valley and out along the shelf break almost to the Shumagin Islands. The whole distribution is rather patchy, and the area of lowest abundance of nauplii is seen along the coast just east of the Shumagin Islands. Very low levels are still seen in 1989 (mostly <25,000 m^{-3}, Fig. 3.37), with the only region of somewhat higher abundance seen near Mitrofania Island. In 1991 (Fig.3.37), the abundances in the sea valley are high (to 55,000 m^{-3}) with patches associated with stream function

meanders. A tongue of abundances to 40,000 m^{-3} is seen extending along the shelf break to the west of the sea valley exit. In 1994 (Fig. 3.37), a similar tongue down the sea valley exists, with somewhat higher abundances and a moderate amount of patchiness.

Abundance levels in all years for DOY 141 (Figs. 3.38) were similar, with levels somewhat higher (background levels >20,000 m^{-3}), except 1991, when naupliar levels went down. An eddy pair is seen in 1978 with high abundances of nauplii around and within the cyclonic eddy, and lower abundances in the anticyclonic eddy. In 1988, a region of low abundance of nauplii is seen in a anticyclonic eddy near Wide Bay. Regions of high abundance were very broad in 1978,1988 and 1991, and somewhat less so in 1994. Regions of high abundance were very small in 1987, and virtually nonexistant in 1989. This pattern was repeated on DOY 151 (Fig. 3.39) and DOY 161 (Fig. 3.40). On DOY 151 in 1987, an area of low naupliar concentration was associated with the center of an anticyclonic eddy, with high levels around the eddy's perimeter extending between this eddy and the corresponding cyclonic eddy to the south. On DOY 151, 1988, a region of low abundance is seen within a anticyclonic eddy near Wide Bay. For most years, the regions between the Semidi Islands and the Shumagins, particularly near the coast, had consistently lower numbers than the sea valley, as, to some degree, did the shelf break to the west of the exit of the sea valley. In 1988 by DOY 151 (Fig. 3.39) numbers in this region were higher than in the other years, and in 1989 (Fig. 3.39) the numbers in this area were somewhat higher than in the sea valley, however, they were not elevated much (to ~35,000 m^{-3}). In 1994 on DOY 161, high abundances of nauplii are again associated with a cyclonic eddy and low abundances with a anticyclonic eddy in mid-sea valley.

By DOY 161, naupliar levels in 1978 (Fig. 3.40) were generally high (to 50,000 in the sea valley) and patchy, with a tongue of higher abundance again along the shelf break out of the sea valley to the Shumagins. In 1987 (Fig. 3.40) the region of high abundance did not extend as far down the sea valley, but the Shumagin Gully area still had moderately high levels (to 40,000 m^{-3}). In 1989 (Fig. 3.40) , a region of moderately high abundances existed on the coastal side of the upper sea valley, extending almost to Sutwik Island. In

1988 (Fig. 3.40) and 1991 (Fig. 3.40) abundances were high over most of the region. In 1994 (Fig. 3.40), patchy areas of high abundance existed, but were not so widespread as in 1988 and 1991.

Coupled Models

Some illustrative results from the coupled IBM and NPZ models for mid-June, 1987 are shown in Figs. 3.41a-c. A total of 1600 individuals are used in the IBM, with mortalities set to zero. A cyclonic eddy is located in the deepest part of the sea valley, near 56.5°N, -156°E (Fig. 3.41a). Total numbers of all copepodite stages of *Pseudocalanus*, spp. are shown for zooplankton (Fig. 3.41b). Positions of individual fish are shaded according to length (Fig. 3.41c). The individual lengths vary, due to the different prey fields encountered during their life history; larvae greater than 8 mm ingest a mixture of *Pseudocalanus*, spp. naupliar and copepodite stages. A cluster of medium-sized larvae (8-16 mm) is trapped within the eddy. A tongue of low zooplankton concentration is being advected around the southern rim of the eddy, and shorter fish are associated with that feature. A tongue of higher zooplankton concentration, advecting around the northern rim of the eddy, has fewer but generally longer fish associated with it. Regions downstream and shoreward of this feature also exhibit greater lengths.

While some patchiness of fish size can be produced through purely kinematic effects related to the time of spawning (e.g. a cluster of late-spawned, smaller individuals trapped in an eddy), clearly the spatially variable prey field contributes to the patchiness of fish attributes in this model. The use of a dynamic prey field also results in a different mean growth and survival for groups of individuals spawned at different places and times.

3.4.5 Spatial Statistics

Two useful statistics for quantifying advection and patchiness of individuals among years are (i) the number of individuals remaining on the shelf between Kodiak Island and the Shumagins on any given date, and (ii) Lloyd's index of patchiness for individuals remaining in that area.

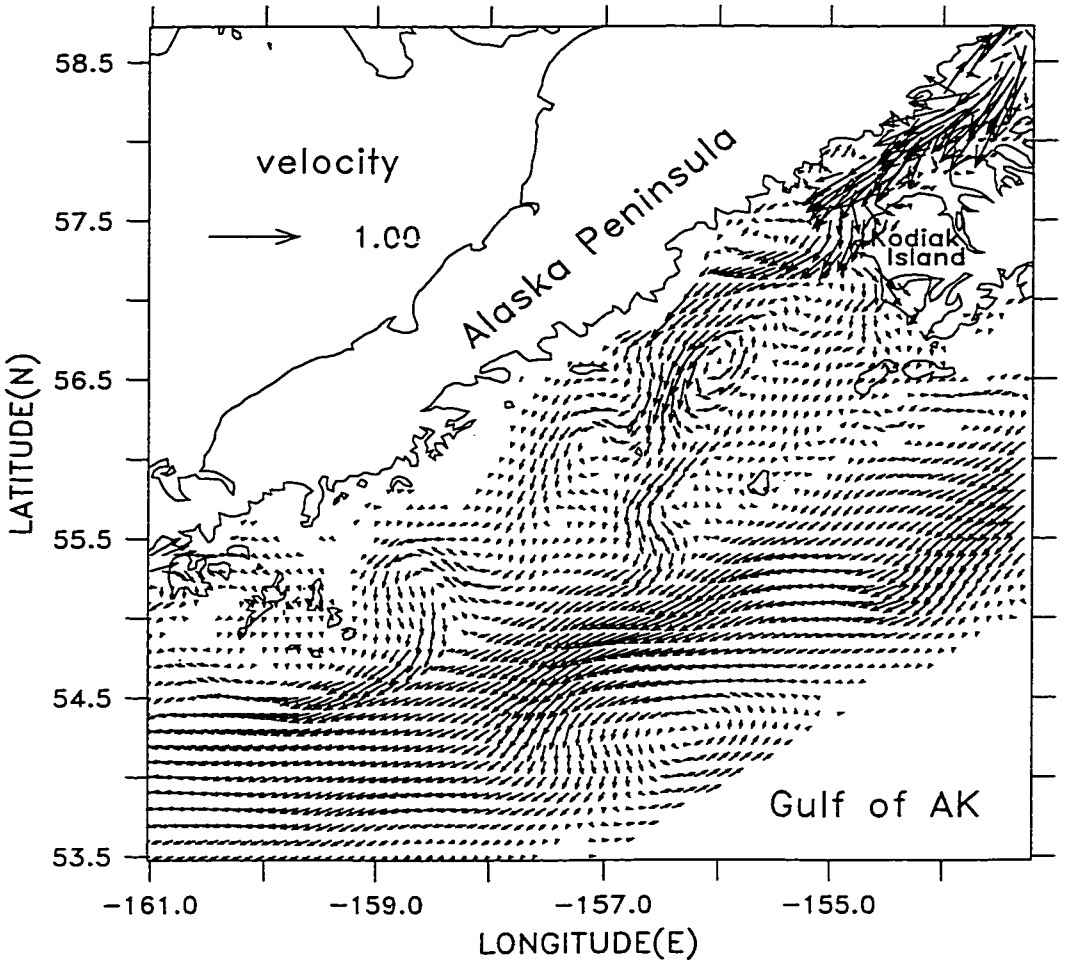

Figure 3.41a. Results of coupled models for mid-June, 1987. Surface velocities (m s^{-1}) from the circulation model.

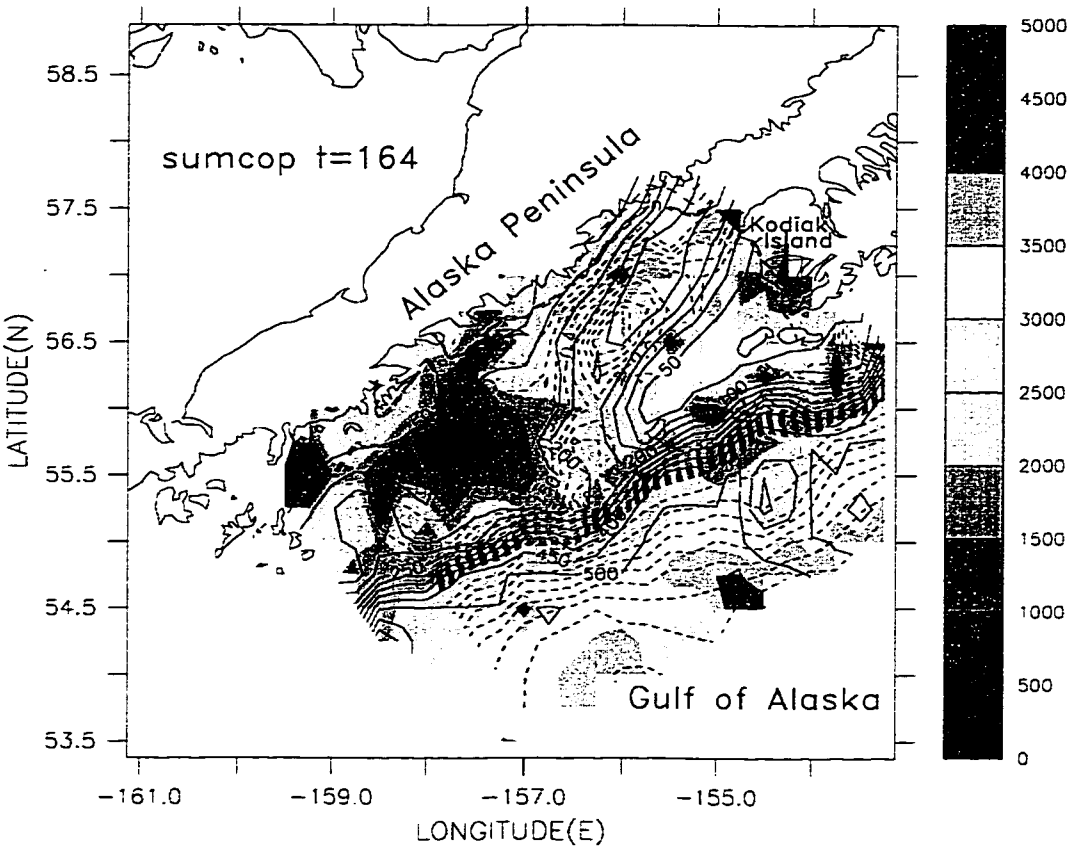

Figure 3.41b. Results of coupled models for mid-June, 1987. NPZ model output. Shading represents total concentration of all copepodite stages of *Pseudocalanus*, spp. in the mixed layer (no. m^{-3}).

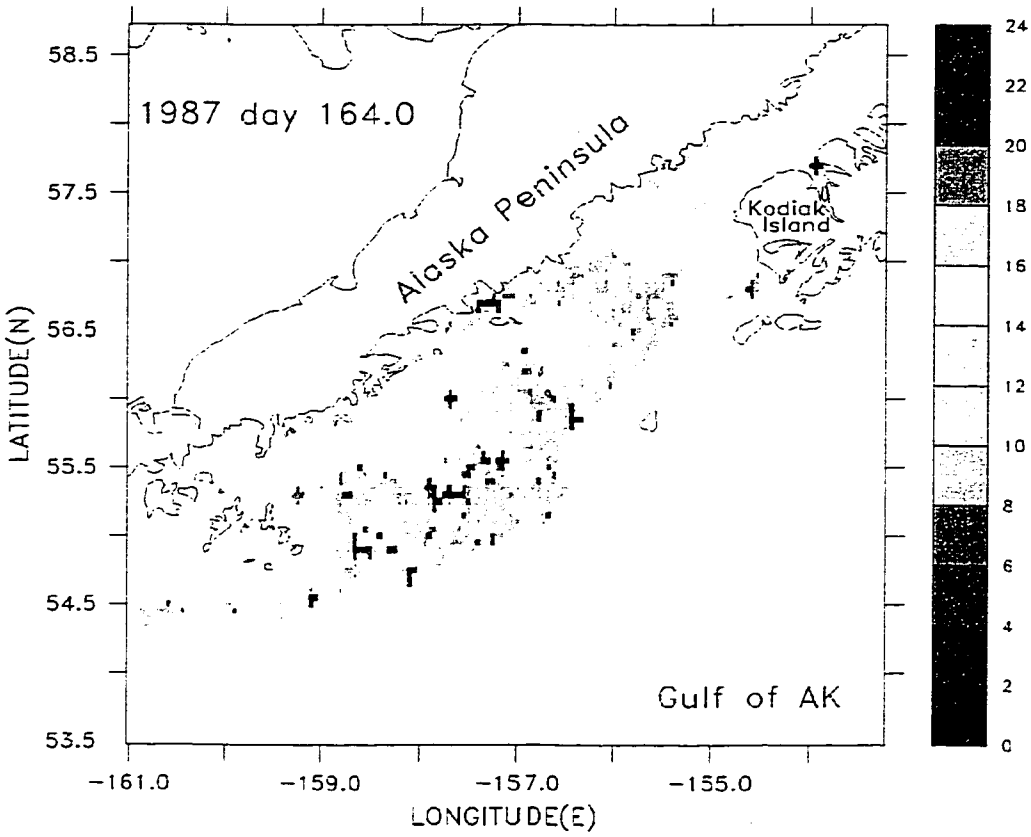

Figure 3.41c. Results of coupled models for mid-June, 1987. IBM output. Position of individual pollock are shaded by length (mm).

Prior to DOY 120, the 1988 run exhibited the largest number of retained larvae (Fig. 3.42a). The 1989 run yielded the largest number of retained larvae on DOY 135 and subsequently, whereas the 1988 run yielded the least beyond that day. Year 1987 yielded high retention of larvae through DOY 175, after which large numbers were lost from the area.

Lloyd's index of patchiness (Lloyd 1967) is defined as:

$$P = 1 + (\sigma^2 - \bar{x})/\bar{x} \qquad \text{(EQ 3.2)}$$

where $\bar{x}$ is the mean density of larvae in the area and σ^2 is the variance in that area. We calculate this statistic by grouping the modeled larvae into 0.2° longitude by 0.1° latitude bins for the shelf area between the southwestern edge of Kodiak Island and the northeastern edge of the Shumagins. The number of grouped larvae per bin serves as our density estimate. Bin size was chosen to correspond approximately with the sampling grids used in the data of Stabeno et al. (1996). Typically, Lloyd's index is computed by assuming a negative binomial distribution for field data; here we are sampling the entire population of modeled individuals and therefore may calculate the index directly.

The calm, dry year (1989) yielded an especially patchy distribution of larvae, with $P \approx 6.0$ on DOY 142 (Fig. 3.42b). Larvae in other years were more evenly distributed at that time. Patchiness values for 1989 dropped subsequently, but remained near $P = 4.0$ by the end of the simulation. For 1978 and 1991, patchiness generally increased beyond the early larval stage. In 1987, patchiness acheived a maximum in the middle of the run (DOY 175-225) but ultimately dropped to lower values than all other years on DOY 262 ($P \approx 3.0$). Year 1988 achieved maximum patchiness around DOY 160 ($P \approx 5.0$), with low values thereafter. An average time series of P for all years matches observed trends in P derived from multi-year data in the region, with values of $P \approx 5.0$ for both model and data at DOY 142 (Stabeno et al. 1996).

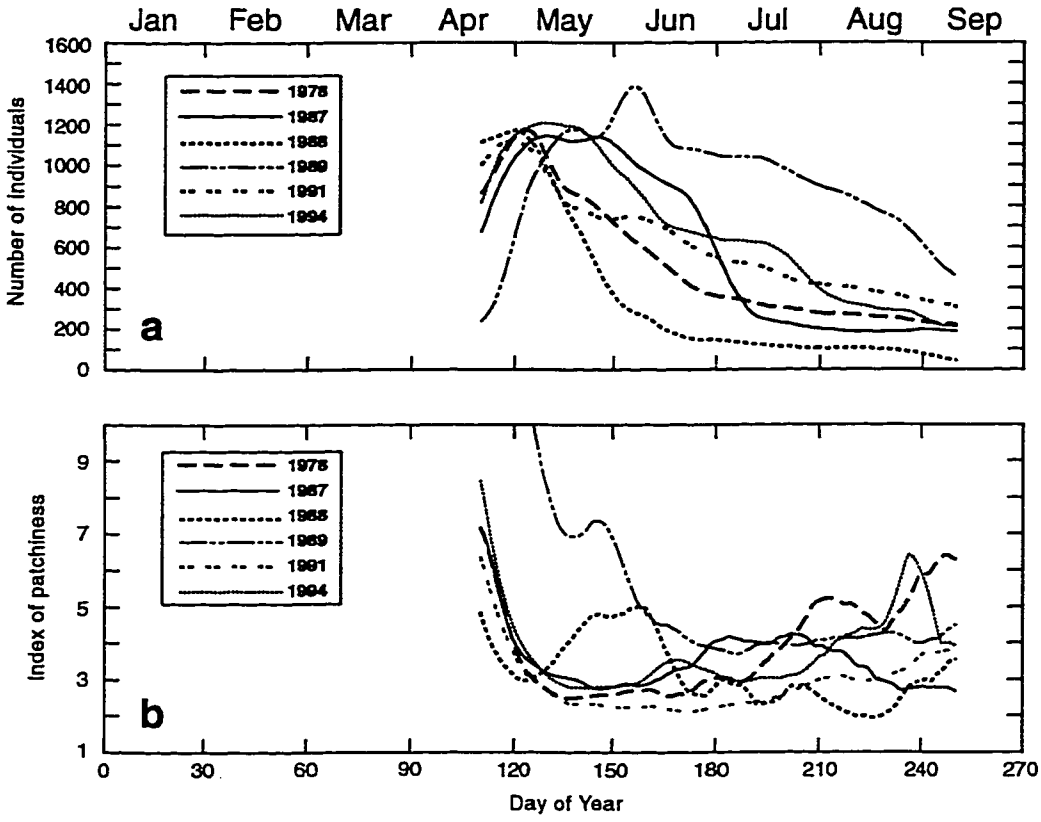

Figure 3.42. Statistics of individuals within the sea valley and shelf area (excluding Shelikof Strait), as a function of time for the 5 years modelled: (a) number of individuals on the shelf between Kodiak Island and the Shumagin Islands, (b) Lloyd's patchiness index for individuals within the same area.

3.5 Simulation 5. The importance of spawning location and timing

Examination of the contingency table containing the raw data (Table) shows that almost no fish (only ~1%) from the spawning region outside Kodiak Island were transported to the Shumagin Island nursery area. This table also shows that no fish from the Early spawning time, and that very few (~2%) from the Very Late spawning time made it. These particular levels of the factors were not included in the loglinear model. The log-linear model was therefore used to determine the effects of regions 1 (Central Shelikof Strait), 2 (Northern Shelikof Strait), 4 (Northwest Shelikof Sea Valley), and 5 (Southeast Shelikof Sea Valley), and only spawning times 2 (Middle) and 3 (Late) on success in reaching the nursery area. After looking at six hierarchical models based on this reduced dataset, depth was found to be independent of all factors and was removed entirely from the model. This resulted in a fixed sample size of 160 at each combination of region and spawning time.

Table 3.1. Contingency table for In/Out and Juvenile/Not Juvenile analyses

Region	Spawning Time	Spawning Depth	% Success In/Out 1978	In/Out 1994	Juv/Notjuv 1978	Juv/Notjuv 1994
Central Shelikof Strait	Early	On	0	0	2.50	1.25
		Off	0	0	3.75	1.25
	Middle	On	5.00	16.25	86.25	81.25
		Off	3.75	18.75	85.00	83.75
	Late	On	12.50	31.25	75.00	76.25
		Off	10.00	33.75	73.75	71.25
	Very Late	On	0	0	1.25	0
		Off	0	1.25	2.50	1.25
North Shelikof Strait	Early	On	0	0	2.50	1.25
		Off	0	0	1.25	0

Table 3.1. Contingency table for In/Out and Juvenile/Not Juvenile analyses

Region	Spawning Time	Spawning Depth	% Success In/Out 1978	In/Out 1994	Juv/Notjuv 1978	Juv/Notjuv 1994
	Middle	On	20.00	22.50	87.50	87.50
		Off	17.50	27.50	83.75	87.50
	Late	On	20.00	25.00	70.00	81.25
		Off	21.25	27.50	72.50	85.00
	Very Late	On	0	0	3.75	2.50
		Off	0	0	3.75	0
Outside Kodiak	Early	On	0	0	1.25	0
		Off	0	0	1.25	1.25
	Middle	On	0	0	100.00	93.75
		Off	0	1.25	98.75	96.25
	Late	On	0	0	100.00	87.50
		Off	0	0	97.50	93.75
	Very Late	On	0	0	1.25	0
		Off	0	0	1.25	1.25
Northwest Shelikof Sea Valley	Early	On	0	0	0	0
		Off	0	0	0	0
	Middle	On	26.25	15.00	83.75	77.50
		Off	18.75	18.75	76.25	77.50
	Late	On	37.50	35.00	80.00	83.75
		Off	36.25	33.75	77.50	86.25
	Very Late	On	2.50	5.00	5.00	6.25
		Off	3.75	6.25	12.50	7.50
Southwest Shelikof Sea Valley	Early	On	0	0	0	0
		Off	0	0	0	0
	Middle	On	7.50	1.25	88.75	83.75
		Off	6.25	0	86.25	78.75

Table 3.1. Contingency table for In/Out and Juvenile/Not Juvenile analyses

Region	Spawning Time	Spawning Depth	% Success In/Out 1978	In/Out 1994	Juv/Notjuv 1978	Juv/Notjuv 1994
	Late	On	13.75	17.50	98.75	96.25
		Off	5.00	11.25	98.75	98.75
	Very Late	On	0	0	5.00	3.75
		Off	0	1.25	2.50	5.00

In the reduced 1978 dataset, success was found to be dependent on spawning time and region, but independent of the spawning time and region interaction. Among all regions except outside Kodiak Island, the highest success rate was in the Northwest Shelikof Sea Valley (30%). The lowest success rate was found in Central Shelikof Strait and Southeast Shelikof Sea Valley (8%). Among spawning times, the Late spawning time had a 19% success rate and the Middle spawning time had a 13% success rate.

In the 1994 reduced dataset, success was found to be dependent on spawning time and region jointly, mainly because of a lower than expected number of successes in the Southeast Shelikof Sea Valley, Middle spawning time. The highest success rate was found in the Northwest Shelikof Sea Valley, and the Late spawning time (34%), and in the Northern Shelikof Strait region and the Late spawning time (33%). The lowest success rate was from the Southeast Shelikof Sea Valley, the Middle spawning time (1%).

For both the 1978 and the 1994 datasets testing whether fish made it to the juvenile stage, at least 98% of the fish from the Early spawning time did not make it to the juvenile stage. This information was noted, and this spawning time was not included in the loglinear model. After looking at six hierarchical models based on this reduced dataset, depth was found to be independent of all factors and was therefore removed entirely from the model.

In the 1978 juvenile/not juvenile reduced dataset, the loglinear model revealed that success of reaching the juvenile stage was dependent on region and spawning time jointly. The highest success rate was found in the region outside Kodiak Island, Middle and Late spawning times (99% and 99% respectively). The lowest success rate was found in Central Shelikof Strait, the Very Late spawning time (2%). It is evident from the complete contingency table (Table , all regions and spawning times) that low success rates are associated with the Early and Very Late spawning times across regions, and that the higher success rates are associated with the Middle and Late spawning times.

In the 1994 reduced dataset, the loglinear model again revealed that success of reaching the juvenile stage was dependent on region and spawning time jointly. The highest success rate was found in the Southeast Shelikof Sea Valley and Late spawning time (98%), although the region outside Kodiak Island, Middle and Late spawning times also had high success (95% and 90%, respectively). The lowest success rate was found in Central Shelikof Strait and outside Kodiak Island, the Very Late spawning time (1%)

Figures 3.43-3.48 show the locations on September 1st (DOY 244) of fish from different years, spawning regions and spawning times. Fig. 3.43 shows fish released from Central Shelikof Strait (Region 1), the observed spawning location. No fish spawned during the Early spawning time survived until September 1st (Fig 3.43a). A few from the Middle (observed, Sptime 2) spawning time were transported to the nursery area (Fig 3.43b). Note that some fish from this spawning time and location were found to the north of Kodiak Island. An animation of transport of individuals (not shown) shows that these fish were carried around the north end of Kodiak Island by the currents. More fish from the Late spawning time (Sptime 3, Fig 3.43c) were transported to the Shumagin nursery area, although many remained both upstream and downstream of the nursery region. The fish spawned in the Very Late spawning time (Sptime 4, Fig 3.43d) were still in the feeding larval stage on September 1st.

The plot of the locations of fish spawned in Region 1 in 1994 (Fig 3.44) shows similar patterns to 1978, except that a few more fish from both the Middle (Fig 3.44b) and the Late

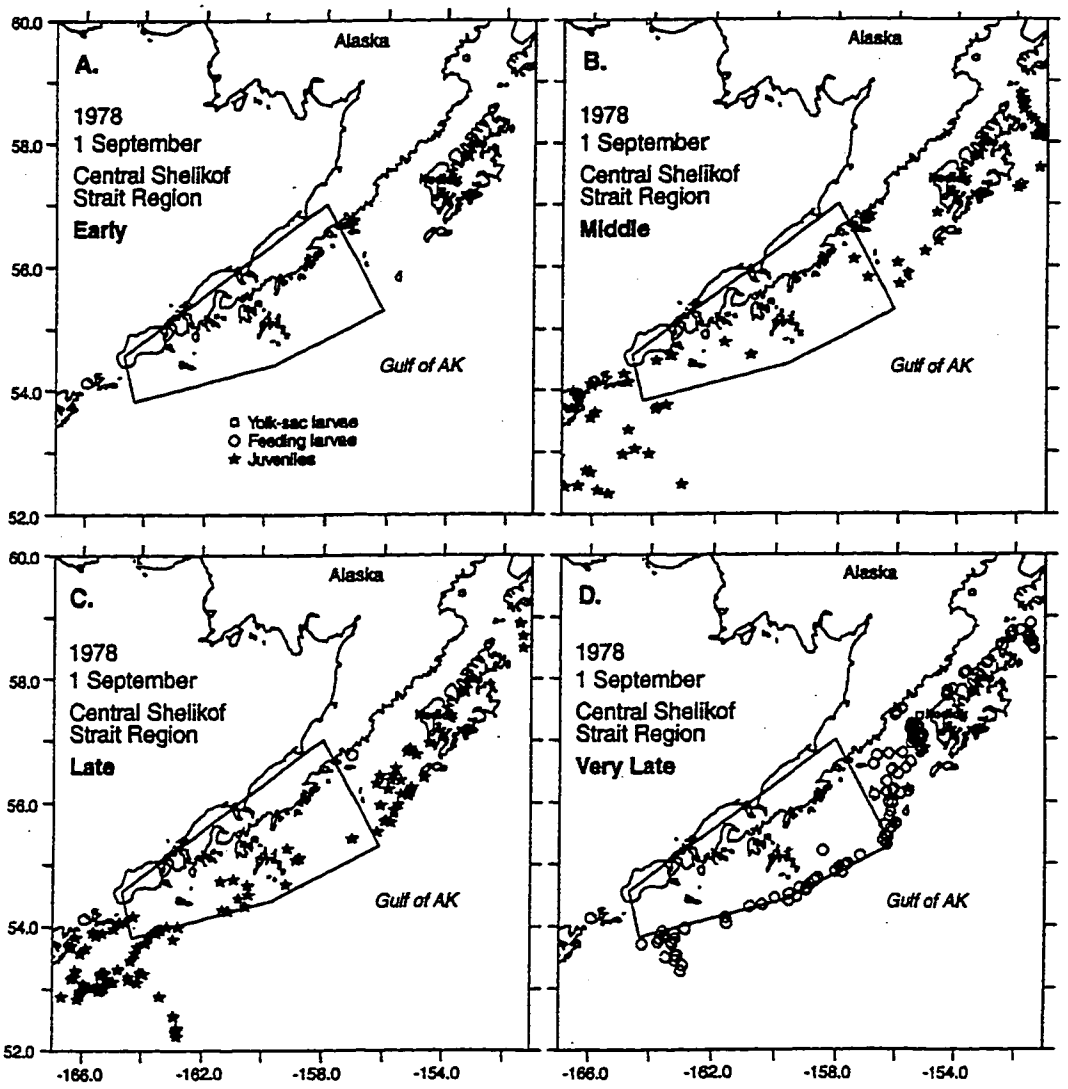

Figure 3.43. Locations on September 1 of yolk sac and feeding larvae and juveniles from eggs spawned in Central Shelikof Strait, for 1978. A. Eggs released during the Early spawning time, B. eggs released during the Middle spawning time, C. eggs released during the Late spawning time, D. eggs released during the Very Late spawning time.

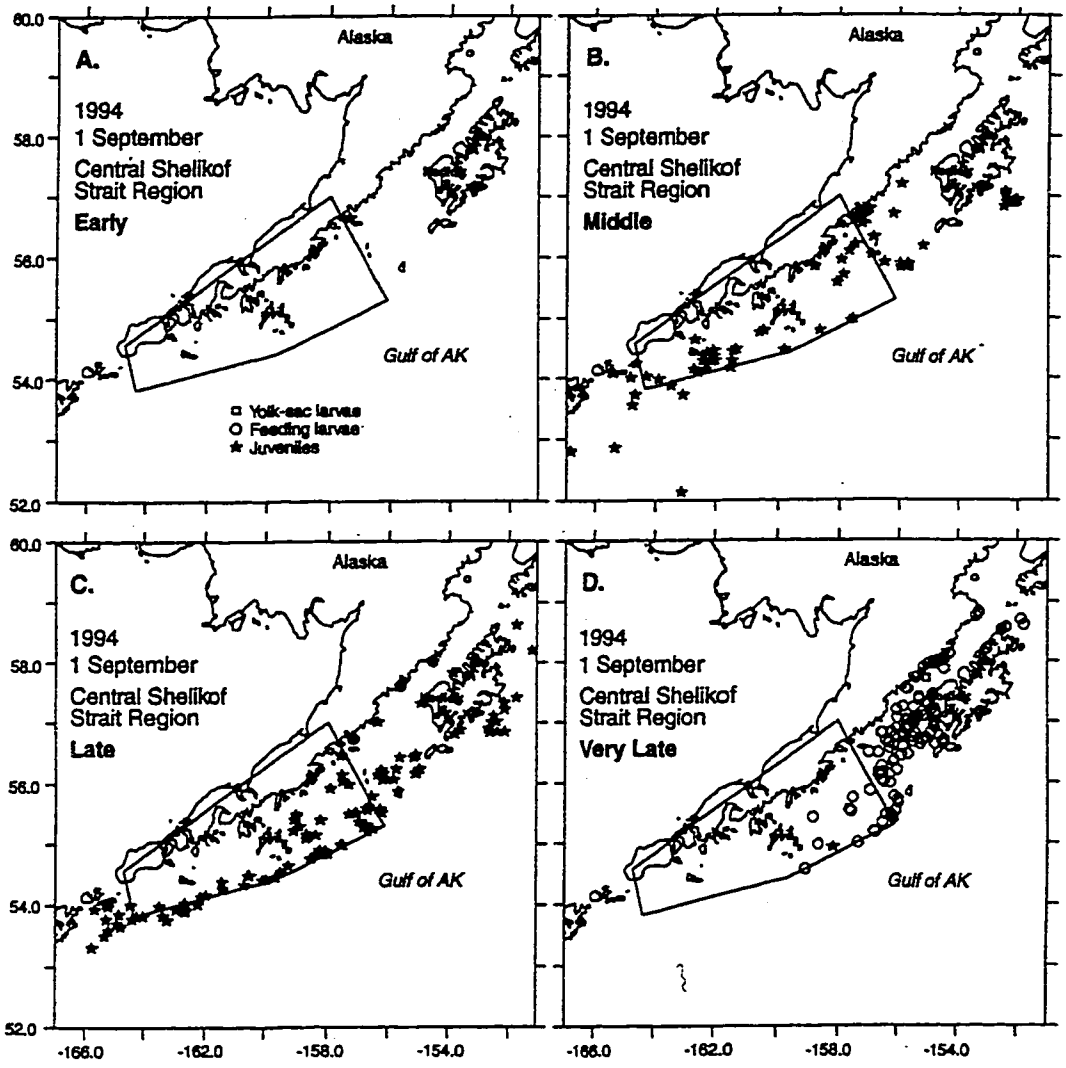

Figure 3.44. Locations on September 1 of yolk sac and feeding larvae and juveniles from eggs spawned in Central Shelikof Strait, for 1994. A. Eggs released during the Early spawning time, B. eggs released during the Middle spawning time, C. eggs released during the Late spawning time, D. eggs released during the Very Late spawning time.

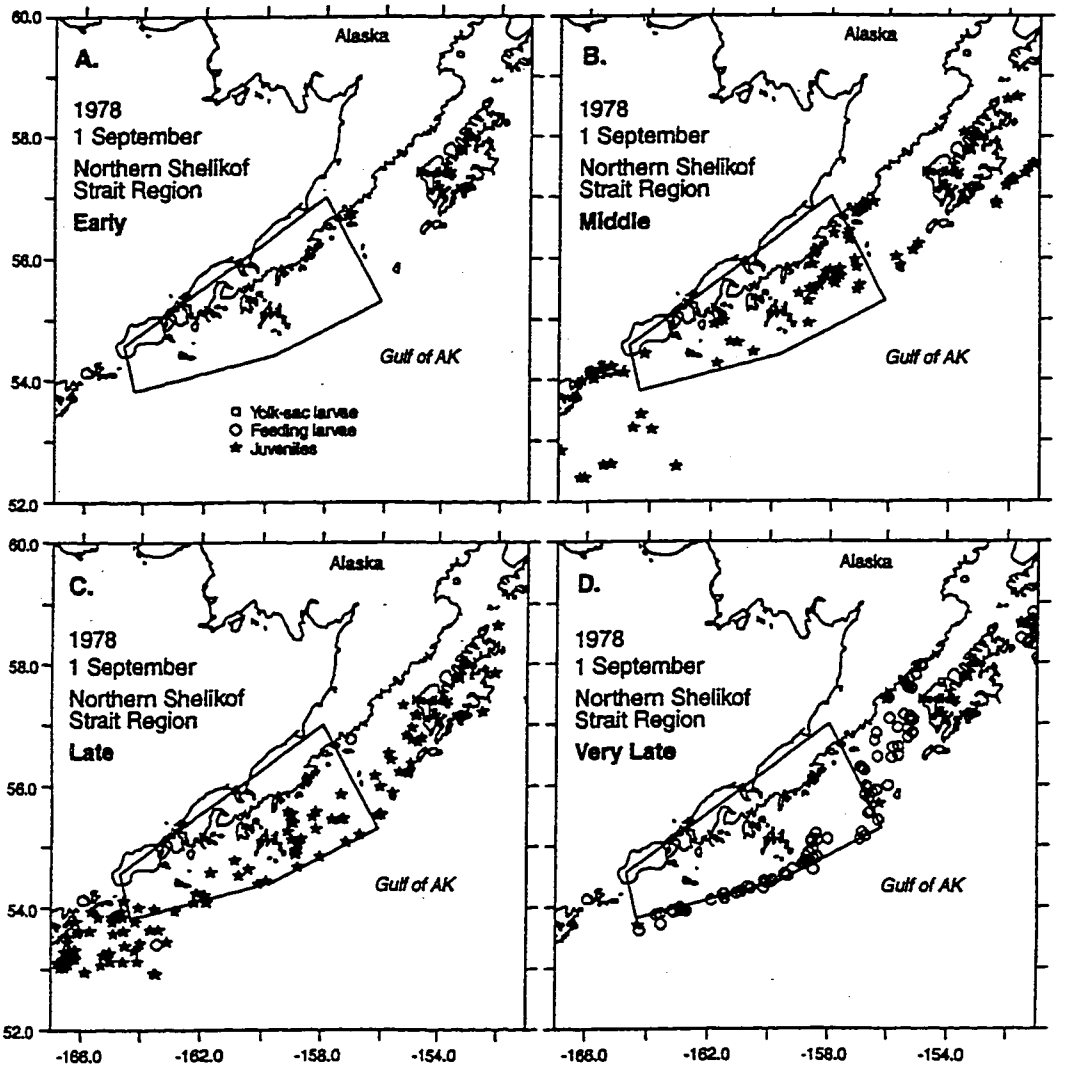

Figure 3.45. Locations on September 1 of yolk sac and feeding larvae and juveniles from eggs spawned in Northern Shelikof Strait, for 1978. A. Eggs released during the Early spawning time, B. eggs released during the Middle spawning time, C. eggs released during the Late spawning time, D. eggs released during the Very Late spawning time.

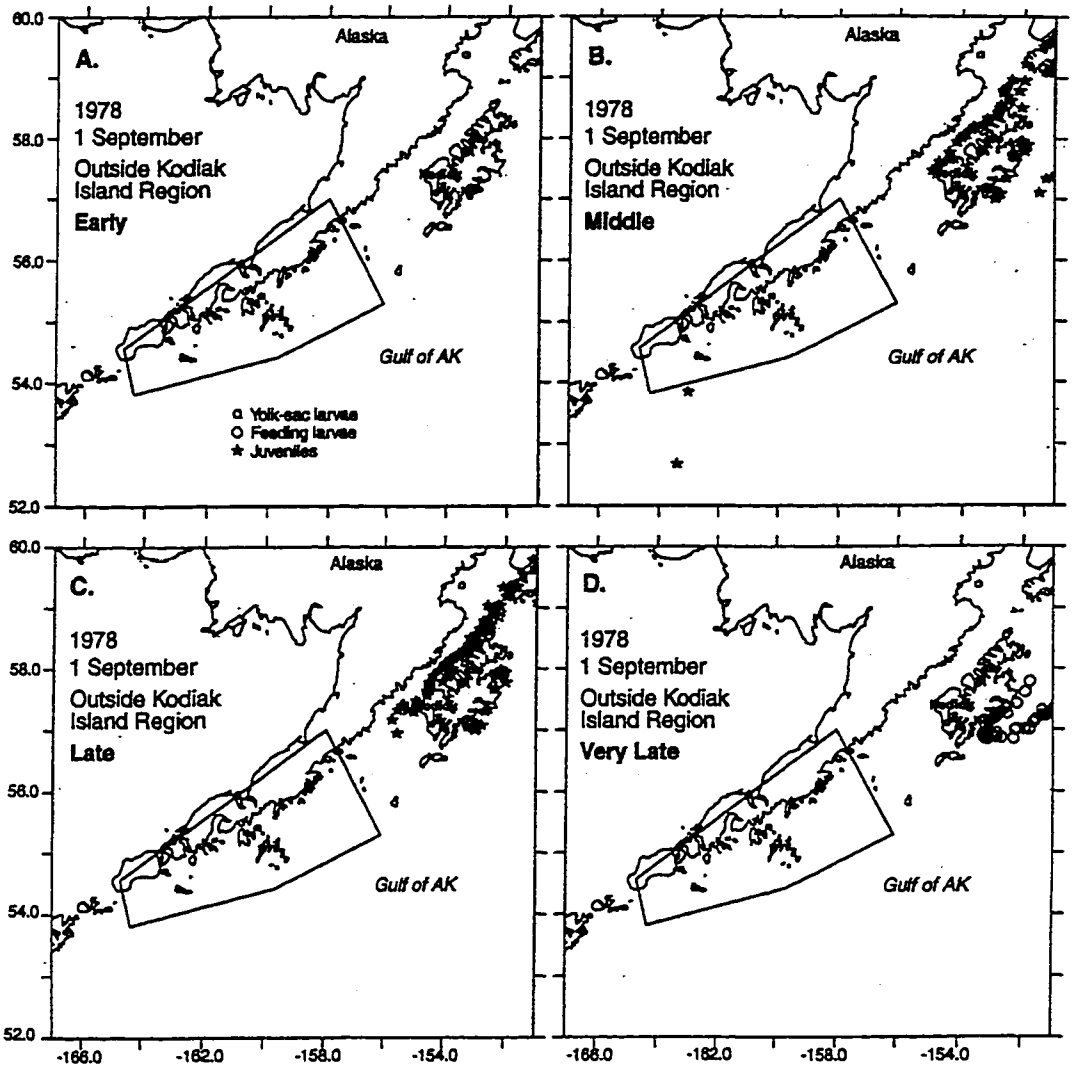

Figure 3.46. Locations on September 1 of yolk sac and feeding larvae and juveniles from eggs spawned outside Kodiak Island, for 1978. A. Eggs released during the Early spawning time, B. eggs released during the Middle spawning time, C. eggs released during the Late spawning time, D. eggs released during the Very Late spawning time.

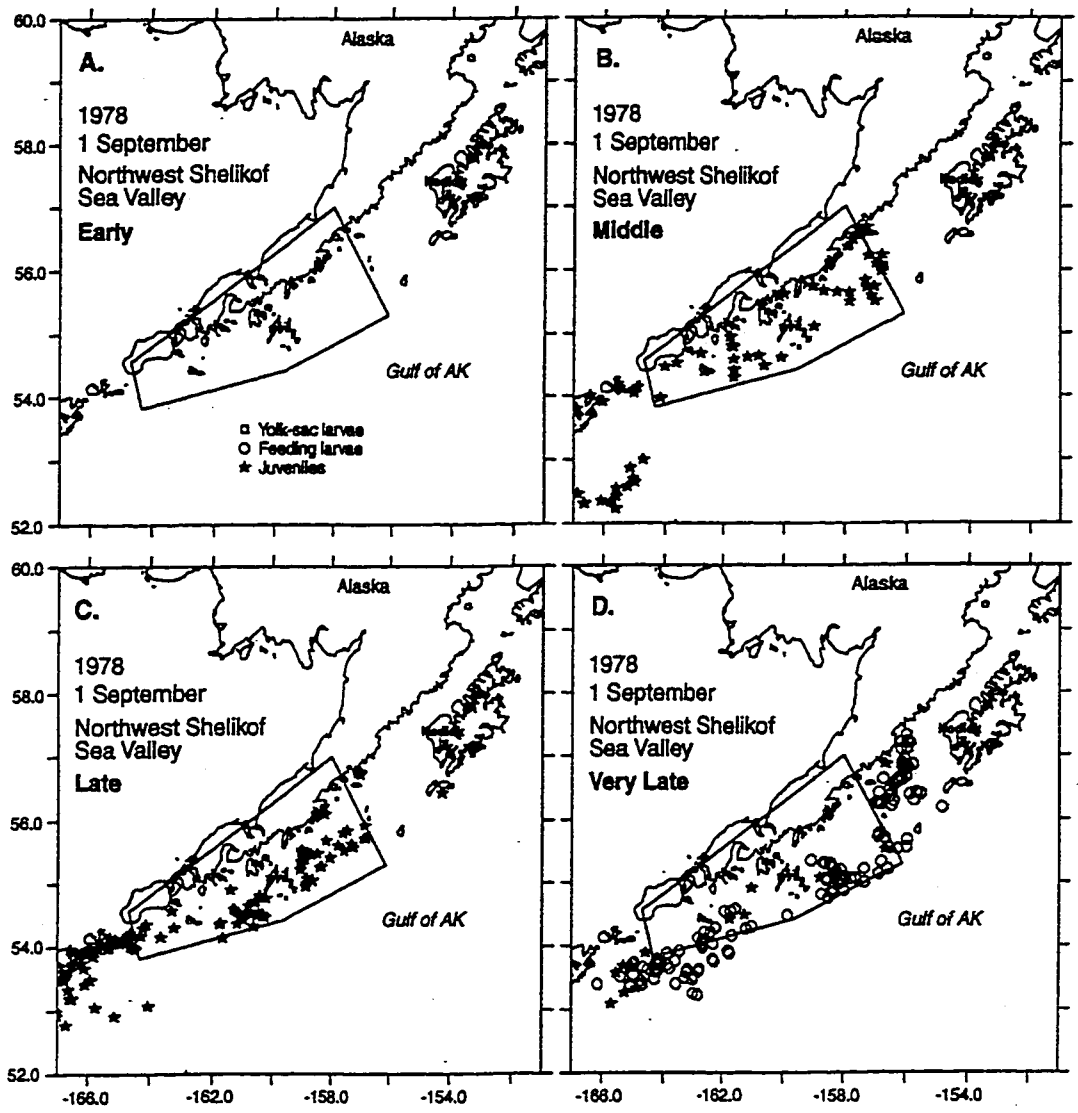

Figure 3.47. Locations on September 1 of yolk sac and feeding larvae and juveniles from eggs spawned in Northwest Shelikof sea valley, for 1978. A. Eggs released during the Early spawning time, B. eggs released during the Middle spawning time, C. eggs released during the Late spawning time, D. eggs released during the Very Late spawning time.

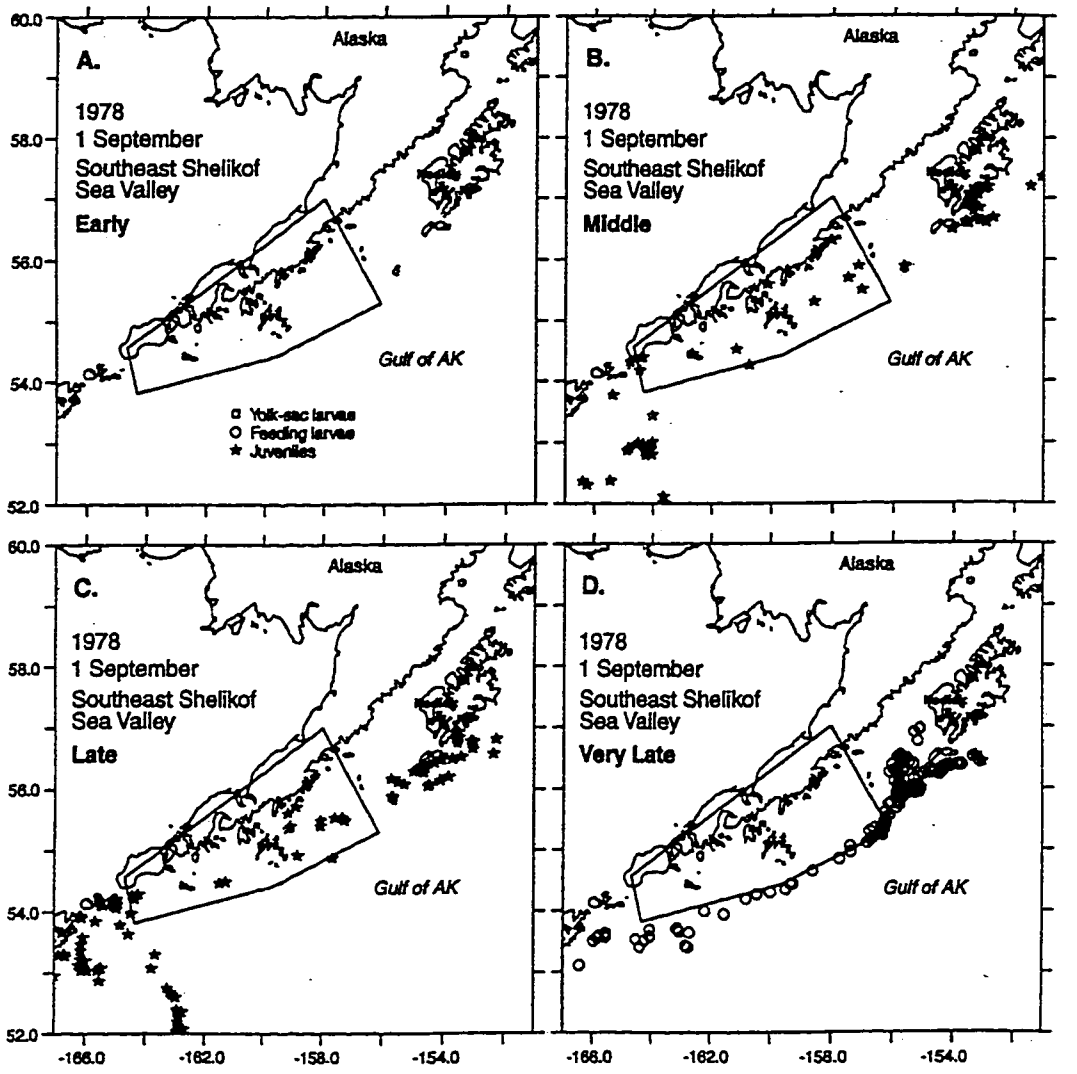

Figure 3.48. Locations on September 1 of yolk sac and feeding larvae and juveniles from eggs spawned in Southeast Shelikof sea valley, for 1978. A. Eggs released during the Early spawning time, B. eggs released during the Middle spawning time, C. eggs released during the Late spawning time, D. eggs released during the Very Late spawning time.

(Fig 3.44c) spawning times ended up in the nursery area. Also, more fish from the Late spawning period were transported to the outside of Kodiak Island. Fish spawned during the Very Late spawning time (Fig 3.44d) were in the feeding larval stage on September 1st, as in 1978, but note that most of them were still upstream of the Shumagin nursery area, probably due to the lower overall transport rates in this year. Since patterns for both years are similar, only plots for 1978 will be shown subsequently.

Fig. 3.45 shows fish spawned in Northern Shelikof Strait (Region 2) for 1978. As before, no fish from the Early spawning time (Fig 3.45a) survived. Many more fish from this region, from both the Middle (Fig 3.45b) and the Late (Fig 3.45c) spawning times, were found in the Shumagin nursery area on September 1st, than were fish from Region 1 (Central Shelikof Strait). Again, nearly all fish spawned in the Very Late spawning time (Fig 3.45d) were still in the feeding larval stage. Patterns were similar in 1994, except that somewhat fewer fish were swept past the nursery area due to lower transport.

Fish spawned outside Kodiak Island (Region 3) were not found in the Shumagin nursery area (Fig 3.46). Fish remained in the region outside Kodiak Island and moved to within Shelikof Strait proper from the outside areas (Fig 3.46b-d). The same pattern was seen in both 1978 and 1994.

Fish from the Northwest Shelikof Sea Valley (Region 4) were very successful in reaching the Shumagin nursery area, from both the Middle (Fig 3.47b) and Late (Fig 3.47c) spawning times. Again, similar patterns were observed in both years. Fish originating from the Southeast Shelikof Sea valley (Fig 3.48) did not, for the most part, reach the nursery area; most were swept downstream. Some fish from the Middle (Fig 3.48b) and Late (Fig 3.48c) spawning times ended up to the southeast of Kodiak Island in both years.

3.6 Simulation 6. The effect of turbulence on feeding.

We evaluated the performance of the IBM model by examining model output with respect to the model's predicted influence of wind-generated turbulence on feeding. We compare

model results to theoretical results such as Figure 3 in MacKenzie et al. (1994) which shows the expected dome-shaped relationship of the effect of turbulence on encounter rate and fish larval ingestion. Output from the model (Fig. 3.49) conforms nicely to the theory by showing a well defined peak in consumption at intermediate wind speeds of about 8 m s^{-1}. Wind speeds above 8 m s^{-1} theoretically cause pursuit time to become limiting with the net effect of decreasing rates of ingestion.

Another measure of model performance was the relationship between starvation mortality and average probability of successful pursuit (Fig. 3.50). These result indicate that as probability of successful pursuit increases, starvation mortality decreases, with the decrease being more pronounced for older larvae (DOY 160). On average, the starvation mortality was lower for older larvae compared to young larvae. Older larvae (DOY 160) were more successful at pursuing their prey as indicated by the tendency of the data points to be clustered toward the right hand side of the bottom panel. The probability of successful pursuit was also less variable for older larvae (DOY 160) compared to younger larvae (DOY 130).

The IBM generated copious amounts of information. Figure 3.51 shows one example of the magnitude and direction of the sensitivity of all 24 output variables to the one model input parameter, reactive distance. An output variable was considered sensitive to the parameter (indicated by a black bar) if the absolute value of the correlation coefficient was greater or equal to 0.15. The selection of 0.15 was an approximation based on the critical value (0.113) of a Pearson's correlation coefficient at $\alpha = 0.05$ and $n = 300$. These data show that increasing reactive distance significantly increased mean growth rate (MGR130), mean length (MLEN130), and mean weight (MWT130) but only for the young larvae (DOY 130), and increased mean cumulative feeding as well as mean pursuit time for small (MCFSL130, MPSSL130) and large larvae (MCFLL160, MPSSL160), on both DOY 130 and 160. Increasing reactive distance had a positive effect on mean numbers for both DOY 130 (MNO130) and 160 (MNO160) but not to a significant degree. Increases in reactive distance caused significant decreases in mean metamorphosis date on

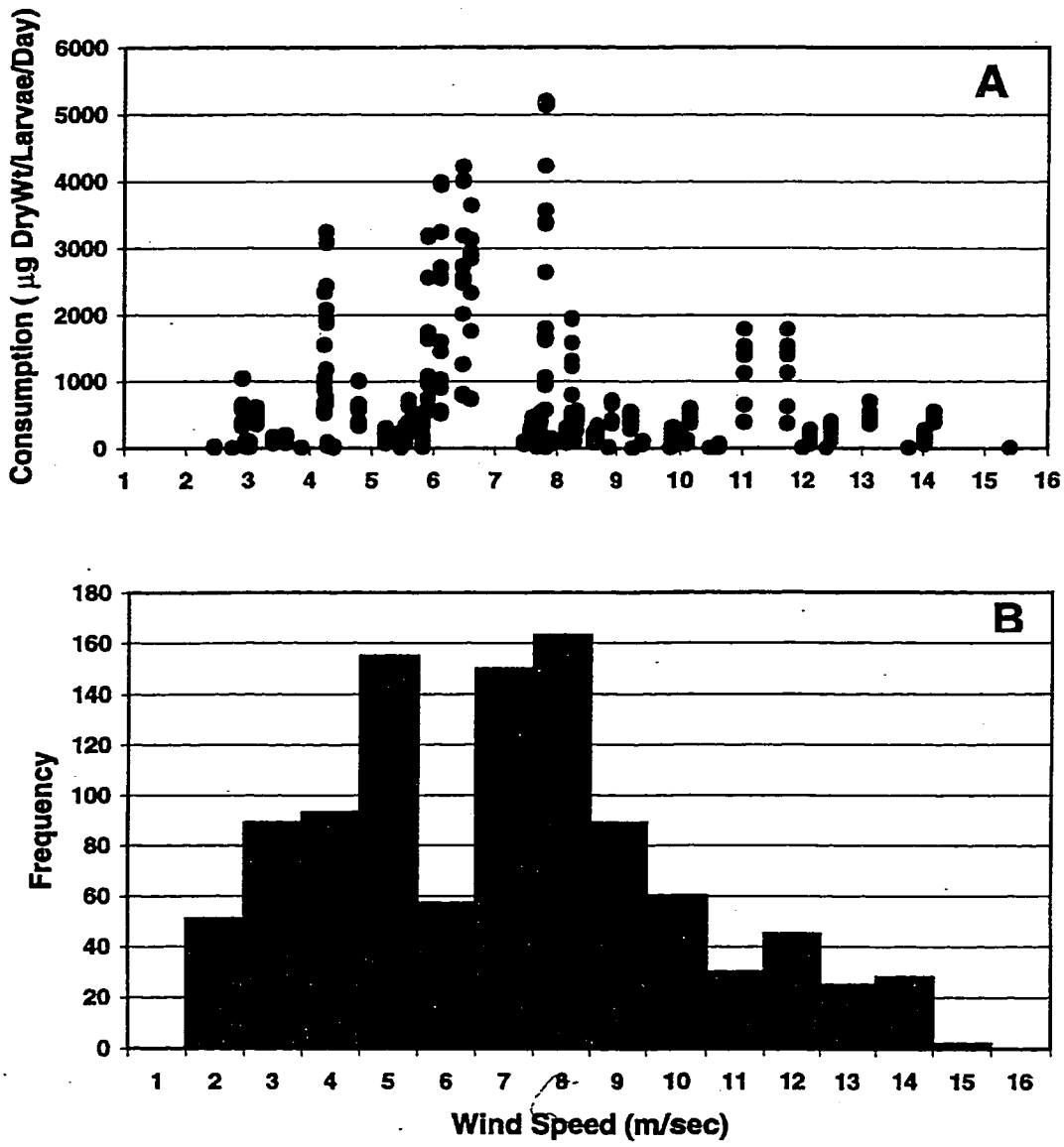

Figure 3.49. IBM model output from Simulation 6 showing (A) the distribution of Consumption with Wind Speed, and (B) a frequency histogram of wind speeds.

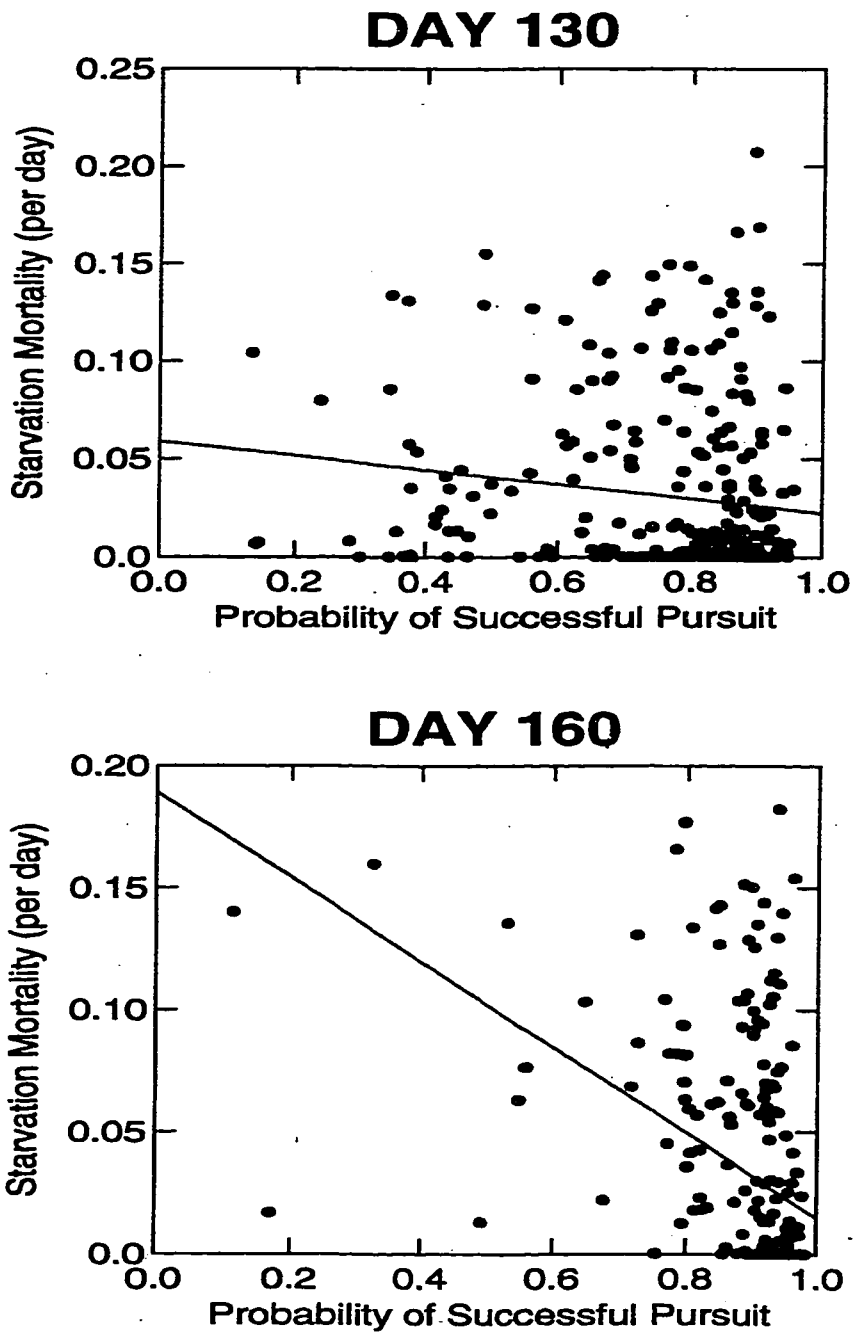

Figure 3.50. IBM model output from Simulation 6 showing starvation mortality related to the probability of successful pursuit on (top) DOY 130 and (bottom) DOY 160.

both DOY 130 (MMD130) and DOY 160 (MMD160). This is a consequence of increased growth; faster growing larvae will reach metamorphosis sooner. Increased reactive distance decreased mean total mortality on both DOY 130 (MZ130) and DOY 160 (MZ160) but not to a significant degree. There was, however, a significant decrease in starvation mortality on both DOY 130 (MSZ130) and 160 (MSZ160) as a result of reactive distance increasing. Also of note is a consistent trend that the magnitude of the effect of reactive distance for all output variables is more pronounced for young larvae compared to old larvae, as indicated by the larger absolute value of the correlation coefficient for an output variable on DOY 130 versus DOY 160. This trend holds true regardless of the direction of the effect of the input variable on the output variable.

Sensitivity was generally evaluated by considering which model input parameter significantly influenced output variables and which output variables were most influenced by the suite of input parameters (Table 3.2 and Table 3.3). This analysis shows which input parameters most control model behavior as well as which output variables were the most sensitive. The rank order of important input parameters (Table 3.2) shows that the weight-length conversion power coefficient (LWYBB) and reactive distance (RDA) input parameters were the two that influenced the largest number of output variables (17 out of 24), influencing 70.8% of all output variables. Larval feeding depth (FDEPTHG) was ranked third, influencing 50% of the output variables. The routine metabolism power coefficient (MROFDLB) ranked fourth, affecting about 42% of the output variables. The intercept parameter of the larval length-maximum prey size function (MAXPREYA), the base mortality when larval length is less than 7 mm (MFDLSM), and the proportionality constant in the turbulent velocity function (WA) all affected about 30% of the output variables. The rank order of important output variables (Table 3.3) show that mean metamorphosis date on both DOY 130 (MMD130) and DOY 160 (MMD160) were sensitive to 39 and 28 input parameters out of a total of 119, respectively. The next five output variables, dealing mainly with starvation and predation mortality, were sensitive to 5-8% of the input parameters.

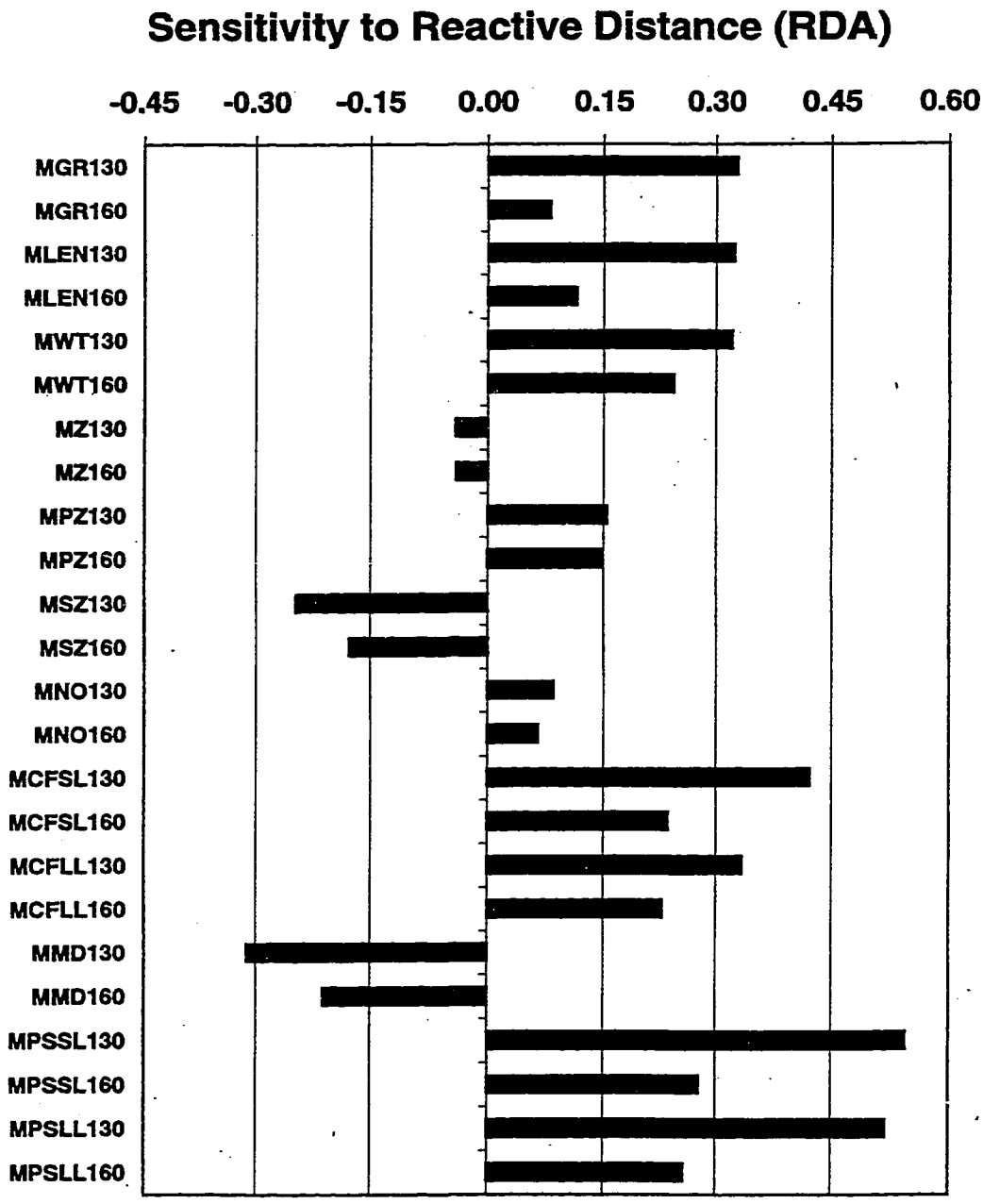

Figure 3.51. One example of the magnitude and direction of the sensitivity of all 24 output variables to one model input parameter, reactive distance.

Table 3.2. List of input parameters ranked by their influence on 24 output variables

Input parameter	Sensitive Output Variables	
	Number	Percent of Total
LWYBB	17	70.8%
RDA	17	70.8%
FDEPTHG	12	50.0%
MROFDLB	10	41.7%
MAXPREYA	8	33.0%
MFDLSM	8	33.3%
WA	7	29.2%

Table 3.3. List of output variables ranked by their sensitivity to 119 input parameters.

Output Variable	Sensitive Input Parameters	
	Number	Percent of Total
MMD130	39	28.6%
MMD160	28	20.3%
MPZ130	11	7.9%
MSZ160	10	7.3%
MLEN130	9	6.5%
MPZ160	9	6.5%
MSZ130	8	5.8%

A summary table of sensitivity results, organized by process, day of the year, and output variable, is presented in Table 3.4. Within the growth process, on DOY 130 the input parameter most influencing the growth, length and weight processes was identical. Reactive distance (RDA) had a similar positive effect ($r \sim 0.33$) on growth, length and weight processes, while the length-weight conversion coefficient (LWYBB) had a negative effect. This effect was much more pronounced ($r = -0.59$) for the length and weight variables compared to the growth variable ($r = -0.25$). Turbulent velocity (WA), pause duration-larval length function coefficient under conditions of no turbulence and low prey density (PD1A), and reactive distance (RDA) had positive effects on growth, length and weight, with RDA having the largest effect ($r = 0.24$). Probability of prey capture of copepod nauplii for 15-16 mm larvae (PNAUP11), length-weight conversion coefficient (LWYBB), and routine metabolism power coefficient (MROFDLB) had negative effects on growth, length and weight. On DOY 160, the magnitude of the correlation coefficients for RDA and LWYBB were smaller compared to DOY 130. On DOY 160 there was a wider range of important input parameters compared to DOY130, however RDA, and LWYBB appeared as they did on DOY 130 with respect to the sign of the effect.

Table 3.4. Sensitivity of output variables to input parameters organized by process, day of the year and magnitude and direction of the effect.

	DOY 130				DOY 160			
	Positive r		Negative r		Positive r		Negative r	
OUTPUT VARIABLE	INPUT PARAMETER	r	INPUT PARAMETER	r	INPUT PARAMETER	r	INPUT PARAMETER	r
			GROWTH					
Growth	RDA	0.33	LWYBB	-0.25	WA	0.16	PNAUP11	-0.18
Length	RDA	0.32	LWYBB	-0.59	PD1A	0.18	LWYBB	-0.32
Weight	RDA	0.32	LWYBB	-0.59	RDA	0.24	MROFDLB	-0.28
			MORTALITY					
Z	MFDLSM	0.57	MSIZEB1	-0.32	MFDLSM	0.46	PNAUP7	-0.16
Predation Z	LWYBB	0.42	MSIZEB1	-0.26	LWYBB	0.39	PEGGS9	-0.19
Starvation Z	MFDLSM	0.25	LWYBB	-0.42	FDEPTHG	0.35	PEGGS9	-0.19
Number	MSIZEB1	0.24	MFDLSM	-0.73	MSIZEB1	0.31	MFDLSM	-0.36
			CONSUMPTION					
Cum. Feeding SL	RDA	0.42	FDEPTHG	-0.30	RDA	0.24	FDEPTHG	-0.25
Cum. Feeding LL	RDA	0.33	LWYBB	-0.27	RDA	0.23	FDEPTHG	-0.19
Prob. Suc. Pursuit SL	RDA	0.54	t	-0.48	RDA	0.28	t	-0.34
Prob. Suc. Pursuit LL	RDA	0.52	t	-0.46	RDA	0.26	t	-0.32

Within the mortality process, on DOY 130, we see that base mortality (MFDLSM) had a positive effect on the total mortality (r = 0.57) and a corresponding negative effect on numbers (r = -0.73). Similarly, the mortality-length function slope coefficient (MSIZEB1) had a positive effect on numbers (r = 0.24) and a negative effect on total mortality (r = 0.32). The length-weight conversion parameter (LWYBB) had a positive effect on predation mortality (r = 0.42) and an equal negative effect on starvation mortality (r = -0.42). This result was caused by predation mortality being calculated by difference from total and starvation mortality. On DOY 160, the magnitude of the correlation coefficients were generally smaller compared to DOY 130. Input parameters having a positive effect on mortality processes were similar to those indicated on DOY 130, except that feeding depth (FDEPTHG) was important to starvation mortality (r = 0.35) for DOY 160. Parameters having a negative effect on mortality processes on DOY 160 included two prey capture probability parameters for 11-14 mm larvae (PNAUP7 and PEGGS9). Of the parameters having a negative effect on mortality processes, base mortality for small larvae (MFDLSM) for DOY 160 had the greatest effect, influencing numbers (r = -0.36).

Within the consumption process, there was a surprising uniformity in the effect (magnitude and direction of the correlation coefficient) of input parameters to the cumulative feeding and the probability of successfull pursuit output variables. The trends held up over both days and for both small and large larval comparisons. Reactive distance (RDA), minimum pursuit time (t), and feeding depth (FDEPTHG) were the three most important input parameters. Reactive distance had a uniform positive effect of similar magnitude and minimum pursuit time and feeding depth had negative effects of similar magnitude.

Chapter 4. Discussion

Spatially explicit biophysical models, spanning multiple trophic levels, can be a powerful tool for probing hypotheses about the early life history of marine fish. Throughout our ongoing work with coupled hydrodynamic, population (IBM), and trophodynamic (NPZ) models, we have attempted to balance desirable features with practical limits on computing power. Our experience in Simulation 1 (Float-tracking experiments) has led to the following conclusions. (1) Storage of prefiltered and decimated model velocity and scalar fields for later use by Lagrangian and Eulerian biological models is both feasible and efficient using presently available computers. Supercomputing platforms with reasonable large (several gbyte) storage capacity are necessary for much of this work, however. (2) The results are reasonably accurate given a sufficiently small time step for spatial tracking; however, care must be taken to consider the information lost through filtering. Practical techniques exist to recover some of the lost information, such as tides or cross-shelf transport.

As our models evolve to greater complexity, there is a continuing need for calibration and sensitivity analyses of the coupling methods which link them. For example, there is a strong need for further sensitivity analyses of grid spacing in our NPZ model. Equally important is the need for further comparison of three-dimensional NPZ model with chlorophyll and zooplankton data. For chlorophyll, satellite-derived estimates may be useful for comparing at least broad spatial patterns, and possible higher-order spatial statistics, with those produced from the model. These and other issues will be explored in future research.

In Simulations 2 (The importance of Lagrangian factors) and 3 (The importance of vertical location), we attempted to answer the questions: (1) "How sensitive are growth characteristics and other attributes of larval pollock to spatial differences in a physical forcing variable such as temperature acting on individuals, and how do these differences affect population-level distributions of attributes?", and (2) "How sophisticated does the predic-

tion of the depth of individuals in the IBM need to be in a coupled model such as ours in order to correctly predict horizontal advection?" It is appropriate to keep in mind that in the biological IBM, the effects of abiotic factors on the attributes of young fish were simplified for these early simulations. With the additions of abiotic factors other than temperature or salinity (such as mixed layer depth or varying Q_{10}), and biotic factors such as predators and prey, and with mortality due to starvation and predation (not included in these early simulations), patterns observed in model output will undoubtedly be somewhat different in detail from what we observed in these simulations. Even with future additions, we cannot expect model output to replicate data exactly, especially spatial distributions. This is because, in general, models can never reproduce reality, only approximate it, hopefully in some statistically acceptable manner.

Simulation 2 illustrates how the inclusion of even rudimentary spatial information can radically alter the outcome of the IBM. Even a simple example, using the Lagrangian approach without behavioral feedback, yields strikingly different distributions of population attributes than the same model with no spatial information. In particular, the added Lagrangian information yields a bimodal distribution of weights and lengths of larval fish, as opposed to a unimodal distribution seen in the case with no spatial tracking (Fig. 3.4). Bimodal distributions have been noted in field data on length distributions of pollock in the Shelikof Strait region. Intracohort cannibalism is a possibility when significant differences in length exist within a cohort. Intracohort cannibalism has been seen in young pollock (P. Livingston, Alaska Fisheries Science Center, Seattle, WA, Unpublished data, Sogard and Olla 1994) when significant differences in size within a cohort did exist. This factor has the potential to affect both recruitment levels and the characteristics of the recruiting population. The Lagrangian method produced significantly more variability in weights and lengths apparently through both individual temperature histories and random mortality, life-stage transitions and feeding factors.

Simulation 3 (The importance of vertical location) shows how the inclusion of a complex algorithm for describing vertical movement of individuals can significantly alter their hor-

izontal advection and growth relative to a scheme where depths for each life stage are fixed. Vertical locomotion will, over time, significantly alter the spatial paths and the life history of individuals relative to those whose depths are constant. Although unnecessary complications are to be avoided in modelling, there are compelling arguments for such vertical movement algorithms in the coupled model versus a more simplified approach to determining individual depths. Such reasons include (1) we know that complex vertical movements occur, (2) they appear to have a significant effect on the horizontal trajectory of individuals, and (3) they appear to have significant effects on growth and other attributes of individuals.

Page et al. (1989) suggest that 'the vertical distribution of pelagic organisms plays an important role in determining the rate and direction of their horizontal displacement and their interaction with prey and predators.' Hjort (1914, 1928) was the first to suggest that transport to favorable nursery areas could be important in the survival of early life stages of marine fish which spawn pelagic eggs. Knowledge of advection patterns of eggs and larvae from the spawning area to the nursery grounds is therefore important to recruitment studies, especially in highly advective systems like Shelikof Strait. Transport or retention patterns can also determine the overlap of larvae with their predators and prey, and expose young pollock to varying suites of environmental factors, thereby affecting mortality and growth rates (Frank and Leggett 1982, Leggett et al. 1984, De Blois and Leggett 1993). The distribution and abundance of eggs and larvae, as these change through time and space, depend both on biological characteristics (such as spawning intensities with time and place, developmental periods, buoyancy of eggs and larvae, existance of predators and food organisms, etc.), as well as interactions with environmental variables (e.g. current velocities and directions, water temperatures and water densities).

Walleye pollock eggs are spawned and develop at depths of 150 to 200 m, and later the larvae reside in the upper layers (20 to 50 m, Kendall et al. 1987 and 1994). During the 2 week (at 5°C) incubation period, eggs exhibit vertical movement in the water column due to changes in the egg's density during development, and movement toward the depth

where they are neutrally buoyant. Kendall and Kim (1989) developed a model of distribution of eggs in the water column based on these changes in buoyancy and assumed differences in water density at depth. Their model could not, however, predict differences in distribution of eggs of different stages in the water column, as it did not take into account the horizontal variability of water density that can arise due to the highly variable current system in Shelikof Strait, and interannual differences in this factor. Kendall and Kim's model also did not take into account the likelihood that the initial density of eggs is neutrally buoyant, (due to uptake of ovarian fluid at hydration and fertilization of the eggs which balances the higher density of egg proteins) our model was able to do this.

Prior to first feeding, larvae move quickly from depths of 150 to 200 m to the upper parts of the water column (Kendall et al. 1994). This movement is probably due to negative geotaxis or barotaxis since there is insufficient light to induce phototaxis at the hatching depth (Olla and Davis 1990). Kendall et al. (1994) propose that movement to a preferred light level may be the controlling factor in diel migrations of larval pollock and that 'this cycle may allow larvae to maximize their daily feeding period by being shallower in the early morning when visual feeding is possible as the sun comes up than during midday, and by rising to such depths as light fades in the evening.' Lab studies indicate that larvae avoid bright light, possibly to avoid visual feeding predators and demonstrate negative geotaxis or barotaxis during low light levels, which could produce this cycle. Diel migration starts when larvae are > 6 mm in length (Kendall et al. 1994).

A complex suite of factors may drive vertical migration (Appenzeller and Leggett 1995). The daytime depths of larvae coincide with the depths of maximum concentrations of copepod nauplii, the main food source of pollock larvae. Temperature, later in May when the water column is vertically stratified, may be used as a cue to stay in the upper parts of the water column. Turbulence in the water column has been hypothesized to have both positive effects [increased encounters with prey (Rothschild and Osborn 1988), enhanced primary production due to the infusion of nutrients from below the photic zone] and negative effects [dilution of vertically enriched layers of prey to levels below successful feed-

ing threshholds, reduced naupliar production (Lasker 1978), and reduced capture success (MacKenzie et al. 1994)]. In the laboratory, larval pollock avoid turbulence (Olla and Davis 1990) although it is difficult to compare levels of turbulence induced in the laboratory with those seen in the field. Kendall et al. (1994) found one instance where larvae were deeper during periods of high winds. Wind speeds of between 12 and 15 m s^{-1} were seen once during this study, and during this occurrence, average larval depth increased by about 10 m.

By explicitly including only light and the location of the mixed layer as external factors regulating larval depth, we are neglecting the possible modification of the diel migration cycle by other factors, such as prey distribution and patchiness, temperature, feeding motivation, bioenergetics or predator avoidance. Neilson and Perry (1990) state that 'combinations of external stimuli may act to modify or override the dominant influence of light intensity.' Prey movements, for example, are likely to have an influence; however, prey distributions are probably responding directly to light (Neilson and Perry 1990, Kendall et al. 1994), therefore light may be a good proxy for prey effects. We know very little about direct effects of predator avoidance on vertical movement in the field. We are also ignoring arguments for energetic motivations for diel migration (Neilson and Perry 1990), as they seem unlikely to be controlling the cycle, except, perhaps, when food is scarce (Sogard and Olla 1996).

In later simulations which included a dynamic prey source, we found that larvae which spent much time below the mixed layer starved, as prey levels declined below this depth. In Simulation 6 (The effect of turbulence on feeding), we fixed the larval feeding depth (FDEPTH), and found that model output was very sensitive to this parameter, indicating that prey density, as it varied with depth, was a controlling factor. In our most recent simulations we have included a dynamic mixed layer, derived from the SPEM model, and have constrained the larvae to remain above this level.

The simulation which used two schemes to predict juvenile depth indicated that treating juveniles as passively advected particles did not result in large discrepancies between modelled and real distributions, at least for September, 1990 and that depth of the juveniles mainly affected their onshore-offshore distribution. This suggests that active, directed horizontal swimming behaviors during the juvenile (or earlier) stages may be less important than advective processes over all of the early life stage in determining fall distributions. The directed behaviors that do exist appear to transport juveniles toward inshore areas.

There are several other factors which will affect spatial variability in growth and other life history attributes that were not yet added in the preliminary versions of the IBM used for these simulations. For Simulations 2 and 3 there was no spatial or temporal variability in food or predators in the model. Spatial and temporal variation in prey is seen, in later simulations, to cause increased spatial and temporal variability in growth and survival. Spatial variation in predation mortality is extremely difficult to parameterize, but would undoubtedly result in more variability, especially if predation is size-based. Note that there is no mortality in Simulation 3, whereas there is constant mortality within each life stage in Simulation 1, with higher mortalities in earlier life stages. In Simulation 1, individuals seeded in areas with colder water experienced extended early stage durations, therefore higher cumulative mortalities, and this affected the size distribution by selectively eliminating a group of individuals with a particular temperature history.

Results shown in Simulation 4 (Hindcasts) showing distributions of young pollock compare favorably with observed larval and juvenile distributions from data. Interannual comparisons suggest that 2 years with subsequent good recruitment, 1978 and 1988, and one year with subsequently poor recruitment, 1991, experienced flow fields which quickly carried many individuals near or into the Alaskan Stream. At the same time, the vigorous flow fields in each of these years carried other individuals quickly onto the shelf area to the south-west of the spawning site, especially near the Shumagin Gully and the outer half of the continental shelf. The modelled tendency to carry individuals quickly out of the

sea valley and to the west may be somewhat affected by the reduced degree of cross-shelf transport due to filtering the physical model output. Future runs of the model should account for this.

Years 1987 and 1994 were notable in the strength and frequency of eddy activity, which early on served to trap larvae and hence reduce dispersion, but later tended to spread larvae and juveniles more uniformly across the shelf than in other years. Year 1989 was notable for the weakness of the circulation, and the extended retention of larvae near the spawning site.

These model results underscore how both winds and runoff could play an important role in affecting levels of recruitment, because the spatial paths of individuals vary so widely from year to year. Both winds and runoff were found to correlate with age-2 recruitment in the regression analyses of Megrey et al. (1995). In particular, their regression analysis found that enhanced precipitation in January-February correlates with greater recruitment ($r^2 = .58$). The hydrodynamic and individual-based model results demonstrate that greater runoff leads to greater larval retention by eddies near Shelikof Strait and enhanced shelfward flux. These phenomena may contribute to the observed correlation of recruitment with freshwater input.

Simulations of the temporal and spatial dynamics of copepod nauplii, the main prey resource of young pollock resulted in some interesting observations. For example, certain regions, such as the coastal area between the Semidi Islands and the Shumagin Islands (except for near Mitrofania Island) showed consistently lower levels of nauplii, especially early in the year (Figs. 3.36-3.70). It would not appear to be advantageous for young pollock to be transported to this area.

Another observation of interest is that prey are probably advected in the same water parcels as larvae, including those transported out of the sea valley and along the shelf break towards the Shumagin Islands. This was seen in the model years 1988, and to a somewhat lesser extent in 1978 and 1991. Both 1978 and 1988 were exceptional year classes

(Megrey et al. 1995). These larvae may not, therefore, be subject to food deprivation, as has been hypothesized. It is also possible that these larvae are not actually entrained into the Alaskan Stream, resulting in their loss from the region, but are actually able to return to shelf areas via the Shumagin Gully or to the west of the Shumagin Islands, as was seen for some larvae in these model years. Since the NPZ model domain does not extend to the west of the Shumagins and no measurements are available, prey levels in these regions are unknown. If cross-shelf transport is reduced as a result of the filtering process, or due to behavioral mechanisms not included in the model, correction of this factor could also result in fewer young pollock being transported out of the region by the model.

Nauplii were often seen concentrated in higher abundances in cyclonic eddies, with anticyclonic eddies showing lower abundances. Cyclonic eddies are characterized by more stratification higher in the water column, whereas anticyclonic eddies show a depressed density interface. Nutrients may be limiting later in the spring near the surface in anticyclonic eddies due to depression of the nutricline, which may decrease photosynthesis by phytoplankton if the photic zone only penetrates partway down and cells are mixed below their compensation depth, eventually limiting production of nauplii. Whatever the mechanism, this dichotomy suggests that, under certain circumstances, larvae entrained in cyclonic eddies may do better than those in anticyclonic eddies. In the modelled years, cyclonic and anticyclonic eddies were both seen frequently.

One model year, 1989, which showed an anomalously late spring bloom and production of nauplii, resulted in a very poor year class (Megrey et al. 1995). There is little data to confirm this result, but if it is true, then the poor recruitment seen could perhaps be explained by the lack of food for the larval stages.

1978 was the largest year class on record for this stock of pollock (Megrey et al. 1995). 1988 was also strong, although not nearly as strong as 1978, and 1994 was strong but less than 1988 (Megrey, B.A, Alaska Fisheries Science Center, Seattle, WA, pers. comm.). All three years showed similar time traces of naupliar abundance over the model domain, although absolute abundances in 1994 were somewhat lower (Figs 3.23-3.34). The poor

year classes of 1987 and 1991, however, showed similar evolution over time. Two years, 1987 and 1989, did show somewhat delayed spring blooms and naupliar production (especially 1989), which may have resulted in low food levels for larvae early in the year.

One feature of the NPZ model output which was significantly different between the good year classes of 1978, 1988 and 1994 and the poor year classes of 1987 and 1989, was that in the former, the regions of high naupliar abundances were significantly broader in area, especially early in the year, than in the latter. 1991, also a weak year class, showed a narrower distribution of high abundances of nauplii early in the year, but not later. Abundances of nauplii west of the Semidi Islands was also somewhat higher in 1978. This broad distribution of prey resources, especially early in the year when it is may be especially critical, may have aided in making these years, especially 1978 and 1988, particularly strong year classes.

Results from these hindcasts do not clearly imply one set of physical or biological conditions to guarantee recruitment success; rather, success appears to be dependent on a complex chain of favorable events during the early life history of pollock. However, the results indicate that strong advection of larvae after late May does not preclude a strong year class, while weak advection or the presence of mesosclae eddies do not by themselves guarantee a strong year class. Also, the temporal and spatial dynamics of the prey resources of young pollock appears important, especially perhaps, a broad distribution of high abundances of nauplii.

Factors which appeared in this modelling effort to contribute to good recruitment, therefore, are:

- Moderate to strong freshwater runoff, combined with moderate-strong winds (except around the time of first-feeding of larvae), as these factors contribute to the formation of eddies.
- Larvae remaining in the sea valley early in the year (before early May), as food is low in the regions between the Semidi Islands and the Shumagin Islands at this time.

- Eddies, especially cyclonic ones, which appear to contribute to cross-shelf transport from the sea valley onto the continental shelf areas east of the Shumagin Islands, and which contain more food.
- Larvae remaining in the upper water column, which helps in cross-shelf transport to the nursery areas; this may be aided by cyclonic eddies.
- A broad distribution of high abundances of copepod nauplii, especially early in the year.
- A peak in naupliar abundance between DOY 120 and 140.
- Wind speeds distributed around the optimum level for consumption, especially around the time of first-feeding of larvae.

Some very clear results arose from Simulation 5 (The importance of spawning location and timing). First, an extremely low number of fish were transported to the Shumagin Island nursery area if they were spawned outside of Kodiak Island. A few fish found around Kodiak originated from other spawning regions. In some (but not all) years, many juveniles are actually seen in the bays around Kodiak, but it is not clear where they came from. This study indicates that they most likely originated from spawning outside of Kodiak, but the possibility exists that a few of them originated in Shelikof Strait. Significant spawning has not been observed in the region outside of Kodiak, however the area is not often surveyed for spawning adults or eggs. It should be recognized that uncertainties exist in the modelled flow field in the region outside Kodiak Island, as there is very little data from this region to validate the model.

Second, fish spawned early in the year (February) in the model died of starvation. The common food of pollock larvae are the nauplii of coastal copepod species, such as *Pseudocalanus*, spp., which reproduce in response to the spring bloom, which generally occurs in early May in this region (Napp et al. 1996).

Third, fish spawned very late in the year (July), would not grow fast enough to reach the juvenile stage by September 1st. Larval pollock grow at about 0.2 mm d^{-1} (Bailey and Stehr 1986, Bailey et al. 1996a), so to make it from hatching at about 4.0 mm to metamor-

phosis at about 25 mm would take more than 100 days, or until late October if they were spawned in mid-July.

Fourth, the depth of spawning, at least in the way it is defined in this analysis, was not significant in determining whether or not a fish was transported to the Shumagin nursery area or whether they reached the juvenile stage. This could be because the time they spend at the spawning depth is very short relative to the time spent in the later stages. Larvae quickly rise to the upper water column not long after hatching.

Of those fish that did reach the Shumagin nursery area, most came (in 1978) from the Northwest Shelikof sea valley and from the Middle and Late spawning times, and in 1994, from this spawning region and the Late spawning time. This may be due to the fact that circulation between the Semidi Islands, near where these fish were released, and the Shumagin Islands is sluggish, with average current speeds of 10 cm s^{-1} or less, compared to the middle of the Shelikof sea valley, where current speeds average 25-100 cm s^{-1}.

In 1978, the observed spawning area (Central Shelikof Strait) and time (Middle) resulted in fewer fish reaching the Shumagin nursery area than other regions and times. This was somewhat less true in 1994 than in 1978. This general result was counter to our initial hypothesis, ie. that the reason for the specificity of spawning of pollock in central Shelikof Strait in early April is to maximize transport of young fish to the Shumagin Islands. The necessary conclusion is that factors other than physical tranpsort alone must be considered as important in the evolution of the specificity of timing and location of spawning of this population. These other factors could include the spatial and temporal availability of prey, the presence or absence of predators on the early stages or details of mesoscale or submesoscale circulation or physical factors that are not captured by the hydrodynamic model.

The window of opportunity for spawning, then, if fish are to reach the Shumagin Island juvenile nursery area by September, would appear to be the region between Northern Shelikof Strait and the Northwest Shelikof sea valley, sometime after February (and probably not much before April) and before July.

The specificity of timing and location of spawning must have evolved to take into account the variability in physical forcing factors such as wind and freshwater runoff. The similarity of results from the two years of significantly different forcing simulated supports this notion. 1978 was about 30% windier overall than 1994, and 1994 was about 50% wetter than 1978. Flow fields were vigorous in 1978, and the model shows many individuals carried to the west early in the simulation. 1994 was a year of significant mesoscale activity, resulting in more larvae being retained in the sea valley by eddies until later in the simulation. However, both years resulted in strong recruitment.

Examination of the NPZ model simulations of the distribution and timing of the production of *Pseudocalanus*, spp. nauplii, the main prey of larval pollock, helps us to narrow this window of opportunity for spawning further. There is a definite peak in naupliar production, occurring in most years between DOY 140 and DOY 160. If larvae were spawned during the Early time period (DOY 47), they would reach first-feeding at about DOY 68. By this time the increase in nauplii has not yet begun, and concentrations are significantly below the 20,000 nauplii m^{-3} (20 l^{-1}) thought to be necessary (Theilacker et al. 1996) for successful feeding and growth. If larvae were spawned during the Late period (DOY 168), they would miss the peak of naupliar production. The spawning date observed (Middle, about DOY 90) results in first-feeding larvae in the water column about DOY 110, after the production of nauplii has begun to rise.

The spatial distribution of prey helps narrow the spawning location further. If pollock were spawned in the Northwest Shelikof sea valley, they would (as is apparent by looking at movies of the movement of fish) be quickly carried into the coastal region between the Semidis and the Shumagins, at times when naupliar abundances in this area are quite low. Fish spawned further to the north and east, in Shelikof Strait proper, are more likely to remain in areas of high prey abundance.

It would appear then that a combination of advection and prey dynamics may be sufficient to explain the evolution of the specificity of the timing and location of spawning in Shelikof Strait. (Spawning is actually observed in the Northern Shelikof region; we could not

locate this region farther away from the center of the observed spawning location due to the physical model boundaries.) The necessity of transport to the nursery area is enough to narrow the spawning time and location somewhat, but when prey dynamics are added, the reasons for the choice of location become clear.

We do not really know why the Shumagin area is the preferred nursery area, except that once a fish is carried into this area, it may be less likely to be advected either into the Bering Sea through Unimak Pass, or to be carried significantly further to the west by the Alaskan Stream. This probably ensures that young fish are able to return to the Shelikof region to spawn at age 2 or 3.

The timing of spawning is clearly a response to the timing of prey production. Actual spawning peaks around the first week of April in Shelikof Strait, but begins mid-March and continues until early May. Fish spawned earlier than the peak of spawning probably have difficulty finding food at the time of first feeding in early April, however those spawned in early May would reach first feeding still in time to hit the peak of naupliar biomasses (mid-late May). This timing ensures a match between larval pollock production and the production of their prey, showing agreement with the "match-mismatch" hypothesis of Cushing (1972, 1974).

Simulation 6 (The effect of turbulence on feeding) showed the magnitude of wind speed at which the feeding optimum for walleye pollock should occur for a given average feeding depth. Sundby and Fossum (1990) speculate that there should exist an optimal level of turbulence with respect to the number of successful attacks larvae can inflict on their prey. Above such a level successful attacks should decrease because the residence time of the prey within the range of attack will be shorter than the reaction time of the predator, causing the prey to pass the predator before it is able to react. They speculate that this optimum should occur at wind speeds higher than 6 m s^{-1}. Results from this simulation indicate that the optimum (about 8 m s^{-1}) for pollock is not much higher than 6 m s^{-1}.

Sundby (1995) suggested that minimum pursuit time was recognized as a critical parameter in MacKenzie et al.'s (1994) turbulence/comsumption model by the fact that they used a range of values in their calculations (t = 0.9, 1.7 and 2.6 s). The minimum pursuit time (t) used in our sensitivity analysis was a random variable from a triangular distribution with a mean of 1.7 s, a minimum of 0.85 s, and a maximum of 2.55 s. These values correspond closely to the range of t values used by MacKenzie et al. (1994). Sundby (1995), interpreting Figure 4 of MacKenzie et al. (1994) , reports that the wind speed which generates a level of turbulence that optimizes ingestion depends on the assumed value of t. Sundby (1995) gives wind speed values of 10 m s^{-1} for a t of 2.6 s, 15.3 m s^{-1} for a t of 1.7 s, and 20 m s^{-1} for a t of 0.9 s. Results from our simulation, using mostly MacKenzie et al. (1994) values, indicate that optimum feeding occurs at a wind speed of 8 m s^{-1} for the average larval feeding depth and larval size. Our results, which are specific to 1987, also indicate that winds speeds in excess of 15 m s^{-1} are somewhat rare at larval locations in Shelikof Strait just as they appear to be on the coast of Norway in May (Sundby 1995). However, Brower et al.'s climatology (1988) show that in general wind speeds in Shelikof Strait often exceed 15 m s^{-1}, doing so 13% of the time in April and 6% of the time in May.

Sundby (1995, 1997) argued that the negative effects of turbulence on larval feeding might not really be an issue because wind speeds necessary to cause feeding to fall to the right of the consumption-turbulence optimum are rare in nature. His statement is based on the model results reported in MacKenzie et al. (1994) that optimum feeding occurs at wind speeds of about 15 m s^{-1} and Sundby's observation that wind speeds off Norway do not typically reach that level. Our results, which basically replicate the physics and parameters of the MacKenzie et al. (1994) model, predict optimum feeding at wind speeds of about 8 m s^{-1}. We believe that lower optimum level predicted from our simulations is due to three factors. First, some of the parameters are specific to larval pollock. Second, our formulation of the turbulence-consumption process is stochastic. Many of the deterministic values described in MacKenzie et al. (1994), such as minimum pursuit time, turbulent dissipation and turbulent velocity equation parameters were random variables in our sensi-

tivity analysis. Thirdly, our formulation of the feeding process is more complex than described in MacKenzie et al. (1994) in that we include size-dependent prey capture probability, 14 prey groups covering the three major zooplankton life stages each with different nutritional characteristics, and prey values based on modelled observations. From the second point alone, we might expect our optimum to occur somewhere in the range of 10-20 m s^{-1} since, for the most part, we parameterized our model with values from MacKenzie et al. (1994). However, we feel that the parameters specific to pollock, plus the additional complexity of our feeding formulation had the tendency to reduce the wind speed at which optimum feeding would take place. If this is true, then the negative effects of wind speed on feeding should be very common occurrences in nature. More results will be needed to validate this result.

Of the input parameters which affect many output variables, two were associated with the turbulence/feeding formulations (RDA and WA), two with prey dynamics and consumption processes (FDEPTHG and MAXPREYA), two with growth and bioenergetics processes (LWYBB and MROFDLB), and one with mortality (MFDLSM). Metamorphosis date, starvation and predation mortality output variables were the most sensitive to input parameters due to the fact that these variables integrate a host of biophysical processes. The importance of feeding depth from our analysis is due to the fact that in the model prey concentration decreases with depth. Also MacKenzie and Leggett (1991) show that the influence of turbulence on the encounter rate between larvae and their prey decreases downwards through the water column, because the rate of turbulent dissipation energy decreases with depth..

Two parameters of the encounter rate model, minimum pursuit time and reactive distance, both played a central role in affecting feeding, growth and mortality processes. Werner et al. (1995) also saw that a decrease in the time required for a larvae to pursue and capture a prey particle as it is being advected through the larvae's visual field increases growth and survival.

The model described here still leaves unanswered questions, such as are there other components of the feeding process (i.e. prey search) affected by turbulence? What are the relative effects of turbulence on larval pollock predator's encounter rate and probability of successful pursuit of pollock? What are the effects on the timing of the prey production cycle, wind-induced changes in the mixed layer, or dilution or maintenance of prey patches? Munk and Kiørboe (1985) have shown that herring larvae are capable of altering their swimming behavior after encountering a prey patch so as to improve the likelihood of remaining in the patch. Are there turbulence-induced changes in larval and prey behavior, such as swimming speed, turn angles, or avoidance of turbulence? Olla and Davis (1990) have noted avoidance of turbulence by larval pollock in the laboratory. How do the levels of turbulence used in the lab relate to those found in the field. Do larvae in the field show the same behavior? Unless turbulence causes physical damage to a larva, it seems the larva might be better off staying at the depth where the food is, despite a level of turbulence which causes decreases in feeding, rather than expending energy in swimming deeper, and then when the turbulence subsides, having to return to areas of high prey abundance.

Even with the above issues unresolved, we feel that this simulations shows that this type of modeling is a viable way to explore the complex issues related to turbulence and its effect on the biophysical environment, and ultimately on growth and recruitment of fish larvae. Modelling provides a framework to examine the complex biophysical relationships concerned with the effect of turbulence on the ability of larval fishes to encounter, detect, pursue and capture prey. Our results show that smaller and younger larvae are more sensitive to turbulent effects than are larger and older larvae. Also, reactive distance, mimimum pursuit time, and weight-length conversion parameters were the most important input parameters of the turbulence-consumption processes. Letcher et al. (1996) also reported the importance of larval length-weight conversion parameters, especially in highly size-dependent formulations. Fortunately, data on larval length-weight parameters is relatively easy and inexpensive to obtain.

Results of this study argue for more research on interactions between fish larvae and their prey, especially individual processes at very fine scales (such as larval reactive distance) and the conditions of the *in situ* feeding environment in turbulent conditions. In addition, features such as a larva's ability to pursue and encounter prey should be an important component of larval growth and survival models.

This work supports that of Bailey and Macklin (1994) which indicates a correlation between larval survival and periods of calm winds during the first-feeding phase. They found that (with limited data) while not all calm periods resulted in strong year classes, all strong survival periods were associated with calm winds. They conclude, as did Bailey and Spring (1992), that high larval survival rates are a necessary but not sufficient condition for a strong year class, as year-class strength may be modified during the juvenile stage. However, adverse wind conditions resulting in diminished larval survival should be linked with poor recruitment.

Our work includes a mechanism by which this correlation may be produced, ie. the dome-shaped relationship between consumption and turbulence levels in the water column. Other mechanisms, particularly the avoidance of turbulence by swimming to deeper levels in the water column, may be operating, and simulations including both mechanisms should be tested to see whether one or the other does a better job in replicating the results of Bailey and Macklin (1994). One advantage of this type of modeling in performing such simulations is that the history of exposure to wind, turbulence and prey levels can be tracked precisely for each individual, rather using aggregate measures, as field studies must do.

Our results do, however, indicate several reasons why the dome-shaped relationship between consumption and turbulence may be the correct mechanism for explaining the effects of turbulence. First, the results are stronger in the simulation for small larvae than for large larvae, supporting Bailey and Macklin's hypothesis that the negative effects of wind-induced turbulence are especially important for first-feeding larvae. Second, our work showed an optimum wind speed for consumption of about 8 m s^{-1}. The exact loca-

tion of this optima is somewhat dependent on larval size and depth, however it correlates well with Bailey and Macklin's definition of a calm period, i.e. a period with winds less than 10 m s^{-1}.

The coupled biophysical model presented here consists of a detailed 3-dimensional hydrodynamic model, a spatially-explicit lower trophic level ecosystem model and an i-state configuration IBM containing significant biological detail. Very few i-state configureation IBMs have included detailed dynamic spatial information along with the biological detail (Tyler and Rose 1994). Many of the early IBMs were developed within the CompMech (Compensatory Mechanisms in Fish Populations) program funded by the Electric Power Research Institute, however most of these models characterize the habitat as a homogeneous unit (Tyler and Rose 1994), where abiotic factors may either be constant or time-varying. An early biophysical model of walleye pollock larvae (which included a biological IBM) was developed by Walsh et al. (1981), however both the biology and the physics were very simple. Bartsch et al. (1989) developed a model to describe the movement through the North Sea of herring larvae, which combined a 3-dimensional circulation model with an extremely simple biological IBM. Larvae were represented as 'tracer particles' which were moved by advective forces. The biology was limited to a simplified vertical movement using mean daytime and nighttime depths from observations, and spawning areas and times. Walters et al. (1992) describe a biophysical model similar to Bartsch's for English sole larvae in British Columbia, Canada. Werner et al. (1993) developed a biophysical model of advection and behavior of cod and haddock early life stages on Georges Bank. This model consisted of a finite elemental circulation model which produced a steady state circulation field. The biology consisted of simple vertical distributions by life stage, some horizontal movement of later stage larvae, and spawning distributions. This model was further developed (under the auspices of the U.S. Global Ocean Ecosystem Dynamic (GLOBEC) program, Werner et al. 1996) and now includes more biological detail in the IBM, such as feeding, growth and starvation mortality. We do not know of other modelling efforts which include a spatially and temporally dynamic food source for individuals in an IBM, provided by an NPZ model.

Development of biophysical modelling techniques which combine both detailed circulation models with biological models, including IBMs and NPZ models will most likely occur rapidly in the near future. Several other large-scale fisheries oceanography programs, such as NOAA's Coastal Oceans Program, the Canadian Ocean Production Enhancement Network (OPEN) program, and U.S. GLOBEC have biophysical modelling efforts of this sort underway at this time. This approach shows promise in clarifying mechanisms affecting recruitment processes and year-to-year variations in year-class strength of marine fish.

Chapter 5. Conclusions and Speculations

What have we learned from this modelling excercise? How has it added to our understanding of the four hypotheses outlined in the Introduction? What new insights about pollock early life history and recruitment have been gained? Let us first address the initial hypotheses.

Hypothesis 1. "The survival of early life stages of walleye pollock is enhanced by transport along the Alaska Peninsula. Larvae which are advected out of the sea valley into the Gulf of Alaska and are entrained in the Alaskan Stream are lost to the population. Larvae which are initially advected out of the sea valley may be returned to the shelf and eventually recruit to the juvenile nursery areas around the Shumagin Islands. Recruitment to the juvenile nursery areas (and thereby, by implication, to the year class) is enhanced when there is a low percentage of flow which goes offshore and joins the Alaskan Stream."

A very early finding of this work is that it is particularly important that the transport shown by the physical model be believable. Not only must the output of the physical model replicate reality in some statistical sense, but our filtering of these outputs must not remove important scales of motions. In our case, some of the cross-shelf transport was probably removed by filtering. This was necessary for practical reasons. A scheme of adding random noise to the movement of floats could obviate this problem.

The model domain did not extend far enough west of the Shumagin Islands to allow us to assess the fate of young pollock which were transported beyond this area. The work did indicate, however, that to be carried out of the sea valley and along the continental slope to the westward was not to necessarily be lost to the population. These fish may not have actually been entrained into the Alaskan Stream, but may have been in some intermediate waters. Many of them were carried back onto the shelf via the Shumagin Gully, or to areas west of the Shumagin Islands. Even if this transport occurred early in the year, patches of copepod nauplii apparently could be advected along with the larvae, indicating that starvation was not a necessary corollary of transport out of the sea valley.

This modelling work does not indicate any one particular set of physical forcing circumstances necessary for transport to the juvenile nursery areas. On the contrary, the results of Simulation 5 (The importance of spawning location and timing) indicates that pollock life history in this region of strong and variable currents, is adapted to a range of physical forcing and transport scenarios.

A year with very weak circulation, 1989, in which many larvae were retained in the sea valley, resulted in a very poor year class, so weak transport and retention in this region is not necessarily good, as has been proposed. Prey for larvae, as indicated by the NPZ model, was scarce however, and this may have been more important for the eventual failure of the year class.

Hypothesis 2. The choice of spawning time and location of adult walleye pollock in the western Gulf of Alaska is controlled mainly by the necessity to optimize transport of eggs and larvae to the juvenile nursery areas, versus the necessity to optimize conditions of feeding, growth and survival along the way.

This hypothesis proved to be false. Transport alone could not narrow the window of spawning time and location as narrowly as is actually observed in Shelikof Strait. The combination of the timing and distribution of the production of the prey of young pollock, plus the transport scenario appeared to be sufficient, however, to explain the specificity of spawning. This finding supports Cushing's (1972, 1974) idea that the production of the young of marine fish species is matched to the timing of production of their prey. We add here that the details of spatial distribution of prey may also be a factor in this match or mismatch. In other words, the spatial aspect of match-mismatch is critical.

Hypothesis 3: Entrainment of eggs and larvae in mesoscale eddies in Shelikof Strait enhances advection to appropriate juvenile nursery areas around the Shumagin Islands, and aids in larval growth and survival by retaining larvae in areas of higher prey.

This work supports the notion that eddies may enhance tranport to nursery areas by retaining them in the sea valley and then dispersing them in regions close to the nursery areas. Years of strong mesoscale eddy formation do not always result in good year classes, however. Also, several years with strong transport which resulted in larvae being carried out

of the sea valley and to the west resulted in good year classes, so it appears that retention in the sea valley may not be a necessary condition for a good year class.

Cyclonic eddies in the model contained higher abundances of food than the background level, whereas anticyclonic ones contained lower abundances. This is probably because of the increased shallow stratification in these eddies and the shallower nutricline. Shelikof Strait is not a nutrient-limited region until after the spring bloom, when nutrient levels in the mixed layer can reach zero. The effect noted, therefore, would only be significant later in the spring. Conditions within an eddy are likely to be critical to those larvae entrained in them for any length of time. It seems that not all eddies are beneficial, as far as prey levels are concerned.

Bailey and Macklin (1994) and Stabeno et al. (1996) have proposed a hypothesis that retention in eddies may be advantageous to larvae due to an interaction of wind, stratification, and prey conditions. They propose that because cyclonic eddies tend to be stratified higher in the water column and this shallow stratification retards the penetration of wind-induced turbulence, larvae that would otherwise swim downward to avoid the turbulence can remain in the upper water column where prey are more abundant, facilitating survival.

An alternative to this hypothesis could be that cyclonic eddies aid in cross-shelf transport to the juvenile nursery areas. This is because if larvae do avoid turbulence or stay within the mixed layer to find food, in eddies where they could remain shallower in the water column they would be removed from the bottom-following tendency of deep currents which would take them into offshore regions. They would also be exposed to onshore transport in the upper regions due to the downwelling nature of the Gulf of Alaska regime and less exposed to offshore transport in deep regions due to the downwelling.

Satellite-tracked drifter trajectories in the Shelikof region show anticyclonic eddies to be more common than cyclonic ones. However, these drifters are drogued at 40 m, and constraining them to a fixed depth may make them less likely to follow mesoscale circulation patterns and remain in eddies than if they were free particles (Hermann et al., In Press). It

is possible, therefore, that cyclonic and anticyclonic eddies are both common in Shelikof Strait, as they are in this model.

Hypothesis 4: The depth of an individual, which varies by life stage and time, is an important life history trait which strongly affects their chance of survival.

This work indicates that the depth of an individual is probably an important adaptation which aids in transport to the nursery areas, in cross-shelf transport, and in keeping young pollock at depths of high food concentrations. Correct specification of depth, by life stage and time of day is critical for modelling transport in a realistic manner. Feedback between the float-tracking of particles, and the biological model is therefore necessary in this type of modelling. The modelling also demonstrates that the depth history of an individual can affect their growth and survival due to its history of exposure to environmental variables and food. We also see that larvae may need to remain mostly within the mixed layer in order to get enough food.

What else have we learned?

This modelling shows that spatial variability in physical factors such as temperature and salinity at the scales resolved by these models have important effects on individuals and significant consequences at the level of the population.

We have underscored the idea that the temporal and spatial dynamics of the prey of walleye pollock is of primary importance to their growth and survival. It is most likely an important factor, along with transport, in determining the specificity of timing and location of pollock spawning in Shelikof Strait. We find evidence supporting the match-mismatch theory of fish production, in both the spatial and temporal sense. The mesoscale details of prey distribution are probably critical. Model results suggest that cyclonic eddies may be good environments for larvae due to higher prey concentrations at certain periods, whereas anticyclonic eddies may be less beneficial environments. Certain regions may consistently have higher or lower prey abundances. Years which turn out to produce good pollock year classes seem to be characterized by broader distributions of

high abundances of prey, which may aid in the spatial overlap of larvae with their prey. A model year characterized by an extremely late spring bloom and late production of copepod nauplii turned out to be one of the poorest pollock year classes since we have been studying this population.

We have explored one possible mechanism by which wind-induced turbulence may affect larval feeding and survival, outcomes of which supports the hypothesis of Bailey and Macklin 1994. This work underscores how turbulence effects and size-dependent processes interact, ie. the effects are stronger on smaller larvae. This mechanism also suggests that there is an optimal wind speed of about 8 $m\ s^{-1}$ for pollock larvae, a number which compares well with other theoretical work and data on this subject. If this optimum is real, it suggests that the negative consequences of wind-induced turbulence may be common in the western Gulf of Alaska, as wind speeds greater than this are relatively common.

Other mechanisms could underlie the observed correlation of wind-induced turbulence and survival. Chief among the possibilities, suggested by laboratory studies, is that they avoid turbulence by swimming deeper in the water column. It would be useful to perform a model experiment to assess the relative impact of these two mechamisns, and to see which, if either, could best succeed in replicating Bailey and Macklin's (1994) results.

It would also be of use to design and perform model experiments to assess the hypotheses proposed by Bailey and Macklin (1994) and Stabeno et al. (1996) and this author to explain possible interactions among turbulence, stratification in eddies, prey dynamics and transport. These hypotheses are complex, and not particularly amenable to field or laboratory experimentation.

What is the value of this type of modelling?

First of all, I would like to stress that the goal of this modelling is not to explicitly predict recruitment. The goal is to explore possible mechanisms underlying the recruitment pro-

cess for walleye pollock. To assess different processes thought to be responsible for the observed correlations between wind mixing and survival, between eddies and larval growth and possibly survival, and between freshwater input and recruitment. To explore these mechanisms at different temporal and spatial scales that may be important. An understanding of these mechanisms should help us to understand how larger and longer scales of change in the environment will affect recruitment, allowing fisheries managers to predict longer term consequences of environmental change.

This modelling can aid in the development of new hypotheses concerning the effects of the biological and physical environment on recruitment, and aid in exploration of these hypotheses. It also allows exploration of the effects of processes at varying time and space scales and interation over these scales, something extremely difficult to do in the field or laboratory.

Mortality is an important process which is presently oversimplified in these versions of the model. Spatial and temporal differences in mortality will have consequences for recruitment which must be assessed. We have made assumptions about the affects of larval size on mortality that are presently under dispute in the community studying recruitment processes. These assumptions need better assessment. Also, at present our state of knowledge of the processes of mortality affecting young pollock are rudimentary. We cannot specify spatial variation in mortality, as we lack sufficient data. The suite of predators affecting different ages and sizes of young pollock are beginning to be understood, but spatial and temporal dynamics of these species are little known. It would be extremely difficult to implement coupled models of all the predator species to fill the gaps in our data. This is an area of development important to this type of modelling, but substantial field and laboratory must be done as well.

What have we learned about recruitment?

We have shown reasonable mechanisms apparently underlying the observed specificity of the timing and location of spawning of pollock in Shelikof Strait. This specificity is an

adaptation to optimize the chances for successfull recruitment back to the spawning population in this region. This specificity of pollock spawning time and location is not seen in the Bering Sea. There, pollock spawning occurs over a broad region and long time period. The reasons for such a striking difference between these two regions is a question of considerable interest, and the answers may lie, as they did for Shelikof, in some combination of transport and prey dynamics, although the Bering Sea is characterized by much weaker overall transport levels. Similar modelling efforts occuring now for the Bering Sea may help us understand this process in that region.

We have demonstrated how critical the depth of different life stages of pollock is for successful transport to nursery areas and successful feeding. We have known that characteristic patterns of depth distribution and movement exist, although the reasons and mechanisms underlying these are not well understood, but this modelling effort has underscored how important they are as a characteristic of pollock early life history.

We have shown details of the transport process, one of the triad of factors thought to be most important to recruitment: transport, feeding and mortality, and how transport and prey dynamics may interact. This type of modelling makes it possible to examine the whole process in detail, whereas field studies are only capable of giving us snapshots of the process. The modelling suggests that transport out of the sea valley and along the shelf break may not mean starvation or loss of larvae to the population. It also supports the notion that eddies aid in cross-shelf transport, which is ultimately critical in getting young pollock to eventual nursery areas.

This work has provided support to the match-mismatch theory of marine fish recruitment. It suggests that spatial variability in larvae and prey is critical in this match or mismatch, as well as the temporal variability usually discussed in this context.

We hope that what we have learned from this type of modelling can be integrated into our growing knowledge of the recruitment process for walleye pollock. Recruitment is an extremely complex process, operating at many time and space scales and including many

nonlinear interactions between processes. It is unlikely that any one type of investigation, be it modelling, field or laboratory studies, will be sufficient to provide an "answer" to the question of why and how variability in recruitment occurs. It is only in the synthesis of results from all of these different types of analyses that advances in understanding may be made.

Literature Cited

Alton, M. and R. Deriso. 1983. Walleye pollock. *In*: Ito, D.H. and J. Balsiger (eds), Condition of groundfish resources in the Gulf of Alaska in 1982. NOAA Tech. Memorandum. NMFS F/NWC-52, Seattle, WA.

Appenzeller, A.R. and W.C. Leggett. 1995. An evaluation of light-mediated vertical migration of fish based on hydroacoustic analysis of the diel vertical movements of the rainbow smelt (*Osmeridus mordax*). Can. J. Fish. Aquat. Sci. 52: 504-511.

Bailey, K.M. and E.D. Houde. 1989. Predation on eggs and larvae of marine fishes and the recruitment problem. Adv. Mar. Biol. 25: 1-83.

Bailey, K.M. and A. Macklin. 1994. Analysis of patterns in larval walleye pollock: *Theragra chalcogramma* survival and wind mixing events in Shelikof Strait, Gulf of Alaska. Mar. Ecol. Prog. Ser. 113: 1-12.

Bailey, K.M. and S.M. Spring. 1992. Comparison of larval, age-0 juvenile and age-2 recruit abundance indices of walleye pollock, *Theragra chalcogramma*, in the western Gulf of Alaska. ICES J. Mar. Sci. 49: 297-304.

Bailey, K.M. and C.L. Stehr. 1986. Laboratory studies on the early life history of the walleye pollock, *Theragra chalcogramma* (Pallas). J. Exp. Mar. Biol. 99: 233-246.

Bailey, K.M., Canino, M.F., J.M. Napp, S.M. Spring and A.L. Brown. 1995. Contrasting years of prey levels, feeding conditions and mortality of larval walleye pollock *Theragra chalcogramma* in the western Gulf of Alaska. Mar. Ecol. Prog. Ser. 119: 11-23.

Bailey, K.M., A.L. Brown, M.M. Yoklavich and K.L.Mier. 1996a. Interannual variability in growth of larval and juvenile walleye pollock *Theragra chalcogramma* in the western Gulf of Alaska, 1983-91. Fish. Oceanogr. 5(Suppl. 1): 137-147.

Bailey, K.M., S.J. Picquelle and S.M. Spring. 1996b. Mortality of larval walleye pollock *Theragra chalcogramma* in the western Gulf of Alaska. 1988-91. Fish. Oceanogr. 5(Suppl. 1): 124-136.

Bartsch, J., K. Brander, M. Heath, P. Munk, K. Richardson and E. Svendsen. 1989. Modelling the advection of herring larvae in the North Sea. Nature 340: 632-636.

Blood, D.M., A.C. Matarese and M.M. Yoklavich.1994. Embryonic development of walleye pollock *Theragra chalcogramma*, from Shelikof Strait, Gulf of Alaska. Fish. Bull. U.S. 92: 207-222.

Bograd, S.J., P.J. Stabeno, and J.D. Schumacher.1994. A census of mesoscale eddies in Shelikof Strait, Alaska, during 1989. J. Geophys. Res. 99: 18243-18254.

Botsford, L.W., C.L. Moloney, A. Hastings, J.L. Largier, T.M. Powell, K. Higgins and J.F.Quinn. 1994. The influence of spatially and temporally varying oceanographic conditions on meroplanktonic metapopulations. Deep Sea Res. 41: 107-145.

Brett, J.R. and T.D.D. Groves. 1979. Physiological energetics. *In*: Hoar, W.S. and D.J. Randall (eds) Fish physiology, Vol. 8. Academic Press, New York, p. 279-352.

Brodeur, R.D. and M.T. Wilson. 1996a. A review of the distribution, ecology and population dynamics of age-0 walleye pollock in the Gulf of Alaska. Fish Oceanogr. 5(Suppl. 1): 148-156.

Brodeur, R.D. and M.T. Wilson. 1996b. Mesoscale acoustic patterns of juvenile walleye pollock (*Theragra chalcogramma*) in the western Gulf of Alaska. Can. J. Fish. Aquat. Sci. 53: 1951-1963.

Brodeur, R.D., S.J. Picquelle, D.M. Blood and N. Merati. 1996. Walleye pollock egg distribution and mortality in the western Gulf of Alaska. Fish. Oceanogr 5(Suppl. 1): 92-111.

Brown, A.L. and K.M. Bailey. 1992. Otolith analysis of juvenile walleye pollock *Theragra chalcogramma* from the western Gulf of Alaska. Mar. Biol. 112: 23-30.

Buckley, T.W. and P.A. Livingston. 1994. A bioenergetics model of walleye pollock (*Theragra chalcogramma*) in the eastern Bering Sea: Structure and documentation. NOAA Tech. Memo. NMFS-AFSC 37, Alaska Fisheries Science Center, 7600 Sand Point Way, NE, Seattle, WA 98115, 52 p.

Canino,M.F., K.M. Bailey and L.S. Incze. 1991. Temporal and geographic differences in feeding and nutritional condition of walleye pollock larvae *Theragra chalcogramma* in Shelikof Strait, Gulf of Alaska. Mar. Ecol. Prog. Ser. 79: 27-35.

Caswell, H. and A.M. John. 1992. From the individual to the population in demographic models. *In*: DeAngelis, D.L. and L.J. Gross (eds) Individual-based models and approaches in ecology: populations, communities, and ecosystems. Routledge, Chapman and Hall, Inc., New York, p. 36-61.

Chambers, R.C. 1993. Phenotypic variability in fish populations and its representation in demographic models. Trans. Am. Fish. Soc. 122: 404-414.

Chambers, R.C. and E.A. Trippel. 1997. Early life history and recruitment in fish populations. Chapman & Hall, Fish and Fisheries Series 21.

Checkley, D.M. 1984. Relation of growth to ingestion for larvae of Atlantic herring *Clupea harengus* and other fish. Mar. Ecol. Prog. Ser. 18: 215-224.

Coombs, S.H., C.A. Fosh and M.A. Keen. 1985. The buoyancy and vertical distribution of eggs of sprat (*Sprattus sprattus*) and pilchard (*Sardinia pilchardus*). J. Mar. Biol. Ass. U.K. 65: 461-474.

Corkett, J. and I.A. McLaren. 1978. The biology of *Pseudocalanus*. Adv. Mar. Biol. 15: 1-231.

Cowan, J.H., K.A. Rose and E.D. Houde. 1997. Size-based foraging success and vulnerability to predation: selection of survivors in individual-based models of larval fish populations. *In*: Chambers, R.C. and E.A. Trippel (eds) Early life history and recruitment in fish populations, Chapman & Hall, Fish and Fisheries Series 21.

Craik, J.C.A. and S.M. Harvey. 1987. The causes of buoyancy in eggs of marine teleosts. J. Mar. Biol. Ass. U.K. 67: 169-182.

Crowder, L.W., J.A. Rice, T.J. Miller and E.A. Marschall. 1993. Empirical and theoretical approaches to size-based interactions and recruitment variability in fishes. *In*: DeAngelis, D.L. and J.L. Gross (eds) Individual-based models and approaches in ecology. Chapman and Hall, pp. 237-255.

Cushing, D.H. 1972. The production cycle and the numbers of marine fish. Symp. Zool. Soc. London 29: 213-232.

Cushing, D.H. 1974. The natural regulation of fish populations. *In*: (Harden Jones, F.R. Sea fisheries research, Elek Science, London, pp. 399-412.

Cushing, D.H. 1975. Fisheries ande marine ecology. Cambridge Univ. Press, Cambridge.

Dagg, M.J., M.E. Clarke, T. Nishiyama and S.L. Smith. 1984. Production and standing stock of copepod nauplii, food items for larvae of walleye pollock *Theragra chalcogramma* in the southeastern Bering Sea. Mar. Ecol. Prog. Ser. 19: 7-16.

DeAngelis, D.L. and L.J. Gross. 1992. Individual-based models and approaches in ecology: populations, communities and ecosystems. Routledge, Chapman and Hall, Inc. New York.

DeAngelis, D.L. and K.A. Rose. 1992. Which individual-based approach is most appropriate for a given problem? *In*: DeAngelis, D.L. and L.J. Gross (eds) Individual-based models and approaches in ecology: populations, communities and ecosystems. Routledge, Chapman and Hall, Inc. New York, p. 67-87.

DeAngelis, D.L., L. Godbout and B.J Shuter. 1991. An individual-based approach to predicting density-dependent dynamics in the smallmouth bass populations. Ecol. Model. 57:91-115.

DeBlois, E.M. and W.C. Leggett. 1993. Match/mismatch between the abundance of marine fish eggs and invertebrate predators: an analysis of *Calliopus laeviusculus* (Amphipoda: Gammaridae) population growth relative to the seasonal spawning cycle of capelin (*Mallotus villosus*). Can. J. Fish. Aquat. Sci. 50: 2581-2590.

Dimou, K.N. and P.E. Adams. 1992. Representation of sources in a 3-D Eulerian-Lagrangian mass transport model. *In*: Wrobel, L.C. and C.A. Brebbie (eds) Water pollution modeling, measurement and predition 1991, pp. 251-264.

Dunn, J.R. and A.C. Matarese. 1987. A review of the early life history of Northeast Pacific gadoid fishes. Fish. Res. 5: 163-184.

Eppley, R.W. 1972. Temperature and phytoplankton growth in the sea. Fish. Bull. U.S. 70: 1063-1085.

Fienberg, S.E. 1980. The analysis of cross-classified categorical data. The MIT Press, Cambridge, Mass. 151 p.

Flierl, G.R. and C.S. Davis. 1993. Biological effects of Gulf Stream meandering. J. Mar. Res. 51: 529-560.

Frank, K.T. and W.C. Leggett. 1982. Coastal water mass replacement: its effect on zooplankton dynamics and the predator-prey complex associated with larval capelin (*Mallotus villosus*). Can. J. Fish. Aquat. Sci. 39: 991-1003.

Frank, P.J.S. and L.J. Walstad. 1997. Phytoplankton patches at fronts: a model of formation and response to wind events. J. Mar. Res. 55: 1-29.

Frost, B.W. 1987. Grazing control of phytoplankton stock in the open subarctic Pacific Ocean: a model assessing the role of mesozooplankton, particularly the large calanoid copepods *Neocalanus*, spp. Mar. Ecol. Prog. Ser. 39: 49-68.

Frost, B.W. 1993. A modeling study of processes regulating plankton standing stock and production in the open subarctic Pacific Ocean. Prog. Oceanogr. 32: 17-56.

Gardner, R.H., B. Rojder and U. Bergstrom. 1983. PRISM: A systematic method for determining the effect of parameter uncertainties on model predictions. Technical Report, Studsvik Energiteknik AB Report/NW-83/555, Nyköping, Sweden.

Haidvogel, D.B. 1982. On the feasibility of particle tracking in Eulerian ocean models. Ocean Modelling 45: 4-9.

Haidvogel, D.B., J.L. Wilkin and R. Young. 1991. A semi-spectral primitive equation ocean circulation model using vertical sigma and orthogonal curvilinear horizontal coordinates. J. Comput. Physics 94: 151-185.

Harris, R.K. 1985. Body composition (carbon, nitrogen and calories) and energetics of immature walleye pollock, *Theragra chalcogramma* (Pallas), in the southeast Bering Sea. Masters Thesis, Univ. of Alaska, Fairbanks.

Harris, R.K., T. Nishiyama and A.J. Paul. 1986. Carbon, nitrogen and caloric content of eggs, larvae, and juveniles of the walleye pollock, *Theragra chalcogramma*. J. Fish. Biol. 29: 87-98.

Haynes, E.G. and S.E. Ignell. 1983. Effect of temperature on the rate of embryonic development of walleye pollock, *Theragra chalcogramma*. Fish. Bull. U.S. 81: 890-894.

Herman, A.W and T. Platt. 1983. Numerical modelling of diel carbon production and zooplankton grazing on the Scotian shelf based on observational data. Ecol. Model. 18: 55-72.

Hermann, A.J. and P.J. Stabeno. 1996. An eddy resolving model of circulation on the western Gulf of Alaska shelf. I. Model development and sensitivity analysis. J. Geophys. Res. 101: 1129-1149.

Hermann, A.J., W.C. Rugen, P.J. Stabeno and N.A. Bond. 1996a. Physical transport of young pollock larvae (*Theragra chalcogramma*) near Shelikof Strait as inferred from a hydrodynamic model. Fish. Ocean. 5(Suppl. 1): 58-70.

Hermann, A.J., S. Hinckley, B.A. Megrey and P.J. Stabeno. 1996b. Interannual variability of the early life history of walleye pollock near Shelikof Strait as inferred from a spatially explicit, individual-based model. Fish. Oceanogr. 5(Suppl. 1): 39-57.

Hermann, A.J., S. Hinckley, B.A. Megrey and J.M. Napp. In press. Applied and theoretical considerations for constructing spatially explicit individual-based models of marine fish early life history which include multiple trophic levels. ICES J. Mar. Sci.

Hinckley, S. 1990. Variation of egg size of walleye pollock (*Theragra chalcogramma*) with a preliminary examination of the effect of egg size on larval size. Fish. Bull. U.S. 88: 471-483.

Hinckley, S., B.A. Megrey and A.J. Hermann. 1996a. An individual-based model of the juvenile stage of walleye pollock, *Theragra chalcogramma*, in the western Gulf of Alaska (extended abstract). *In* U.S. Dep. Commer. NOAA Tech. Rep. NMFS 126.

Hinckley, S., K.M. Bailey, S.J. Picquelle, J.D. Schumacher and P.J. Stabeno. 1991. Transport, distribution and abundance of larval and juvenile walleye pollock (*Theragra chalcogramma*) in the western Gulf of Alaska. Can. J. Fish. Aquat. Sci. 48: 91-98.

Hinckley, S., A.J. Hermann and B.A. Megrey. 1996b. Development of a spatially explicit, individual-based model of marine fish early life history. Mar. Ecol. Prog. Ser. 139: 47-68.

Hinckley, S. A.J. Hermann, K.L. Mier and B.A. Megrey. In press. The importance of spawning location and timing to successful transport to nursery areas: a simulation modeling study of Gulf of Alaska walleye pollock. ICES J. Mar. Sci.

Hjort, J. 1914. Fluctuation in the great fisheries of northern Europe. Rapp. PV Réun. Cons. Int. Explor. Mer 20: 1-20.

Hjort, J. 1928. Fluctuations in the year classes of important food fishes. J. Cons. Int. Explor. Mer 1: 5-38.

Hofmann, E.E., K.S. Hedstrom, J.R. Moisan, D.B. Haidvogel and D.L. Mackas. 1991. The use of simulated drifter tracks to investigate general transport patterns and residence times in the coastal transition zone. J. Geophys. Res. 96: 15041-15052.

Holloway, G. 1994. On modeling vertical trajectories of phytoplankton in a mixed layer. Deep-Sea Res. II 41: 957-959.

Hollowed, A.B., B.A. Megrey and E. Brown. 1993. Walleye pollock. *In*: Stock assessment and fishery evaluation report for the groundfish resources of the Gulf of Alaska as projected for 1994. Unpubl. MS, p. 1-1-1-54. Complied by the plan team for the groundfish fisheries of the Gulf of Alaska. North Pacific Fishery Management Council, P.O. Box 103136, Anchorage, AK 99510.

Houde, E.D. 1989. Comparative growth, mortality, and energetics of marine fish larvae: temperature and implied latitudinal effects. Fish. Bull. U.S. 87: 471-495.

Houde, E.D. and R.C. Shekter. 1981. Growth rates, rations and cohort comsumption of marine fish larvae in relation to prey concentration> Rapp. PV. Réun. Cons. Int. Explor. Mer 178: 441-453.

Hunter, J.R. P.D. Craig and H.E. Phillips. 1993. On the use of random walk models with spatially variable diffusivity. J. Comput. Phys. 106: 366-376.

Huston, M.A., D.L. DeAngelis and W.M. Post. 1988. New computer models unify ecological theory. BioScience 38: 682-691.

Incze, L.S. and T. Ainaire. 1994. Distribution and abundance of copepod nauplii and other small (40-300 μm) zooplankton during spring in Shelikof Strait, Alaska. Fish. Bull. U.S. 92: 67-78.

Incze, L.S., A.W. Kendall, Jr., J.D. Schumacher and R.K. Reed. 1989. Interactions of a mesoscale patch of larval fish (*Theragra chalcogramma*) with the Alaska Coastal Current. Cont. Shelf Res. 9: 269-284.

Incze, L.S., P.B. Ortner and J.D. Schumacher. 1990. Microzooplankton, vertical mixing and advection in a larval fish patch. J. Plankton Res. 12: 365-379.

Incze, L.S., D.W. Seifert and J.M. Napp. 1997. Mesozooplankton of Shelikof Strait, Alaska: abundance and community composition. Cont. Shelf Res. 17: 287-305.

Jamart, B.M., D.F. Winter, K. Banse, G.C. Anderson and R.K. Lam. 1977. A theoretical study of phytoplankton growth and nutrient distribution in the Pacific Ocean off the northwestern U.S. coast. Deep Sea Res. 24: 753-773.

Jamart, B.M., D.F. Winter and K. Banse. 1979. Sensitivity analysis of a mathematical model of phytoplankton growth and nutreint distribution in the Pacific Ocean off the northwestern U.S. coast. J. Plankton Res. 1: 267-290.

Judson, O.P. 1994. The rise of the individual-based model in ecology. Trends Ecol. Evol. 9: 9-14.

Kändler, R. and E.O. Tan. 1965. Investigations on the osmoregulation in pelagic eggs of gadoid and flatfishes in the Baltic. Part 1. Changes in volume and specific gravity at different salinities. ICES Baltic-Belt Council Meeting 43.

Kendall, A.W., Jr. and S. Kim. 1989. Buoyancy of walleye pollock (*Theragra chalcogramma*) eggs in relation to water properties and movement in Shelikof Strait, Gulf of Alaska. *In*: Beamish, R.J. and G.A. McFarlane (eds) Effects of ocean variability on recruitment and an evaluation of parameters used in stock assessment models. Can. Spec. Fish. Aquat. Sci. 108: 169-180.

Kendall, A.W., Jr. and T. Nakatani. 1992. Comparisons of early life history characteristics of walleye pollock *Theragra chalcogramma* in Shelikof Strait, Gulf of Alaska, and Funka Bay, Jokkaido, Japan. Fish. Bull. U.S. 90: 129-138.

Kendall, A.W., Jr. and S.J. Picquelle. 1990. Egg and larval distributions of walleye pollock *Theragra chalcogramma* in Shelikof Strait, Gulf of Alaska. Fish. Bull. U.S. 88: 133-154.

Kendall, A.W. Jr., M.E. Clarke, M.M. Yoklavich and G.W. Boehlert. 1987. Distribution, feeding and growth of larval walleye pollock, *Theragra chalcogramma*, from Shelikof Strait, Gulf of Alaska. Fish. Bull. U.S. 85: 499-521.

Kendall, A.W., Jr., L.S. Incze, P.B. Ortner, S.R. Cummings and P.K. Brown. 1994. The vertical distribution of eggs and larvae of walleye pollock (*Theragra chalcogramma*) in Shelikof Strait, Gulf of Alaska, Fish. Bull. U.S. 92: 540-554.

Kendall, A.W., Jr., J.D. Schumacher and S. Kim.1996. Walleye pollock recruitment in Shelikof Strait: applied fisheries oceanography. Fish. Oceanogr. 5(Suppl. 1): 4-18.

Kinoshita, R.K., A. Greig, J.D. Hastie and J.M. Terry. 1995 (draft), Economic status of the groundfish fisheries off Alaska (1994). Socioeconomic Task. Alaska Fishery Science Center, 7600 Sand Point Way, NE, Seattle, WA 98115, 104 p.

Kiørboe, T., P. Munk and K. Richardson. 1987. Respiration and growth in larval herring *Clupea harengus*: relation between specific dynamic action and growth efficiency. Mar. Ecol. Prog. Ser. 40: 1-10.

Lackmann, GM and J.E. Overland. 1989. Atmospheric structure and momentum balance during a gap-wind event in Shelikof Strait, Alaska. Mar. Wea. Rev. 116: 1817-1833.

Lande, R. and M.R. Lewis. 1989. Models of photoadaptation and photosynthesis by algal cells in a turbulent mixed layer. Deep Sea Res. 36: 1161-1175.

Lasker, R. 1975. Field criteria for survival of anchovy larvae: the relation between inshore chlorophyll maximum layers and successful first feeding. Fish. Bull. U.S. 73: 453-462.

Lasker, R. 1978. The relation between oceanographic conditions and larval anchovy food in the California Current: identification of factors contributing to recruitment failure. Rapp. P.V. Réun. Cons. Int. Explor. Mer 173: 212-230.

Leggett, W.C. and E. DeBlois. 1994. Recruitment in marine fishes: is it regulated by starvation and predation in the egg and larval stages? Neth. J. Sea Res. 32: 119-134.

Leggett, W.C., Frank, K.T. and J.E. Carscadden. 1984. Meteorological and hydrographic regulation of year-class strength in capelin (*Mallotus villosus*). Can. J. Fish. Aquat. Sci. 41: 1193-1201.

Letcher, B.H., J.A. Rice, L.B. Crowder and K.A. Rose. 1996. Variability in survival of larval fish: disentangling components with a generalized individual-based model. Can. J. Fish. Aquat. Sci. 53: 787-801.

Lewis, C.V.W., C.S. Davis and G. Gawarkiewicz. 1994. Wind-forced biological-physical interactions on an isolated offshore bank. Deep Sea Res. 41: 51-73.

Lloyd, M. 1967. Mean crowding. J. Anim. Ecol. 36: 1-30.

Lomnicki, A. 1992. Population ecology from the individual perspective. *In*: DeAngelis, D.L. and L.J. Gross (eds) Individual-based models and approaches in ecology. Chapman and Hall, pp. 3-17.

Macklin, S.A., P.J. Stabeno and J.D. Schumacher. 1993. A comparison of over-the-water winds along a mountainous coast. J. Geophys. Res. 98: 16555-16579.

MacKenzie, B.R. and T. Kiørboe. 1995. Encounter rates and swimming behavior of pause-travel and cruise larval fish predators in calm and turbulent laboratory environments. Limnol. Oceanogr. 40: 1278-1289.

MacKenzie, B.R. and W.C. Leggett. 1991. Wind-based models for estimating the dissipation rates of turbulent energy in aquatic environments: empirical comparisons. Mar. Ecol Prog. Ser. 94: 207-216.

MacKenzie, B.R., W.C. Leggett and R.H. Peters. 1990. Estimating larval fish ingestion ratees: can laboratory derived values be reliably extrapolated to the wild? Mar. Ecol. Prog. Ser. 67: 209-225.

MacKenzie, B.R., T.J. Miller, S. Cyr and W.C. Leggett. 1994. Evidence for a dome-shaped relationship between turbulence and larval fish ingestion rate. Limnol. Oceanogr. 39: 1790-1799.

Mantua, N.J., S.R. Hare, Y. Zhang, J.M. Wallace and R.C. Francis. 1997. A Pacific interdecadal climate oscillation with impacts on salmon production. Bull. Am. Meteorol. Soc. 78: 1069-1079.

McKay, M.D., R.D. Beckman, and W.J. Conover. 1979. A comparison of three methods for selecting values of input variables in the analysis of output from computer code. Technometrics 21: 239-245.

Megrey, B.A., S.J. Bograd, W.C. Rugen, A.B. Hollowed, P.J. Stabeno, S.A. Macklin, J.D. Schumacher and W.J. Ingraham, Jr. 1995. An exploratory analysis of associations between biotic and abiotic factors and year-class strength of Gulf of Alaska walleye pollock (*Theragra chalcogramma*). *In*: Climate change and northern fish populations. Beamish, R.J. (ed). Can. Spec. Publ. FIsh. Aquat. Sci. 121: 227-243.

Megrey, B.A., A.B. Hollowed, S.R. Hare, S.A. Macklin and P.J. Stabeno. 1996. Contributions of FOCI research to forecasts of year-class strength of walleye pollock in Shelikof Strait, Alaska. Fish. Oceanogr. 5(Suppl. 1): 189-203.

Megrey, B.A. and S. Hinckley. In press. The effect of turbulence on feeding of larval fishes: a sensitivity analysis using an individual-based model. ICES J. Mar. Sci.

Metz, J.A. and O. Diekmann. 1986. The dynamics of physiologically structured populations. Lecture notes in biomathematics, Vol. 68. Springer-Verlag, Berlin.

Moisan, J.R. and E.E. Hofmann. 1996a. Modeling nutrient and plankton processes in the Coastal Transition Zone. Part 1: A time- and depth-dependent model. J. Geophys. Res. 101(C10): 22647-22676.

Moisan, J.R. and E.E. Hofmann 1996b. Modeling nutrient and plankton processes in the Coastal Transition Zone. Part 3: Lagrangian drifters. J. Geophys. 101(C10): 22693-22704.

Moisan, J.R., E.E. Hofmann and D.B. Haidvogel. 1996. Modeling nutrient and plankton processes in the Coastal Transition Zone. Part 2: A three-dimensional physical-bio-optical model. J. Geophys. Res. 101(C10): 22677-22691.

Munk, P. and T. Kiørboe. 1985. Feeding behavior and swimming activity of larval herring (*Clupea harengus*) in relation to density of copepod nauplii. Mar. Ecol. Progr. Ser. 24: 15-21.

Musgrave, D.L., T.J. Weingartner and T.C. Royer. 1992. Circulation and hydrography in the northwestern Gulf of Alaska. Deep Sea Res. 39: 1499-1519.

Napp, J.M., L.S. Incze, P.B. Ortner, D.L.W. Seifert and L. Britt. 1996. The plankton of Shelikof Strait, Alaska: standing stock, production, mesoscale variability and their relevance to fish survival. Fish. Oceanogr. 5(Suppl. 1): 19-38.

National Renewable Energy Laboratory. 1992. User's Manual: National Solar Radiation Database (1961-1990), Version 1.0, Vol. 1. Asheville, NC, U.S. Dept. Energy Resource Assessment Program. National Climatic Data Center.

Neibauer, H.J. 1988. Effects of El Niño-Southern Oscillation and North Pacific weather patterns on interannual variability in the subarctic Bering Sea. J. Geophys. Res. 93: 5051-5068.

Neill, W.H. 1979. Mechanisms of fish distribution in heterothermal environments. Am. Zool. 19: 305-317.

Neilson, J.D. and R.I. Perry. 1990. Diel vertical migrations of marine fishes: an obligate or facultative process? Adv. Mar. Biol. 26: 115-168.

Nisbet, R.M. and S.C.Gurney. 1982. Modelling fluctuating populations. John Wiley & Sons, New York.

Nishiyama, T., K. Hirano and T. Haryu. 1983. The early life history and feeding habit of larval walleye pollock, *Theragra chalcogramma* (Pallas) in the southeast Bering Sea.

Paper No. P-10, Int. N. Pac. Fish. Council Groundfish Symposium, Oct 26-28, Anchorage, Alaska.

Olla, B.L. and M.W. Davis. 1990. Effects of physical factors on the vertical distribution of larval walleye pollock *Theragra chalcogramma* under controlled laboratory conditions. Mar. Ecol. Prog. Ser. 63: 105-112.

O'Rourke, J. 1993. Computational geometry in C. Cambridge Univ. Press. pp. 233-236.

Page, F.H., K.T. Frank and K. Thompson. 1989. Stage dependent vertical distribution of haddock (*Melanorammus aeglefinus*) eggs in a stratified water column: observation and model. Can. J. Fish. Aquat. Sci. 46(Suppl 1): 55-67.

Parsons, T.R., M. Takahashi and B. Hargrave. 1977. Biological Oceanographic Processes, 2nd Edition. Pergamon Press, Oxford.

Paul, A.J. 1986. Respiration of juvenile pollock, *Theragra chalcogramma* (Pallas), relative to body size and temperature. J. Exp. Mar. Biol. 97: 287-293.

Paul, A.J., J.M. Paul and R.L. Smith. 1990. Energy ingestion and conversion rate in pollock (*Theragra chalcogramma*) fed different prey types. J. Cons. int. Explor. Mer 46: 232-234.

Pepin, P. and T.J. Miller. 1993. Potential use and abuse of general empirical models of early life history processes in fish. Can. J. Fish. Aquat. Sci. 50: 1343-1345.

Picquelle, S.J. and B.A. Megrey. 1993. A preliminary spawning biomass estimate of walleye pollock, *Theragra chalcogramma*, in the Shelikof Strait, Alaska, based on the annual egg production method. *In*: Proceedings from the Symposium on the Advances in Estimating the Biomass of Marine Fish Stocks Using Ichthyoplankton, During the 15th Annual Early Life History Section of the American Fisheries Society. J. R. Hunter and N.C.H Lo (eds.). Bull. Mar. Sci. 53: 728-749.

Pope, J.G., J.G. Shepard and J. Webb. 1994. Successful surf-riding on size spectra: the secret of survival in the sea. Phil. Trans. Royal Soc. London 343: 41-49.

Pritchett, M. and L.Haldorson. 1989. Depth distribution and vertical migration of larval walleye pollock (*Theragra chalcogramma*). *In*: Proceedings of the international symposium on the biology and management of walleye pollock; 14-16 November, 1988, Anchorage. Alaska Sea Grant Rep. 89-1, University of Alaska, Fairbanks, Alaska, p. 173-183.

Redfield, A.C., B.H. Ketchum and F.A. Richards. 1963. The influence of organisms on the composition of sea water, *In*: Hill, M.N. (ed) The sea. Wiley Interscience 1: 26-77.

Reed, R.K. 1984. Flow of the Alaskan Stream and its variations. Deep Sea Res. 31: 369-386.

Reed, R.K., J.D. Schumacher and L.S. Incze. 1987. Circulation in Shelikof Strait, Alaska. J. Phys. Oceanogr. 17: 1546-1554.

Rice, J.A., T.J. Miller, K.A. Rose, L.B. Crowder, E.A. Marschall, A.S. Trebitz and D.L DeAngelis. 1993. Growth rate variation and larval survival: inference from an individual-based size-dependent predation model. Can. J. Fish. Aquat. Sci. 50: 133-142.

Roach, A.T. and J.D. Schumacher. 1991. Observations of seasonal and interseasonal variability in Shelikof Strait, Alaska. *In*: Proc. of the 7th Symposium on Coastal and Ocean Management, Coastal Zone 91. ASCE/Long Beach, CA, July 8-12, 1991, pp. 3304-3317.

Rose, K.A. and J.H.Cowan, Jr. 1993. Individual-based model of young-of-the-year striped bass population dynamics. I. Model description and baseline simulations. Trans. Am. Fish. Soc. 122: 415-430.

Rose, K.A., E.P. Smith, R.H. Gardner, A.L. Brenkert and S.M. Bartell. 1991. Parameter sensitivities, Monte Carlo filtering and model forecasting under uncertainty. J. Forecasting 10: 117-133.

Rose, K.A., S.W. Christensen, and D.L. DeAngelis. 1993. Individual-based modeling of populations with high mortality: a new method for following a fixed number of model individuals. Ecol. Model. 68: 273-292.

Rothschild, B.J. 1986. Dynamics of marine fish populations. Harvard Univ. Press, 277 p.

Rothschild, B.J. and T.R. Osborn. 1988. Small-scale turbulence and plankton contact rates. J. Plankton Res. 10: 465-474.

Royer, T.C. 1981. Baroclinic transport in the Gulf of Alaska. Part II. Freshwater driven coastal current. J. Mar. Res. 39: 251-266.

Royer, T.C. 1982. Coastal freshwater discharge in the northeast Pacific. J. Geophys. Res. 87: 2017-2021.

Savage, D. 1990. Fisheries Oceanography Coordinated Investigations Field Operations 1989. NOAA Data Rep. ERL-PMEL-26.

Scheffer, M., J.M. Baveco, D.L. DeAngelis and K.A. Rose. 1995. Super-individuals: a simple solution for modeling large populations on an individual basis. Ecol. Model. 80: 161-170.

Schumacher, J.D. and A.W. Kendall, Jr. 1991. Some interactions between young walleye pollock and their environment in the western Gulf of Alaska. CalCOFI Rep. 32: 22-40.

Schumacher, J.D., P.J. Stabeno and A.T. Roach. 1989. Volume transport in the Alaska Coastal Current. Cont. Shelf Res. 9: 1071-1083.

Schumacher, J.D., P.J. Stabeno and S.J. Bograd. 1993. Characteristics of an eddy over a continental shelf: Shelikof Strait, Alaska. J. Geophys. Res. 98: 8395-8404.

Seifert, D.L.W. and L.S. Incze. 1989. Zooplankton of Shelikof Strait, Alaska, April to July 1987: Data from Fisheries-Oceanography Coordinated Investigations (FOCI) Cruises. NWAFC Proc. Rep. 89-22. Alaska Fisheries Science Center, 7600 Sand Point Way, NE, Seattle, WA 98115.

Sissenwine, M.P. 1984. Why do fish populations vary? *In*: May, R.M. (ed), Exploitation of marine communities. Springer-Verlag, Berlin, pp. 59-94.

Smith, M. 1974. Models in ecology. Cambridge University Press, Cambridge, England.

Smith, G.B., G.E. Walters, P.A. Raymore and W.A. Herschberger. 1984. Studies of the distribution and abundance of juvenile groundfish in the northwestern Gulf of Alaska, 1980-82, Part 1. Three-year comparisons. NPAA Tech. Memo. NMFS F/NWC-59, Seattle, WA.

Smith, R.L., A.J. Paul and J.M. Paul. 1986. Effect of food intake and temperature on growth and conversion efficiency of juvenile walleye pollock (*Theragra chalcogramma*): a laboratory study. J. Cons. int. Explor. Mer 42: 241-253.

Sogard, S. M. and B.L. Olla. 1994. The potential for intracohort cannibalism in age-0 walleye pollock, *Theragra chalcogramma*, as determined under laboratory conditions. Env. Biol. Fishes 39: 183-199.

Sogard, S.M and B.L. Olla. 1996. Food deprivation affects vertical distribution and activity of a marine fish in a thermal gradient: potential energy-conserving mechanisms. Mar. Ecol. Prog. Ser. 133: 43-55.

Sokal, R.R. and F.J. Rohlf. 1995. Biometry. Third Ed. W.H. Freeman & Co. NY.

Solemdal, P. 1967. The effect of salinity on buoyancy, size and development of flounder eggs. Sarsia 29: 431-442.

Solemdal, P. 1973. Transfer of Baltic flatfish to a marine environment and the long-term effects on reproduction. Oikos Suppl 15: 268-276.

SOLMET Vol. 1. 1979. Hourly Solar Radiation - Surface Meteorological Observations. Asheville, NC. Final Rep. TD-9724. National Climatic Center.

Spring, S.M. 1996. Swimming behavior of larval walleye pollock, *Theragra chalcogramma*, in relation to food. Masters Thesis, Univ. of Washington, Seattle.

Spring, S. and K.M. Bailey. 1991. Distribution and abundance of juvenile pollock from historical shrimp trawl surveys in the western Gulf of Alaska. AFSC Proc. Rep 91-18, Alaska Fisheries Science Center, 7600 Sand Point Way, NE, Seattle, WA 98115.

Stabeno, P.J. and A.J. Hermann. 1996. An eddy resolving model of circulation on the western Gulf of Alaska shelf. II. Comparison of results to oceanographic observations. J. Geophys. Res. 101: 1151-1161.

Stabeno, P.J., A.J. Hermann, N.A. Bond and S.J. Bograd. 1995a. Modelling the possible impact of climate change on the survival of larval walleye pollock (*Theragra chalcogramma*) in the Gulf of Alaska. *In*: Beamish, R.J. (ed) Climate change and northern fish populations. Can. Spec. Pub. Fish. Aquat. Sci. 121: 719-727.

Stabeno, P.J., R.K. Reed and J.D. Schumacher. 1995b. The Alaska Coastal Current: continuity of transport and forcing. J. Geophys. Res. 100: 2477-2485.

Stabeno, P.J., J.D.Schumacher, K.M. Bailey, R.D. Brodeur and E.D. Cokelet. 1996. Observed patches of walleye pollock eggs and larvae in Shelikof Strait, Alaska: their characteristics, formulation and persistance. Fish. Oceanogr. 5(Suppl. 1): 81-91.

Strickland, R.M. and T.H. Sibley. 1989. Potential effects of water transport on the walleye pollock (*Theragra chalcogramma*) fishery in the Gulf of Alaska. CRC Critical Reviews in Aquatic Sciences 1: 281-293.

Sundby, S. 1983. A one-dimensional model for the vertical distribution of pelagic fish eggs in the mixed layer. Deep Sea Res. 30: 645-661.

Sundby, S. 1995. On the dome-shaped relationship between wind-generated turbulence and larval feeding. Neth. J. Sea Research 34: 243-244.

Sundby, S. 1997. Turbulence and ichthyoplankton: influence on vertical distributions and encounter rates. Scientia Marina 61(Suppl 1): 159:176.

Sundby, S. and P. Fossum. 1990. Feeding conditions of Arcto-Norwegian cod larvae compared with the Rothschild-Osborn theory on small-scale turbulence and plankton contact rates. J. Plankton Res. 12: 1153-1162.

Taylor, G.I. 1921. Diffusion by continuous movements. Proc. London Math. Soc. (ser.2) 10: 196-212.

Theilacker, G.H. and A.S. Kimball. 1984. Comparative quality of rotifers and copepods as foods for larval fishes. Calif. Coop. Ocean. Fish. Invest. Rep. 15: 80-86.

Theilacker, G.H., K.M. Bailey, Canino, M.F. and Porter, S.M. 1996. Variations in larval walleye pollock feeding and condition: a synthesis. Fish. Oceanogr. 5(Suppl. 1): 112-123.

Tilseth, S. 1984. The distribution of cod larvae and prey organisms in the Lofoten area related to critical prey concentrations. *In*: Godø, O.R. and S. Tilseth (eds) Proceedings of Soviet-Norwegian symposium on the reproduction and recruitment of Arctic cod, Leningrad, 26-30 Sept. 1983. Inst. Mar. Res., Bergen, Norway.

Tyler, J.A. and K.A. Rose. 1994. Individual variability and spatial heterogeneity in fish population models. Rev. Fish. Biol. FIsh. 4: 91-123.

Van Winkle, W., K.A. Rose and R.C. Chambers. 1993. Individual-based approach to fish population dynamics: an overview. Trans. Am. Fish. Soc. 122: 397-403.

Vastano, A.C., L.S. Incze and J.D. Schumacher. 1992. Observations and analysis of fishery processes: larval pollock at Shelikof Strait, Alaska. Fish. Oceanogr. 1: 20-31.

Walsh, J.J., C.D. Wirick, D.A. Dierterle and A.G. Tingle. 1981. Environmental constraints on larval fish survival in the Bering Sea. Rapp. P.V. Réun. Cons. Int. Explor. Mer 178: 24-27.

Walters, C.J., C.G. Hannah and K. Thompson. 1992. A micro-computer program for simulating effects of the physical transport process on fish larvae. Fish. Oceanogr. 1: 11-19.

Walters, G.E., G.B. Smith, P.A. Raymore and W. Hirschberger. 1985. Studies of the distribution and abundance of juvenile groundfish in the northwest Gulf of Alaska, 1980-82: Part 2, Biological characteristics in the extended region. NOAA Tech. Memo. NMFS F/NWC-77, Seattle, WA.

Webb, P.W. 1978. Partitioning of energy into metabolism and growth. *In*: Gerking, S.D. (ed) Ecology of greshwater fish production. Wiley, New York, p. 184-214.

Werner, F.E., F.H. Page, D.R. Lynch, J.W Loder, R.G. Lough, R.I Perry, D.A. Greenberg and M.M. Sinclair. 1993. Influences of mean advection and simple behavior on the distribution of cod and haddock early life stages on Georges Bank. Fish. Oceanogr. 2: 43-64.

Werner, F.E., R.I. Perry, B.R. MacKenzie, R.G. Lough and C.E. Naimie. 1995. Larval trophodynamics, turbulence, and drift on Georges Bank: A sensitivity analysis of cod and haddock. ICES C.M./Q:26.

Werner, F.E., R.I Perry, R.G. Lough and C.E. Naimie. 1996. Trophodynamic and advective influences on Georges Bank larval cod and haddock. Deep Sea Res. II. Topical Studies in Oceanography, Georges Bank Research Vol. 43: 1793-1822.

Wilson,M.T., R.D. Brodeur and S. Hinckley. 1996. Distribution and abundance of age-0 walleye pollock, *Theragra chalcogramma*, in the western Gulf of Alaska during September, 1990. *In*: Brodeur, R.D., P.A. Livingston, T.R. Loughlin and A.B. Hollowed (eds), Ecology of juvenile walleye pollock, *Theragra chalcogramma*, pp. 11-24.

Winberg, G.H. 1956. Rate of metabolism and food requirements of fishes. Belorussian Univ., Minsk, 253 p. (Translated by Fish. Res. Bd. Can. Translation Ser. No. 164, 1960).

Wooster, W.S. and K.M. Bailey. 1989. Recruitment of marine fishes revisited. *In*: Beamish, R.J. and G.A. McFarlane (eds), Effects of ocean variability on recruitment and evaluation of parameters used in stock assessment models, Can. Spec. Pub. FIsh. Aquat. Sci. 108: 153-159.

Wroblewski, J.S. 1977. A model of phytoplankton plume formations during variable Oregon upwelling. J. Mar. Res. 35: 357-394.

Yamashita, Y and K.M. Bailey. 1989. A laboratory study of the bioenergetics of larval walleye, *Theragra chalcogramma*. Fish. Bull. U.S. 87: 525-536.

Yoklavich, M.M. and K.M Bailey. 1990. Hatching period, growth and survival of young walleye pollock *Theragra chalcogramma* as determined from otolith analysis. Mar. Ecol. Prog. Ser. 64: 13-23.

VITA

SARAH HINCKLEY

Education

1999	Ph.D. Fisheries University of Washington, Seattle, WA
1986	M.S. Fisheries University of Washington, Seattle, WA
1977	B.A. Biology and Ecology College of the Atlantic, Bar Harbor, ME

Employment

1981-present.	Fisheries research biologist National Marine Fisheries Service Northwest and Alaska Fisheries Center Seattle, WA
1980-1981	Biological Technician National Marine Mammal Laboratory Northwest and Alaska Fisheries Center Seattle, WA
1980	Research Assistant Hawaii Volcanos National Park
1979	Fishery Observer National Marine Fisheries Service Northwest and Alaska Fisheries Center Seattle, WA
1977-1978	Research Assistant College of the Atlantic Bar Harbor, ME

Selected Publications

Hinckley, S. A.J. Hermann, K.L. Mier and B.A. Megrey. In press. The importance of spawning location and timing to successful transport to nursery areas: a simulation modeling study of Gulf of Alaska walleye pollock. ICES J. Mar. Sci.

Hermann, A.J., S. Hinckley, B.A. Megrey and J.M. Napp. In press. Applied and theoretical considerations for constructing spatially explicit individual-based models of marine fish early life history which include multiple trophic levels. ICES J. Mar. Sci.

Megrey, B.A. and S. Hinckley. In press. The effect of turbulence on feeding of larval fishes: a sensitivity analysis using an individual-based model. ICES J. Mar. Sci.

Hinckley, S., A.J. Hermann and B.A. Megrey. 1996. Development of a spatially explicit, individual-based model of marine fish early life history. Mar. Ecol. Prog. Ser. 139: 47-68.

Hinckley, S., B.A. Megrey and A.J. Hermann. 1996. An individual-based model of the juvenile stage of walleye pollock, *Theragra chalcogramma*, in the western Gulf of Alaska (extended abstract). *In* U.S. Dep. Commer. NOAA Tech. Rep. NMFS 126.

Hinckley, S., S. Picquelle, K.M. Bailey and J.D. Schumacher, M.M. Yoklavich. 1993. Mortality rates of larval walleye pollock (Theragra chalcogramma) in the Gulf of Alaska as determined from field sampling. Mar. Ecol. Progr. Ser. 98:17-29.

Hinckley, S., K.M. Bailey, S.J. Picquelle, J.D. Schumacher and P.J. Stabeno. 1991. Transport, distribution and abundance of larval and juvenile walleye pollock (*Theragra chalcogramma*) in the western Gulf of Alaska. Can. J. Fish. Aquat. Sci. 48: 91-98.

Hinckley, S. 1990. Variation of egg size of walleye pollock (*Theragra chalcogramma*) with a preliminary examination of the effect of egg size on larval size. Fish. Bull. U.S. 88: 471-483.

Hinckley, S. 1987. The reproductive biology of walleye pollock, Theragra chalcogramma, in the Bering Sea, with reference to spawning stock structure. Fish. Bull. U.S. 85: 481-498.

Awards

1992-1993 Electric Power Research Institute Fellowship

IMAGE EVALUATION TEST TARGET (QA-3)

150mm

6″

APPLIED IMAGE . Inc
1653 East Main Street
Rochester, NY 14609 USA
Phone: 716/482-0300
Fax: 716/288-5989